Electrochemical Society

NEW TECHNICAL DATA SHEETS AVAILABLE TO GLC ANODE CUSTOMERS

Recently issued data sheets prepared by our Technical Department contain important information about graphite anode properties.

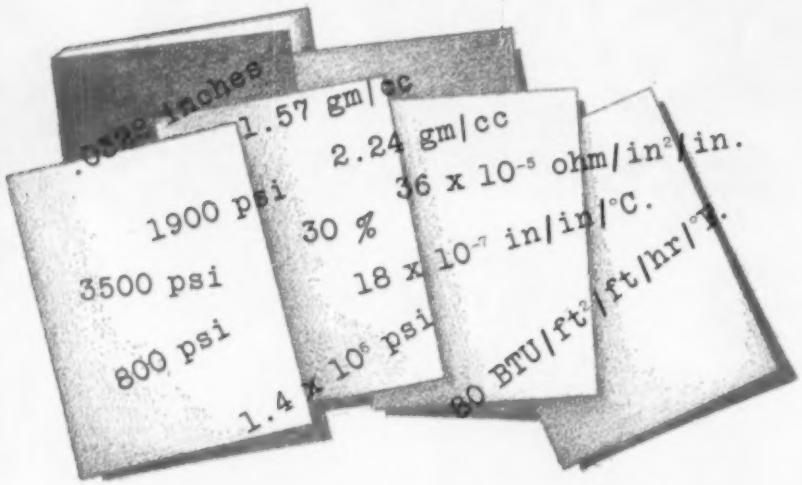

Among the typical physical properties detailed for anodes in various grades and sizes are maximum particle sizes... apparent and real density... porosity... resistivity... rupture... compressive and tensile strength... elasticity... thermal expansion and conductivity.

Typical chemical properties of the anode grades show percentages of ash, sulfur, silicon, iron, calcium, aluminum, vanadium sodium, titanium and other impurities.

Data on the surface finishing obtainable in various machining operations are also included.

We shall be happy to furnish a set of these technical data sheets, with our compliments, to anode users everywhere. Your request will be most welcome.

PRODUCTS ELECTRODE GLC DIVISION YOU CAN TRUST ®

GREAT LAKES CARBON CORPORATION

18 EAST 48TH STREET, NEW YORK 17, N. Y.

EDITORIAL STAFF

C. L. Faust, Chairman, Publication Committee

Cecil V. King, Editor

Norman Hackerman, Technical Editor

Ruth G. Sterns, Managing Editor

U. B. Thomas, News Editor

H. W. Salzberg, Book Review Editor

Natalie Michalski, Assistant Editor

DIVISIONAL EDITORS

W. C. Vosburgh, Battery

Milton Stern, Corrosion, I

R. T. Foley, Corrosion, II

T. D. Callinan, Electric Insulation

Seymour Senderoff, Electrodeposition

H. C. Froelich, Electronics, I

Ephraim Banks, Electronics, II

Ernest Paskell, Electronics—Semiconductors

Sherlock Swann, Jr., Electro-Organic, I

Stanley Wawzonek, Electro-Organic, II

John M. Blocher, Jr., Electrothermics and Metallurgy, I

A. U. Seybolt, Electrothermics and Metallurgy, II

N. J. Johnson, Industrial Electrolytic

C. W. Tobias, Theoretical Electrochemistry, I

A. J. deBethune, Theoretical Electrochemistry, II

ADVERTISING OFFICE

ECS

1860 Broadway, New York 23, N. Y.

ECS OFFICERS

R. A. Schaefer, President
The Bunting Brass and Bronze Co.,
Toledo, Ohio

Henry B. Linford, Vice-President
Columbia University, New York, N. Y.

F. L. LaQue, Vice-President
International Nickel Co., Inc.,
New York, N. Y.

W. J. Hamer, Vice-President
National Bureau of Standards,
Washington, D. C.

Lyle I. Gilbertson, Treasurer
Air Reduction Co., Murray Hill, N. J.

I. E. Campbell, Secretary
National Steel Corp., Weirton, W. Va.

Robert K. Shannon, Executive Secretary
National Headquarters, The ECS,
1860 Broadway, New York 23, N. Y.

Manuscripts submitted to the Journal should be sent, in triplicate, to the Editorial Office at 1860 Broadway, New York 23, N. Y. They should conform to the Instructions to Authors, last published in the Sept. 1960 issue, pp. 229C-230C. Manuscripts so submitted become the property of The Electrochemical Society and may not be published elsewhere, in whole or in part, unless permission is requested of and granted by the Editor.

Inquiries re positive microfilm copies for volumes should be addressed to University Microfilms, Inc., 313 N. First St., Ann Arbor, Mich.

The Electrochemical Society does not maintain a supply of reprints of papers appearing in its Journal. A photoprint copy of any particular paper, however, may be obtained by corresponding directly with the Engineering Societies Library, 29 W. 39 St., New York 18, N. Y.

Journal of the

Electrochemical Society

NOVEMBER 1960 **VOL. 107 • NO. 11**

CONTENTS

Editorial

University Research Equipment 250C

Technical Papers

The Cathodic Behavior of AgO in Alkaline Solutions. *T. P. Dirkze* 859

Relation of Electron Configuration to Passivity in Cr-Ni-Fe Alloys. *H. G. Feller and H. H. Uhlig* 864

Dissolution of Iron in Sulfuric Acid and Ferric Sulfate Solutions. *A. C. Makrides* 869

Inhibition of Metal Dissolution by Ferric Sulfate. *A. C. Makrides and M. Stern* 877

The Influence on the Oil Dielectric Strength of the Gas Pressure in Equilibrium with the Oil. *P. G. Priaroggia and G. Palandri* 884

Electropolishing in Cyanide Electrolytes. *F. Sullivan and E. H. Newton* 886

Particle Growth during Zinc Sulfide Phosphor Preparation. *A. Kremheller and S. Faria* 891

Electroluminescence Maintenance. *W. A. Thornton* 895

Determination and Identification of Impurities in Silicon from Low-Temperature Hall Data. *R. T. Bate, L. R. Weingarten, and D. J. Shombert* 908

A Modified Closed Box System for the Diffusion of Boron in Silicon. *R. S. Yatsko and J. S. Kesperis* 911

Properties of PbSe Prepared by Powder-Metallurgy Techniques. *J. F. Miller and R. C. Himes* 915

Kinetics of the Formation of the Iron-Tin Alloy $FeSn_2$. *R. P. Frankenthal and A. W. Loginow* 920

Properties of Vanadium-Columbium Alloys. *S. T. Wlodek* 923

Technical Notes

NMR Measurements of the Knight Shift in Conducting PbO_2. *D. A. Frey and H. E. Weaver* 930

Determination of the Standard Free Energy of Formation of Lead Selenide. *C. B. Finch and J. B. Wagner, Jr.* 932

Microalloy Junction for Silicon. *L. Maissel* 933

Electrolytic Production of Zirconium in a Fused Salt Voltaic Cell. *M. L. Freedman* 934

Technical Feature

Fuel Cell Thermodynamics. *A. J. deBethune* 937

Current Affairs **253C-260C**

Published monthly by The Electrochemical Society, Inc., from Manchester, N. H., **Executive Offices, Editorial Office** and **Circulation Dept.,** and **Advertising Office** at 1860 Broadway, New York 23, N. Y., combining the JOURNAL and TRANSACTIONS OF THE ELECTROCHEMICAL SOCIETY. Statements and opinions given in articles and papers in the JOURNAL OF THE ELECTROCHEMICAL SOCIETY are those of the contributors, and The Electrochemical Society assumes no responsibility for them. Nondeductible subscription to members $5.00; subscription to nonmembers $18.00. Single copies $1.25 to members, $1.75 to nonmembers.

Copyright 1960 by The Electrochemical Society, Inc.

Entered as second-class matter at the Post Office at Manchester, N. H., under the act of August 24, 1912.

One of a series

Catching the Drift of Gyro Bearings

The fantastic accuracies needed by inertial guidance systems for space flight depend on the suppression of gyro drift, the tendency of a gyro to precess from minutely occurring internal torques. Particularly puzzling has been the problem of "jogs," or sudden axial shifts, within gyro spin-axis bearings. Shifts of but one ten-millionth of an inch can cause serious steering error.

Specialists at the GM Research Laboratories have found that the real key to drift lies in the thickness and distribution patterns of bearing lubricating films. Only a tenth of a milligram of oil – equivalent in volume to less than two-thousandths of a drop of water – is required in a gyro bearing, but even this amount unevenly distributed may cause jogs.

Conducting unique studies of single bearings apart from rotor assemblies, GM Researchers use a hydrostatic spindle and special instrumentation to take film-thickness measurements they compare with hydrodynamic theory. Jogs, due to excess oil supply, have been analyzed in relation to surface oil transfer and separator feed control, ball spin orientation, displacement, and differential heating and ball wander.

This experimental and analytical approach is achieving progress toward jog-free, stably distributed, and suitably thick oil films required in high-precision bearings. It is a further example of the critical and advanced research General Motors carries out in seeking "more and better things for more people."

General Motors Research Laboratories

Warren, Michigan

The fluoresced streaks show the disturbed "wake" of the lubricating film during bearing operation. The active part of the film, too thin to fluoresce visibly, averages ten-millionths of an inch in thickness.

FIRST PHONE CALL VIA MAN-MADE SATELLITE!

"Project Echo" satellite went into a near-perfect circular orbit 1000 miles high, circling the earth once every two hours. Its orbital path covered all parts of the U. S.

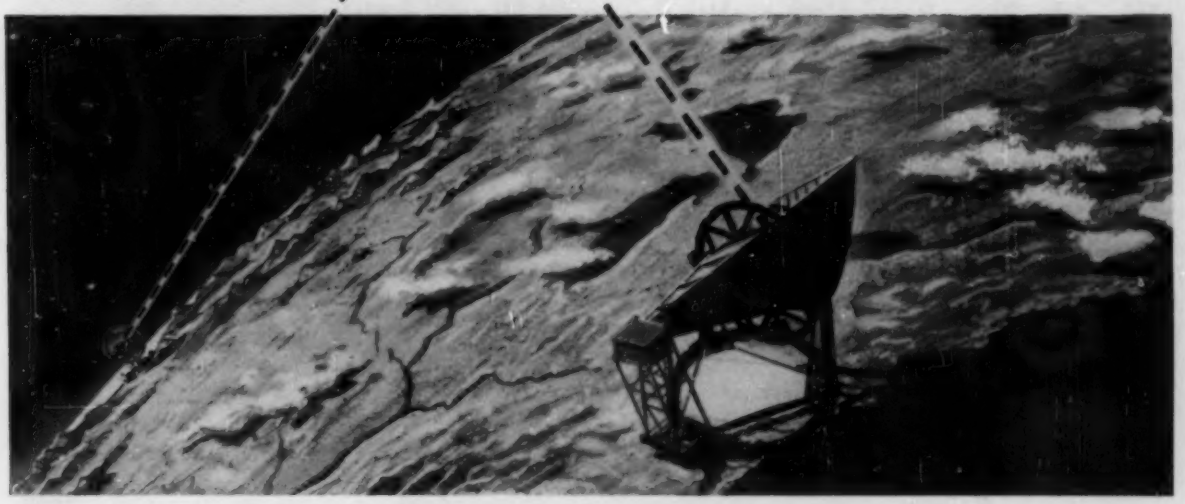

BELL TELEPHONE LABORATORIES BOUNCES VOICE OFF SPHERE PLACED IN ORBIT A THOUSAND MILES ABOVE THE EARTH

Think of watching a royal wedding in Europe by live TV, or telephoning to Singapore or Calcutta—*by way of outer-space satellites!* A mere dream a few years ago, this idea is now a giant step closer to reality.

Bell Telephone Laboratories recently took the step by successfully bouncing a phone call between its Holmdel, N. J., test site and the Jet Propulsion Laboratory of the National Aeronautics and Space Administration (NASA) in Goldstone, California. The reflector was a 100-foot sphere of aluminized plastic orbiting the earth 1000 miles up.

Dramatic application of telephone science

Sponsored by NASA, this dramatic experiment—known as "Project Echo"—relied heavily on telephone science for its fulfillment . . .

- The Delta rocket which carried the satellite into space was steered into a precise orbit by the Bell Laboratories Command Guidance System. This is the same system which recently guided the remarkable Tiros I weather satellite into its near-perfect circular orbit.

- To pick up the signals, a special horn-reflector antenna was used. Previously perfected by Bell Laboratories for microwave radio relay, it is virtually immune to common radio "noise" interference. The amplifier—also a Laboratories development—was a traveling wave "maser" with very low noise susceptibility. The signals were still further protected from noise by a special FM receiving technique invented at Bell Laboratories.

"Project Echo" foreshadows the day when numerous man-made satellites might be in orbit all around the earth, acting as 24-hour-a-day relay stations for TV programs and phone calls between all nations.

This experiment shows how Bell Laboratories, as part of the Bell System, is working to advance space communication. Just as we pioneered in world-wide telephone service by radio and cable, so we are pioneering now in using outer space to improve communications on earth. It's part of our job, and we are a long way toward the goal.

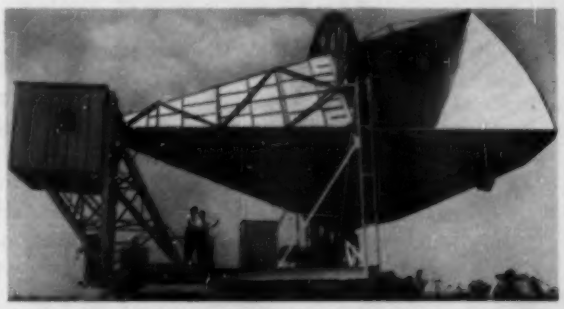

Giant ultra-sensitive horn-reflector antenna which received signals bounced off the satellite. It is located at Bell Telephone Laboratories, Holmdel, New Jersey.

BELL TELEPHONE LABORATORIES

WORLD CENTER OF COMMUNICATIONS RESEARCH AND DEVELOPMENT

Editorial

University Research Equipment

LAST August, *Chemical and Engineering News* called attention to the difficulties which university science departments may have in obtaining expensive research instruments, and explored the extent to which different departments, or even different universities, cooperate in buying and using such equipment. There is, of course, a great deal of such cooperation, much of it on an informal basis, especially if it involves only brief use of instruments. However, many professors thought it too much trouble and effort to cooperate in this way, especially in buying, installing, and maintaining expensive items, and, if travel is involved, to do what should be routine experimentation. Consequently, they plan their research programs around less expensive but more easily available equipment.

If an industrial laboratory decides that an expensive instrument is needed—say something costing $50,000 to $100,000—then certainly the problems of maintenance and use will be carefully planned, and sufficient trained personnel will be assigned to insure full value from the investment. (Of course, there are rumors that costly mistakes have been made.) On the other hand, if a college professor in some way picks up an expensive item (say a "surplus" mass spectrometer), he may feel that his research program must be tied to the one instrument for years. It is unlikely that he could count on trained technical help to maintain such instruments as tools for a broader program; he and his students must be their own technicians.

We are, naturally, not concerned here with the professor who becomes the Director of Well-Financed Research, and is able to find funds to keep a well-equipped laboratory and a staff to operate it; who perhaps glances hastily over his notes a few minutes before the occasional lecture. There are many more professors who teach from 8 to 18 hours per week in the classroom and laboratory, and maintain minor or major research programs with a few students, with or without expensive equipment.

If a university, with Government assistance, sets up a million-dollar nuclear reactor, it is quite certain that the problems of operation will be in the hands of experienced personnel. Then faculty members and their students can use the reactor as a research tool and as a teaching aid, with little or no responsibility for the actual maintenance. Why not apply the same principle to lesser equipment? Some universities do, but more do not. The university administration can make a valuable contribution to its science departments and their research by encouraging the setting up of cooperative instrument laboratories, to be maintained by experienced technicians rather than by the professors and their students. Many professors have special problems which require special apparatus; nearly all could benefit by having additional standard instruments available, if they were tools and not maintenance problems.

—CVK

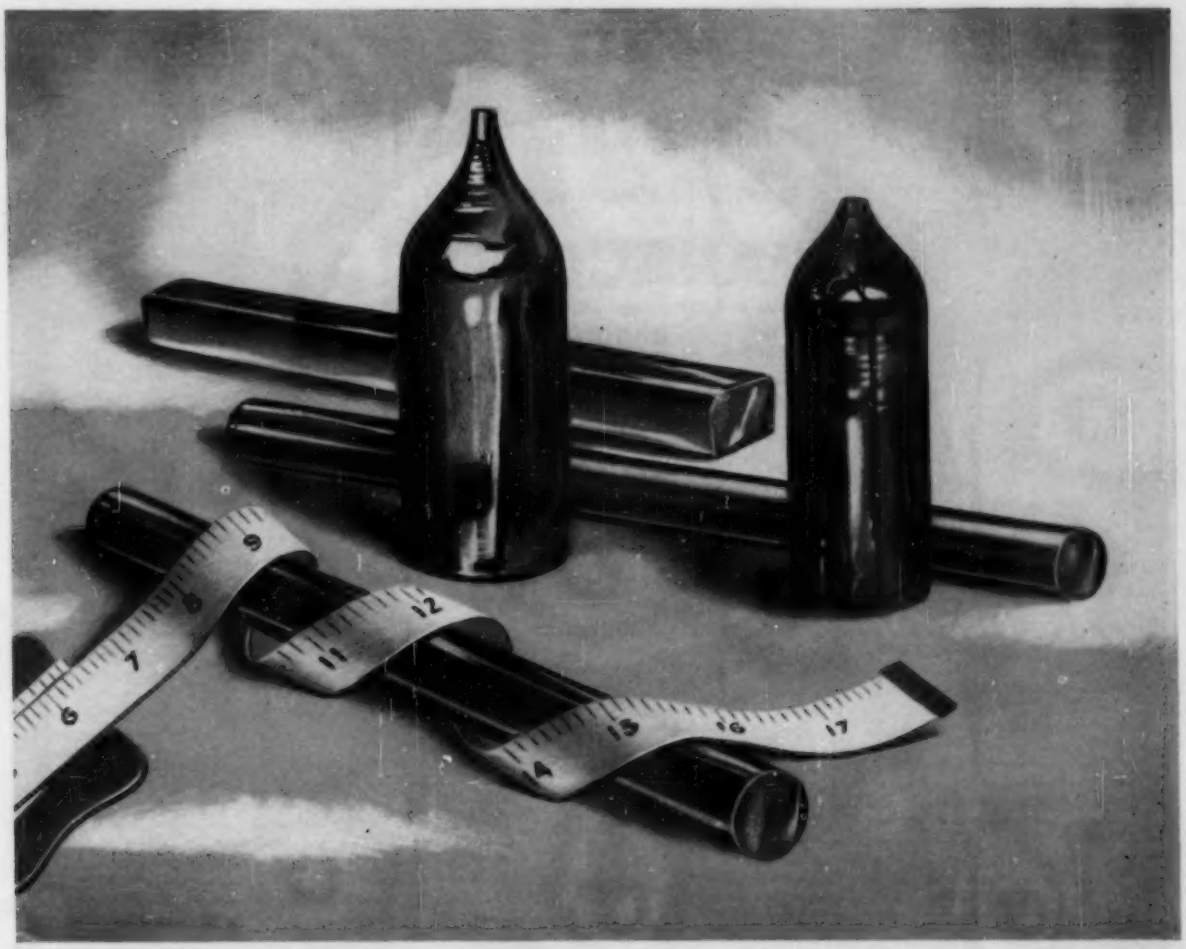

Now! Tailored to your budget!

Sylvania offers Germanium and Silicon Single Crystals in Production Quantities—at Attractive Prices

Now Sylvania offers to all device manufacturers the advantages of quantity production in the highly specialized field of germanium and silicon single crystals. These crystals are available at competitive prices and to desired specifications. Through the use of stringent quality-control techniques, you are assured of top-quality material—ready to use!

By specifying Sylvania crystals, you save the capital needed to invest in your own crystal-growing equipment. You save valuable space, time and technical manpower, too.

Another step in the Sylvania program to offer semiconductor materials and services to the device manufacturer is the completeness of product line. Sylvania now supplies germanium dioxide, intrinsic polycrystalline germanium, and doped germanium single crystals and slices. Polycrystalline silicon and doped silicon single crystals and slices are also available. To the germanium device manufacturer we can also offer our scrap-refining facilities.

For full details, a price on your quantity needs, plus your copy of a report on measuring and evaluating crystals for many specifications, write Chemical & Metallurgical Division, Sylvania Electric Products Inc., Towanda, Pennsylvania.

SYLVANIA

Subsidiary of **GENERAL TELEPHONE & ELECTRONICS**

A new idea in plating

ANACONDA

announces

"PLUS-4"

phosphorized copper anodes

in a new form

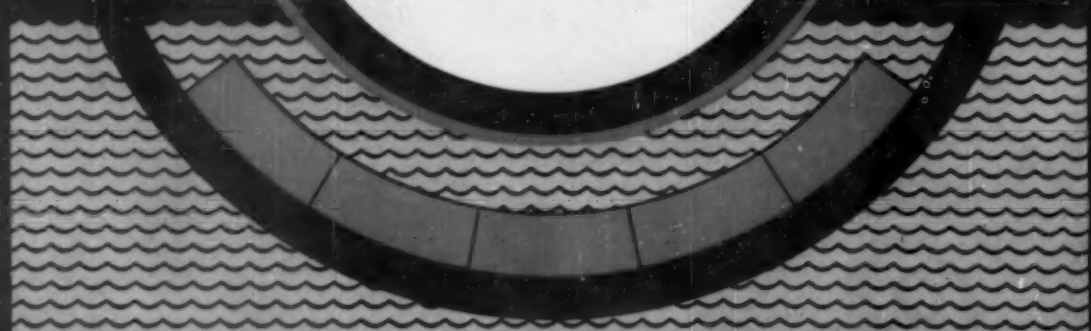

CURVED ANODES

for plating cylinders faster and more uniformly

To make anode surfaces parallel the rotogravure cylinder being plated, and to fit the curve of the current-carrying slings, Anaconda "Plus-4" phosphorized copper anodes are now extruded to precisely curved shapes.

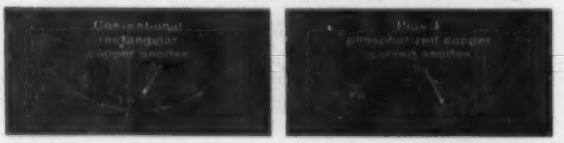

This design gives both cost savings and improved cylinder quality:

1. A more evenly plated cylinder. Because the distance between the cylinder and the anode surface is more uniform, the copper deposit is smoother and more uniform.

2. Finishing operations in most cases are reduced, as much as 50%, because of the uniform copper deposit.

3. Less scrap because anodes corrode more evenly.

4. Improved electrical efficiency and faster plating because of better contact with sling.

For more information, write: Anaconda American Brass Company, Waterbury 20, Conn. In Canada: Anaconda American Brass Ltd., New Toronto, Ont.

Note: When you request information, please specify inside radius of anode.

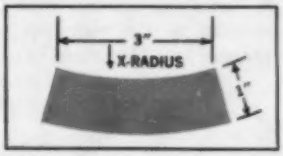

"PLUS-4"® phosphorized copper anodes

products of

ANACONDA®

Anaconda American Brass Company

The Cathodic Behavior of AgO in Alkaline Solutions

Thedford P. Dirkse

Calvin College, Grand Rapids, Michigan

ABSTRACT

A study has been made of the discharge of AgO to determine why only a part of the discharge capacity of AgO is delivered at the potential of the AgO-Ag_2O couple and to determine the role of oxygen in this process. The difference in discharge capacity of electrodes produced by constant-current and by constant-potential anodization also has been studied. A mechanism involving the transport of $O^=$ ions through the electrode material and the reaction of these ions with the electrolyte is presented.

When a fully charged silver-zinc battery is discharged, the voltage-time curve usually has two levels (Fig. 1). The higher of these is generally attributed to the presence of AgO in the silver electrode. However, the processes occurring when AgO is discharged are not well understood. The capacity delivered at this higher level on discharge is usually but a fraction of that theoretically available. Furthermore, this capacity appears to depend on a variety of circumstances, some of which are unknown. In recent years several facts have been brought to light in connection with this capacity. A good deal of the capacity available as AgO on the electrode is delivered at a voltage level corresponding to that of Ag_2O (1, 2). The exact amount delivered at this lower voltage level depends on the current density. It also has been shown that the capacity of AgO delivered at this higher voltage level decreases on stand with no loss in total capacity (3). Recently, Wales and Burbank (4) have shown that during certain periods of discharge the reduction of AgO to Ag_2O and that of Ag_2O to Ag likely proceed simultaneously. Their results fail to give any evidence for the presence of solid solutions of AgO in Ag_2O on discharge.

A second problem associated with the cathodic behavior of AgO arises from the fact that oxygen can be added to AgO without changing the emf of the substance (5). This added oxygen does not alter the x-ray diffraction pattern of AgO except to make it more diffuse.

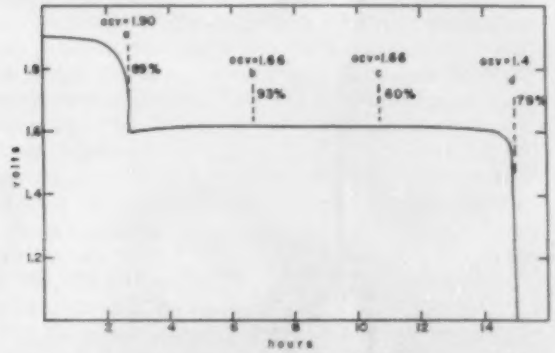

Fig. 1. Voltage-time curve for the discharge of an AgO-Zn-40% KOH cell at room temperature. Percentages are discharge efficiencies.

The present work was carried out to obtain more information on the cathodic behavior of AgO and to investigate more thoroughly the role of oxygen in this process.

Experimental and Discussion

The experimental techniques used in this work were the same as those described earlier (5). When electrodes were to be weighed they were first soaked in distilled water for at least 8 hr, then dried in a stream of purified nitrogen at room temperature, and finally placed in a desiccator for at least 24 hr. All these operations were carried out in the absence of light. After this, the electrodes were weighed and the change in weight was considered to be due to changes in oxygen content. Where possible the electrode was finally reduced to Ag and weighed. The weight of Ag at this time agreed, within experimental error, with the weight at the beginning of the charging process.

Oxygen content.—In the work reported earlier (5) it was shown that when silver is treated anodically in KOH solutions the addition of oxygen to form Ag_2O and AgO follows Faraday's laws. When the gassing potential is reached some oxygen is still added to the electrode. This was determined by weighing the electrode before and after such gassing treatment. At constant-current charging the oxygen added during gassing often corresponded to about 10% of the current passed. Apparent current densities of 0.25 to 2.5 ma/cm^2 were used, yet there was no stoichiometric evidence for complete transformation of all the Ag to AgO even though these electrodes were allowed to remain at the gassing potential for periods of up to 10 hr.

With constant-potential charging, oxygen also can be added to the silver electrode even when the potential is kept below that needed for gassing. Products having oxygen contents corresponding to $AgO_{1.5}$ have been prepared in this manner.

The question then arises whether the oxygen added to the electrode during gassing on constant-current charging or during prolonged constant-potential charging at a potential about 100 mv

below the gassing potential contributes to the discharge capacity of the electrode.

To check this, a commercially prepared sintered Ag electrode, 1.5 x 3.8 cm, weighing 2.4 g, was charged at 0.1 amp in 40% KOH. Its capacity was determined by charging up to the gassing potential and then allowing it to stand 20 hr before being discharged. The discharge capacity exactly equaled the charge input (0.68 amp-hr). The electrode then was given a series of cycles in which it was charged at the same rate and allowed to remain at the gassing potential for 8 to 15 hr. It was discharged immediately after each of these charges, and the discharge capacity was only 3% larger than the previous charge input up to the gassing potential. Thus while prolonged gassing on constant-current charge does add oxygen to the electrode as noted above, this oxygen contributes very little to the discharge capacity. In all these instances, however, there was no complete conversion to AgO. Since this electrode accepted 0.68 amp-hr of charge, its composition when charged corresponded to about $AgO_{1.2}$. Since there definitely was AgO present, as determined by x-ray diffraction and by observation of the discharge voltage-time curve, free silver also was present.

Wales and Burbank (4) observed that prolonged gassing on constant-current charge appeared to produce more perfectly crystalline AgO. This suggests that when the electrode reaches the gassing potential on charge the surface has not been completely converted to crystalline AgO. During gassing more oxygen is added to the surface, forming more completely crystalline AgO. Perhaps it is this oxygen that gives the small increase in discharge capacity which is obtained on prolonged gassing.

This oxygen, however, is not the only oxygen added during the gassing period. The weight gained during gassing is larger than that corresponding to the extra discharge capacity. Earlier work (6) has shown that, when an electrode is charged at constant-current and is allowed to charge at the gassing potential for several hours or more, appreciable amounts of oxygen can be added. This oxygen is held firmly by the electrode material, but it does not add correspondingly to the discharge capacity. Moreover, this oxygen is released on discharge. For example, a sintered Ag electrode, 3.8 cm square and weighing 6.2 g, was charged at a constant-current of 0.04 amp in 15% KOH for 3 days. It was then soaked in distilled water and dried overnight in an oven at 60°C. The weight gain corresponded to a product having the composition $AgO_{1.2}$. This electrode was stored dry in the dark for 2 years and then charged again, this time at 0.7 amp in 40% KOH for 24 hr. It was gassing profusely during the latter part of the charge. When it was soaked in distilled water much gas was evolved. It was then dried for 24 hr at 60°C. There was a slight gain in weight, corresponding to less than 1% of the charge applied. After 3½ weeks the electrode was discharged at 0.1 amp in 42% KOH. After 10 hr the voltage *vs.* Zn fell below 1 v and the discharge was terminated even though there was still visible evidence of oxides on the plate. The electrode again was soaked in distilled water and dried for a day at 60°C. The loss in weight was 0.57 g. Assuming that this loss was due to oxygen, this corresponds to 1.9 amp-hr. Yet only 1 amp-hr had been removed during the discharge. Apparently, about 0.27 g oxygen escaped as bubbles during the discharging process, but no attempt was made to observe this.

Changes do occur if the electrode is stored for some time. Several electrodes similar to the one just described were charged at constant-current and were stored dry for 1 to 2 years. None of them was completely converted to AgO, and none lost weight during this storage. With some, the open-circuit voltage (ocv) after storage was that associated with Ag_2O. Others, however, gave an ocv associated with AgO. Thus, this dry storage does not necessarily lead to complete conversion of AgO to Ag_2O (reaction [1]).

$$AgO + Ag \rightarrow Ag_2O \qquad [1]$$

This reaction does take place when electrodes are stored in electrolyte or even in water. Figure 2 is a picture of electrodes which had been partially discharged. The white portions are Ag whereas the darker portions are oxides of silver. One such electrode was placed in electrolyte, and after about 3 weeks all the Ag had been oxidized to Ag_2O. In such a situation, Eq. [1] represents the net effect of a local cell reaction consisting of a AgO cathode and a Ag anode. This reaction may take place rapidly at first, but as Ag_2O is produced the internal resistance of the local cell is increased and the reaction slows down.

These electrodes did not deliver their total available capacity after storage. After discharge, such

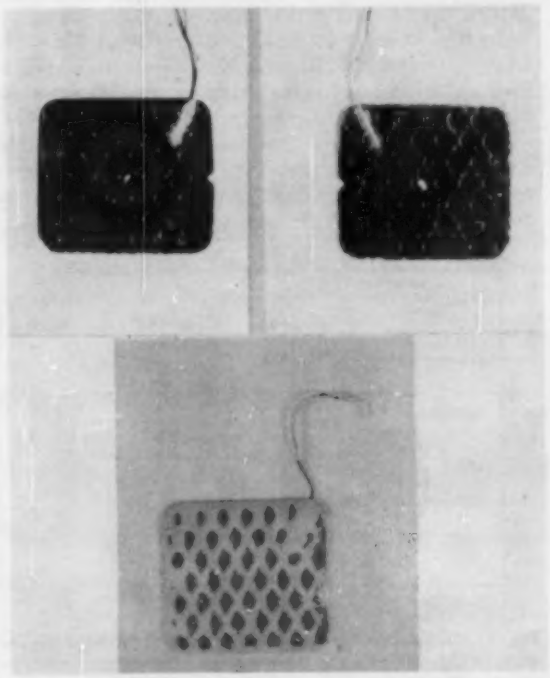

Fig. 2. Partially discharged AgO electrodes

an electrode was heavier than it was before being charged, indicating that discharge had not removed all the oxygen from the electrode material. With one charged electrode, 25% of the theoretical discharge capacity (calculated from oxygen content) was unavailable after storage. This phenomenon has been noted with other electrodes also.

An attempt was made to follow this change during storage by x-ray analysis. Freshly charged electrodes gave good sharp patterns for AgO. In some electrodes there were also areas giving good Ag_2O patterns. After dry storage for 1.5 years the electrodes still gave the AgO pattern, but it was weak and the lines were broader. This indicates a deterioration of the crystallinity of the oxide structure and is likely due to diffusion of oxygen ions to areas of lower oxygen content. There was no loss of oxygen. This diffusion during storage apparently also affects the current path through the electrode, and this may be responsible for the reduction in capacity. The current path is altered, as will be noted later, so that some of the oxygen in the interior of the electrode cannot escape from the silver lattice.

With constant-potential charging (at potentials slightly below the gassing potential) large amounts of oxygen can be introduced into the silver lattice. This oxygen may exceed the stoichiometric ratio of AgO, and yet many of the physical properties are the same as those of AgO (5). It has been suggested that at least part of this oxygen is physically adsorbed rather than chemically bound. This idea is consistent with the following results.

A small electrode was charged in 30% KOH at a constant potential of 350-400 mv above the reversible potential of Ag-Ag_2O. After charge its composition was $AgO_{1.2}$. After standing one week it was discharged in 42% KOH at about 1 ma/cm^2. At intervals the discharge was interrupted, the electrode was dried, weighed, and x-rayed. Then it was inserted in the cell and the discharge continued. The x-ray patterns showed the same variations as have been reported earlier (4). Discharge results are given on Fig. 1. The electrode was weighed at points a, b, c, and d. The loss in weight was considered to be due to a loss of oxygen. This was justifiable since the weight of the silver on the electrode at the end of the discharge was within 0.3% of that on the electrode at the beginning of the experiment. The theoretical weight loss was calculated from the ampere-hours of discharge. This value divided by the actual weight loss was called the discharge efficiency. The discharge efficiency at point a on Fig. 1 refers to the interval from the beginning of discharge to point a, that at point b refers to the interval between a and b, etc. Perhaps as the electrode discharges, adsorbed oxygen escapes in a mechanical fashion from the lattice. On the basis of the efficiencies, this is more easily accomplished toward the end of the discharge.

Three other electrodes were prepared on platinum grids. They were made by pasting the grid with moist Ag_2O, air drying, and thermally reducing them at 550°C to Ag. Then they were subjected to constant-potential charging until they had an oxygen content greater than AgO. Two of them (A and B) were stored dry for 3 months at room temperature and the third was stored dry for 1.5 years after 4 months' storage in the dark in 30% KOH. None of these electrodes lost any appreciable weight over this period of time. This shows that the extra oxygen is bound rather firmly to the silver. Their emf values and x-ray diffraction patterns were those of AgO. There was nothing to indicate a new type of oxide, *e.g.*, Ag_2O_3.

Electrodes A and B were discharged at a very low current density in 28% KOH. Typical discharge curves were obtained, although relatively little discharge capacity (2% and 15% of the total) was obtained at the higher voltage level. Electrode C was discharged in 40% KOH at an 11 hr rate. No discharge capacity was obtained at the voltage level corresponding to AgO. The ocv, however, was 1.9 v *vs.* Zn.

The fact that so little discharge capacity was obtained at the higher level in each case may at first seem to be normal. These electrodes stood for some time before being discharged, and it has been shown that standing reduces the amount of capacity delivered at the high voltage level but does not reduce the total discharge capacity (3). This has been attributed to the fact that on stand reaction [1] takes place (4). If this is the case, there must have been more than a trace of unoxidized silver present in the charged electrodes. It follows then that constant-potential charging does not bring about complete conversion to AgO even though the composition of the material can be represented by $AgO_{1.0}$. It can be argued that reaction [2] takes place at the platinum

$$2AgO \rightarrow Ag_2O + 1/2\ O_2 \qquad [2]$$

grid and that the formation of the Ag_2O increases the internal resistance of the electrode so that the discharge voltage is polarized to the Ag_2O-Ag level. This reaction then would take place in the dry state since these electrodes were stored dry. Ohse (7) noted a lack of evidence for this reaction in 1N KOH.

A comparison was made of the capacity obtained to that theoretically available. The theoretical capacity was calculated on the basis of both silver and oxygen content. Results are given in Table I.

It is obvious that all the oxygen present in these electrodes was not useful for discharge purposes. This also follows from the fact that with electrode C, *e.g.*, the loss in weight of oxygen during discharge was 130% of that corresponding to the actual capacity obtained. Some of this oxygen was apparently released from the electrode during dis-

Table I. Capacity of "AgO" electrodes

Electrode	Composition	% Theoretical capacity on basis of		
		O_2	Ag^{++}	Ag^{+++}
A	$AgO_{1.0}$	56	91	60
B	$AgO_{1.0}$	55	85	57
C	$AgO_{1.2}$	23	27	18

charge without entering into the discharge reaction. The small value for per cent theoretical capacity is due to the prolonged storage of this electrode, as noted earlier in this paper. Since electrode C had a 4 month wet stand it is very possible that reaction [1] proceeded to a significant extent. This could build up sufficient Ag_2O to increase the internal resistance of the electrode, alter the current path within it, and thus bypass some of the oxide during the discharge reaction.

If one assumes that the silver present in the electrode was all in the divalent state, then the actual discharge capacity still is less than theoretical. At the current densities used one would expect practically 100% discharge/charge efficiency. The fact that the actual discharge capacity is less than theoretical supports the idea that some unoxidized silver was present in the charged electrodes. It also makes unnecessary the suggestion that trivalent silver is present in the electrodes. These results support the idea that divalent silver is the highest oxidation state of silver in the charged electrodes. Furthermore, even prolonged constant-potential charging fails to convert all the silver to the divalent state.

It follows from these results that the oxygen content of the electrodes charged by the constant-potential method is no measure of the oxidation state of the silver. This method of charging may be rather inefficient. Although the weight of oxygen added to the electrode follows Faraday's laws (5), the discharge of such an electrode does not necessarily give a capacity equal to the oxygen content. This oxygen is strongly held and not readily released from the dry solid at room temperature. On discharge it appears to be released as the positive charge on the silver atoms (ions) is decreased. It may be forced out of the electrode as the lattice changes from AgO to Ag_2O. As this reduction takes place the silver ions move closer together leaving less room for occluded oxygen. Furthermore, the reduced charge on silver ions decreases the power to attract or adsorb oxygen atoms.

With constant-current cycling the discharge capacity generally equals the charge input up to the gassing potential (8). The weight of oxygen added during charge at moderate rates follows Faraday's laws (5). Prolonged gassing does result in the addition of oxygen and a small increase in discharge capacity. This indicates that the oxygen added during normal charging is a good measure of the state of oxidation of silver. With prolonged gassing, however, much of the oxygen added appears to be merely physically adsorbed.

Polarization.—One of the questions in connection with the discharge of AgO is the extent of polarization. Less than half the discharge capacity of an electrode usually is delivered at the higher voltage level. This raises the possibility that the $AgO \rightarrow Ag_2O$ process is polarized to such an extent that it operates at the lower potential of $Ag_2O \rightarrow Ag$.

The extent of this polarization was studied by an interrupter method (9). Electrodes in which the surface is almost completely AgO showed very little polarization in the initial stages of discharge. A rapid increase in polarization was noted as the AgO was converted to Ag_2O and this polarization at times was so great that it caused the discharge of AgO to take place at a potential below that of Ag_2O (9). After this the potential rose to that of the $Ag_2O \rightarrow Ag$ process. The point at which the voltage drops to that of the $Ag_2O \rightarrow Ag$ level seems then to be determined by the current density on the surface layer of AgO. When this exceeds a certain value the potential drops. This drop in potential also is influenced by the formation of increasing amounts of Ag_2O. This highly resistive material may bring about an *IR* drop in the electrode itself.

With small wire electrodes on which but thin films of oxide were produced, about 40% of the discharge was obtained at the higher voltage level over a modest range of current densities. Conceivably this fact can be used to indicate that the fall of potential from the higher to the lower level is determined more by the resistance of the Ag_2O formed than by the increase of current density on the AgO. Since only thin films of oxide are produced, the resistance of the Ag_2O is not as great as with thicker films. Under these conditions the fall in potential occurs at a later stage in the discharge. It also may be that a greater fraction of the AgO present is on the surface and therefore the higher voltage level on discharge lasts relatively longer.

In Fig. 2 the pattern of the silver spots is the same as that of the grid of the electrode, indicating the importance of the current path in the discharge process. Furthermore, this suggests that the electrical resistance is an important factor in this process.

This polarization also is due in part to the electrolyte. This was shown by varying the KOH concentrations. At an apparent current density of about 1 ma/cm^2 the polarization amounted to 3, 6, and 32 mv in 1*N*, 0.5*N*, and 1.0*N* KOH, respectively. These values are corrected for the *IR* drop in the solution.

Mechanisms.—In discussing possible mechanisms for the cathodic behavior of AgO one should know whether the discharge reaction proceeds from the grid to the electrode-electrolyte interface or in the opposite direction. The discharge reaction is the removal of $O^=$ ions from the electrode material. To determine where in the electrode this process begins, the silver oxides were pressed into pellets about 1.25 cm diameter and 0.65 cm thick. They were discharged in a cell shown on Fig. 3. Only a small

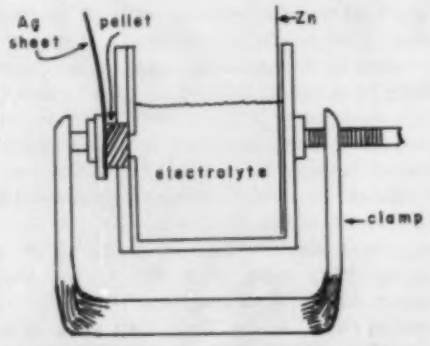

Fig. 3. Cell for use with pelletized electrodes

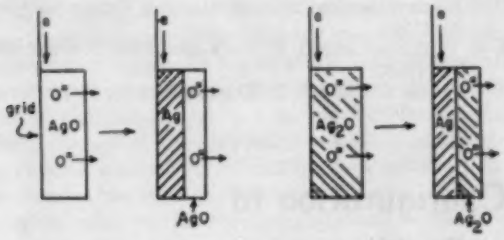

Fig. 4. Mechanism for the reduction of AgO

surface area was exposed to the electrolyte, and the grid (the Ag sheet) was completely outside the cell case. The electrolyte did seep into and penetrate the pellet.

Pellets of both Ag_2O and AgO were prepared and discharged at 35 ma/cm², considering only the surface area exposed to the bulk electrolyte. In either case the material was reduced to Ag during discharge and gave the capacity calculated from its weight, i.e., 231 ma-hr/g of Ag_2O and 432 ma-hr/g of AgO. When the material was discharged only long enough to deliver about half the discharge capacity of the material, it was found that with the Ag_2O pellet the reduced Ag was at the grid and not at the electrolyte. With the AgO pellet the same thing occurred. In fact, there was almost a plane surface that separated the Ag from the unreduced oxide. This plane was practically at the mid-point of the pellet. Furthermore, the unreduced oxide was AgO and not Ag_2O. This was determined by x-ray analysis, and it is possible that small amounts of Ag_2O were present. However, the bulk of the material was AgO. This suggests that on discharge the removal of $O^=$ ions proceeds from the grid toward the electrode-electrolyte interface (Fig. 4). Moreover, no large amounts of Ag_2O need be produced during the discharge of the AgO.

During the discharge of AgO small amounts of Ag_2O may be formed at the electrode-electrolyte interface as the $O^=$ ions are removed from the electrode by the electrolyte. X-ray evidence (4) indicates that this occurs, and the extent of this Ag_2O formation would depend on the current rate. This Ag_2O will be formed then because $O^=$ ions are removed from the surface at a faster rate than they are transported through the electrode material. The current path available is a significant factor since the $O^=$ ions begin to migrate from the areas where the current enters the electrode (Fig. 2).

Because the polarization of AgO is determined to some extent by the concentration of the KOH, it is apparent that some solvent or solute species are involved in this cathodic process. The species available are OH^-, K^+, and H_2O.

The cathodic process involves the removal of $O^=$ ions from the oxide. As the silver is reduced these ions are ejected from the electrode material. It is unlikely that the negatively charged OH^- ions would be responsible for this removal of the negatively charged oxygens. They would, no doubt, be repelled from the electrode.

It is possible that the free H_2O molecules are involved in this process. During discharge the H part of the molecule would be oriented toward the electrode and then the following process could occur

$$\begin{matrix} Ag=O & H \\ & \diagdown \\ & + \quad O + 2e \rightarrow Ag_2O + 2OH^- \\ & \diagup \\ Ag=O & H \end{matrix} \qquad [3]$$

If this explanation is correct, then the cathodic polarization should increase with increase in KOH concentration. In a dilute solution more H_2O molecules would be available for reaction. However, as noted above, no such effect was observed.

Since, as indicated earlier, it is unlikely that the OH^- ions are involved, one is left with the K^+ ions as the reacting species. These ions are hydrated in solution, probably $K(H_2O)_4^+$ (10). Conceivably, these ions are drawn to the electrode with the H atoms oriented toward the electrode surface and then reaction [3] takes place. The charge on the K^+ ion aids in attracting the $O^=$ ions of the solid. It also weakens the O — H bonds in the H_2O. Thus the H_2O molecules bound to the K^+ ions are more reactive than the uncombined H_2O molecules. Attempts were made to determine the effect of substituting Na^+ ions for K^+ ions by using 0.1*N* NaOH solutions and also 7M solutions of $NaC_2H_3O_2$ and $KC_2H_3O_2$. However, any differences observed were within the limits of experimental error.

In summary, the cathodic reaction of AgO involves the removal of $O^=$ ions from the lattice by the H_2O molecules that are bound to the K^+ ions. This reaction occurs at the electrode-electrolyte interface. The amount of interfacial area is extensive because the KOH solution permeates the bulk AgO so thoroughly. As reaction proceeds, $O^=$ ions from the interior of the lattice migrate to this interface. Thus there are two factors responsible for the polarization of the AgO: (*a*) the reaction of $O^=$ ions with hydrated K^+ ions; and (*b*) the transport of $O^=$ ions through the electrode material. If the second process is not as fast as the first one, then the $O^=$ ion concentration at the electrode-electrolyte interface is reduced and the emf of the electrode decreases.

Acknowledgment

This work was supported by the Office of Naval Research. Thanks are also due to the Yardney Electric Company and to the M. Ames Chemical Works for furnishing some of the materials used in this work, and to Dr. W. C. Vosburgh for his help in preparing this manuscript.

Manuscript received March 30, 1960.

Any discussion of this paper will appear in a Discussion Section to be published in the June 1961 JOURNAL.

REFERENCES

1. I. A. Denison, *Trans. Electrochem. Soc.*, **90**, 387 (1946).
2. J. C. White, T. P. Dirkse, and R. T. Pierce, *ibid.*, **90**, 467 (1946).
3. C. P. Wales, NRL Report 5167, Aug. 11, 1958, Naval Research Laboratory, Washington, D. C.
4. C. P. Wales and J. Burbank, *This Journal*, **106**, 885 (1959).
5. T. P. Dirkse, *ibid.*, **106**, 920 (1959).

6. T. P. Dirkse and L. A. Vander Lugt, "A Study of the Oxides of Silver," Techn. Report No. 4 on Contract No. N onr-1682(01), June 30, 1957, Calvin College, Grand Rapids, Mich.
7. R. W. Ohse, *Z. Elektrochem.*, **63**, 1063 (1959).
8. T. P. Dirkse and J. De Vries, Paper presented at Electrochemical Society Meeting, Columbus, Oct. 20, 1959.
9. T. P. Dirkse and G. J. Werkema, *This Journal*, **106**, 88 (1959).
10. G. W. Brady and J. T. Krause, *Norelco Reporter*, **5**, 111 (1958).

Relation of Electron Configuration to Passivity in Cr-Ni-Fe Alloys

H. G. Feller and H. H. Uhlig

Corrosion Laboratory, Department of Metallurgy

Massachusetts Institute of Technology, Cambridge, Massachusetts

ABSTRACT

Critical current densities for passivity were measured for single phase Cr-Ni-Fe alloys as a function of Cr content for 20%, 40%, 50% and 60% Ni compositions. Major discontinuities in slope approximate the ratio 12/88 for Cr to Fe in the 20 and 40% Ni alloy series, and 14/86 for Cr to Ni in the 50 and 60% Ni alloy series. These ratios correspond to observed critical compositions for passivity in the Cr-Fe and Cr-Ni binary systems. Additional discontinuities occur at the critical binary Cr to Fe ratio in the 50 and 60% Ni series. This behavior is interpreted in terms of separate electron interaction in the ternary system between Cr and Fe distinct from interaction between Cr and Ni. Flade or activation potentials become more active with increasing Cr content, corresponding to increased stability of passivity. In accord with greater stability, average time for breakdown of passivity increased exponentially with Cr content.

The austenitic Cr-Ni-Fe stainless steels are passive alloys of which the 18% Cr, 8% Ni, balance Fe alloy (18-8) is an important example. These alloys, including the ferritic and martensitic Cr-Fe stainless steels, must contain a minimum of 12% Cr in order to exhibit optimum passivity or corrosion resistance. This critical concentration of Cr has been related to the tendency of an "unfilled" *d* band (or uncoupled *d* orbitals) of Cr to fill (or become coupled) with electrons donated by Fe, a process which is assumed to be just complete at 12%. Larger amounts of alloyed Cr correspond to residual uncoupled electrons or vacancies in surface atoms of Cr accounting for an alloy best able to chemisorb its environment, e.g., $O_2 + H_2O$, and become passive in a manner similar to pure chromium. Below 12% Cr, the *d* orbitals of Cr are coupled and the alloy has chemical properties more nearly resembling Fe, i.e., it is not passive. Similar electron interaction occurs in other binary transition metal alloys, a summary of known relations having been presented recently by one of us (1).

Electron interaction in relation to passivity has also been described for the ternary Mo-Ni-Fe and quaternary Cr-Fe-Ni-Mo passive alloys (2). It was in the interest of exploring this matter further using relatively pure ternary alloys instead of commercial compositions that this investigation was initiated. The Cr-Fe-Ni system is ideally suited to such a study because the phase diagram shows (3) that the alloys at low temperatures (650°C), are solid solution, face-centered cubic, over a wide range of composition. Metallographic examination of several alloys prepared for the present investigation confirmed that they were single-phase.

Measurement of Passivity

Passive behavior of the alloys was evaluated by measuring critical anodic current densities to produce passivity. Data of this kind provide a better criterion of the relation between alloy composition and passivity than do corrosion rates, as was discussed previously by Bond and Uhlig (4). A discontinuity in slope of critical current density plotted with composition, or minima in values of current density are observed at a relatively specific alloy composition. This critical composition has been found to be insensitive to pH or temperature of environment in the case of the Cr-Fe alloys (5), or to pH in the case of the Cr-Ni alloys (4), whereas similar alloy compositions corresponding to discontinuities in slope or to minima in corrosion rates tend to shift with environment. The discontinuity in slope of critical current densities for the Cr-Fe alloys, for example, comes at 10-12% Cr. This is also the critical composition derived from corrosion rate measurements of these alloys in water or in the atmosphere, but in acids or alkalis, passivity occurs at lower or higher Cr percentages.

The electrochemical mechanism of passivation (6-8) makes it clear why this is so. It has been shown, for example, that stainless steels achieve passivity whenever the anodic current density accompanying corrosion reaches or exceeds the critical current density. The same relation is expected to hold for other passive alloys. But the cathodic

reaction rate varies with environment and shifts the corrosion rate accordingly, thereby inducing passivity at higher or lower alloy compositions depending on the actual rate and the value of the critical current density in a particular environment. The influence of the cathodic reaction is eliminated by relying instead on critical current densities as a measure of the ease or difficulty with which an alloy becomes passive. In addition, constant renewal of the alloy surface by anodic dissolution during measurements avoids compositional changes caused for example by redeposition of ions in solution.

The important consideration from the present standpoint is that discontinuities in the critical current density for passivity are observed as a function of Cr content in the Cr-Ni-Fe alloy system as for the Cr-Fe system. These discontinuities can be interpreted in terms of electronic interaction between components of the alloy, similar to interactions hypothesized previously for the binary Cr-Fe, Cr-Ni, and other alloy systems (1).

Preparation of Alloys, Experimental Procedure

Alloys were prepared from electrolytic Fe and Cr, and from carbonyl Ni, melted in vacuum (10^{-4} mm Hg) by induction in high-purity alumina crucibles. No deoxidizers were added. Casting was carried out in a helium atmosphere by drawing the melts into 7 mm Vycor tubes and quenching in water. The helium was purified by passage over titanium sponge at 800°C, then through a liquid N_2 cold trap. In general, a single series of alloys was prepared by withdrawing a portion of the initial composition melt and quenching, then adding additional calculated amounts of Ni and Fe for the next composition, melting, withdrawing a portion, etc. This procedure was repeated several times. Ingots were homogenized in silica tubes in a helium atmosphere at 1050°C for 20 to 50 hr. Chips were then machined for chemical analysis of Ni and Cr and the remaining alloy was lightly cold-swaged to approximately 5 mm diameter rods. The swaged rods were annealed at 1050°C for 30 min and air-cooled. Representative analyses of 16 alloys showed a carbon content of 0.01-0.02%, and 5 representative samples showed a nitrogen content of 0.007-0.008%.

Electrodes measuring 1 to 2 cm long by 3.4 mm diameter were machined from the annealed rods with a small diameter stem at one end to which a nickel wire was silver-soldered. The wire was enclosed by a Pyrex tube, with a Teflon gasket insuring that only the alloy specimen came into contact with the electrolyte. The surfaces were abraded, using successively finer emery paper to 3/0 grit. After degreasing with benzene, the electrode was inserted into the cell, the latter being arranged so that pickling and washing, and final introduction of electrolyte could be carried out without exposing the electrode surface to air. The pickle was either dilute HNO_3 in the case of low Cr alloys, or dilute H_2SO_4 in the case of high Cr alloys. Deaerated electrolyte and deaerated distilled water for washing were contained in 5-gal carboys connected to the cell by glass tubing. Deaeration was accomplished by bubbling through nitrogen, first purified by passing over copper turnings at 450°C. After pickling of the electrode, the cell was filled and emptied 3 times with water and twice with electrolyte. The electrode was finally pickled anodically for 10 min with electrolyte in the cell using about 1/20th to 1/10th the current density required for passivation. Measurement of critical current density followed immediately.

The cell was all-glass with sealed-in glass electrical connections, separated into two halves by a ground glass joint. It contained two Pt cathodes spaced equally on either side of the test electrode to insure uniform current density. The test electrode fitted into the cell by means of a ground-glass joint. The reference cell was Ag-AgCl in 0.1*N* KCl, connected to a salt bridge filled with H_2SO_4, the tip of which (asbestos fiber sealed in glass) was located near the electrode surface.

The electrolyte for all measurements was deaerated 1.28*N* H_2SO_4, whose pH was about 0.4. Measurements were carried out in a constant temperature room maintained at 25° ± 0.5°C.

Critical current densities were determined by measuring times to reach a steady passive potential for a series of current densities, each above the critical value. The reciprocal of these times $1/t$ were then plotted with current densities i in accord with the relation:

$$i - i\ (\text{Crit.}) = K/t$$

where K is a constant equal to the coulombs required for passivation and i (Crit.) is the critical current density for passivity below which passivity is not achieved no matter how long the time. Applied current was obtained from 30 dry cells operating through a high resistance so as to maintain a constant value. The current densities chosen were within a factor of 2 or 3 times the critical current density, over which range the above equation is known to hold.

Potentials were also measured in 1.28*N* H_2SO_4 at which passivity decays spontaneously to an active potential on shutting off the anodic current. These are called "activation" or Flade potentials. A typical decay curve for the 4.8% Cr, 20% Ni, balance Fe alloy, as recorded by a high-input-resistance recorder, is shown in Fig. 1. In general, decay curves were obtained by first polarizing the electrodes to the passive region and holding for ½ to 1 min in order to allow the passive film to form. If insufficient time was allowed, no Flade potential was observed. Based on many measurements, it was found that the Flade potential was independent of time held at the passive potential; however, time to reach the Flade potential after shutting off the current increased the longer the electrode was maintained in the passive state. Flade (9) also observed much earlier that, when iron was held in the passive state for a long period, the time observed for decay tended to be longer.

Results

Critical current densities for 15 alloys all containing 20% Ni (average = 20.1% with a maximum

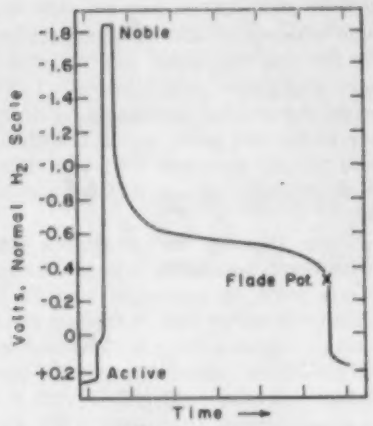

Fig. 1. Recorded potential decay of passivated 4.8% Cr, 20% Ni, balance Fe alloy in deaerated 1.28N H_2SO_4, 25°C.

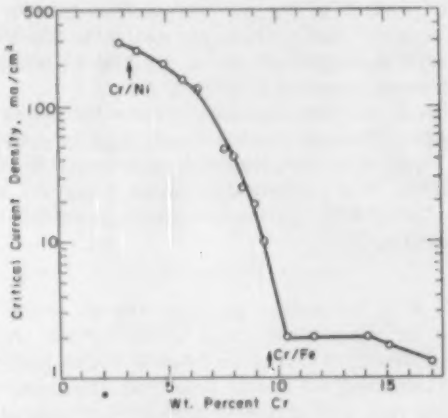

Fig. 2. Critical current densities for passivity of 20% Ni alloys in 1.28N deaerated H_2SO_4, 25°C.

deviation of 0.6%) and variable Cr and Fe are shown in Fig. 2. It is noted that alloys within the low Cr range require current densities in the order of 100-300 ma/cm² for passivation, whereas for alloys of greater than 10.5% Cr, current densities only about 1/100th as large are required. Optimum conditions for passivity can be said to initiate, therefore, at a minimum of 10.5% Cr. Although the corrosion rate corresponding to a critical current density of 2 ma/cm² is approximately 5,000 mdd, which is a high rate, in more dilute acids, of course, the critical current density and corresponding corrosion rate would be much lower. It should also be noted that the current density required to maintain passivity, corresponding to the steady-state corrosion rate of passive alloys, is much less than the critical current density. The important consideration is that as Cr content increases, the critical current density falls markedly and, at 10.5% Cr, achieves relatively low values which remain low for higher Cr compositions. This is typical of the behavior of Cr-Fe and other alloys as they progress from the active to the passive range of composition. The value 10.5% Cr, therefore, is a unique or critical composition.

Similar data for 40% (av. = 40.1%, max. deviation of 0.5%), 50% (av. = 50.0%, max. deviation of 0.6%) and 60% (av. = 60.0%, max. deviation of 0.7%) Ni alloys are shown in Fig. 3, 4 and 5. Major changes in slope occur as for 20% Ni alloys, but with some additional smaller changes in slope also apparent. A possible cause for these smaller changes will be discussed later.

Flade potentials for 20 and 60% Ni alloys are summarized in Fig. 6, each point representing an average of several determinations. Values for 40 and 50% Ni show a similar scatter, with all values for low Cr alloys starting at about −0.45 v to the normal H_2 electrode and ending at about 0 to −0.15 v for 15-20% Cr alloys. The value for the Flade potential E_F of Fe in H_2SO_4 of pH 0.4, as calculated from the relation (5) $E_F = -0.63 + 0.059$ pH, is

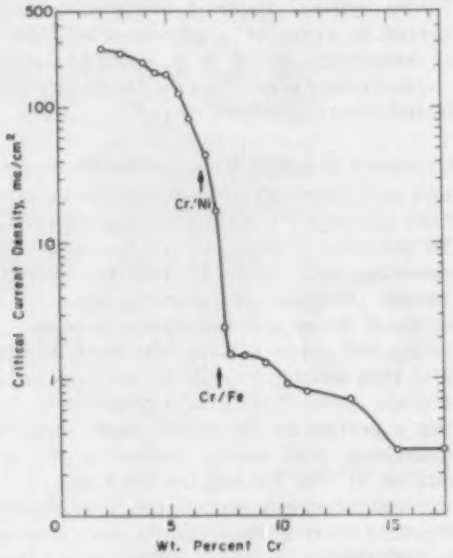

Fig. 3. Critical current densities for passivity of 40% Ni alloys in 1.28N deaerated H_2SO_4, 25°C.

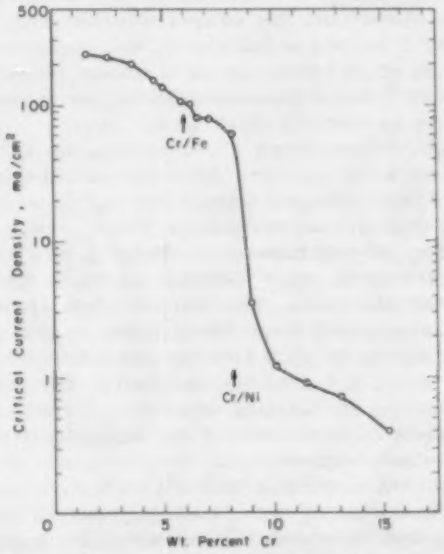

Fig. 4. Critical current densities for passivity of 50% Ni alloys in 1.28N deaerated H_2SO_4, 25°C.

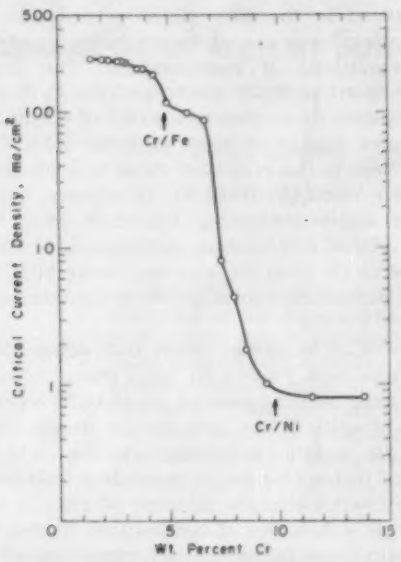

Fig. 5. Critical current densities for passivity of 60% Ni alloys in 1.28N deaerated H_2SO_4, 25°C.

equal to −0.61 v. The less noble values for the alloys indicate that their passivity is more stable than that of iron. The standard Flade potential ($pH = 0$) for Cr, by way of example, is +0.2 v. Some potentials of Fig. 6 fall off the best curve through all the points. It may not be coincidence that these marked deviations occur mostly at alloy compositions corresponding to discontinuities in slope of critical current density as observed in Fig. 2 and 5. The extent to which the two sets of data can be correlated is not entirely clear, however, and any attempt in this direction would probably require additional measurements on alloys of composition falling in between present compositions.

The over-all shape of the Flade potential curves in Fig. 6, allowing for deviations mentioned above, are similar to those reported for the Cr-Fe alloys in H_2SO_4 by Rocha and Lennartz (10). There is a

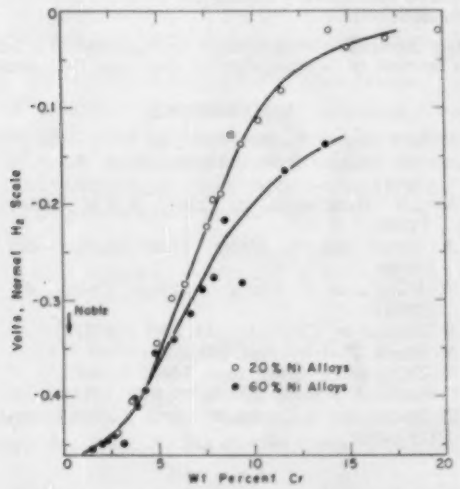

Fig. 6. Activation or Flade potentials of Cr-Ni-Fe alloys in 1.28N deaerated H_2SO_4, 25°C.

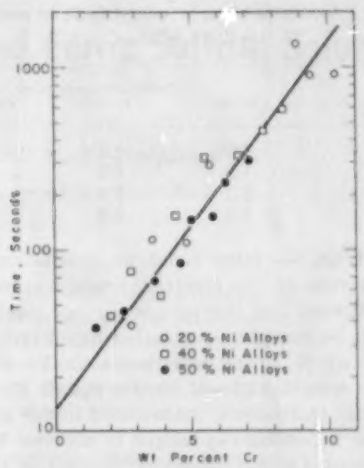

Fig. 7. Relation of Cr content of Cr-Fe-Ni alloys to time for breakdown of passivity in 1.28N deaerated H_2SO_4, 25°C.

bending of the curve both at low and high Cr compositions with relatively steep rise in the region of the critical Cr composition.

Time t_s in seconds required for passivity to break down increases with Cr content, as Fig. 7 shows, in accord with the approximate relation $\log t_s = 0.2$ (% Cr) + 1.15. The recorded data are for the 20, 40, and 50% Ni alloy series where the time held at the passive potential in each instance was 15-20 sec. Values for the 60% Ni series also fall on the best straight line through all the points but with greater scatter in the 1 to 3% Cr range. It is concluded that without any Cr, the median life of the passive film in 1.28*N* H_2SO_4 is about 14 sec, which is consistent with the observed behavior of passive iron, including probably also the Fe-Ni alloys. The prolonged life of the passive film as Cr content increases is consistent with the more active values of the Flade potential for higher Cr alloys, which, as mentioned before, parallel increased stability of passivity.

Discussion

Major changes in the slope of critical current densities plotted with respect to per cent Cr presumably can be interpreted in terms of a more protective oxide film initiating at the critical Cr compositions, or alternatively in terms of a stronger bond between discharged OH^- (or O_2) and the base metal, leading in either case to a passive film. A stronger bond between adsorbate and adsorbent would be expected to occur for compositions in which the *d* orbitals of Cr are uncoupled. Under such conditions, corresponding to Cr compositions above the critical value, the observed critical current density is low and tends to change only slightly with increasing % Cr, as shown in Fig. 2 through 5. For compositions corresponding to coupled *d* orbitals of Cr, critical current densities are much higher and the change with alloy composition is greater.

Although a passive film hypothesized to consist of metal oxide may meet the immediate *qualitative* requirements for an explanation of critical Cr compositions in the stainless steels, no quantitative evaluation has been offered by proponents of this

Table I. Calculated values for critical % Cr for passivity in Cr-Ni-Fe alloys

% Ni	Donor electrons from Fe only	Ni only	Fe and Ni
20	9.6%	3.3%	12.5
40	7.2	6.5	12.9
50	6.0	8.2	13.2
60	4.8	9.8	13.4

viewpoint. On the other hand, an evaluation is possible in terms of the electron configuration theory which proposes that the vacant surface d orbitals of Cr should be completely coupled by electrons from Fe at 12 wt % Cr or less in the Cr-Fe alloys, or when the weight ratio of Cr/Fe equals 12/88. Assuming that this ratio is maintained in the Cr-Ni-Fe alloys, the following expression is derived for critical per cent Cr for passivity assuming electrons donated only by Fe: Crit. % Cr = 12/88 (100 − Crit. % Cr − % Ni) or Crit. % Cr = 0.120 (100 − % Ni).

On the other hand, if the surface d orbitals of Cr are coupled by electrons donated from Ni only, the corresponding value is: Crit. % Cr = 14/86 (% Ni), where 14/86 is the empirical ratio for passivity observed for the Cr-Ni alloys based on observed critical current densities (4). A third case can be considered for which electrons are donated both from Fe and Ni. Using the same empirical ratios for Cr/Fe and Cr/Ni, this leads to: Crit. % Cr = 14/86 (% Ni) + 12/88 (100 − Crit. % Cr − % Ni) = 0.023 (% Ni) + 12.0.

The calculated values for critical Cr compositions are summarized in Table I, and are also indicated for the first 2 cases cited above on Fig. 2 through 5.

For 20% Ni alloys, it is seen in Fig. 2 that the major predicted change of slope at 9.6% Cr for the case of donor electrons from iron comes close to the observed change in slope at about 10.5% Cr. There is no observed change in slope at 3.3% Cr for the case of donor electrons from Ni. For 40% Ni, the predicted change of slope at 7.2% Cr for donor electrons from Fe again comes close to the observed value at 7.6% Cr. Because of the rapidly changing slope in this region, it is not possible to observe whether a change in slope also results from donor electrons from Ni predicted to occur at 6.5% Cr. Furthermore, it is not certain that the slight discontinuity in slope observed at 5% Cr is real.

For 50% Ni alloys, the observed change in slope at about 10% Ni lies to the right of the predicted values based on donor electrons from either Fe or Ni. The observed value, however, comes closer to the predicted value based on donor electrons from Ni equal to 8.2% Cr than it does to the value based on electrons from Fe. In this connection, some significance may attach to the fact that alloys at 50% Ni contain more Ni than Fe. It should be noted in Fig. 4 that a slight change in slope also occurs close to the value of 6% Cr predicted for donor electrons from Fe. This slight change of slope becomes more pronounced in the 60% Ni alloy series in Fig. 5 where the change can no longer be ascribed to possible variations of measurement. The predicted change based on donor electrons from Fe is at 4.8% Cr compared to an observed value of 4.5 to 5% Cr. The major change of slope at about 9.5% Cr now comes close to the predicted value of 9.8% Cr based on donor electrons from Ni. It appears, therefore, that in alloys containing less than 50% Ni, the major critical composition corresponds to electrons donated to Cr from Fe, whereas above 50% Ni, the critical composition corresponds to electrons donated by Ni.

There is no strong evidence that donor electrons come from both Fe and Ni, even though this might be expected on fundamental grounds. The predicted values of critical per cent Cr for donor electrons from both metals lie definitely to the right of the observed major changes in slope. It should be noted that any small changes in slope of critical current density as a function of composition in this higher chromium range fall within the experimental errors of measurement since the maximum change on the logarithmic scale as plotted amounts to only a few ma/cm^2. The same situation does not apply to changes of slope in the lower chromium composition range where deviations from a smooth curve through the observed points amount to tens or hundreds of ma/cm^2.

The primary features of the critical current density curves are described reasonably well, therefore, by the separate electron interaction between Cr and Fe distinct from interaction between Cr and Ni. Furthermore, the critical compositions in the ternary system approximate in each case the critical composition typical of the corresponding binary system. Further experiments are needed to establish whether similar relations can be expected in other passive alloy systems.

Acknowledgment

The authors are grateful for support of this research by the Shell Oil Company Foundation Inc.

Manuscript received April 13, 1960. This paper was prepared for delivery before the Houston Meeting, Oct. 9-13, 1960.

Any discussion of this paper will appear in a Discussion Section to be published in the June 1961 JOURNAL.

REFERENCES

1. H. H. Uhlig, *Z. Elektrochem.*, **62**, 700 (1958).
2. H. H. Uhlig, *Trans. Electrochem. Soc.*, **85**, 207 (1944).
3. Metals Handbook, p. 1261, A.S.M., Cleveland (1948).
4. A. Bond and H. Uhlig, *This Journal*, **107**, 488 (1960).
5. P. King and H. Uhlig, *J. Phys. Chem.*, **63**, 2026 (1959).
6. N. Tomashov, *Corrosion*, **14**, 229t (1958).
7. M. Stern, *This Journal*, **105**, 638 (1958).
8. H. Uhlig and P. King, *ibid.*, **106**, 1 (1959).
9. F. Flade, *Z. physik. Chem.*, **76**, 513 (1911).
10. H. Rocha and G. Lennartz, *Arch. Eisenhüttenw.*, **26**, 117 (1955).

Dissolution of Iron in Sulfuric Acid and Ferric Sulfate Solutions

A. C. Makrides[1a]

Metals Research Laboratories, Union Carbide Metals Company, Division of Union Carbide Corporation, Niagara Falls, New York

ABSTRACT

Dissolution of iron in sulfuric acid solutions containing ferric sulfate is described by the superposition (without distortion) of the partial processes of hydrogen evolution, reduction of ferric ion, and anodic dissolution of iron. Reduction of ferric ion occurs at a diffusion-limited rate. Derived relations between electrode potential and the concentration of ferric sulfate, the linear flow velocity, and time are verified. A comparison of potential-current density curves obtained by polarization and from addition of ferric sulfate suggests that adsorption of ferric ion, if any, has no appreciable effect on iron dissolution

Corrosion or dissolution of metals in environments found in practice often involves a reaction proceeding at a rate limited by diffusion. For example, the corrosion rate of iron in nearly neutral aerated salt solutions is determined, to a large extent, by the rate of diffusion of oxygen to the iron-solution interface. Similarly, dissolution of nickel in acid solution is accelerated by oxygen which apparently is reduced as fast as it diffuses to the interface. A study of such systems is of interest therefore not only in general electrochemical theory but also in developing methods for minimizing corrosion in industrial processes.

It is essential in a study of a heterogeneous reaction proceeding at a diffusion-limited rate to control mass transport to the interface precisely and reproducibly. The rotating cylinder electrode (1-3) meets these requirements and possesses the advantage of a uniform mass transport rate over the whole of its lateral surface. An application of the rotating electrode to dissolution of iron in ferric sulfate solutions is presented here. The results are discussed on the basis of the Wagner-Traud postulate of superposition of partial processes together with elementary hydrodynamic considerations.

Electrochemistry of Iron Dissolution

Iron dissolves in aqueous acid solutions through an electrochemical mechanism (4-6). In moderately concentrated acid solutions and in the absence of reducible substances other than hydrogen ions, the partial processes are described by

$$\eta_c = -b_c \log \frac{i_c}{i_{oc}} \quad \text{for } 2H^+ + 2e^- \rightarrow H_2 \qquad [1]$$

and

$$\eta_a = b_a \log \frac{i_a}{i_{oa}} \quad \text{for } Fe \rightarrow Fe^{++} + 2e^- \qquad [2]$$

where the η's are overpotentials associated with current densities i_a and i_c and the i_o's are exchange current densities. At the steady state,

$$i_a = i_c = i_{corr} \qquad [3]$$

at a common electrode potential. The corresponding overpotentials are

$$\eta_c = E_{corr} - E_c^{rev} \qquad [4]$$

$$\eta_a = E_{corr} - E_a^{rev} \qquad [5]$$

where E_{corr} is the corrosion or dissolution potential and E^{rev} the reversible potential for each partial process.

If another reducible substance is introduced in the solution, the partial cathodic current is the sum

$$i_c = i_H + i_r \qquad [6]$$

where i_H is the partial current of hydrogen evolution and i_r the reduction current of the added oxidant. Only the case where i_r is equal to the limiting diffusion current, i_d, is considered here.

Equation [6] expresses the basic assumption of this development, viz., that the partial processes taking place during dissolution can be superimposed without interference. The only restriction imposed is that at the common electrode potential the sum of all cathodic processes equals the sum of all anodic processes. An electrochemical description of dissolution based on this assumption was given first by Masing (7) and in detail by Wagner and Traud (8).

Dependence of the dissolution potential on i_d.—The diffusion current depends on the concentration of oxidant and its diffusion coefficient, and on the flow rate. It is similar to an anodic current applied externally since it is independent of the electrode potential. This analogy is developed below.

If $i_d >> i_H$, then

$$i_c \cong i_d \qquad [7]$$

and the corrosion current for an electrode dissolving under these conditions is given by the diffusion current, while the potential is determined by the anodic polarization curve (Eq. [2]). Formally,

$$i_d = i_{corr} = i_a$$

and

$$\eta_a = E - E_a^{rev} = b_a \log \frac{i_d}{i_{oa}}$$

[1a] Present address: Research Department, Socony Mobil Oil Company, Inc., Dallas, Texas.

or

$$E = b_a \log \frac{i_d}{i_{ox}} + E_a^{rev} \qquad [8]$$

Therefore, it is possible to obtain the anodic polarization curve for the electrode by determining E as a function of i_d.

If $i_c \sim i_H$, both hydrogen discharge and oxidant reduction must be considered. Proceeding similarly to the above

$$E = b_a \log \frac{(i_d + i_H)}{i_{ox}} + E_a^{rev} \qquad [9]$$

with i_H a function of potential. Equation [9] reduces to [8] at sufficiently positive potentials where i_H becomes negligible.

Dependence of potential on concentration.—If the dependence of i_d on the concentration of oxidant, C_{ox} (moles cc^{-1}), is known, we can immediately write down E as a function of C_{ox}. Since under most conditions $i_d >> i_H$, Eq. [8] rather than [9] is used in what follows.

The diffusion-limited current is

$$i_d = nF \frac{dj}{dt} = nFkC_{ox} \qquad [10]$$

Here, j is the number of moles of oxidant transported across a unit area of metal-solution interface, t the time in seconds, n the number of equivalents per mole of oxidant, $\mathbf{F}$ Faraday's constant, and k the rate constant in cm/sec. For turbulent flow, and in excess of an indifferent electrolyte (constant ionic strength), k may be assumed independent of C_{ox} (9). From Eq. [8] and [10]

$$E = b_a \log C_{ox} + b_a \log \frac{nFk}{i_{ox}} + E_a^{rev} \qquad [11]$$

Therefore, at constant k and i_{ox}, the potential is a linear function of the logarithm of the concentration of depolarizer with a slope equal to the Tafel slope of the anodic polarization curve.

Time dependence of the dissolution potential.—The change of E with time can be calculated from Eq. [8] and [10]. The potential of an electrode immersed in a solution originally C_{ox} in oxidant moves in a cathodic (active) direction as oxidant is depleted by reaction. The rate at which oxidant is used is given by Eq. [10]. From Eq. [8]

$$\frac{dE}{dt} = \frac{b_a}{2.30(i_d)} \frac{d(i_d)}{dt}$$

with i_{ox} independent of time. Noting that

$$dj = -\frac{V_s d(C_{ox})}{A}$$

where V_s is the solution volume and A the surface area of the electrode, we have from Eq. [10] for constant k (fixed flow),

$$\frac{d(i_d)}{dt} = nFk \frac{d(C_{ox})}{dt} = -nFk^2 \frac{A}{V_s} C_{ox}$$

Substituting above and using Eq. [10]

$$\frac{dE}{dt} = \frac{-A}{2.30V_s} k\, b_a \qquad [12]$$

The potential is therefore a linear function of time with a slope given by Eq. [12]. If dE/dt and b_a are known, k can be obtained from Eq. [12].

Dependence of potential on hydrodynamic flow conditions.—Equations [8] and [10] yield a relation between E and k from which we may derive the dependence of the potential on various hydrodynamic parameters. Some useful relations are given below.

The rate constant of a diffusion-controlled reaction occurring at a cylindrical electrode in turbulent flow is

$$k = \frac{D}{\delta} = (C_1)\, V\, (R_d)^{-\beta}\, (Pr)^{-\gamma} \qquad [13]$$

where D (cm^2/sec) is the diffusion coefficient of the oxidant, δ (cm) the effective thickness of the boundary layer, and V (cm/sec) the linear velocity. R_d is Reynolds number, d_1V/ν with d_1 (cm) the diameter of the electrode and ν (cm^2/sec) the kinematic viscosity, and Pr is Prandtl's number, ν/D. Equation [13] is based on an extended Reynolds momentum-mass transfer analogy (the Chilton-Colburn analogy) and is in good agreement with experiments [2] with $C_1 = 0.079$, $\gamma = 0.644$, and $\beta = 0.2$ to 0.3. As noted previously (3), β depends on the range of Reynolds numbers and on the roughness of the electrode. For hydrodynamically rough surfaces β approaches zero, while for smooth electrodes $\beta \cong 0.3$ at small Reynolds number ($\sim 10^2$) and $\cong 0.2$ at large Reynolds numbers ($\sim 10^5$).

Two useful relations can be derived from Eq. [13]. At constant C_{ox}, from Eq. [8] and [10]

$$E = b_a \log k + b_a \log \frac{nF\, C_{ox}}{i_{ox}} + E_a^{rev}$$

And from Eq. [13]

$$E = b_a \log V^{(1-\beta)} + (\text{Constant}) \qquad [14]$$

Therefore, the potential varies linearly as the logarithm of the velocity at any constant C_{ox} with a slope of $b_a(1-\beta)$.

At constant potential, from Eq. [8],

$$i_a = i_d = \text{const}$$

And from Eq. [10] and [13]

$$(\text{Constant})_3 = nFk\, C_{ox} = nF\, (\text{Constant})_2\, V^{(1-\beta)}\, C_{ox}$$

Rearranging,

$$-\log C_{ox} = (1-\beta) \log V + (\text{Constant}) \qquad [15]$$

The value of β for a particular experimental arrangement can be obtained from a log-log plot of the oxidant concentration against the linear velocity at constant potential.

Relations [1], [2], [8], [10], [11], [12], [14], and [15] have been verified for iron electrodes in ferric sulfate solutions 0.5N in sulfuric acid.

Experimental

The experimental arrangement reported previously (3) was modified to reduce the concentration

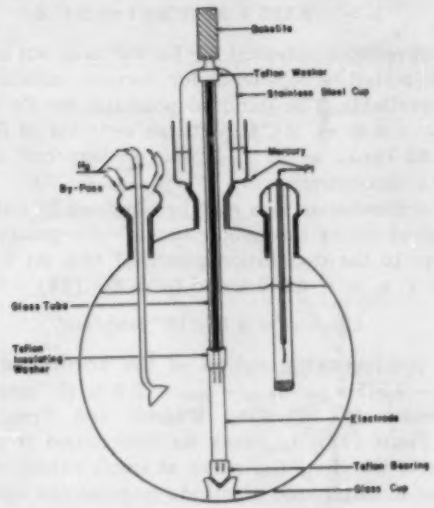

Fig. 1. Reaction cell

of oxygen in solution and to make it easier to vary the rotational speed.

The cell is shown in Fig. 1. The electrode, generally a cylinder 1 cm in diameter and about 4 cm long, was attached to a stainless steel shaft isolated from the solution with a glass tube. A Teflon washer gave a water-tight seal at the point of attachment of specimen to shaft and also isolated the top surface of the cylinder from solution. At the other end of the cylinder, a Teflon bearing riding in a glass cup fused to the cell minimized eccentric motion and at the same time isolated the lower surface of the cylinder from solution. Smaller electrodes, about 1 cm^2 in surface area, were used in polarization studies. In these cases, the Teflon washer at the top was extended to leave only about 0.3 cm of the electrode exposed to the solution.

The steel shaft ended in an inverted steel cup which rotated in mercury and sealed the system from the atmosphere. Electrical contact to the electrode was made through the mercury pool.

Hydrogen, purified over copper at 500°C and through sodium plumbate, concentrated sulfuric acid, triply distilled water, a drying tower, and a cold trap, was passed through the solution prior to a run and over the solution during a run.

Potentials were measured against S.C.E. and platinized platinum with a high impedance L&N pH meter connected to a multiple range, adjustable zero, Dynamaster Bristol recorder. Alternatively, a Rubicon potentiometer was used together with a galvanometer of 0.007 μa/mm sensitivity. A capillary probe with a bridge filled with solution of the same acid concentration was used in polarization measurements. The bridge led to an external S.C.E. A greaseless, closed, stopcock prevented mixing of (air-saturated) solution outside the cell with solution in the cell, but had sufficient conductivity when wetted with solution to maintain electrical contact. Constant current was obtained through appropriate resistances from two banks of three 45-v batteries arranged in series to give 135 v.

Greaseless ground glass joints were used to avoid possible contamination from lubricant. Although some air probably diffused into the cell, any contribution from dissolved oxygen to the cathodic current was negligible (see below).

Electrodes were rotated with a Bodine motor at speeds continuously variable up to 4000 rpm. The motor was electrically insulated from the electrode by a short Bakelite sleeve, friction-fitted on the upper part of the shaft (Fig. 1). Rotational velocities were measured to 0.2% with both a Jaquet tachometer (via an auxiliary shaft driven through an 18:1 reduction gear) and a stroboscope.

Through a ground glass joint (not shown in Fig. 1) small amounts of a concentrated solution of $Fe_2(SO_4)_3$ were added to the solution from a precision (±0.01 ml) buret equipped with a greaseless Teflon stopcock.

Analytical reagent-grade ferrous sulfate was recrystallized twice, washed with absolute alcohol and anhydrous spectroscopic-grade ether, and dried. Ferric sulfate was prepared from ferrous sulfate by oxidation with hot, concentrated sulfuric acid. Ferric sulfate solutions also were prepared from recrystallized C.P. ferric sulfate. Water was triply distilled, one distillation being carried out of dilute, alkaline potassium permanganate. The reaction vessel and all glass parts were cleaned with a saturated solution of potassium dichromate in concentrated sulfuric acid (cleaning solution) and rinsed with triply distilled water prior to use. Water drained uniformly and with zero contact angle from glass surfaces cleaned in this way.

Electrodes were prepared from Ferrovac E iron (99.92+ iron). They were abraded with 2/0 emery paper, washed with reagent-grade carbon tetrachloride, left to dry, etched in 1:3 HNO_3, washed with distilled water, etched in 1:3 H_2SO_4, and washed again.

Concentrations of various solutions were determined by analysis. The cell was thermostated at 30.0 ± 1°C.

Results and Discussion

Dissolution in Sulfuric Acid

In 0.52*N* H_2SO_4 the steady-state dissolution potential changed by less than 0.2 mv on varying the speed from zero to 4000 rpm (200 cm/sec). Concentration overpotentials therefore were negligible for both partial processes. Also it may be inferred that the partial current for reduction of any trace of oxygen present in solution was negligible in comparison with the corrosion current.[1]

Metal dissolution in acid alone is described by Eq. [1]-[5], i.e., by specifying the exchange current and Tafel slope for hydrogen evolution and for metal oxidation. These parameters were not always reproducible with iron. In general, electrodes belonged to one of two sets: (i) the steady-state corrosion potential was about −0.510 to −0.520 v vs.

[1] It was suggested (3) that an observed dependence of potential on rotational speed in solutions which were thought to be air-free was attributable to an electrokinetic effect. It is apparent that some dissolved oxygen must have been present in these solutions. As with other oxidants, the partial current for oxygen reduction increases and the dissolution potential becomes more positive when the flow velocity is increased.

S.C.E., the corrosion current about 400 μa/cm^2, b_a = 0.050 to 0.060 v, and b_c = 0.095 to 0.105 v; (ii) the corrosion potential was −0.495 to −0.505 v vs. S.C.E., the corrosion current about 2200 μa/cm^2, b_a = 0.030 to 0.040 v and b_c = 0.095 v. The hydrogen exchange current was considerably larger than in (i) (see below).

The time dependence of the corrosion potential differed for (i) and (ii). For set (i), E_{corr} increased from about −0.550 to −0.515 in about 3-4 hr and remained essentially constant at about this value. For set (ii), the drift continued, although at a smaller rate, for at least 24 hr. The corrosion current increased during this time to the value given above.

The cause of these differences is obscure. The rather wide variation in results obtained in electrochemical studies (4-6, 9-12) with iron and other metals of Group VIII, notably nickel, has been ascribed variously to impurities in solution, impurities in the metal, or to solution of hydrogen in the metal (10, 11). It is possible that some impurities, e.g., carbon and sulfur, have a pronounced effect on the kinetics of dissolution even if present in very small quantities. Since the system was designed primarily for the study of dissolution in solutions with oxidants, results for dissolution in acid alone are limited. The work reported for acid solutions is considered preliminary to a more extensive study with a more suitable experimental arrangement.

The variability of b_a made it necessary in most cases to obtain polarization curves prior to a run in order to compare anodic slopes observed directly and by addition of ferric sulfate. In other cases, the corrosion rate and corrosion potential were used to characterize the electrode.

Figure 2 gives anodic and cathodic polarization curves typical of electrodes belonging to set (i). The reversible H^+/H_2 potential was −0.275 v vs. S.C.E. Hydrogen overpotentials were

$$\eta_c = -(0.105) \log \frac{i_c}{2.2 \times 10^{-6}} \qquad [16]$$

with i_c in amp/cm^2. From $b_c = 2.30\ RT/\alpha_c F$, the transfer coefficient α_c is 0.57. For the anodic polarization curve

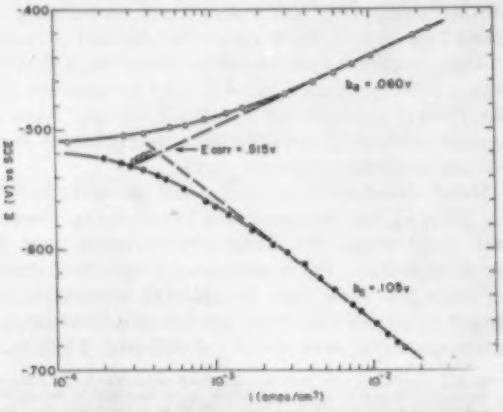

Fig. 2. Polarization diagram for iron in 0.52N H_2SO_4 at 30°C. The diagram is typical of set (i). The electrode was in solution for 10 hr E_{corr} = −0.515 v.

$$E = -0.320 + 0.060 \log i \text{ vs. S.C.E.} \qquad [17]$$

The reversible potential for Fe/Fe^{++} was not known, since activity coefficients for ferrous sulfate were not available. The standard potential for Fe/Fe^{++} is $E' = -0.68$ vs. S.C.E. With an estimate of $E_e^{rev} \cong -0.80$ ($a_{Fe^{++}} \cong 10^{-4}$), $i_{ex} \cong 10^{-6}$ amp/cm^2 at this $FeSO_4$ concentration.

The dissolution rate may be obtained by extrapolation of either the anodic or cathodic polarization curves to the dissolution potential (6). At E = −0.515 v, η_c = −0.240 v and from Eq. [16]

$$i_c = i_{corr} = 4.1 \times 10^{-4} \text{ amp/cm}^2$$

A similar extrapolation of the anodic curve to E = −0.515 v yields $i_a = i_{corr} = 5.6 \times 10^{-4}$ amp/cm^2. Alternatively, following Wagner and Traud (8) and Stern (12), i_{corr} may be determined from the slope of the E vs. i_{appl} curve at small values of i_{appl}. If, for example, the electrode is polarized cathodically

$$i_{appl} = i_c - i_a \qquad [18]$$

For convenience, the steady-state dissolution potential (instead of the reversible potential) may be taken as the reference potential so that

$$\begin{aligned} i_c &= i_{corr} \exp(-2.30\,\epsilon/b_c) \\ i_a &= i_{corr} \exp(+2.30\,\epsilon/b_a) \end{aligned} \qquad [19]$$

where $\epsilon = E - E_{corr}$. Substituting [19] in [18]

$$i_{appl} = i_{corr}\left[\exp\left(\frac{-2.30\epsilon}{b_c}\right) - \exp\left(\frac{2.30\epsilon}{b_a}\right)\right] \qquad [20]$$

Expanding around $\epsilon = 0$, neglecting higher terms for small ϵ, and rearranging we obtain the equation given by Stern (12)

$$i_{corr} = \frac{b_a b_c}{2.30\,(b_a + b_c)\,(\epsilon/i_{appl})} \qquad [21]$$

Figure 3 shows a plot of ϵ vs. i_{appl} at small ϵ, from which $i_{corr} = 4.1 \times 10^{-4}$ amp/cm^2.

Figure 4 gives results typical of electrodes belonging to set (ii). The curves drawn through the open triangles were obtained 4 hr after immersion of the electrode in the solution, while the curves through the full triangles were obtained 24 hr after

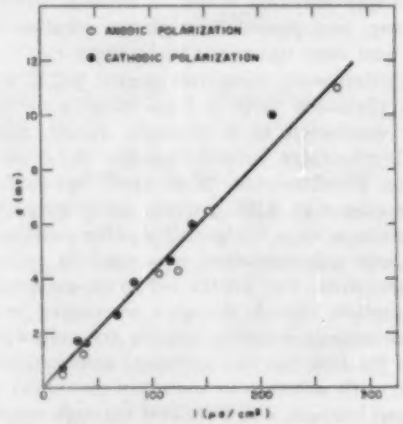

Fig. 3. Polarization data at small applied current densities in 0.52N H_2SO_4 at 30°C.

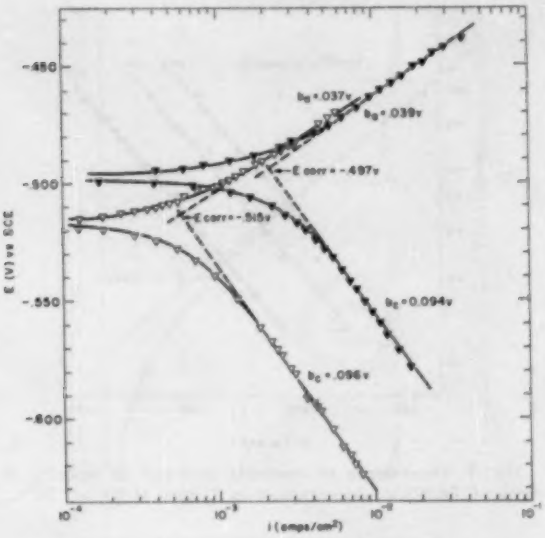

Fig. 4. Polarization diagram for iron in 0.52N H_2SO_4 at 30°C. The diagram is typical of set (ii). Curves through open points were obtained 4 hr after the electrode was in solution, and those through the full points after 20 hr in solution.

immersion. Hydrogen overpotentials for the two cases are

$$\eta_c = -0.096 \log \frac{i}{2 \times 10^{-6}}$$

and

$$\eta_a = -0.094 \log \frac{i}{1 \times 10^{-5}}$$

The anodic polarization curve was essentially unaltered during this time. The two sets of results are described by

$$E = -0.385 + 0.038 \log i \text{ vs. S.C.E.}$$

which yields on assumptions similar to those made above, $i_{co} \cong 10^{-11}$ amp/cm². Therefore, the shift of the corrosion potential to more noble values and the increased corrosion rate result essentially from the increase of the hydrogen exchange current.

Dissolution in Ferric Sulfate Solutions

The behavior of iron electrodes in ferric sulfate solutions paralleled that on anodic polarization. Data with electrodes belonging to set (i) are presented in Fig. 5 which shows the dependence of potential on the concentration of ferric sulfate over the range of velocities 50 to 200 cm/sec. The potential is a linear function of the logarithm of ferric ion concentration at potentials sufficiently removed from the corrosion potential. According to Eq. [11], the slope of the linear sections of these plots should be equal to b_a. Values of b_a determined in this way range from 0.057 to 0.066 v while 0.060 v was measured directly (see Fig. 2).

Rate constants at various velocities are required for comparison of results from anodic polarization and from addition of ferric sulfate. Rate constants were determined by withdrawing 5 ml portions of the solutions at various times and analyzing for iron. Equation [10] was used in the integrated form

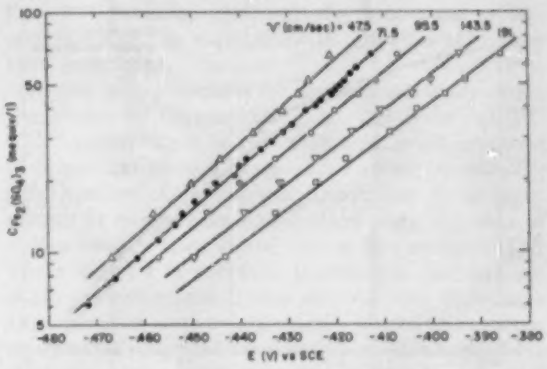

Fig. 5. Electrode potential as a function of ferric sulfate concentration at various linear velocities. The slopes are, from left to right, 0.057, 0.058, 0.062, 0.066, and 0.066 v.

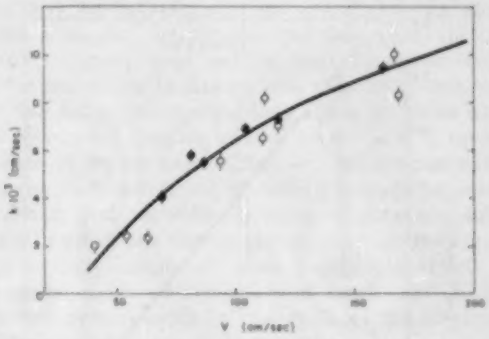

Fig. 6. First order rate constants as a function of velocity in 0.52N H_2SO_4 at 30°C. Values shown by open circles were calculated from the change (determined by analysis) of ferric ion concentration with time using Eq. [22]; solid circles were obtained from the time dependence of the dissolution potential and from the anodic Tafel slope (b_a = 0.060 v) using Eq. [12].

$$k = \frac{2.30\, V_s}{A\, t} \log (C^\circ/C) \qquad [22]$$

Results are shown in Fig. 6. Rate constants cannot be computed from Eq. [13] since the diffusion constant of ferric ion in 0.5*N* H_2SO_4 solution is not known. From experimental values of k, with β = 0.20 (see below), and $\nu = 0.87 \times 10^{-2}$ cm²/sec, we find from Eq. [13] $D \cong 3 \times 10^{-6}$ cm²/sec. The estimated equivalent thickness of the boundary layer is then $\delta = D/k \cong 0.5 \times 10^{-4}$ cm at V = 100 cm/sec.

Potential-current density curves obtained by anodic polarization and from addition of ferric sulfate are compared in Fig. 7. Points obtained by the two methods differ by less than 10 mv at any current density.

Dependence of Dissolution Rate and Potential on Flow Velocity

According to [15], a plot of log C vs. log V at constant potential is linear with a slope of $(1-\beta)$. Data from Fig. 7 are plotted in Fig. 8 at E = const = − 0.420 v vs. S.C.E. Over the limited range of velocities used (50-200 cm/sec), $(1-\beta)$ = 0.80 or β = 0.20. Using this value for β, it is expected from Eq. [14] that a plot of log V vs. E at constant C is linear with a slope of 0.80 b_a. Figure 9 gives such

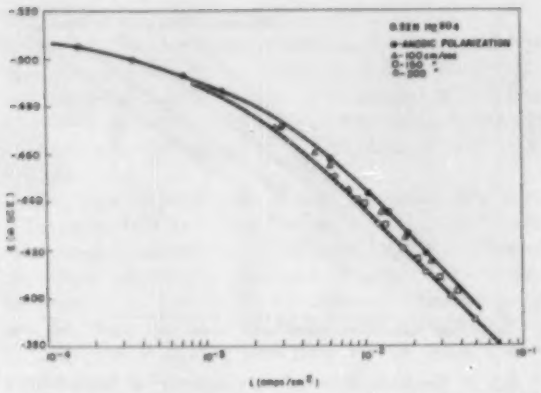

Fig. 7. Comparison of anodic curves obtained directly and by addition of $Fe_2(SO_4)_3$ for electrodes of set (i).

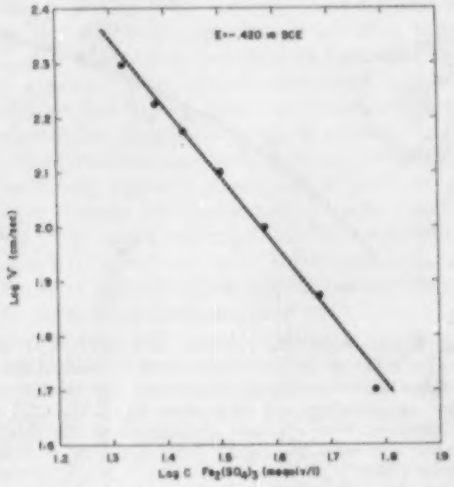

Fig. 8. Plot from data given in Fig. 5 at constant potential

plots for an electrode having a mean value of $b_a = 0.060$ v ($E_{corr} = -0.521$) at 34.6, 46.1, and 67.5 mequiv/l of $Fe_2(SO_4)_3$. The observed mean slope of 0.044 is in good agreement with a calculated value of 0.048 v.

Time Variation of Potential

The change of potential with time at various flow velocities is given in Fig. 10. From the slope, dE/dt, and with $b_a = 0.060$ v, rate constants were obtained from Eq. [12]. These are shown as solid circles in Fig. 6. The good agreement with k's found by analysis confirms the validity of Eq. [12].

Electrodes of set (ii).—Figure 11 shows the dependence of potential on ferric ion concentration for electrodes belonging to set (ii). The slope of the linear section of the curve is 0.040 v. Results were similar to those described above. The smaller Tafel slope of the anodic curve led however to relatively smaller changes of potential.

General Discussion

Although the anodic reaction for dissolution of iron in sulfuric acid solution followed a Tafel relation, both the slope and the exchange current varied

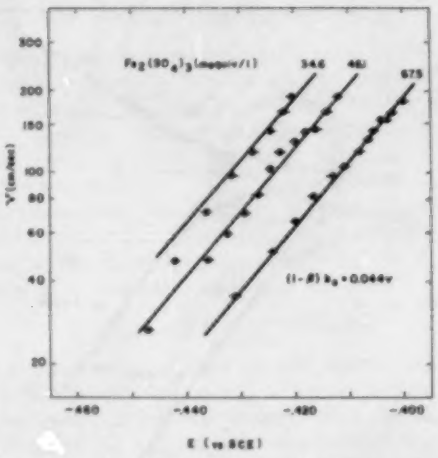

Fig. 9. Dependence of electrode potential on velocity at constant $Fe_2(SO_4)_3$ concentration in 0.52N H_2SO_4 at 30°C.

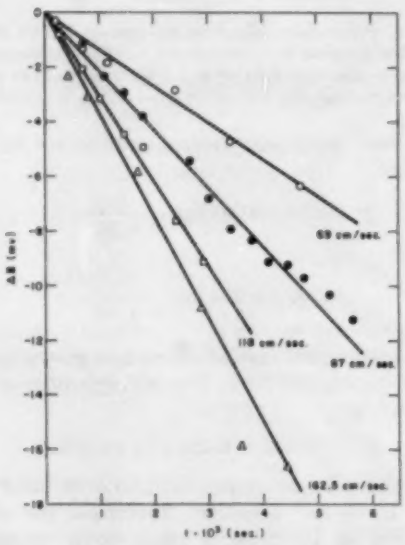

Fig. 10. Change of potential with time at various flow velocities.

within rather wide limits. As noted above, Tafel slopes were generally either about 0.035 or 0.060 v; exchange currents were smaller by 10^3 for electrodes having the former slope.

Reported Tafel slopes for the Fe/Fe^{++} couple also vary widely. Roitar, Jura, and Polujan (13) found for "electrolytic iron" in 1.25M $FeSO_4$, $b_a = 0.060$ or 0.075 v, depending on the history of the electrode, with $i_o \cong 3 \times 10^{-6}$ amp/cm². Stern and Roth (14) reported $b_a = 0.068$ v in 4% NaCl at pH of 1.5. Okamoto, Nagayama, and Sato (11) found $b_a = 0.10$ with Armco iron in 0.3N H_2SO_4. Hoar and Hurlen (15) determined $b_a = 0.030$ and $i_o \cong 3 \times 10^{-11}$ amp/cm² in 0.5M $FeSO_4$ + 0.1M $NaHSO_4$. Bonhoeffer and Heusler (16) obtained $b_a = 0.030$ in perchlorate solutions, a value also reported by Kaesche (17) in similar solutions.

Pronounced time dependence of the anodic polarization curve is also generally observed and is frequently associated with an open hysteresis loop

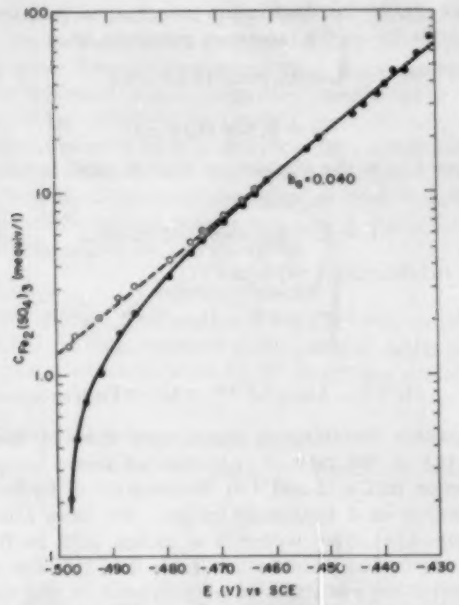

Fig. 11. Electrode potentials as a function of $Fe_2(SO_4)_3$ concentration at V = 58 cm/sec. Data are typical of electrodes of set (ii). Open circles were calculated from Eq. [27] as explained in text.

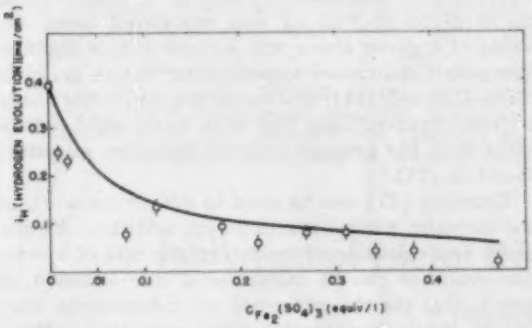

Fig. 12. Rate of hydrogen evolution as a function of $Fe_2(SO_4)_3$ calculated from Eq. [28]. Points are experimental average rates given in ref. (21).

(6, 11). The curve traced on decreasing the current density falls below the curve obtained on increasing the current, the corrosion potential being displaced after a cycle to a more negative value. A similar drift toward lower overpotentials, particularly at high current densities, was observed here. In obtaining anodic polarization curves, each current setting was held for about 1 min during which time the potential decreased by about 1 mv. The electrode returned to a potential 10-15 mv more negative than E_{corr} after anodic polarization and drifted to within a few millivolts of E_{corr} in about 15 min.

A number of hypotheses have been advanced to account for the anodic behavior of iron. It has been suggested repeatedly (4, 11, 18) that the extent of adsorption of atomic hydrogen on the surface of an iron electrode decreases with increasing (more noble) potential. It is possible to account for some of these effects on the assumption that an adsorbed film of hydrogen interferes with the rate of the $Fe \rightarrow Fe^{++}$ reaction. Alternatively, adsorption of hydroxyl ion and its variation with potential (19) have been postulated.

Anodic overpotentials for iron are relatively large, the exchange current being of the order of 10^{-6} -10^{-11} amp/cm^2. It is probable that small amounts of impurities have a pronounced effect on dissolution kinetics. One expects dissolution to proceed mainly at sites where metal cations are in states of higher energy than at the rest of the surface (20). These may be at subgrain boundaries, dislocations, edges of incomplete layers, etc. As ions from such sites dissolve, near neighbors are placed in positions energetically favored for dissolution. However, these sites are probably also preferred for adsorption of impurities. It is thus probable that impurities in quantity far less than a monolayer may have a large effect on the anodic partial reaction. Some impurities may be introduced from the dissolving electrode. Okamoto, Nagayama, and Sato (11), for example, suggest that sulfide ions produced from sulfur inclusions in Armco iron may be responsible for the anodic hysteresis loop. It is probable that the divergent results quoted above are a consequence of extraneous impurities and are not characteristic of clean iron electrodes. It should be noted, however, that impurities present in quantities sufficient to affect the anodic partial reaction may have a relatively small or even negligible effect on processes, such as reduction of ferric ion, which proceed over essentially the whole of the electrode surface.

Dissolution in Ferric Sulfate Solutions

Previous work (1, 3) has shown that reduction of ferric ion on iron and mild steel in acid solution proceeds at a diffusion-limited rate. The first order kinetics, the dependence of the rate on flow velocity, and the absolute magnitude of the rate constants ($\sim 10^{-2} - 10^{-3}$ cm/sec) are all in accord with the assumption that dissolution is limited only by the rate of diffusion of ferric ion to the interface.

It is in general possible to determine the anodic partial curve from the dependence of potential on the concentration of oxidant when the oxidant is reduced at a diffusion-limited rate (Eq. [11]). The question to be answered experimentally is whether the oxidant, ferric ion in this case, modifies the anodic partial curve or the reduction kinetics for hydrogen evolution.

The anodic partial curve is not changed by ferric ion. Although the anodic slope was variable, values obtained with the same electrode by anodic polarization and from the dependence of potential on the ferric ion concentration coincided closely. It may be concluded that ferric ion has no specific effect on the anodic partial curve.

The absence of specific effects is not surprising. If reduction occurs at a rate limited by diffusion, a concentration gradient of an equivalent thickness δ is established in the steady state.[2] If sufficient in-

[2] The equivalent thickness of the boundary layer is obtained by assuming that the concentration of the diffusing species changes linearly with distance from a value of zero at the interface to its bulk concentration at δ. The physical thickness of the boundary layer may be approximated with sufficient accuracy for the purpose of this discussion by δ.

different electrolyte is present, changes of ionic strength caused by ferric ion may be neglected. Ferric ion could then influence the kinetics of metal dissolution or of hydrogen reduction either by adsorption in the fixed part of the electrical double layer or through reaction with some intermediate formed in either process.

There is no apparent intermediate in the anodic process with which ferric ion could interact. At the same time, adsorption of ferric ion is unlikely since it is precisely in the region of the Helmoltz layer that its concentration approaches zero ($C \cong (10^{-5} C_{bulk}) \cong 10^{-6}$ to 10^{-7} equiv/l). The concentration gradient for ferrous ion is, of course, opposite to that for ferric ion. However, the results show that the local excess of ferrous ion had little effect on the anodic curve.

Ferric ion could modify the hydrogen evolution reaction (h.e.r.) by reacting with adsorbed hydrogen atoms formed when hydrogen is discharged. Interference effects, if any, will be significant in the neighborhood of the corrosion potential. At more positive potentials the h.e.r. reaction becomes negligible.

The two most likely mechanisms for the h.e.r. on iron are slow discharge and the adsorbed hydrogen-hydrogen ion reaction.[5] These may be written as

$$H_3O^+ + e \rightarrow H_{ad.} + H_2O \qquad [23]$$

and

$$H_3O^+ + H_{ad.} + e \rightarrow H_2 + H_2O \qquad [24]$$

with

$$H_2O + H_{ad.} + Fe^{+++} \rightarrow H_3O^+ + Fe^{++} \qquad [25]$$

possible in the presence of ferric ion.

If we denote the rate by v, and if [23] is rate controlling, i.e., $v_2 > 10\ v_1$, the over-all rate of h.e.r. is unaffected by [25] in the range $i_d \sim V_2 \sim V_{h.e.r.}$. Similarly, if [24] is slow and [23] fast, again [25] is negligible for $V_{h.e.r.} \sim V_2$. In either case, the stationary concentration of $H_{ad.}$ is not changed to any appreciable extent by reaction [25]. Only if [23] and [24] are comparable in rate will reaction [25] have an appreciable effect on the h.e.r. It is shown below that no effect was detected.

It must be emphasized that the possible effects on the h.e.r. discussed above are in addition to the expected decrease in rate at the more positive potentials in ferric sulfate solutions. This decrease is, of course, allowed for in superposing partial processes.

It has been proposed (21) that ferric ion reduction and hydrogen evolution are competitive not because of indirect reduction (process [25] above) but through competition between ferric and hydrogen ions for available adsorption sites. The suggestion was based on an interpretation of the dissolution rate of mild steel in stagnant ferric sulfate solutions (21).

Let us examine the dependence of the dissolution rate of ferric ion concentration, particularly in the range $i_d \sim i_H$. The dissolution rate (equiv/cm²/sec) is

$$\text{(dissolution rate) } F = i_a = i_d + i_H$$

[5] It is not likely that a combination of absorbed hydrogen atoms is the slow step for the h.e.r. on iron since the Tafel slope is about 0.1 v.

If we choose the dissolution potential in the absence of ferric ion as the reference potential, then

$$i_a = i_{corr} \exp (2.30\ \epsilon/b_a) \qquad [26]$$

or

$$\epsilon = b_a \log (i_a/i_{corr})$$

where i_{corr} is the dissolution rate in acid alone. But from $i_a = i_d + i_H$,

$$i_a = i_d + i_{corr} \exp (-2.30\ \epsilon/b_a) \qquad [27]$$

and substituting [26] into [27]

$$i_a = i_d + i_{corr} (i_{corr}/i_a)^{b_a/b_c}$$

from which

$$i_a - i_{corr} (i_{corr}/i_a)^{b_a/b_c} = i_d = nFk\, C_{Fe^{+++}} \qquad [28]$$

Possible interference effects may then be looked for (a) in the rate of reduction of ferric ion as a function of $C_{Fe^{+++}}$ and (b) in the rate of hydrogen evolution as a function of $C_{Fe^{+++}}$. We have already shown (22) that within the range 0.01 to 0.467 equiv/l for which data are given in (21), the rate of ferric ion reduction is proportional to the ferric ion concentration with an average rate constant of 1.75×10^{-4} cm/sec.[6]

The rate of hydrogen evolution is given in Eq. [28] by the second term on the left-hand side. From (21), $i_{corr} = 0.39$ ma/cm² and $b_a = 0.060$ v. The curve given in Fig. 12 was calculated using the value of k given above and assuming $b_c = 0.100$ v. The points shown are experimental values given in Table II of ref. (21). The curve lies somewhat above a "least squares" line but is in fairly good agreement with the average rates of hydrogen evolution found in (21).[7]

Equation [27] can be used to determine whether the cathodic partial reactions are additive. At any given concentration of ferric ion, the rate of hydrogen evolution can be calculated if it is assumed, as above, that the two processes are independent. Figure 11 shows the results of this calculation. Here, $i_{corr} = 390\ \mu$a/cm² at $E_{corr} = -0.500$ vs. S.C.E., and $b_c = 0.100$ v. For each concentration i_d was calculated from the rate constant ($k = 3.1 \times 10^{-4}$ cm/sec) and i_H was obtained from the second term on the r.h.s. of Eq. [27]. Anodic currents obtained in this way were converted to equivalent concentrations of ferric ion and are shown as open circles on the same figure. They fall, within experimental error, on the line extrapolated from high concentrations of ferric ion ($i_d >> i_H$). It may be concluded that hydrogen evolution and ferric ion reduction do not interfere with each other.

Conclusions

An analysis of changes of electrode potential with concentration and flow velocity shows that the Tafel line for the Fe/Fe^{++} couple is unaffected by ferric ion. Specific effects expected if adsorption of ferric ion took place are not found. The overpotential curve

[6] For the experimental conditions employed in (21), a dependence of the reduction rate on $(C_{Fe^{+++}})^{5/4}$ is expected (23). However, experimental scatter made it impossible to distinguish between a 5/4 power and linear dependence (see (22)).

[7] A decrease of the rate of hydrogen evolution with time was observed in (21). The experimental points shown are, therefore, average rates over 5 hr.

for hydrogen evolution is also apparently unaffected but the experimental evidence is less extensive in this case. These conclusions may be extended to other systems where reduction occurs at a rate limited by diffusion. In general, it is unlikely that the oxidant will have a specific effect, either on the anodic reaction or on hydrogen evolution, since its concentration approaches zero at the interface. Specific effects may appear however if the reduction products adsorb on the electrode.

Acknowledgment

The author thanks Mr. R. Aikin who skillfully assisted in the experimental part of this work. Helpful discussions with Dr. M. Stern are gratefully acknowledged.

Manuscript received March 23, 1960.

Any discussion of this paper will appear in a Discussion Section to be published in the June 1961 JOURNAL.

REFERENCES

1. C. V. King and W. H. Catchart, *J. Am. Chem. Soc.*, **59**, 63 (1937); C. V. King and P. L. Howard, *Ind. Eng. Chem.*, **29**, 75 (1937); C. V. King and L. Weidenhammer, *J. Am. Chem. Soc.*, **58**, 602 (1936); M. B. Abramson and C. V. King, *J. Am. Chem. Soc.*, **61**, 2290 (1939); C. V. King, "Pittsburgh International Conference on Surface Reactions," p. 5, Corrosion Publishing Co., Pittsburgh (1948).
2. M. Eisenberg, C. W. Tobias, and C. R. Wilke, *Chem. Eng. Progr.*, **51**, [16] (1955); *This Journal*, **101**, 306 (1954).
3. A. C. Makrides, N. Komodromos, and N. Hackerman, *This Journal*, **102**, 363 (1955); A. C. Makrides and N. Hackerman, *ibid.*, **105**, 156 (1958).
4. O. Gatty and E. C. R. Spooner "The Electrode Behaviour of Corroding Metals in Aqueous Solutions," p. 253, Oxford (1938) (and references therein).
5. K. Bonhoeffer and W. Jena, *Z. Elektrochem.*, **56**, 585 (1952).
6. M. Stern, *This Journal*, **102**, 609 (1955).
7. G. Masing "Die Korrosion Metallischer Werkstoffe," by O. Bauer, O. Kröhnke, and G. Masing, Vol. 1, p. 45, Leipzig (1936) [quoted by C. Wagner and W. Traud, see ref. 8].
8. C. Wagner and W. Traud, *Z. Elektrochem.*, **44**, 391 (1938).
9. J. N. Agar, *Discussions Faraday Soc.*, **1**, 26 (1947).
10. A. M. Azzam, J. O'M. Bockris, B. E. Conway, and H. Rosenberg, *Trans. Faraday Soc.*, **46**, 918 (1950); J. O'M. Bockris and E. C. Potter, *J. Chem. Phys.*, **20**, 614 (1952).
11. G. Okamoto, M. Nagayama, and N. Sato, "International Committee of Electrochemical Thermodynamics and Kinetics" 8th Meeting Madrid 1956, p. 72, Butterworths (1958).
12. M. Stern, *Corrosion*, **14**, 440 (1958).
13. W. Roitar, W. Jura, and E. Polujan, *Acta Physichochim.*, **10**, 389 (1939).
14. M. Stern and R. M. Roth, *This Journal*, **104**, 390 (1957).
15. T. P. Hoar and T. Hurlen, "International Committee of Electrochemical Thermodynamics and Kinetics," 8th Meeting Madrid 1956, p. 445, Butterworths (1958).
16. K. Bonhoeffer and K. Heusler, *Z. Phys. Chem.*, **8**, 390 (1956).
17. H. Kaesche, *Z. Elektrochem.*, **63**, 492 (1959).
18. K. Bonhoeffer, Paper presented at ECS Meeting, San Francisco, April 30, 1956.
19. K. E. Heusler, *Z. Elektrochem.*, **62**, 582 (1958).
20. T. P. Hoar, "Modern Aspects of Electrochemistry, No. 2", J. O'M. Bockris, Editor, p. 270, Academic Press, New York (1959).
21. H. C. Gatos, *This Journal*, **103**, 286 (1956).
22. A. C. Makrides, *ibid.*, **103**, 706 (1956).
23. C. Wagner, *J. (and Trans.) Electrochem. Soc.*, **95**, 161 (1946).

Inhibition of Metal Dissolution by Ferric Sulfate

A. C. Makrides and Milton Stern

Metals Research Laboratories, Union Carbide Metals Company,

Division of Union Carbide Corporation, Niagara Falls, New York

ABSTRACT

Iron-chromium alloys are passivated in acid solution at a critical ferric sulfate concentration which depends on acid normality and flow velocity. Smaller concentrations of ferric ion increase the dissolution rate of active electrodes by providing a cathodic partial process occurring at a diffusion-limited rate. Once passivity is achieved, however, considerably less than the critical ferric ion concentration is required to maintain the electrode passive. The dependence of the electrode potential on the concentration of ferric ion is quantitatively related to the anodic polarization curve of the electrode. Polarization curves obtained in the active region coincide with curves derived from studies with ferric ion. The inhibitor concentration required to produce passivity is directly proportional to the anodic critical current density, while the primary passive potential is not changed by ferric ion. These results suggest that adsorption of ferric ion is not responsible for inhibition by this ion.

A number of oxidizing substances inhibit metal dissolution by inducing a transition from the active to the passive state (1). A characteristic electrochemical difference between the action of these substances and that of nonoxidizing inhibitors is the change of electrode potential which they produce. Oxidizing inhibitors displace the mixed potential in the positive (noble) direction by about 1 v, while nonoxidizing inhibitors produce changes which may be of either sign and which rarely exceed 0.1 v.

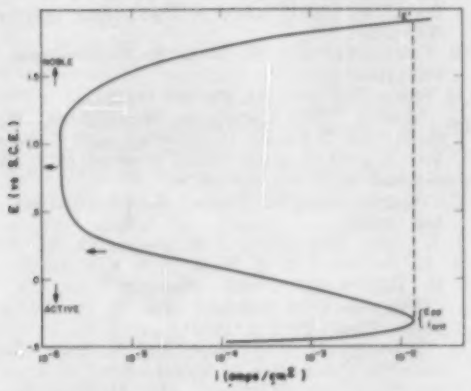

Fig. 1. Schematic polarization curve typical of iron-chromium alloys (series 400 stainless steels). Dashed curve shows transition to oxygen evolution with constant current source. Full curve is obtained in a potentiostatic experiment. E_{pp} is the primary passive potential and i_{crit} the critical current density. Arrows at left indicate decreasing current with time in this potential region.

It is generally agreed that nonoxidizing inhibitors reduce the dissolution rate by forming an adsorbed film at the metal-solution interface (2). Conflicting mechanisms have been proposed for inhibition by oxidizing substances. It has been suggested (3) that oxidizing inhibitors induce passivity by adsorption. It is possible however to give an account of inhibition in which specific effects, such as expected from a model postulating adsorption, are not assumed (1). A study of inhibition by ferric ion was carried out to determine whether specific effects are, in fact, present. As shown below, the results are consistent with the generalized description given in (1). It may therefore be concluded that inhibition is not related to adsorption of ferric ion.

Passivating inhibitors.—The anodic polarization curve of a number of common metals and alloys (1, 4, 5) is of the general type shown in Fig. 1. The full curve is the result of a potentiostatic and the dashed curve of a galvanostatic experiment.

With no applied current, the electrode dissolves at some rate i_{corr} corresponding to a mixed potential E_{corr}. If the electrode is polarized anodically with a constant current source, the rate of the anodic partial reaction increases smoothly with potential until at some current i_p a large, discontinuous potential jump occurs (from E_{pp} to E' on the diagram). Oxygen evolution takes place at E'. However, if a polarization curve is obtained by controlling the potential and allowing the current to vary, potentials intermediate between E_{pp}, the primary passive potential (6), and E' are attainable. At first, the steady-state current decreases in this potential region. After some low value is reached, it becomes more or less independent of potential over an interval of several tenths of a volt. Oxygen is again evolved at sufficiently positive potentials.

In general, several hours are required to achieve a steady state at potentials more positive than E_{pp}. In some cases time dependent results are also observed at potentials somewhat more negative than E_{pp}.

The reversible potential of a redox couple whose oxidized form is an inhibitor lies in the passive potential region. Since a mixed potential in the passive region can be maintained with such redox couples, stable inhibition (small dissolution rate) is observed when the metal is passivated either externally or by the added redox couple. The redox couple may displace the potential to the passive region when its reduction rate exceeds some current equivalent i_p'.

A specific effect by an inhibitor can be detected experimentally by comparing anodic polarization curves with and without inhibitor. If the inhibitor alters the anodic reaction in some specific way, then at any given potential the anodic partial current will be less than that indicated by the anodic curve determined in the absence of inhibitor. If this is the case, one expects i_p to differ from i_p'. Further, the potential, say E_{pp}', at which the inhibitor induces a transition to a passive state should also differ from E_{pp}. If, on the contrary, the inhibitor has no specific effect, the anodic partial current will depend only on the potential. Therefore, $i_p' = i_p$ as well as $E_{pp}' = E_{pp}$. This study was directed toward determining these quantities with and without ferric sulfate.

Experimental

Previous work (7, 8) established that ferric ion is reduced on iron and mild steel at a rate limited only by diffusion. Since it appeared probable that this would also be true for the iron-chromium alloy used here, it was essential to control the rate of mass transport to the interface precisely and reproducibly. A rotating, cylindrical electrode was chosen since it satisfied these requirements and possessed the advantage of a uniform mass-transport rate over the whole of its lateral surface.

The experimental arrangement was described in detail previously (8). Briefly, electrodes of various projected surface areas were rotated at equivalent linear velocities up to 200 cm/sec in hydrogen- or argon-saturated sulfuric acid solutions. Small amounts of a concentrated solution of ferric sulfate were added from a precision buret.

Only glass and Teflon were in contact with solution. Greaseless ground glass joints were used to avoid possible contamination from lubricant.

Ferric sulfate was prepared from ferrous sulfate by oxidation with hot, concentrated sulfuric acid. Solutions were also prepared from recrystallized C. P. ferric sulfate. Water was triply distilled, one distillation being from dilute, alkaline potassium permanganate. The reaction vessel and all glass parts were cleaned with a saturated solution of potassium dichromate in concentrated sulfuric acid (cleaning solution) and rinsed with triply distilled water prior to use. Water drained uniformly and with zero contact angle from glass surfaces cleaned in this way.

Potentials were measured against S.C.E. and platinized through a high impedance L&N pH meter connected to a multiple-range, adjustable-zero, Dynamaster Bristol recorder. Alternatively, a Rubicon potentiometer was used together with a galvanometer of 0.007 μa/mm sensitivity. A capillary probe

with a bridge filled with solution of the same acid concentration was used in polarization measurements. The bridge led to an external S.C.E. A greaseless, closed stopcock prevented mixing of (air-saturated) solution outside the cell with solution in the cell, but had sufficient conductivity when wetted with solution to maintain electrical contact. Constant current was obtained through appropriate resistances from two banks of batteries, each consisting of three 45 v cells arranged in series to give 135 v.

Potentiostatic measurements were conducted with an Analytical Instruments Company potentiostat, an electromechanical device. It was necessary to use the same material for the test electrode and for a potentiostat reference electrode and to place the two electrodes in the same solution, since this potentiostat does not operate properly if a high impedance exists between the electrodes. Auxiliary electrodes of the same material as the test electrode were placed directly in the cell. Electrodes were cut from a bar of an iron-chromium alloy (stainless steel 410) of the following per cent composition: 12.39 chromium, 0.09 carbon, 0.44 manganese, 0.024 phosphorus, 0.022 sulfur, 0.27 silicon, 0.24 nickel, 0.07 molybdenum, and 0.12 copper. They were abraded with 2/0 emery paper, washed with reagent-grade carbon tetrachloride, left to dry, etched in 1:3 HNO_3, washed with conductivity water, etched in 1:3 H_2SO_4, and washed again.

Concentrations of various solutions were determined by analysis. The cell was thermostated at 30° ± 1°C.

Results and Discussion

General observations.—Electrodes were active in hydrogen-saturated sulfuric acid solutions with potentials in the neighborhood of −0.490 v *vs.* S.C.E. The corrosion potential increased with time at first, but drift became negligible (< 2 mv/hr) after about 3 hr of immersion. Electrodes were aged therefore for at least 3 hr before a run.

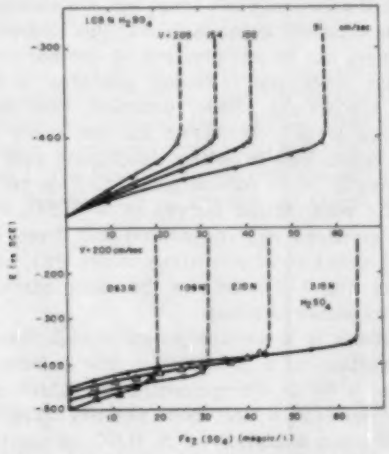

Fig. 2. Electrode potential as a function of ferric sulfate concentration at (top figure) various velocities in solutions of constant acidity and (bottom figure) in solutions of varying acidity at constant velocity. Dashed lines indicate discontinuous transition to potentials about +0.4 v vs. S.C.E. Transitions to passive potentials were irreversible (see text).

The potential moved in the anodic direction when ferric sulfate was added (Fig. 2). About a minute was required to establish a steady state after each increment in ferric ion concentration. A discontinuous transition from active to noble potentials occurred at a critical ferric ion concentration. The increase of potential was about 0.8 v. The critical concentration varied with flow velocity and acid normality as shown in Fig. 2.

Once passivity (noble potential) was produced, the electrode remained passive when the flow velocity was decreased. In the cases studied here, the electrode remained passive even when the rotational velocity was reduced to zero.

Passive specimens could be activated by cathodic polarization. The current required for activation increased with the amount of ferric ion in solution and with rotational velocity.

Detailed studies of the active region, of the transition to a passive potential, and of the passive potential region are presented below.

Active potential region.—Anodic polarization curves were obtained with a constant current source, with a potentiostat, and by following the potential as a function of ferric ion concentration.

For an electrode dissolving at a rate i_{corr} in a hydrogen-saturated acid solution

$$i_a = i_H = i_{corr} \qquad [1]$$

Here i_a is the partial anodic current corresponding to metal dissolution and i_H the partial cathodic current corresponding to hydrogen evolution. Both i_a and i_H are functions of potential.

If the electrode is polarized anodically by a constant current source, then

$$i_a = i_{appl} + i_H \qquad [2]$$

at a potential E more positive than the corrosion potential, E_{corr}. Since i_H decreases exponentially with potential, at sufficiently positive potentials

$$i_a \simeq i_{appl} \qquad [3]$$

where i_{appl} is the externally applied current. At sufficiently positive potentials, therefore, an anodic polarization curve obtained with a constant current source coincides with the anodic partial curve for the metal.

The same remarks apply to a polarization curve obtained with a potentiostatic device in this potential region.

If another reducible substance is introduced in the solution, the cathodic partial current, i_c, is the sum of the hydrogen evolution current and of the reduction current of the added oxidant. If reduction of oxidant occurs at a diffusion-limited rate, then

$$i_a = i_c = i_H + i_d \qquad [4]$$

where i_d is the limiting diffusion current and is independent of potential. At large flow velocities and large concentrations of oxidant, $i_d >> i_H$ and

$$i_a = i_c \simeq i_d \qquad [5]$$

A plot of potential against i_d under these conditions yields the anodic partial curve for the metal. Specific effects attributable to the oxidant (or to its reduction product) may be detected by comparing anodic partial curves obtained in this way with curves measured directly (Eq. [3]).

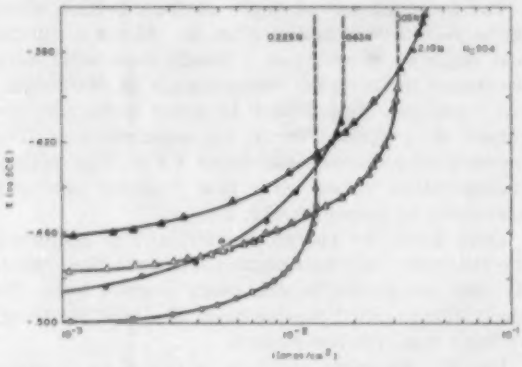

Fig. 3. Polarization curves with a constant current source in solutions of varying acidity. Dashed lines indicate transitions to potentials where oxygen is evolved ($> +1.0$ vs. S.C.E.).

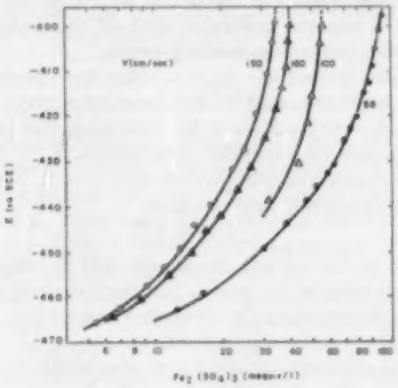

Fig. 4. Potential as a function of ferric sulfate concentration in N H_2SO_4 at various velocities.

Polarization curves obtained with a constant current source are shown in Fig. 3. Results were not time dependent in the active region, even at potentials close to the primary passive potential. Electrodes polarized for long periods (30 min) at a current density only 0.2 ma/cm² less than the critical did not show any tendency to become passive and the potential did not drift. In general, each current setting was held for 3 min, the same time interval used in runs with the potentiostat.

Figure 4 shows the dependence of the potential on concentration of ferric ion in the active region. The curves are similar to the polarization curves of Fig. 3. The primary passive potential, taken as the most positive potential observed before a transition to a passive state occurred, was essentially that found with a constant current source.

The reduction current for ferric ion must be known as a function of concentration and flow velocity in order to compare results of Fig. 4 with those of Fig. 3. If ferric ion is reduced at a diffusion-limited rate (see below)

$$i_d = \frac{nFV_r}{A}\frac{dc}{dt} = nFkC_\infty \qquad [6]$$

Here n is the number of equivalents per mole of oxidant, F Faraday's constant, C_∞ the concentration of oxidant, A the (projected) surface area, V_r the volume of solution, t the time, and k a rate constant. The rate constant depends on various hydrodynamic parameters but is independent of the nature of the electrode since the diffusion gradient is entirely within the liquid phase. Reaction rate constants used here were determined for the same experimental conditions from the dissolution rate of iron electrodes in ferric sulfate solutions (see ref. 8).

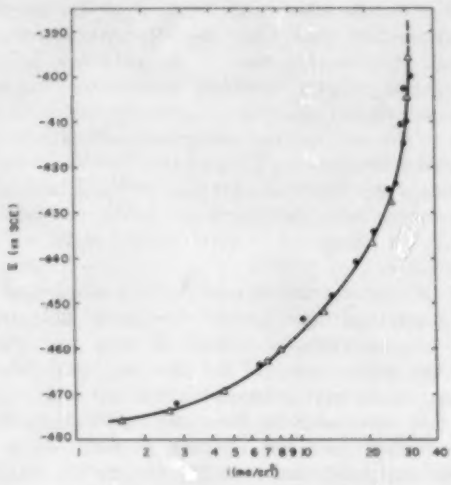

Fig. 5. Comparison of polarization curves obtained with a constant current source (triangles) and indirectly from the dependence of potential on $Fe_2(SO_4)_3$ concentration (circles). In the latter case, current densities were calculated from Eq. [6].

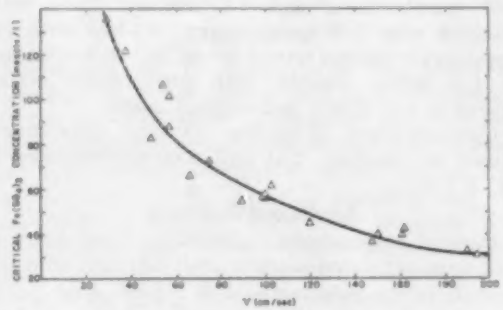

Fig. 6. Critical $Fe_2(SO_4)_3$ concentration required for passivity in N H_2SO_4 as a function of velocity. Points shown were obtained with six different electrodes.

Anodic polarization curves in N H_2SO_4 obtained with a constant current source and from Eq. [5] and [6], using constants given in ref. (8), are compared in Fig. 5. Essentially the same curve is obtained by either method.

Transition to a passive potential.—A discontinuous transition to a potential in the passive region occurs at a ferric ion concentration which depends on acid normality and flow velocity. The critical ferric ion concentration in N H_2SO_4 is plotted as a function of flow velocity in Fig. 6.

If the critical current density required for passivating the electrode is independent of the ferric ion concentration, then from Eq. [6]

$$i_p' = nFkC_{crit} = \text{(constant)} \qquad [6a]$$

Table I. Comparison of the equivalent critical current density for passivity calculated from mass transfer and measured by anodic polarization

Type 410 stainless steel in N H_2SO_4 at 30±1°C

Velocity, cm/sec	Critical $Fe_2(SO_4)_3$ concentration, mequiv/l	k* cm/sec	Calculated equivalent critical current density, i_p', ma/cm²
55	107	2.8	29
58	102	3.2	31.5
58	90	3.2	28
67	66	4.0	25.5
75	71	4.6	31.5
90	55	5.7	30
100	57	6.4	35
103	61	6.6	39
120	44	7.6	32
148	36	8.8	30.5
161	41	9.3	37
162	43	9.4	39
182	30	10.0	29
190	34	10.4	34
194	31	10.5	31.5
			Average 32 ± 3

Measured critical anodic current, i_p by constant current polarization: 31, 31, 28, 27, 32
Average 30 ± 2

In all cases $E_{pp} = E_{pp}' = -0.395 \pm 0.005$ *vs.* S.C.E.

* In 0.5N H_2SO_4 solutions.

where C_{crit} is the concentration of ferric ion required to produce passivity.

For turbulent flow, the rate constant is given by [see ref. (8)]

$$k = (\text{Constant})\ V\ (R_d)^{-s}\ (Pr)^{-n} \qquad [7]$$

Here V is the linear flow velocity, R_d is Reynolds number, $\frac{Vd_i}{\nu}$, with d_i the diameter of the electrode and ν the kinematic viscosity, and Pr is Prandtl's number, ν/D, with D the diffusion coefficient of ferric ion. For the conditions employed here [see ref. (7)]

$$k = (\text{constant})\ V^{0.80}$$

Substituting in Eq. [6a]

$$C_{crit} = (\text{Const.})\ V^{-0.80} \qquad [8]$$

A log-log plot of C_{crit} against the velocity (Fig. 7) has a slope of −0.79 in good agreement with Eq. [8]. Equivalent current densities required for passivity were calculated from Eq. [6a] and are given in Table I. The equivalent current density for passivity is independent of the concentration of ferric ion and differs by less than 10% from the critical current density found by anodic polarization. The rate constants used in calculating i_p' were determined in 0.5N H_2SO_4. Rate constants in N H_2SO_4 are probably smaller, mainly because of a decrease of the activity coefficient of ferric ion. The higher mean value of i_p' is probably due to somewhat larger rate constants in 0.5 than in N H_2SO_4.

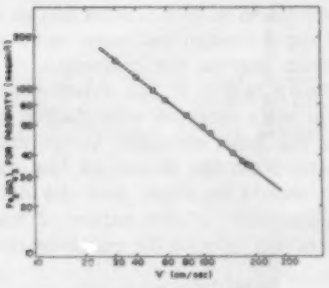

Fig. 7. Critical $Fe_2(SO_4)_3$ concentration for passivity as a function of velocity plotted according to Eq. [8]. The slope of the log-log plot is −0.79.

The conclusions drawn from Table I were confirmed by anodically passivating electrodes in solutions containing less than the critical ferric ion concentration. If ferric ion has no specific effect, the sum of the equivalent reduction current for ferric ion and of the applied current should be constant and equal to the critical current. Table II shows this to be true and also shows that the primary passive potential is not changed by ferric ion (see also Table I).

Table III compares equivalent current densities for passivity with ferric sulfate to critical current densities determined by anodic polarization for various acid normalities. Primary passive potentials are also given.

Passive potential region.—When the critical ferric ion concentration is exceeded, the electrode becomes passive with a mixed potential positive with respect to S.C.E. The potential depends on the ferric ion concentration and to a small extent on the normality of H_2SO_4, but is independent of flow velocity. It drifts slowly to more positive values, reaching a steady state after about 100 hr. At concentrations of the order of 0.010 equiv/l, the mixed potential is negative to the reversible Fe^{+++}/Fe^{++} potential, but it essentially coincides with the reversible potential at larger ferric ion concentrations (0.10 equiv/l).

The time dependence of the mixed potential in the passive region is probably caused by a decrease

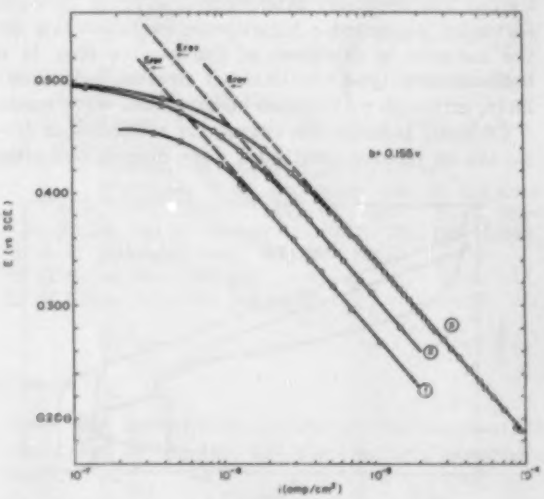

Fig. 8. Cathodic polarization curves of ferric sulfate on passive electrodes. Arrows indicate the reversible potential for the Fe^{+++}/Fe^{++} couple measured with a platinized platinum electrode. Curves 1 and 2 were obtained with solutions 0.0011M in ferrous ion and respectively 0.0138M and 0.0288M in ferric ion. For curve 3, $[Fe^{++}] = 0.005M$ and $[Fe^{+++}] = 0.066M$. Exchange currents are (from 1 to 3) 3.3, 4.3, and 8.1 × 10^{-7} amp/cm² while the Tafel slope is for all cases 0.155 v. The solution was N in H_2SO_4.

Table II. Comparison of measured critical anodic current density to the sum of the current density equivalent to ferric ion reduction and the applied anodic current

Type 410 stainless steel at 30 ± 1°C

V = 100 cm/sec; k = 6.4 cm/sec

H_2SO_4	$Fe_2(SO_4)_3$ concentration, mequiv/l	Equivalent $Fe_2(SO_4)_3$ reduction current, ma/cm²	Applied anodic current density, ma/cm²	Sum of equivalent and applied current densities, ma/cm²	Measured critical anodic current density, ma/cm²	Primary passive potential, E_{pp}, vs. SCE
0.63N	8.0	5	12	17		−0.405
	16.0	10	10	20		±0.005
	29.5	19	0	19	16	
	6.4	4	17	21		
	12.8	8	12	20		−0.410
	19.2	12	9.5	21.5		±0.005
	25.5	16	6.0	22		
	35.0	22	0	22	20	

Table III. Comparison of the equivalent critical current density for passivity calculated from mass transfer and measured by anodic polarization at various H_2SO_4 concentrations

Type 410 stainless steel at 30 ±1°C

Concentration H_2SO_4, N	Velocity, cm/sec	Critical $Fe_2(SO_4)_3$ concentration, mequiv/l	Calculated equivalent critical current density i_p', ma/cm²	Average measured critical current density i_p, ma/cm²	Primary passive potential with ferric sulfate, v vs. S.C.E.	Primary passive potential from anodic polarization, v vs. S.C.E.
0.225	—	—	—	13.5	—	−0.440
0.63	50	82	18			
	75	43	20			
	100	30	19			
	150	26	22	18	−0.415	−0.410
1.05	50-200	—	32*	30*	−0.395	−0.395
2.10	105	72	47			
	155	54	48			
	200	47	49	43	−0.370	−0.360
3.15	75	108	50			
	105	97	64	55	−0.345	−0.350

* Averages from Table I.

in the rate of oxidation of the passive electrode. In similar studies with type 304 stainless steel it was found (9) that the oxidation rate at constant potential was inversely proportional to time. This observation suggested a logarithmic oxidation law for the increase in thickness of the passive film. It is believed that type 410 stainless steel behaves similarly, although no detailed observations were made.

Cathodic polarization curves for reduction of ferric ion on passive electrodes were determined after the electrode had reached a steady state. Curves for various ferric ion concentrations are given in Fig. 8. At any given potential the current increases with ferric ion concentration. The Tafel slope is 0.155 v and is independent of ferric ion concentration. The Tafel curves measured here are similar to the ones reported by Stern (10) for 304 stainless steel.

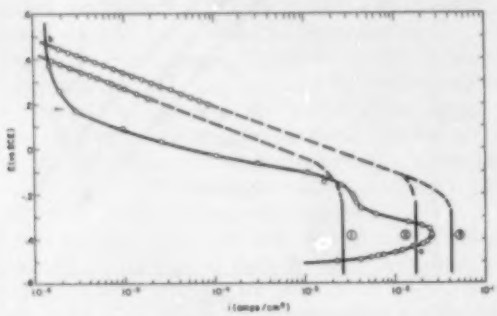

Fig. 9. Superposition of reduction curves for ferric ion and of the anodic polarization curve of Type 410 stainless steel in N H_2SO_4. Reading from curve 1 to 3, 0.010M Fe^{+++} at 55 cm/sec, 0.066M Fe^{+++} at 55 cm/sec, and 0.066M Fe^{+++} at 100 cm/sec. The upper sections of the reduction curves were determined by cathodic polarization on passive electrodes, while the solid lines at lower right are limiting diffusion currents obtained from Eq. [6] (see text). The dashed lines connecting the two are extrapolated from the passive region.

Potentiostatic curves.—Figure 9 gives a potentiostatic anodic polarization curve for type 410 stainless steel in N H_2SO_4. The primary passive potential is −0.380 v; the critical current density 28 ma/cm². These are to be compared with −0.395 v and 30 ma/cm² determined by polarization with a constant current source (see Table I). At each potential setting positive to E_{pp}, the current decreased rapidly at first and then changed slowly with time. The points shown were taken at 3-min intervals at which time the initial rapid change had come to an end.

Polarization curves for reduction of ferric ion are also shown in Fig. 9. The experimentally measured curves are connected with dashed lines calculated from the Tafel constants (slope and exchange current) and from the measured limiting diffusion current. It should be noted that the diffusion current is independent of the nature of the electrode and is a function only of the concentration and flow conditions.

General Discussion

Results shown in Figure 9 account completely for both the accelerating and the inhibitive effect of

ferric ion. Starting with a specimen freely corroding in acid solution, the figure indicates that ferric ion in concentration less than the critical increases the dissolution rate by providing an additional cathodic reaction which occurs at a rate limited by diffusion. The dissolution rate increases with increasing concentration and flow velocity until some critical current, i_p', is exceeded. This current is the same as the critical current found by anodic polarization (either potentiostatically or from a constant current source). When this critical current is exceeded, the electrode becomes passive with a dissolution rate of about 10^{-6} to 10^{-7} amp/cm^2.

At small concentrations and flow velocities two mixed potentials, indicated by points a and b on Fig. 9, are stable. The potential assumed by the system on addition of ferric ion depends on its previous state. Thus, if the electrode is originally active, ferric ion displaces the potential to (a), while if the specimen is already passive, potential (b) is stable. These observations account for the widely different concentrations required to produce and to maintain passivity. Thus, ferric ion causes a transition to a passive state only if its reduction rate exceeds i_{p_1} which is in this case about 3×10^{-5} amp/cm^2. However, the reduction current necessary to maintain the electrode passive is only about 10^{-6} amp/cm^2, and decreases with time to probably less than 10^{-7} amp/cm^2.

An electrode in state (a) may be displaced to state (b) by polarization with an external source. When the sum of the applied anodic current and the equivalent reduction current exceed i_p (see Table II), the electrode undergoes a transition to a passive state which is maintained, since it is stable, even when the applied current is reduced to zero. Similarly, if the electrode is at potential (b), it may be activated by a cathodic current and remains active at (a) even after the applied current is reduced to zero. However, when the reduction rate of ferric ion exceeds the critical current density, the system is no longer bistable. In this case, the only stable mixed potential is in the passive region.

Figure 9 describes adequately the stainless steel-ferric sulfate system both at potentials more active than E_{p_1} and in the neighborhood of the reversible Fe^{+++}/Fe^{++} potential. No experimental information is available, however, for ferric ion reduction at potentials between E_{p_1} and about +0.1 v *vs.* S.C.E. An extrapolated curve is shown in this potential region in Fig. 9. This extrapolation is only approximate since the Tafel parameters for reduction are probably not the same on passive and active surfaces. It is likely that on active surfaces the exchange current is several powers of ten larger than on passive electrodes. An increase in exchange current shifts the reduction curve for ferric ion to the right, i.e. to lower overpotentials at any given current density. The dashed line must therefore be considered as giving a lower limit for the current at any given potential. The limiting current densities indicated by vertical solid lines in Fig. 9 are, of course, independent of the surface state of the electrode; their magnitudes were determined in separate experiments.

The starting point of this investigation was the attempt to determine whether adsorption of an oxidizing inhibitor, such as ferric ion, played a significant role in inhibition. If inhibitor ions are specifically adsorbed, changes in the composition of the surface state of the metal brought about by adsorption will be manifest in the anodic polarization curve of the metal. The results above clearly show that ferric ion produces no detectable change in the anodic behavior of stainless steel 410. It may be concluded that adsorption of ferric ion is unrelated to inhibition by this ion.

Acknowledgment

The authors thank Mr. R. E. Aikin for his assistance in the experimental part of this work.

Manuscript received March 23, 1960.

Any discussion of this paper will appear in a Discussion Section to be published in the June 1961 JOURNAL.

REFERENCES

1. M. Stern, *This Journal*, **105**, 638 (1958).
2. A. C. Makrides and N. Hackerman, *J. Phys. Chem.*, **59**, 707 (1955).
3. H. H. Uhlig and A. L. Geary, *This Journal*, **101**, 215 (1947).
4. N. Y. Bune and Y. M. Kolotyrkin, *Doklady Akad. Nauk S.S.S.R.*, **111**, 1050 (1956).
5. C. Edeleanu, *Metallurgia*, **50**, 113 (1954); *Nature*, **173**, 737 (1954).
6. N. D. Greene, Submitted to *This Journal*.
7. A. C. Makrides, N. Komodromos, and N. Hackerman, *This Journal*, **102**, 363 (1955); A. C. Makrides and N. Hackerman, *ibid.*, **105**, 156 (1958).
8. A. C. Makrides, *ibid.*, **107**, 869 (1960).
9. M. Stern, *ibid.*, **106**, 376 (1959).
10. M. Stern, *ibid.*, **104**, 600 (1957).

Correction

On page 666 of the August 1960 issue of the JOURNAL in the paper by S. Uno Falk "Investigations on the Reaction Mechanism of the Nickel-Cadmium Cell," the approximate values of the temperature coefficients of the emf and the electrode potentials should be:

dE/dT	dE_+/dT	dE_-/dT
Pocket cells	Pocket cells	Pocket cells
−0.00030	−0.00006	−0.00024
Sintered cells	Sintered cells	Sintered cells
−0.00018	−0.00014	−0.00004 v/°K

The Influence on the Oil Dielectric Strength of the Gas Pressure in Equilibrium with the Oil

Paolo Gazzana-Priaroggia and Giuseppe Palandri

Research Laboratories, Società Italiana Pirelli, Milan, Italy

ABSTRACT

A laboratory investigation of the influence of gas pressure on the electrical breakdown of thin oil, as used in oil-filled cables, was carried out at gas pressure between about 5 x 10^{-6} mm Hg and 1000 mm Hg. The test cell consisted of a glass container enclosing a platinum sphere gap (0.5 mm). Tests were carried out at ambient temperature. The results of this investigation showed that the dielectric strength of the oil is absolutely independent of the gas pressure, provided a perfect equilibrium is reached between the gas dissolved in the oil and the free gas remaining in the cell above the oil surface.

The influence of dissolved gas on the dielectric strength of oil has been discussed often and some data have been published giving the relation between oil dielectric strength and gas pressure (1, 2). These experimental results, of course, refer only to gas dissolved in the oil and not to gas in the form of bubbles or films.

This matter is not only of scientific but also of practical interest with regard to the problem of degassing oils used as impregnants of high-voltage electrical equipment. Published data, however, were not obtained under conditions of most interest to the present authors and they therefore undertook this study. For practical reasons it was decided to study the behavior of thin mineral oil as used in oil-filled cables under 50-cycles stress and to use dry air in the range of 5 x 10^{-6} mm Hg to about 1000 mm Hg.

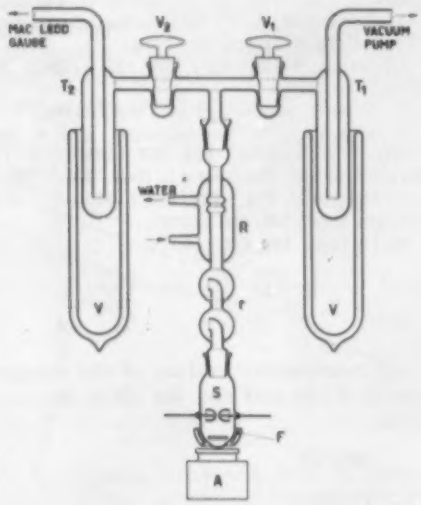

Fig. 1. Testing apparatus. A, magnetic stirrer; F, electric heater; S, sphere gap cell (platinum hemispheres 10 mm diameter, 0.5 mm gap); R, condenser; r, reflux condenser; V, Dewar vessels containing solid CO_2; T_1, T_2, cold traps; V_1, V_2, vacuum tight valves.

Fig. 2. Sphere gap cell

The apparatus is shown schematically in Fig. 1. Detail of the sphere gap cell S is given in Fig. 2.

Preparation of Tests

From the first test it appeared evident that to obtain sufficiently consistent results a certain cleanliness of the oil was necessary. To this end 55 cm^3 of clean, dry oil were introduced into the sphere gap cell. This oil had been filtered previously under vacuum through a glass filter. The sphere gap cell then was connected to the remainder of the testing apparatus. The oil was degassed by heating and stirring under vacuum at 110°C. To avoid fractionation of the oil while it was being degassed, the condenser R and the reflux condenser r were introduced into the vacuum circuit between the sphere gap cell S and the vacuum traps T.

The evacuation of the sphere gap cell was carried out by means of a diffusion pump for pressures below 10^{-4} mm Hg and with a mechanical pump, for

higher pressures. The absolute pressure was measured by means of a MacLeod gauge directly connected to the apparatus through a cold trap. To make sure that no moisture was present in the oil, the oil was degassed thoroughly and then saturated with dry air before reaching the desired pressure by pumping.

Each pressure was obtained and kept constant during the test by means of a vacuum limiter inserted in the vacuum circuit.

Test Results

The oil subjected to the investigation was the NJ 2 thin oil produced by Italian Standard Oil, having a viscosity of 25 centistokes at 20°C. 50-cycle a-c dielectric strength measurements were made as a function of the absolute pressure starting from 6×10^{-4} mm Hg, which was the highest vacuum obtainable with the present equipment, up to atmospheric pressure. The voltage was applied starting from 10 kv and then increasing it in steps of 10 kv/min.

From the first test it became evident that a considerable spread of results was obtained unless the greatest care was taken to make sure that the gas dissolved in the oil was in complete equilibrium with the free gas present in the sphere gap cell above the oil surface. If the saturation pressure of the oil was higher than the pressure of the free gas, the dielectric strength results obtained were considerably lower than the results obtained when a perfect equilibrium was reached. To overcome this difficulty, after the desired absolute pressure value was reached, the oil was left to cool down to the ambient temperature and kept under the desired pressure value with continuous stirring for about 24 hr before making any dielectric strength test.

To limit to as much as possible the influence of the static head of the oil, the oil level was kept at the minimum value necessary to obtain complete covering of the platinum spheres. This requirement determined the amount of 55 cm^3 of the oil which was mentioned before. The static head above the center point of the gap was 30 mm.

The results obtained are shown in the diagram of Fig. 3, in which average values and spread of results are indicated. For each pressure 10 different tests were made. No subsequent tests were made on an oil sample after the first discharge. This was done to avoid trouble due to gas evolution from the oil following breakdown since this could alter the pressure equilibrium. As can be seen, the average dielectric strengths lie on a straight line parallel to the abscissa, having on ordinate value of 400 kv/cm rms. All tests were carried out at ambient temperature (18°+25°C).

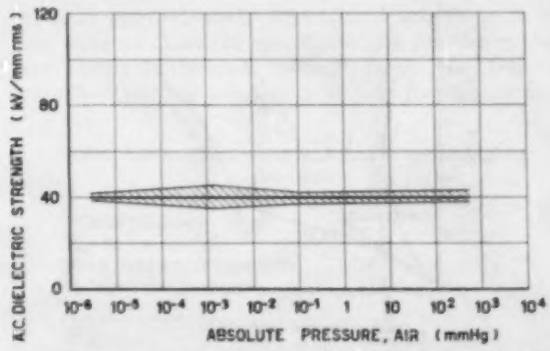

Fig. 3. A-C dielectric strength of thin coble oil vs. absolute air pressure.

Interpretation of Results

The values obtained for the average dielectric strength of about 400 kv/cm rms are lower than the results obtained by other investigators on pure liquid hydrocarbons under controlled physical conditions (3, 4). However, the consistency of the results obtained in the tests described in the present paper indicates that the tests were certainly governed by a well-determined breakdown mechanism. The conclusion could be that this mechanism differs from the breakdown mechanism ruling the tests described by the above-mentioned investigators.

It seems to the authors that an explanation may be found in the fact that the breakdown mechanism of absolutely pure dielectric liquids probably is ruled only by the movement of electrons, accelerated by the electrical field, which ionize the oil molecules; on the other hand the breakdown mechanism with which the tests described above are concerned probably is ruled by particles much bigger than electrons such as molecular aggregates or submicroscopic impurities, still accelerated by the electrical field but unable to ionize the oil molecules.

Two facts are of great importance in understanding these tests: (*a*) the breakdown is practically independent of the saturation pressure of the oil provided a perfect equilibrium is reached between the gas dissolved in the oil and the free gas above the oil surface; and (*b*) the breakdown strength is lowered when the saturation pressure is higher than the pressure of the free gas.

These two facts, combined with the assumption made above that particles much bigger than electrons are responsible for the breakdown of oils as used in industrial apparatus, have suggested the following theory:

A charged particle in suspension in the oil is accelerated by the electrical field and tends to cavitate the liquid in its wake; if the saturation pressure of the gas dissolved in the oil is equal to the pressure of the free gas acting on the oil surface, this tendency is very much reduced. Breakdown occurs when the movement of the particle becomes quick enough to create a cavitation in which gaseous ionization may take place.

Within the conditions of the present investigation it can be concluded that, when this particular state is reached, ionization occurs whatever the pressure of the gas dissolved in the oil, provided this is not higher than a pressure approximately equal to the atmospheric pressure.

Tests not reported in this paper indicate that when the gas pressure is higher than atmospheric the breakdown strength does not remain constant but tends to rise above 400 kv/cm rms. This suggests that in this condition gaseous ionization does not follow immediately when the cavitation onset level is attained but that a higher field is required to pro-

duce bubbles of such a dimension to cause ionization of the gas evolved in the cavity.

Acknowledgment

The authors are grateful to Pirelli S.p.A. for permission to publish the present paper and to Mr. Mazzola for carrying out the laboratory tests.

Manuscript received Feb. 23, 1960. This paper was prepared for delivery before the Philadelphia Meeting, May 3-7, 1959.

Any discussion of this paper will appear in a Discussion Section to be published in the June 1961 JOURNAL.

REFERENCES

1. F. M. Clark, *J. Franklin Inst.*, **215**, 39 (1933).
2. F. M. Clark, *Elec. Eng.*, p. 50 (January 1935).
3. B. Salvage, The Inst. of Electrical Engineers, *Monograph 2*, (May 15, 1951).
4. T. J. Lewis, *Proc. Inst. Elec. Eng.*, **100**, part II, 141 (1953).
5. P. K. Watson and J. B. Higham, *ibid.*, **100**, part II, 168 (1953).
6. J. L. Maksiejewski and H. Tropper, *ibid.*, **101**, part II, 183 (1954).
7. K. A Macfadyen, *British J. Appl. Phys.*, **6**, 1 (1955).
8. A. H. Sharbaugh, J. K. Bragg, and R. W. Crowe, *J. Appl. Phys.*, **26**, 434 (1955).
9. T. J. Lewis, *ibid.*, **27**, n. 6, 645 (1956).
10. (Laboratoria N. V. Philips' Gloeilampenfabrieken, Eidenhoven, Holland)—J. A. Kok and M. M. G. Corbey, Applied Scientific Research B 6, p. 197-206 (1956).

Electropolishing in Cyanide Electrolytes

F. Sullivan and E. H. Newton

Arthur D. Little, Inc., Cambridge, Massachusetts

ABSTRACT

Mirrorlike polished surfaces can be obtained on silver, sterling silver, gold alloys, copper, and brass by electropolishing in cyanide electrolytes. The optimum current density and agitation rate to obtain a brilliant polish varies widely with the metal being polished. For silver and silver plate a current density range of 1.1-2.8 ASD at 45 cm/min is necessary; for copper and brass the range is 2-8 ASD at 1300-2600 cm/min. Agitation is not critical in gold alloy electropolishing because the very high current density (>250 ASD) induces copious gassing. Rapid periodic movement of sterling silver into and out of the polishing bath within a current density range of 10-16 ASD is required to mirror polish this alloy.

Anyone who has observed the anodes in a copper or silver cyanide plating bath may have noted the different appearance they assume at various times, dull and etched, bright or filmed. These surface changes represent the three conditions important in characterizing the events taking place at the anode during electropolishing, that is, the etching region, the polishing region, and the permanent film region of the voltage-current density relationship.

This paper covers details of the commercial electropolishing of silver plate and pilot plant studies on the electropolishing of sterling. Laboratory electropolishing of gold alloys, copper, and brass is also discussed. All of the studies were carried out in cyanide electrolytes.

The relationship between most of the operating variables encountered in polishing cyanide soluble metals in cyanide electrolytes is most conveniently expressed in the form of voltage-current density or polishing curves. The information necessary to construct a polishing curve is obtained by noting the current passing through the cell and the appearance of the anode while increasing the voltage at 0.2 v increments. In order to start with a uniform surface, a light etch is first produced on the anode. The anode is removed at each voltage step and the degree of etch or polish determined.

Electropolishing of Silver Plate

One series of experiments designed to determine the effect of agitation rate on the shape of the polishing curve was carried out in a bath which was 0.3M with respect to silver cyanide, free potassium cyanide, and potassium carbonate (1). The anode was a silver-plated copper panel rotated at various speeds.

Figure 1 shows typical polishing curves for silver plate at three agitation rates. The polishing zone is indicated by the dotted lines at the letter P. In this area the anode was mirror bright all over. Below the polishing zone the silver surface was dull and etched. Above the polishing zone, the anode assumed a cloudy blue appearance. The broadest polishing range occurred at the intermediate agitation rate. With no agitation the polishing range was very

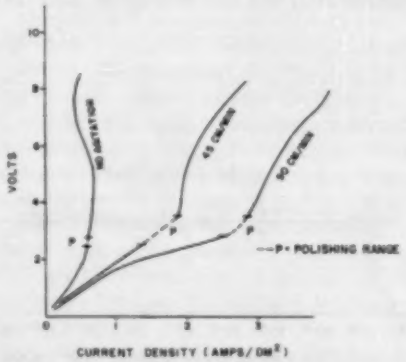

Fig. 1. Typical polishing curves for silver plate at various agitation rates. Bath composition: silver (as metal), 32.4 g/l; KCN (free), 19.5 g/l; K_2CO_3, 42 g/l.

narrow and operating in this range was impractical. At the higher agitation rate the polishing range also narrowed.

Temperatures ranging from 10°-50°C had only minor effects on the polishing results obtained. In general, the higher the temperature the higher the current density at a given voltage. This would be expected from the increased conductivity. While good polishes could be obtained at higher temperatures, the results showed no improvement over those obtained at room temperature. At the higher temperatures, polishing was more difficult to control because of slight etching action after the current had been cut off. Cyanide breakdown was more rapid at higher temperatures. At low temperatures, throwing power appeared somewhat improved.

Commercial electropolishing of silver plate.—Silver plate has been electropolished commercially by several large silver companies on both continuous and batch installations (2). Electropolished surfaces of high quality have been produced on such materials as costume jewelry, novelties, holloware, and flatware. The electropolishing solution most generally used commercially is shown in Table I (3). The cathodes may be either silver or stainless steel with an area at least twice than of the anodes. The work should pass through the bath by either straight line or reciprocal motion at a rate of approximately 45 cm/min. The voltage is generally between 2.5 and 3.5, but these limits may be extended in either direction where conditions demand. The current density is in the range of 1.1-2.8 amp/dm^2 (4).

When the correct polishing conditions exist, a uniform brown film forms on the anode remaining there throughout the polishing cycle. The agitation must be smooth to protect this anodic film which is essential for optimum leveling and brightness. It is believed that this polishing film permits the selective dissolution of the projections or irregularities in the plate thus producing leveling and brightening.

In the continuous flatware process used by a large silver company, spoons, forks, and other articles are mounted in racks and conveyed through a typical cleaning and plating cycle (5). After the plating rinse and pre-dip operations, they pass through an electropolishing bath of the composition previously described. The work moves through the bath at approximately 45 cm/min and remains in the solution about 20 sec. Rinse and pre-dip cycles are advisable, because without these, the drag-in of silver plating solution will rapidly change the composition of the polishing bath and necessitate frequent analysis and adjustment.

Table I. Bath composition and conditions for electropolishing silver plate

Composition	Grams/liter
Silver (as metal)	32.8
Free potassium cyanide	19.5
Potassium carbonate	41.5
Polishing conditions	
Voltage	2.5-3.5
Current density	1.1-2.8 amp/dm^2
Agitation rate	45 cm/min
Temperature	ambient

Holloware.—Silver-plated holloware has also been successfully electropolished by several large silver companies. Articles such as trays, coffee pots, creamers, Paul Revere bowls, baby cups, and many other items have been polished commercially with excellent results. In general, polishing conditions are essentially the same as those for polishing flatware, except the polishing time usually ranges from 1 to 1½ min and the agitation should be reciprocal. Articles to be electropolished should be racked so as to allow the least resistance or turbulence as they pass through the bath.

In articles such as deep bowls, it may be necessary to adjust the distance between the cathodes and anode to obtain maximum throwing power. In some instances internal anodes are necessary for polishing deeply recessed surfaces.

In a few cases, "thieves" have been used to protect certain areas from receiving too much current. These points of high current density, unless shielded, will have a smoky blue appearance.

Advantages and Limitations.—Let us consider a few of the advantages of electropolishing silver. Hand buffing is a slow, expensive, dirty operation. By electropolishing, wheel finishing costs can be reduced from 20 to 100% depending on the class of the article. The 100% figure may sound a bit strange but in costume jewelry and some special lines wheel finishing has been eliminated completely. Electropolishing is ideal for intricate shapes or filagree work where buffing is extremely difficult or impossible. The saving in refining costs compared to the savings realized by refining of buffing dust is appreciable. The silver removed from the work plates out on the cathodes and is recovered in pure metallic form.

Electropolishing in cyanide is a short operation, and many pieces can be processed at one time. Finished articles have more silver more uniformly distributed on them than their buffed counterparts. If properly carried out, it is possible to obtain as high a luster by the removal of 2% of the silver deposit as would be possible by removing 5-10% by hand buffing.

One of the outstanding advantages in electropolishing holloware is the excellent brightness which results in difficult to buff areas such as the inside of handles. The saving in finishing costs and the other advantages previously mentioned in the electropolishing of flatware also apply to holloware.

Although in certain applications a saleable finish can be produced directly from the tank, electropolishing does not necessarily eliminate all finishing operations. Electropolishing cannot exactly duplicate a finished buffed surface. In the field of flatware, for instance, esthetic requirements often demand that the brilliant electropolished glitter be toned down or softened. This would necessitate a wheel operation.

The quality of the plate and the conditions of the basis metal have a marked influence on the resulting polish. The amount of silver removed is generally so small that imperfections in the base

are not eliminated. In fact, the high luster tends to accentuate flaws. Good pre-plate finishing and a smooth electrodeposit are prerequisites for good electropolishing.

There was considerably more interest in electropolishing silver plate ten years ago than at the present time. The popularity of electropolishing now appears to have diminished appreciably due to the advent of several of the modern proprietary bright silver plating baths. Electropolishing does, however, have its place in certain applications such as the continuous production of silver flatware where control of the polishing bath is not as critical as the control of the bright plating bath.

Sterling Silver

In the laboratory sterling silver has been electrolytically polished to a specular brightness in a cyanide bath. Mirror bright polishes have been obtained on flatware, holloware, costume jewelry, and other commercially produced sterling articles (6). Because of certain difficulties which will be discussed later, the electropolishing of sterling has not yet progressed beyond the pilot plant stage.

The bath composition was only slightly different from that used for electropolishing silver plate, but the form and speed of agitation differ greatly. The recommended bath is shown in Table II and was operated at room temperature. The anode, or work, was agitated by repeated immersions and withdrawals from the solution. The cycle of anode movement may be termed a stroke, and the work was lifted clear of the solution with each stroke. This had the effect of cutting the current on and off. The best polishing occurred at current densities between 10 and 16 amp/dm^2 at a potential of from 2.5 to 12 v. The agitation was at least 20 strokes/min and the polishing time approximately 1½ min. Articles were positioned on the racks so as to produce the least turbulence.

The exact reason for the marked improvement in the polishing of sterling silver when repeatedly removed from the solution is not known. Exposure of the film to air may allow the cupric ion formed by evolution of oxygen during the anodic process to be reduced by the cyanide to the more stable cuprous state. Removal of the work from the bath and the consequent draining of excess cyanide could assist in reestablishing the polishing film. The film formed on copper during polishing in cyanide solutions is not as readily dissolved as the film formed on silver. Consequently, the rate of agitation during the polishing of alloys containing copper must be considerably higher than during the polishing of pure silver to increase the cyanide ion concentration of the anodic film. Agitation in the solution without the dunking action is not sufficient to polish sterling. Figure 2 shows typical polishing curves for sterling silver at various agitation rates. Good polishing was noted only in the dotted areas designated by the letter P. Below this area is the etch region and above is the permanent film zone. At the higher agitation rates, the polishing range is extremely broad.

Table II. Bath composition and conditions for electropolishing sterling silver

Composition	Grams/liter
Silver (as metal)	32.8
Free potassium cyanide	26-32
Potassium carbonate	41.5
Polishing conditions	
Voltage	2.5-12
Current density	10-16 amp/dm^2
Agitation rate	20-100 strokes/min
Temperature	ambient

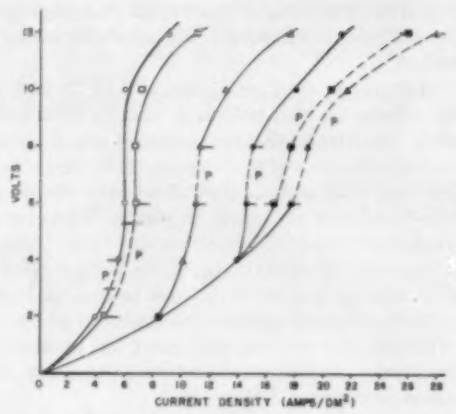

Fig. 2. Polishing curves for sterling silver at various agitation rates. - - P = polishing range; length of stroke = 26 cm. Agitation rate: ○, 10 strokes/min; □, 20 strokes/min; △, 40 strokes/min; ●, 60 strokes/min; ■ 80 strokes/min; ▲, 100 strokes/min.

Interrupting the current without withdrawal of the anode from the solution will result in semi-bright etched surfaces. For example, a piece of sterling with an area of 24 cm^2 was immersed in a bath at 5 v, and the current was turned on and off at a rate of 30 times/min. A brown film appeared and disappeared with the current. At the end of 2 min the sample was semi-bright and etched. Turning the current on and off 60 times/min did not improve the brightness.

A series of experiments was carried out to determine the behavior of sodium and potassium salts in sterling silver polishing baths. Three compositions were investigated: (*a*) containing mixed sodium and potassium salts, (*b*) containing all sodium salts, and (*c*) containing all potassium salts. Figure 3 shows the effect of these cations on the shape and position of the polishing curve. The potassium bath (No. 3) polished at a lower voltage but higher current density than the other two solutions. The composition containing all sodium ions produced the poorest polish. The best polish was noted in the straight potassium bath.

An interesting application is in controlling the weight of sterling while polishing takes place. In the laboratory seven sterling silver soup spoons were suspended from a rack and repeatedly immersed and withdrawn from the polishing bath at a rate of 30 times/min. Five volts was applied at a current density of 15 amp/dm^2. The original weight of the spoons was 304.3 g, but after several minutes of operation the weight was reduced to 278.3 g. The

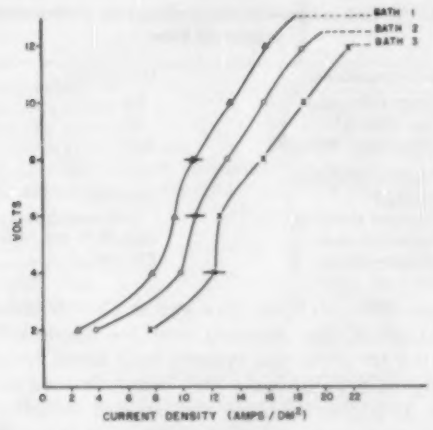

Fig. 3. Polishing curves for sterling silver in various bath compositions; polishing above line, etch region below line; agitation, 60 strokes/min. Composition (g/l): bath 1, 2, 3, AgCN, 40.2; bath 3, KCN, 26; bath 1,2, NaCN, 19.6; bath 1,3, K_2CO_3, 41.5; bath 2, Na_2CO_3, 31.8.

spoons were all very bright and required no mechanical buffing to attain further brilliance.

The sterling silver polishing bath will remove fire scale. This method has many obvious advantages over the nitric acid solution commonly used for this purpose.

Pilot plant studies.—In a 100-gal sterling polishing bath installed at one of the large sterling silver companies, thousands of pieces of flatware and holloware were electropolished to determine the utility of the bath. The brightest polishes were obtained on flatware, and more than 5000 pieces were processed. Although bright polishes could be obtained, difficulty was encountered in pit removal. For example, in manufacturing flatware from heavy wrought material the forming hammer closes up many defects present in the stock. Electropolishing tends to open up these defects. In polishing holloware, the immersing and withdrawing operation sometimes created drainage and racking problems. However, after a 6-month operating period, the bath was still performing well, a fact which indicates that there was no stability problem.

As a result of this study and subsequent laboratory work, it is felt that the process is most suitable for polishing specialty items such as trays or coffee pots and small articles such as costume jewelry. Approximately 1 hr of finishing time could be saved by electropolishing large sterling trays, and 20 min could be saved by electropolishing coffee pots. Since only a few hundred of these items were made per year, the savings from electropolishing these articles did not justify installing the process. Other applications which appear more promising are weight reduction and the removal of fire scale.

Other Metals

Electropolishing of gold alloys.—The investigation into the electropolishing of gold alloys was carried out as part of a general program for determining the anodic behavior of metals in cyanide solutions. Most of the work was done in 3*N* potassium cyanide solutions to avoid complicating reactions. No attempt was made to develop a practical polishing bath.

All the tests were run in 2-l beakers containing 1 l of solution; a new solution was used for each experiment. Four sheet copper cathodes 8.3 cm x 6.4 cm were hung symmetrically around the sides of the beaker. The samples used were silver-gold and copper-gold binary alloys, (18, 16, 12, and 10 karat). All of the copper-gold alloys looked like copper. The silver alloys varied in color from the bright yellow brass of the 18 karat to the silvery color of the 10 karat. Anodes were 2.54 x 5.08 x 0.16 cm. The cathode to anode ratio was approximately 8:1. The cathode to anode distance was 4.3 cm.

For most of the tests the sample was rotated at 22 rpm in a circle of 4.45 cm diameter which corresponds to a linear speed of approximately 310 cm/min.

The potential was increased stepwise from 0 to 20 v. Each voltage was applied for 30 sec, and readings were taken on the ammeter at the start and after equilibrium had been reached. After every few points the voltage was dropped to the etching region and a very light etch given to the surface so that the previous condition of the surface would not influence the results. In the very high current density regions (220-330 amp/dm^2) the time at each point was shortened to 20 sec so the sample would not be dissolved too rapidly. A small microscope lamp was used to illuminate the specimen while in the bath. The sample was removed from the bath, washed, and dried at each point when any change was observed.

Complete polishing over the whole surface of the samples was obtained only at the higher voltages and current densities. (16-20 v, 240-350 amp/dm^2). All the alloys polished like pure gold in 3*N* potassium cyanide. No good polishing was observed in the voltage range where copper or silver are ordinarily polished.

Voltage-current density curves on these alloys showed only slight differences. With the copper alloys at a given voltage, slightly higher current densities were obtained with decreasing gold content. With the silver alloys the curves showed no correlation with gold content. Figure 4 shows a typical polishing curve for a binary gold alloy.

Individual cases varied somewhat, but to reach the polishing range the general pattern as the voltage was increased was as follows: 1, Linear rise of the current with voltage. No films are present in this region and the surface of the anode is etched; 2, polarization point at which film formation begins; 3, polarizing region in which soluble or loosely adherent films are present. In this region the anode has an etched surface with or without edge polishing; 4, more sloping, less polarized region usually accompanied by soluble films with the surface of the anode partly polished; 5, second etch region with no films and a linear rise of current with voltage; 6, partly polished region with no films and a linear rise of current with voltage; 7, polishing region. Surface of the anode is completely polished. Vigorous gassing is present in this region at both the cathode and anode.

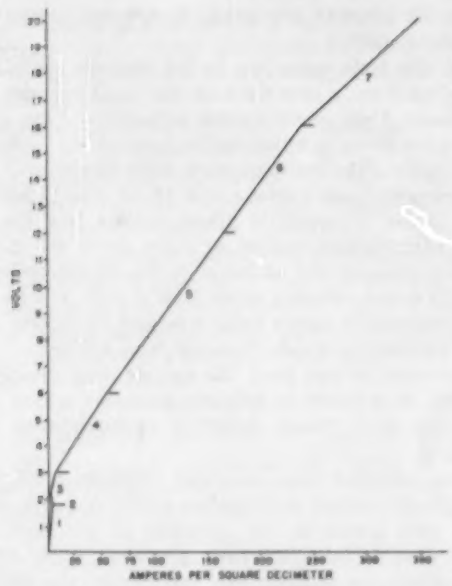

Fig. 4. Typical polishing curves for binary gold alloys; bath composition, 3N KCN; agitation rate, 310 cm/min. Appearance of gold surface: 1, etch; 2, start of film formation; 3, etch and/or edge polishing; 4, part polish, part etch; 5, etch; 6, part polish, part etch; 7, polish.

Agitation of the work was not critical. Comparisons of data obtained in experiments in which the work was not agitated with experiments in which the work was rotated in one direction at 310 cm/min showed only slight differences.

Although all the tests were started at room temperature, no attempt was made to control temperature so by the time a complete curve was plotted, the solution had been warmed up to about 45°C. One experiment was carried out in the reverse order starting with 20 v at room temperature and ending at the low voltage and higher temperature. No significant difference was noted between the curve prepared from this data and the previously described curve. This indicates that temperatures from 20° to 45°C have little or no effect on the polishing curve.

Although most of the work was carried out in 3*N* potassium cyanide solutions, concentrations of 0.3*N*, 1*N*, and 7*N* were also studied. None of these polished as well as the 3*N* solution.

Experiments were also performed with 3*N* sodium cyanide and 3*N* barium cyanide instead of potassium cyanide. The sodium cyanide gave a slightly improved polish at high current densities and voltage. The barium cyanide solution polished similar to the potassium cyanide bath. Current density-voltage curves for these cyanides closely resembled the 3*N* potassium cyanide curve.

Very little change in the quality of polish or current density-voltage curves was obtained by adding the following materials to the 3*N* potassium cyanide bath: additional potassium gold cyanide, copper cyanide, potassium ferrocyanide, potassium ferricyanide. However, the addition of 30 g/l potassium tartrate shifted the polishing range to a lower

Table III. Bath composition and conditions for electropolishing copper and brass

Bath composition:	Grams/liter
Copper cyanide	31
Zinc cyanide	47
Potassium cyanide	126
Polishing conditions:	
Voltage	1.8-3.4
Current density	2-8 amp/dm²
Agitation rate	400-2600 cm/min
Temperature	25°-30°C

voltage. Between 5 and 10 v and at 55-110 amp/dm², a good polish was obtained over the whole surface. With the 3*N* potassium cyanide bath alone, no polish or only part polish-part etch was obtained in this range. At higher voltages and current densities, the tartrate-potassium cyanide bath acted the same as plain potassium cyanide.

Brass and copper polishing.—In the laboratory copper and brass have been electropolished to mirror brightness in cyanide polishing baths. The most brilliant finishes were produced on brasses containing 70% or more copper. Leaded brass could not be polished satisfactorily.

The electropolishing solution which we have found most effective is shown in Table III. Polishing was carried out at a current density of 2-8 amp/dm² at agitation rates ranging from 1300-2600 cm/min. The extremely high rate of agitation was a major problem. On a curved surface where there is streamlined flow, mechanical agitation was possible. However, with flat surfaces and odd shaped items, very fast hand agitation was necessary to produce good polishing. We were unsuccessful in our attempts to duplicate the hand agitation by mechanical means.

Figure 5 shows the effect of three agitation rates on the polishing curves obtained by electropolishing short lengths of red brass pipe in the above bath. The initial "free cyanide" was about 50 g/l and the pH was 12. The pipe was agitated by rotating it in a circular path 7.6 cm in diameter. No polishing occurred at the lowest agitation rate. The best mirrorlike polish was obtained at 2600 cm/min at the knee of the curve, that is, between 2.3 and

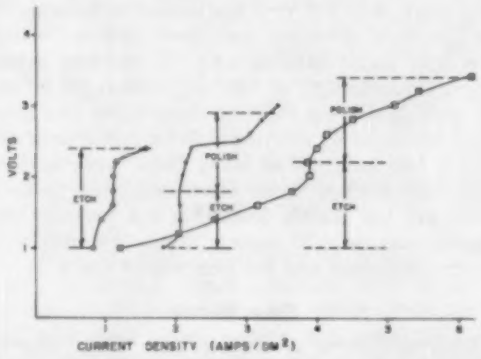

Fig. 5. Polishing curves for red brass at three agitation rates. Bath composition: copper cyanide, 31 g/l; zinc cyanide, 47 g/l; potassium cyanide, 126 g/l; agitation rate: ⊙ 400 cm/min; • 1300 cm/min; dotted square 2600 cm/min; temperature, 27°C.

Table IV. Bath composition and conditions for electropolishing 70/30 brass

Bath composition:	
Potassium cyanide	75 g/l
Potassium tartrate	20 g/l
Potassium ferrocyanide	20 g/l
Potassium dihydrogen phosphate	20 g/l
Conc. ammonium hydroxide	4 ml/l
Operating conditions:	
Voltage	5-6
Current density	25-50 amp/dm²
Agitation rate	very fast hand
Temperature	50°-60°C
Time	3-5 min

2.5 v at about 4 amp/dm². Under these conditions 68% of the metal lost from the polished anode plated out on the copper cathodes.

Pure copper may also be polished in the above bath. An additional stability problem was encountered because the copper tended to build up in the solution while the zinc was being depleted. The addition of a zinc anode remedied this, permitting brass to plate out during the electropolishing operation, thus maintaining the desired solution balance. Occasional readjustments of the copper and zinc concentration and close control of "free cyanide" were necessary for continued operation of the bath.

The quality of an electropolished surface depended to a great extent on the grain size of the metal. The effect of grain size of 70/30 brass on the resulting polish was noted in a series of experiments carried out in the polishing bath shown in Table IV. The composition of this solution departed considerably from that used in previous research and was similar to the type of bath used in brightening or stripping solid gold rings (7). The bath was operated at a higher temperature and current density than the bath described previously. Brass did not plate out at the cathode so periodic analysis of the bath was necessary for continued operation.

Five panels of 70/30 brass with grain sizes varying from 0.010 to 0.075 mm and hardnesses ranging from ½ hard, ¼ hard, and soft were polished for 3 to 5 min using very fast hand agitation. A uniform polish could be produced only on panels that were bent into a semicircle. Although all panels were polished to some degree, rolling marks were not completely removed in any case. The panels with the smallest grain sizes were polished to a mirror bright state. The polish on the larger grain size brass samples was decidedly inferior. The hardness of the panels had no effect on the quality of the polish.

Acknowledgment

The investigation of the electropolishing of silver, sterling silver, and gold alloys was sponsored by Oneida Limited. The authors wish to thank Arthur D. Little, Inc., and Oneida Limited for permission to publish this data.

Manuscript received May 11, 1960. This paper was prepared for delivery before the Columbus Meeting, Oct. 18-22, 1959.

Any discussion of this paper will appear in a Discussion Section to be published in the June 1961 JOURNAL.

REFERENCES

1. S. E. Eaton (to Oneida Ltd.), U.S. Pat. 2,610,144, Sept. 9, 1952.
2. D. Gray and S. E. Eaton, *Metal Finishing*, **45**, 60 (1947).
3. S. E. Eaton (to Oneida Ltd.), U.S. Pat. 2,416,294.
4. S. E. Eaton (to Oneida Ltd.), U.S. Pat. 2,610,143, Sept. 9, 1952.
5. D. Gray, *Metal Finishing*, **47**, 55 (1949).
6. F. Sullivan (to Arthur D. Little, Inc.), U. S. Pat. 2,661,330, Dec. 1, 1953.
7. J. B. Kushner, *Prods. Finishing*, p. 44, Nov. 1942.

Particle Growth during Zinc Sulfide Phosphor Preparation

A. Kremheller[1] and S. Faria

General Telephone and Electronics Laboratories, Incorporated, Bayside, New York

ABSTRACT

The influence of processing conditions, such as time and temperature, and the effect of fluxing agents on the particle size and concomitant properties observed during zinc sulfide phosphor preparation are reported. The particle size increases exponentially with the reciprocal firing temperature and as the square root of the firing time when phosphors are prepared in open boats; the activation energy and frequency constant depend on the flux employed. A particle size anomaly is observed when zinc sulfide powder containing zinc chloride is processed near 1000°C in sealed quartz vials. This anomaly, which can be ascribed to the Hedvall effect, is accompanied by anomalies in chloride retention and crystal structure.

Commercial zinc sulfide phosphors are usually prepared by heat treatment of the host material in the presence of an activator and a coactivator (1). The average particle size of the zinc sulfide crystallites increases during this treatment, and the final particle size depends on the processing conditions and the additives. Tiede and Schleede (2) observed that the fluxing agent promotes crystal growth at low temperatures by lowering the melting point of the base material. A few years later Schleede and Gantzckow (3) proposed that a thin film of the fluxing agent dissolves small particles of the base material, and that subsequent precipitation takes

[1] Present address: Republic Aviation Corp., Farmingdale, N. Y.

place on large particles with concomitant increase of the average particle diameter.

Work and Odell (4) discussed particle size and the growth mechanism during heat treatment of zinc sulfide powder and observed that the development of pigment properties of zinc sulfide is closely related to changes in particle size. The authors indicated that their experimental data agree quite well with the theory of growth by vaporization; they also pointed out that the theoretical considerations are quite similar for particle growth by dissolution and subsequent reprecipitation. They found that the particle size is primarily a function of the processing temperature, and only secondarily of time. Leverenz (5) established that zinc sulfide crystals grow in approximate proportion to exp $(-E/kT)$, where E is the activation energy connected with the growth process. The growth rate decreases with increasing time because the crystals approach a size distribution that is determined largely by the temperature and by the nature and sizes of the initial particles. Bube (6) confirms that the particle size varies exponentially with the reciprocal of the processing temperature and finds an activation energy of 1.3 ev for the host material without additives. Shionoya and Amano (7) showed that the change of the particle volume with processing time is proportional to the reciprocal processing temperature. The proportionality constant is considered to contain the activation energy, which is nearly three times as high without as with the fluxing agent. They found that the increase of the particle volume with time t is constant at constant temperature, which is not in agreement with our results (8) which lead to a $t^{1/2}$ dependence, as explained in the discussion section.

The present paper deals with the influence of time and temperature of heat treatment and the effects of various additives on particle size, crystal structure, and luminescence of zinc sulfide powder. This includes processing in open boats and sealed quartz vials, study of the final product, and elucidation of the growth mechanism as a function of experimental conditions. The implications of the experimental data as to the influence of the various processing parameters on particle growth and related properties are discussed.

Experimental

The zinc sulfide powder and the additives used in these experiments were essentially free of heavy metals to the limit of spectrographic detectability. The zinc sulfide powder contained about 0.45% by weight of sulfate and less than 0.002% of chloride.

The samples are kept in transparent quartz boats and heated in transparent quartz combustion tubes in an atmosphere of helium during open-boat processing; the linear flow rate was about 1 cm/min. Another series of experiments was conducted with sealed evacuated quartz vials containing the base material and the source of the coactivator. The purpose of using sealed vials was to keep the flux concentration constant during the heat treatment.

A simplified gas adsorption method, microscopic counting, x-ray analysis, and electron photomicrography were employed in determining the particle size and the crystal structure, as discussed previously (9). The same publication (9) also describes a semi-quantitative method which was employed in the present investigation to obtain a measure of photoluminescence intensity. The determination of chloride has been discussed in some detail in a previous publication (10). This method permits one to determine quantitatively amounts of 0.001% by weight of chloride in 1 g of zinc sulfide; results have been found to be reproducible and accurate.

Results

Particle growth studies are of interest by themselves and are a first step in controlling the particle size so that phosphors of a given particle size can be prepared. For instance, a given particle size can be attained by processing the powder at low temperature for a long time or at high temperature for a short time; proper selection of processing conditions will depend on other requirements on the final product.

While the processing conditions are important with respect to particle growth, it is well understood that the initial particle size and the size distribution also have to be considered, especially, when zinc sulfide powder is processed at low temperature and/or for very short times. For this reason, our experimental conditions have been selected in such a manner that the initial particle size can essentially be neglected with respect to the final size. In the present study the average initial particle diameter was 0.02 μ, and the final diameter was at least ten times as large.

In order to study the influence of the flux and processing conditions without additional complications, activators were not added. The experiments and results are arranged in two sections. The first part presents phosphor processing in open boats, while the second part deals with the study of material preparation in sealed quartz vials.

Phosphor Preparation in Open Quartz Boats

Zinc sulfide powder without flux addition was processed at temperatures from 200° to 1250°C for up to 40 hr in open boats. It was found that the average particle size increases exponentially with the reciprocal of the processing temperature, as is implicit for a typical case in Fig. 1. In another series of experiments, the processing temperature was

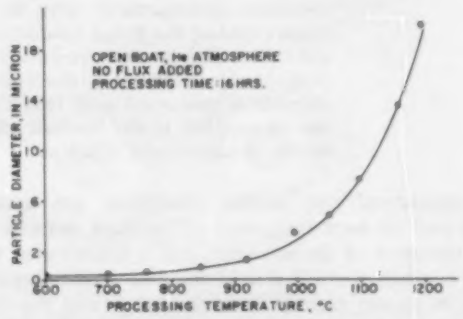

Fig. 1. Average particle diameter as a function of processing temperature.

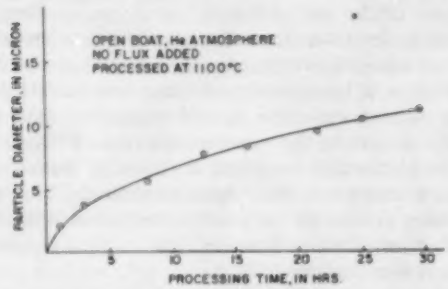

Fig. 2. Increase of average particle diameter with processing time.

kept constant and the processing time was varied. A typical result of this study is presented in Fig. 2. The curve corresponds to the hypothesis that the particle size increases with the square root of the processing time. Accordingly, the average particle diameter X can be expressed[8] as a function of processing temperature T and time t by the equation:

$$X \cong At^{1/2} \exp(-a/T) \qquad [1]$$

Equation [1] contains the constants A and a, which are found to be $A = 3.15 \times 10^4$ micron hr$^{-1/2}$ and $a = 1.25 \times 10^4$ °K, when no coactivator is added.

X-ray diffraction analysis indicates that the originally cubic zinc sulfide powder is transformed into the hexagonal form when processed above 1100°C. At processing temperatures below 900°C the processed material is cubic, while amounts of hexagonal phase that increase with the temperature are found in the intermediate interval. The samples exhibit some luminescence if they are processed above 1000°C.

In another series of experiments, various amounts and kinds of fluxes were added. It was found that the fluxing agent changes the constants A and a in Eq. [1]. Effective fluxing agents lower the value of a, which may be interpreted as a decrease in the activation energy needed for the growth process. Figure 3 represents data that are in good agreement with Eq. [1]; the experimental points are plotted for zinc sulfide without flux and with 2% by weight of NaCl processed for 2 hr at various temperatures. The constants in Eq. [1] are $A = 2 \times 10^5$ micron hr$^{-1/2}$ and $a = 7.5 \times 10^3$ °K when 2% NaCl is used as the additive. The same Eq. [1] is obeyed when 5% by weight of zinc chloride or 0.8% of coprecipitated chloride are present (see also Fig. 3).

Phosphor Preparation in Sealed Quartz Vials

In order to keep the concentration of the fluxing agent constant, zinc sulfide powders with flux addition were heat-treated in sealed quartz vials. In one series of experiments a constant amount of various halides was added before processing for 3 hr at 850°C. The purpose of this study was to compare qualitatively the influence of various halide anions and of the cations zinc and sodium on particle growth and attendant properties. Figure 4 shows photomicrographs of zinc sulfide processed with 0.007 gram atom of halide per mole zinc sul-

[8] The left side of Eq. [1] is equal to $(X^2 - X_o^2)^{1/2}$ which has been approximated by X since $X > X_o$.

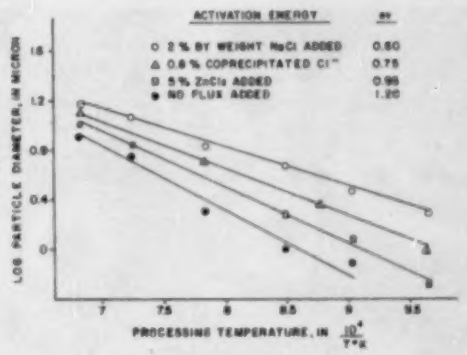
ACTIVATION ENERGY
○ 2 % BY WEIGHT NaCl ADDED 0.50
△ 0.8 % COPRECIPITATED Cl⁻ 0.75
□ 5 % ZnCl₂ ADDED 0.99
● NO FLUX ADDED 1.20
LOG PARTICLE DIAMETER, IN MICRON
PROCESSING TEMPERATURE, IN 10⁴/T°K

Fig. 3. Dependence of average particle diameter on reciprocal processing temperature; fluxing agent as the parameter.

fide. Zinc sulfide with sodium halide leads to a growth habit in the form of triangular plates, while zinc halides lead to spherical polyhedra, similar to those observed without coactivator. Table I presents data on these samples. It is seen that the average particle diameters of samples with sodium halide addition are larger than those with zinc halide addition. The sodium halides favor the formation of cubic structure; however, one also observes that the cubic samples are larger in particle size than the partially hexagonal samples. It appears that flux action leading to large particles requires that the sodium halide be liquid. While there are considerable variations from sample to sample in various properties, the zinc halides are essentially as effective as the sodium halides with respect to the photoluminescence intensity.

Another series of experiments yielded quite unexpected results, when 0.25% by weight of zinc chloride was physically admixed to zinc sulfide in sealed vials which were subsequently heat-treated for various times and temperatures. Equation [1] is not valid in this case, because one observes a peak in particle size as a function of processing temperature near 1000°C, as shown in Fig. 5. The curve in Fig. 5 shows the dependence of the particle size on the temperature of processing from 800° to 1200°C for a processing time of 4 hr; the curves for 2, 8, and 16 hr, which are not shown, vary in absolute particle size while their general shape is the same. The anomalous peak near 1000°C is accompanied by anomalous behavior with respect to the crystal structure and the amount of retained volume chloride,[9] as shown in Fig. 5. It was found that these

[9] See definition of "volume chloride" in ref. (10).

Table I. Some properties of zinc sulfide powders with 0.007 g atom of halide per mole of zinc sulfide added, and processed in sealed, evacuated quartz vials for 2 hr at 850°C

Halide added	Average particle diameter, μ	Ratio of hex.: cubic	Blue photoluminescence, relative	Melting point of halide, °C
NaF	1	1:9	44	992
NaCl	10	0:10	680	801
NaBr	14	0:10	647	755
NaI	8	0:10	357	651
ZnF_2	<1	2:8	2	872
$ZnCl_2$	1	2:8	765	262
$ZnBr_2$	<1	3:7	790	394
ZnI_2	3	0:10	753	446

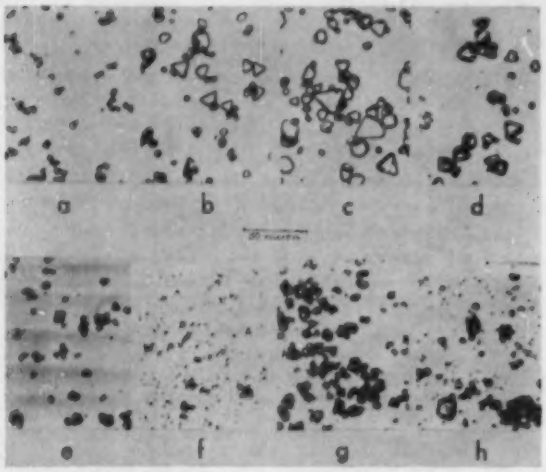

Fig. 4. Zinc sulfide powders with 0.007 g atom of halide per mole of zinc sulfide added and processed for 3 hr at 850°C in sealed quartz vials; the added halides are: a, NaF; b, NaCl; c, NaBr; d, NaI; e, ZnF_2; f, $ZnCl_2$; g, $ZnBr_2$; and h, ZnI_2.

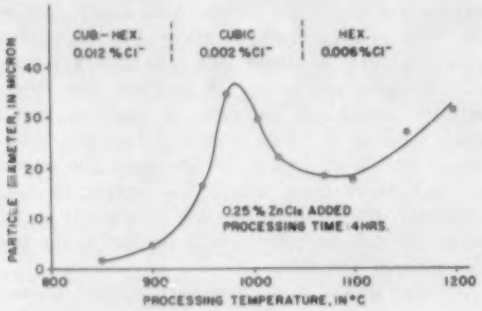

Fig. 5. Anomalous particle growth and attendant chloride retention and crystal structure in sealed quartz vials.

zinc sulfide phosphors contain some hexagonal structure even at processing temperatures below 950°C, while the pure hexagonal structure occurs above 1050°C and pure cubic structure is found in the intermediate range. The amount of retained volume chloride is lowest in the region of the anomalous peak. It appears that the anomaly near 1000°C can be explained as being due to the Hedvall[4] effect (11), since one observes a considerable amount of randomness in the crystal structure of zinc sulfide crystals (especially for those of cubic structure) that are annealed at this temperature (12). The degree of randomness was found to be enhanced considerably during annealing in the presence of halide when compared with samples containing no additives. A series of samples without additives was used as a blank; in this case the anomalous growth peak was absent.

It appears that the randomness in the crystal structure seems to facilitate crystal growth near 1000°C while the degree of incorporation of chloride is actually decreased. One may also conclude that the low concentration of volume chloride in particles processed near 1000°C can be interpreted by assuming that the growth rate is increased by randomness while the diffusion or incorporation of chloride is lowered. It is also possible that chloride is incorporated by diffusion alone and that the diffusion rates in hexagonal and cubic zinc sulfide may differ. In that case one would expect to find the largest amount in the smallest particles because of their large surface area and in those of hexagonal structure because of their open structure. These observations appear to be closely connected with the fact that chloride influences the cubic-hexagonal structure equilibrium (12).

[4] The Hedvall effect ascribes similar anomalies to the increased chemical reactivity near a transition point.

Summary and Discussion

As part of commercial phosphor preparation zinc sulfide powder is submitted to a heat treatment process during which the particle size increases. The average particle diameter is found to increase with the square root of the processing time and exponentially with the reciprocal of the temperature during phosphor preparation in open boats. The growth process is related to the tarnishing reaction, corrosion processes, and similar diffusion-limited growth phenomena (13). For instance, the same exponential dependence of the growth rate on the temperature has been found by Keck (14) for the growth of selenium films in vacuum. The time dependence of particle growth with $t^{1/2}$ has been found, for instance, for $Ba(OH)_2$ on BaO by Jahoda (15) and for germanium oxide films by Lukes (16).

The growth Eq. [1] can be derived theoretically if one considers the particle growth as a quasi-chemical reaction (17). The derivation, which is not discussed here, leads to an expression for a diffusion-limited process. Constant a in Eq. [1] can be interpreted as being equal to the activation energy E for the growth process divided by the Boltzmann constant k. The constant A is then found to be proportional to the concentration of molecules, ions, or atoms in the gaseous phase and inversely proportional to the concentration of mobile molecules in the solid substance. These concentrations and the activation energy may be modified by the presence of additives, so that one would expect, in agreement with our experiments, a variation in a and A with the kind of additive employed. Since additives that are solids at the processing temperature do not affect the particle growth significantly (see NaF-addition in Table I), one may assume that the vapor pressure of the additive must be fairly high in order to be effective in stimulating particle growth. The concentration of the additive appears not to be critical, because in open boats a considerable amount of the additive is lost (10) with processing time and temperature, and the values of a and A in the growth Eq. [1] do not change, as can be seen in Fig. 3.

It is interesting to find that Shionoya and Amano (7) obtained activation energies without an additive and with 2% NaCl added, which are about 2 to 3 times larger than our values. The explanation of this discrepancy is quite simple, since one finds that they consider the particle volume rather than the diameter. In this case the growth Eq. [1] is essentially raised to the third power, so that the activation energy for volume growth should be three times

that for linear growth. According to Eq. [1] the volume should be proportional to $t^{3/2}$, while Shionoya and Amano (7) found a linear dependence between particle volume and the processing time t. It appears that the difference in time dependence can be ascribed to the limited range of experimental conditions that Shionoya and Amano (7) considered.

The other series of experiments in sealed quartz vials which led to the observations of the anomalous behavior near 1000°C has been discussed in the result section. The Hedvall effect (11) offers a possible explanation for the growth anomaly; however, there has to be some additional influence and/or interaction to account for the anomalies in crystal structure and chloride incorporation in the case of sealed vials, because none of the above three anomalies has been observed when processing was conducted in open boats.

It is quite apparent that many problems in this field require further study. The present experimental investigation has led to a growth equation which explains certain results. On the other hand, it is also clear that the growth Eq. [1] can only be considered to be an approximation which does not apply in certain cases. It is expected that future investigations will lead to a better understanding of the anomalous behavior, the growth process and phosphor preparation which may finally contribute to the synthesis of novel or improved phosphor materials.

Acknowledgment

Grateful acknowledgment is made to D. J. Bracco, A. K. Levine, P. Goldberg, V. C. Brophy, C. F. Tufts, and other colleagues for their generous contributions and many helpful discussions. Thanks are due J. T. Ragusin for valuable assistance with the experimental work.

Manuscript received April 25, 1960. This paper was presented in part at the Cincinnati Meeting, May 1-5, 1955.

Any discussion of this paper will appear in a Discussion Section to be published in the June 1961 JOURNAL.

REFERENCES

1. H. W. Leverenz, "Luminescence of Solids," John Wiley & Sons, Inc., New York (1950).
2. E. Tiede and A. Schleede, *Berichte*, **53**, 1921 (1920).
3. A. Schleede and H. Gantzckow, *Z. physik. Chem.*, **106**, 37 (1923).
4. L. T. Work and I. H. Odell, *Ind. Eng. Chem.*, **25**, 411, 543 (1933).
5. H. W. Leverenz, *Science*, **109**, 183 (1949).
6. R. H. Bube, *J. Chem. Phys.*, **20**, 716 (1952).
7. S. Shionoya and K. Amano, *J. Chem. Soc. Japan*, **77**, 303 (1956).
8. A. Kremheller, D. J. Bracco, and P. Goldberg, Particle Size and Structure of Fired Zinc Sulfide Powders, presented at the Cincinnati Meeting, May 1955.
9. A. Kremheller, S. Faria, and A. K. Levine, *This Journal*, **107**, 753 (1960).
10. A. Kremheller, S. Faria, P. Goldberg, and D. J. Bracco, *ibid.*, **107**, 749 (1960).
11. J. A. Hedvall and L. Leffler, *Z. anorg. u. allgem. Chem.*, **234**, 235 (1937).
12. A. Kremheller, *Sylvania Technologist*, **8**, 11 (1955).
13. C. Wagner, *Z. physik. Chem.*, **B21**, 25 (1933).
14. P. H. Keck, *J. Opt. Soc. Am.*, **42**, 221 (1952).
15. F. C. Jahoda, *Phys. Rev.*, **107**, 1261 (1957).
16. F. Lukes, *Czechosl. J. Phys.*, **8**, 491 (1958).
17. G. N. Lewis and M. Randall, "Thermodynamics and the Free Energy of Chemical Reactions," McGraw-Hill Book Co., New York (1923).

Electroluminescence Maintenance

W. A. Thornton

Lamp Division, Westinghouse Electric Corporation, Bloomfield, New Jersey

ABSTRACT

The maintenance of several electroluminescent phosphors, mainly of the ZnS:Cu,Cl type, has been investigated. Data are given illustrating its dependence on phosphor properties, such as copper and chlorine additions, firing temperature and particle size, on conditions of operation, and on lamp construction. Changes in properties other than light emission and recent maintenance improvements are described.

Electroluminescence (1, 2) shows a characteristic slow decrease in light emission, in common with all other practical light sources, over long periods of operation of the lamp. Improvements in the maintenance of electroluminescence have kept pace with increases in brightness and efficiency and have required knowledge of the dependence of electroluminescence maintenance on phosphor properties, conditions of operation, and lamp construction. It is the purpose of this paper to describe the influence of these factors on electroluminescence maintenance. Electroluminescent phosphors have not changed basically from the type discovered by Destriau (3, 4) in 1936, and consist typically of zinc sulfide activated by copper and chlorine. The ZnS:Cu,Cl and ZnS:Cu,Mn,Cl phosphors are in most general use, and it is to these that the data to follow primarily refer.

Electroluminescence maintenance has been the subject of three previous papers. Observations on photoluminescence, dark capacitance and conductance, photoconduction, wave form, and low-temperature deterioration of light emission were related by Thornton (5) (Paper I) to the typical maintenance (brightness-time) curve by assuming field-diffusion of traps or donors within the phosphor

crystal. Roberts published a paper (6) (Paper II) based in part on results obtained much earlier (7), in which he gives an empirical relation accurately describing typical brightness-time behavior, gives some data on voltage and frequency dependence of maintenance, and also concludes that deterioration is due to physical processes within the phosphor grain. Deep traps appearing in the phosphor crystal during deterioration are ascribed by Thornton (8) (Paper III) to incoming oxygen ions; the presence of the deep traps was indicated by thermoluminescence measurements and by the fact that brightness-voltage changes with deterioration could be reproduced by firing into the phosphor deep-trap-producing impurities such as In, Cd, and Ga, and could be removed temporarily simply by heating the deteriorated lamps. That oxygen is involved was indicated by similar thermoluminescence behavior of oxygen (9) in ZnS, by the fact that the brightness-voltage changes with deterioration could also be reproduced by firing small amounts of ZnO into the ZnS phosphor, and by the appearance of free zinc (10) on the phosphor crystals during electroluminescence deterioration.

Most of the data presented in this paper were obtained from conventional electroluminescent lamps which consist of phosphor powder dispersed in a plastic dielectric material (polyvinyl chloride acetate) at room temperature. When organic materials are used as the dielectric, the lamp is subjected to temperatures no greater than 50° to 100°C. Therefore, all the data presented here are characteristic of electroluminescent phosphor powders as prepared. In the case of ceramic lamps, which are subjected to processing temperatures in the neighborhood of 600°-700°C, profound changes occur in the phosphor during this processing and its electroluminescence properties are altered; no consideration is given here to the ceramic type of electroluminescent lamp.

II. Results

A. Dependence of Maintenance on Phosphor Properties

1. Copper and chlorine additions.—ZnS:Cu,Cl phosphors showing blue electroluminescence are known to have much poorer maintenance characteristics than similar phosphors of the same type which show green emission. It is of interest, practically, to determine the dependence of electroluminescence maintenance on the proportions of added copper and chlorine in phosphors[1] made at constant firing temperature and covering a wide range of copper and chlorine additions. The phosphor samples, about forty in all, were sprayed on conducting glass. The phosphor/plastic (Ucilon[2]) weight ratio was unity, gross thickness of the finished lamps was about two mils, and they were coated with evaporated aluminum to form the rear electrode. The lamps were mounted in good thermal contact with a massive metal base and operated together, from a single power supply and simultaneously, in an air-conditioned room (temperature about 70°F., R.H. about 30%). The temperature of the lamps did not rise significantly above room temperature. The deterioration to be described is the "intrinsic" deterioration characteristic of the phosphor rather than that due to its environment. Light output measurements during deterioration were made with an RCA 931-A photomultiplier and battery box for long-time stability. No spectral shift with deterioration was detected (see Section D-3). Initial brightness measurements were made in a castor-oil cell, 60 μ thick, using the Ultrasensitive Spectra Brightness Meter.[3] Cell thickness reproducibility is better in the oil cells than in the sprayed lamps, although brightness readings among the sprayed lamps agreed well with those obtained with the oil cell. All of these measurements were made at 4000 cps, the frequency at which electroluminescent maintenance was determined.

The percentages of added impurities are plotted as ordinate and abscissa, respectively, on logarithmic scales in Fig. 1. In this figure are plotted contours of equal maintenance, in per cent of initial brightness, after operation at 150 v, 4000 cps. Contours plotted for short and long periods of operation show the same configuration. Electroluminescence maintenance improves rapidly with increase of both copper and chlorine additions. The contours are roughly symmetrical about the line of equal copper and chlorine additions; this is the line of unity slope in Fig. 1. Furthermore, again roughly, a schematic representation of these contours may be given as in the inset of Fig. 1. This implies that, for a given maintenance characteristic, certain equal additions of copper and chlorine are required. For example, for 10% maintenance, an addition of 0.5 mole % of copper and 0.5 mole % of chlorine is required. Further additions of chlorine (at constant copper) or of copper (at constant chlorine) will not improve the maintenance; instead a greater addition of both is required. Since the contours show no sign of closing, it may be assumed that further maintenance improvement may be realized by greater impurity addition. This is of interest practically only if maintenance is the only requirement. To a marked degree, there is a correlation between better main-

[1] Supplied by W. Lehmann.

[2] Metal and Thermit Corporation, Rahway, N. J.

[3] Manufactured by Photo Research Corporation, Hollywood, Calif.

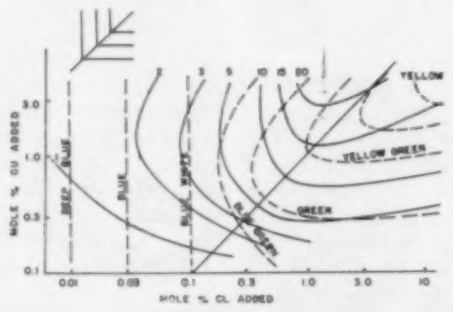

Fig. 1. Dependence of maintenance (solid curves, per cent of initial brightness, 150 v, 4000 cps) and visual color (dashed curves) on copper and chlorine additions. Inset: schematic diagram of same data.

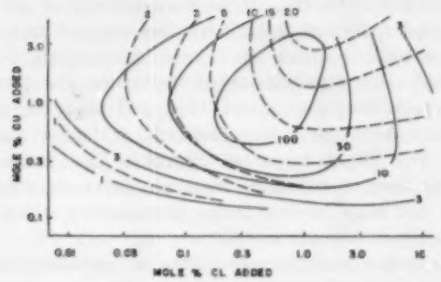

Fig. 2. Dependence of maintenance (dashed lines, per cent of initial brightness, 150 v, 4000 cps) and brightness (solid lines, oil cell, 200 v, 4000 cps, arbitrary units) on copper and chlorine additions.

tenance and longer wave-length emission, as shown in Fig. 1. Here are plotted the maintenance contours and also visual color contours which, although subjective, are correct in their gradation from apparent shorter to longer wave lengths. The maintenance and color contours are not coincident. This means, for example, that there is a definite procedure for obtaining a green-emitting phosphor of optimum maintenance (in this case, by extrapolation to 10 mole % copper and 2 mole % chlorine added). While the blue-emitters are always poorer in maintenance, Fig. 1 demonstrates simple matching of a required color to optimum maintenance and hence the best blue emitter is chosen easily. Note that the color contours of Fig. 1 follow the simple schematic diagram even more closely, and hence the same discussion applies.

The third important characteristic is brightness. Contours of equal brightness (in arbitrary units proportional to ft-L) are given in Fig. 2. Initial brightness contours (not shown) for the sprayed cells which were deteriorated had the same configuration; the plotted brightness data were obtained from oil cells. Figure 2 includes the maintenance contours already described. In the blue region, the brightness and maintenance contours are approximately coincident; that is, maximum brightness and maximum maintenance for a certain color occur at about the same point. In the green and yellow-green regions the contours are not at all coincident, but at least the high brightness contours are elongated in the direction of best maintenance so that not much brightness is sacrificed in realizing good maintenance. Brightness and maintenance are often equally important, and the total light emitted throughout the operating life of the lamp (lumen-hours) is the criterion. Peak "lumen-hours" is obtained in the green and falls off by a factor of twenty toward the yellow; hence, the effect is due neither to decreasing luminosity (since luminosity rises slightly in this range, 5200-5650Å) nor to poorer maintenance but is a marked physical effect. In the blue regions, fortunately, a ridge occurs at about 1 mole % copper along which maximum lumen-hours can be chosen for a given color.

As discussed in Section III, density of trapping sites is thought to be related to the maintenance of a phosphor. For this reason, the thermoluminescence of each phosphor in this series was measured by

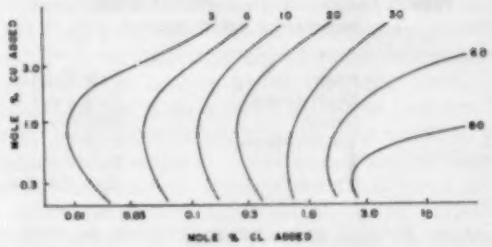

Fig. 3. Dependence of integrated thermoluminescence (—195°C to room temperature, arbitrary units) on copper and chlorine additions.

integrating the thermal glow, between —195°C and room temperature, following equal irradiation at 365 mμ at the lower temperature. In Fig. 3 the total light output due to thermoluminescence (release of trapped electrons followed by recombination) is plotted in arbitrary units.

As a matter of interest, the yellow-emitting ZnS:Mn,Cu,Cl phosphors show similar contours and as wide a maintenance variation as the ZnS:Cu,Cl type described above, depending also on copper and chlorine additions. For samples of yellow phosphors of this type with various copper and chlorine additions, the time to half brightness at 4000 cps ranged from 4 to 350 hr. The initial brightness of the best maintenance phosphor was about 60% of that of the brightest yellow phosphor.

2. Firing temperature.—A series of blue-white ZnS:Cu,Cl phosphors[4] was fired at various temperatures. The experimental procedure was identical to that described in the previous section. The maintenance of those phosphors fired at higher temperatures was much better than the maintenance of those fired at 950°C and below (Table I). The brightness units are proportional to foot-lamberts; maintenance is given in per cent of initial brightness after 24 hr at 150 v, 4000 cps. Comparing the variations with firing temperature with the corresponding contours of Fig. 1, the increasing firing temperature appears to have the effect of causing increased retention of copper. The practical result is a blue-white phosphor of much improved maintenance.

Part but not all of the maintenance improvement with increasing firing temperature is undoubtedly due to the increase in particle size with increasing temperature, as shown in Table I. The dependence of maintenance characteristics on particle size is described in the next section.

3. Particle size.—Any alteration of the phosphor (impurity addition, firing temperature, etc.) re-

[4] Supplied by A. Wachtel.

Table I. Phosphor characteristics as a function of firing temperature

Firing temp, °C	Initial brightness, B	Maintenance, M, %	B x M	Average particle size, μ
650	7.2	1.2	9	2.5
800	5.3	1.2	6	2.5
950	4.9	2.7	13	3
1100	11.0	5.1	56	5
1250	9.5	11.0	104	8

Table II. Phosphors for which effect of particle size on maintenance was determined

B	Blue	ZnS:Cu, Cl
BG	Blue-green	ZnS:Cu, Cl
G	Green	ZnS:Cu, Cl
YG	Yellow-green	ZnS:Cu, Cl
Y (1)	Yellow	ZnS:Cu, Mn, Cl
Y (2)	Yellow	ZnS:Cu, Mn, Cl

sults, in general, in a change in mean particle size also. Efficiency (11) and brightness (11, 12) have been shown to depend on mean particle size. The maintenance of output also depends on particle size. Therefore an observed variation in maintenance, for instance, cannot be attributed entirely to a certain alteration of the phosphor if a particle size change also is induced by the alteration. This section describes a determination of the dependence of maintenance on particle size alone, in order that this effect of particle size may be allowed for in determining true maintenance variation due to phosphor alteration.

From each of the six phosphors listed in Table II five or six fractions were separated out by water settling. Several particle size determinations were made by microscope and the apparent mean particle size averaged to obtain the nominal particle diameter used in plotting the data. These nominal particle sizes are very approximate, and only the large differences in the mean diameter of the fractions make the determination meaningful. Although the number of particles considerably coarser than the nominal size was negligible, there were small numbers of fines present in the coarser fractions. The nominal average particle sizes designated are estimated to be within about 15% of the true average in the case of most of the 30 fractions; one or two fractions, however, consisted of particles of approximately two different diameters, and these were discarded. Each fraction apparently consists of a bell-shaped distribution similar in shape to the original phosphor. Such a distribution is well suited to this maintenance study, since any actual electroluminescent phosphor of interest practically will have such a distribution.

The dependence of maintenance of the phosphors on particle size is shown in Fig. 4. All of the curves are seen to extrapolate approximately through the origin. The dependence of the blue phosphor is nearly linear to 12 μ; it is characteristic of the blue phosphors, having relatively low copper and chlorine additions, that the range of particle size is limited. The dependence of the other phosphors is also quite linear to about 12 μ, and then the maintenance becomes fairly constant at larger particle size. The slight apparent decrease in maintenance of the largest particles in some cases may not be real, but may be due to the presence of a few fine particles as already noted.

Thus, the particle size effect is considerable. On the other hand, particle size is by no means the major consideration in electroluminescence maintenance. Modified firing procedures have been shown to lead to maintenance improvement factors of as much as twenty; no difference in average particle diameter of the original and such modified phosphors is apparent by microscope. Maintenance also has been shown to depend very strongly on copper and chlorine additions during phosphor preparation (Section A-1.); in the array of samples studied, the maintenance of electroluminescence brightness varied by a factor of 50 while the particle size ranged over a factor of 2 or 3. In a method of maintenance improvement over conventional blue phosphors by use of other coactivators (13) the maintenance differs by a factor of 18 while the particle diameter ratio is roughly 2. Higher firing temperatures improve the maintenance of a blue phosphor by a factor of ten while the particle size is increased by a factor of three (Section A-2). Hence, in the last four examples, the particle size effect on maintenance is a minor one, compared to the over-all maintenance variations cited.

4. Emission color variation with particle diameter. —In certain phosphors of the ZnS:Cu,Cl type a definite shift occurs in emission color with variation of particle size from the same phosphor batch. The emission spectra of the five particle size fractions of the blue-green phosphor of Table II are given in Fig. 5 together with mean particle diameter as determined by microscope. The shift of emission toward the blue with increasing particle size is not consistent with the general improvement in maintenance of phosphors the longer wave length their emission color. Small and large particles from the same batch are apparently activated differently, and emission color indicates that the smaller particles are more highly activated. Maintenance has been shown to depend very strongly on activation (per cent addition of copper and chlorine) and also to

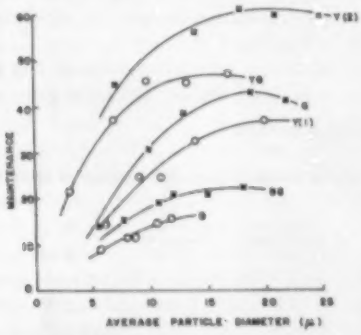

Fig. 4. Dependence of maintenance (per cent of initial brightness, 120 v, 4000 cps) on particle diameter.

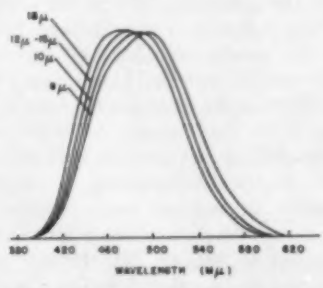

Fig. 5. Variation of emission color with particle size from the same lot of phosphor. Blue-green ZnS:Cu, Cl.

depend somewhat on particle size. These dependences, as determined, are slightly inaccurate due to the interrelation of activation and particle size.

The emission color of the blue and deep yellow-green phosphors (near the extremes of the color range of ZnS:Cu,Cl class) does not vary with particle size, very likely because (*a*) the blue fine particles contain only active blue luminescence centers and so the coarse particles can emit no bluer light, and (*b*) the coarse yellow-green particles contain only active yellow-green luminescence centers so the finer particles can emit no yellower light. The possibility that the yellower emission from smaller particles might be due to their stronger absorption of blue emission, was eliminated by the following experiment. A large-particle fraction (20-30 μ diameter, blue-green emission) was crushed to an average diameter of 1 or 2 μ. No change in the electroluminescence emission spectrum occurred within experimental error due to this mechanical reduction in particle size, and it differed significantly from the spectrum of the original small-particle fraction (4-6 μ diameter, green emission) of the same phosphor batch.

B. Dependence of Maintenance on Conditions of Operation

1. Frequency.—It is well known that electroluminescent phosphors deteriorate more rapidly at higher frequencies (5, 6). This behavior is true generally, with no known exceptions. It was suggested[a] that, at least approximately, a universal deterioration curve results from plotting the per cent of initial brightness against the total number of cycles of operation, rather than the hours of operation. The validity of such a universal deterioration curve was determined for the phosphors in Table II. Figure 6 shows the data plotted in terms of cycles of operation. A universal curve can be drawn approximately for frequencies higher than 1000 cps, but at lower frequencies significant deviations from the universal curve occur. On the basis of these curves, a parameter useful for describing the maintenance properties of an electroluminescent phosphor is the high-frequency half-life under dry conditions, defined as the number of cycles of operation at frequencies greater than 1000 cps after which light emission has been reduced to half the initial value.

[a] By E. A. Sack, Westinghouse Research Laboratories, Pittsburgh, Pa.

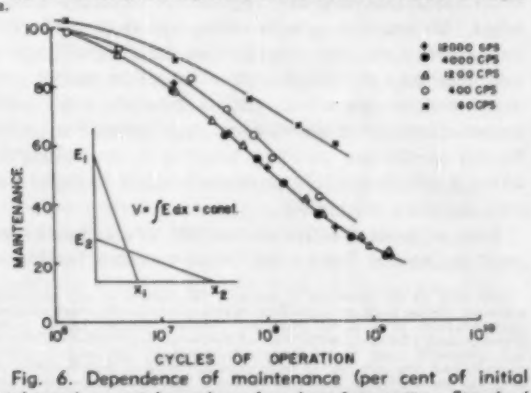

Fig. 6. Dependence of maintenance (per cent of initial brightness) on total number of cycles of operation. Standard green phosphor, 200 v. Inset: Field distribution at (1) high and (2) low frequency.

All the phosphors showed low-frequency deviations from the universal curve which satisfactorily described deterioration above 1000 cps. These deviations ranged from a factor of two in half-life for the phosphor with blue emission to a factor of ten with the yellow-green. Generally, these deviations are in the direction of longer half-life (in cycles) at lower frequency; the blue phosphor, however, showed a shorter half-life in cycles at low frequency. The yellow-emitters showed low-frequency deviations which were intermediate between the blue and yellow-green.

The frequency dependence of maintenance is therefore very strong, covering a range in half-life even greater than the range of frequencies of operation.

It might be expected that if two identical lamps are operated, one at a high frequency and one at a low frequency and at the same applied voltage, that the brightness of the high-frequency lamp would initially be much greater than that of the low-frequency lamp but would eventually fall below; this would follow if the lumen-hour capabilities of the two lamps were about equivalent. It is observed, however, that of two identical lamps operated at the same voltage and different frequencies, the brightness of the lamp operated at the higher frequency never falls below that of the lamp operated at lower frequency. Lamps operated at high frequency, although they have deteriorated to a small percentage of initial brightness, are still brighter than identical low-frequency lamps. The brightness-time curves of these lamps approach each other more and more closely after a period of operation but apparently do not cross even after very long times. Such behavior suggests fast-deterioration and slow-deteriorating components of light emission, the latter being relatively independent of frequency. The presence of two components is particularly marked in the case of an improved-maintenance yellow phosphor described in Section E and in Fig. 14.

2. Voltage (field strength).—It is not unreasonable to expect that an increase in voltage and field strength will lead to more rapid deterioration of the phosphor since the light output is higher. Roberts (6) reported, however, that the maintenance of certain lamps improved slightly with increase in field strength. A determination of the voltage dependence of maintenance was made for blue and green ZnS:Cu,Cl phosphors and a yellow-emitting ZnS:Mn,Cu,Cl phosphor. Some of the results are given in Table III. At low frequency (60 cps) the maintenance of the blue phosphor improves with increasing field strength. At intermediate frequency (400-4000 cps) the blue and green phosphors deteriorate slightly more rapidly at higher field strengths, and the yellow phosphor shows no voltage dependence within experimental error. Thus, electroluminescence maintenance does not depend appreciably on the field strength experienced by the phosphor. The greatest observed variation in half-life over the range of useful voltage is no more than a factor of two or three; this is to be compared

Table III. Dependence of maintenance (half-life) on applied voltage for various phosphors and frequencies

	Initial brightness, arb. units	Voltage	Half-life, hr
	1300	400	380
	700	310	290
Blue	400	230	210
60 cps	50	150	150
	8	75	180
	1600	370	1.0
	1300	340	1.3
Blue	1050	300	1.3
4000 cps	240	203	1.4
	9	95	1.1
	770	370	2.2
	580	340	3.5
Green	320	300	2.6
4000 cps	100	200	3.5
	6	92	5.0
	600	400	14
	380	360	14
Yellow	250	317	14
4000 cps	60	212	16
	2	97	12

to the variation of 1000 to 1 due to frequency. There is little disadvantage, therefore, in operating a lamp close to breakdown in order to obtain maximum brightness, since the maintenance is about that observed at much lower voltages. Conversely, maintenance cannot apparently be improved significantly by reducing the field strength on the phosphor.

3. Temperature.—Electroluminescence deterioration proceeds (5) at a rate too slow to measure if the phosphor is maintained at liquid nitrogen temperature (−195°C). On the other hand, the maintenance is poorer at temperatures higher than room temperature than it is at room temperature. This behavior is illustrated by Fig. 7.

4. Humidity.—It is well known generally in electroluminescence work that moisture has a strong deleterious effect on the maintenance of output. Atmospheric water vapor is perhaps the most important adverse influence on electroluminescence maintenance from the point of view of practical

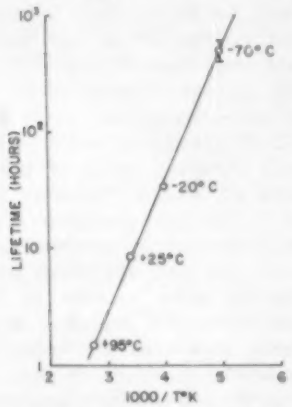

Fig. 7. Dependence of lifetime (time to half of initial brightness) on temperature. Standard green phosphor, 150 v, 4000 cps.

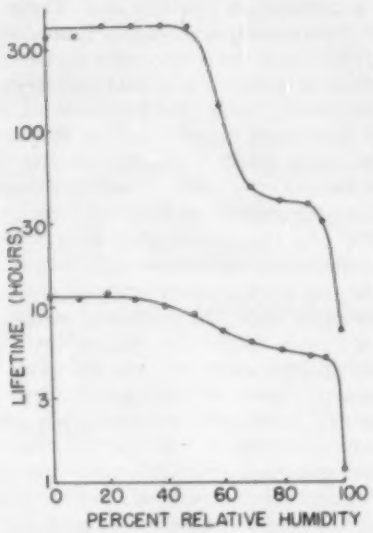

Fig. 8. Dependence of lifetime (hours to half of initial brightness) for two green ZnS:Cu, Cl, phosphors as a function of per cent relative humidity. 4000 cps, PVCA dielectric, 23°C.

application. Operation at zero humidity is certainly the ideal condition for obtaining information on the intrinsic maintenance behavior of a phosphor, and this has been done for much of the testing reported in this paper. For experimental unprotected lamps, when the relative humidity of the air-conditioned laboratory rose above 30% the lamps were always operated in a closed vessel of the desiccator type at zero humidity. The dependence of lifetime on per cent relative humidity is shown in Fig. 8 for a standard and an improved green ZnS:Cu,Cl phosphor. The curves shown were obtained with sulfuric acid solutions, and similar results were obtained with saturated solutions of solid materials. The reduction in lifetime from low to high humidity (excluding 100%) is by a factor varying from 2 to 10. The deterioration observed when a phosphor is operated in a vacuum (10^{-5} mm Hg) either with or without plastic dielectric[e] is similar to what is observed if a lamp is operated in air at zero humidity or in 100% humidity so long as perfect protection from moisture is achieved; the plastic dielectric apparently serves only to slow the ingress of moisture somewhat. Moisture has apparently no detectable adverse effect on the phosphor so long as voltage is not applied; if the phosphor layer is thoroughly dried before operation, the maintenance is unaffected. Storage of an already aged phosphor under humid conditions, or even wetting it, will show no adverse effects so long as the phosphor is dried before the field is applied.

Zinc selenide electroluminescent phosphors which emit in the red have been found to show far better

[e] As long as no moisture is present, the nature of the dielectric material seems to have no effect whatsoever on the maintenance characteristics of a given phosphor. Various waxes, epoxy resin, nitrocellulose, Lucite, polyvinyl chloride acetate (PVCA) which was generally used in the lamps described in this report, castor oil, air, and vacuum led to very similar rates of deterioration so long as the humidity was low or zero. This conclusion does not apply (a) to solid dielectric materials which are not stable with time, such as plastics containing volatile plasticizers, or (b) to glass dielectrics during the firing of which the phosphor is altered because of the higher temperatures necessary.

maintenance than zinc sulfides. It has been found also that the electroluminescence of a selenide phosphor is remarkably maintained in the presence of moisture.

5. Two lifetimes from electroluminescent lamps. —An electroluminescent lamp deteriorated at high frequency and low voltage to a fraction of its initial brightness may show no evidence of deterioration under low frequency and high voltage excitation. In other words, a lamp excited to brightness L_o at high frequency and low voltage (HFLV) can be quite completely deteriorated and then can be excited to L_o again by the same LFHV conditions which produced an equivalent brightness L_o initially. When excited by the low frequency and high voltage, the phosphor is as fresh as initially and an entirely new "lifetime" is begun. The first deterioration has little or no effect on the rate of the second deterioration. Coarse (15 μ) particles and fine (3 μ) particles show the same behavior; namely, deterioration at a high frequency is not seen at a much lower frequency as long as the operating voltage is higher than that at which the deterioration took place; this will usually be the case in practice since higher voltage is required to reproduce a given brightness at lower frequency. A typical pair of frequencies at which the two "lifetimes" may be obtained is 60 and 4000 cps. Since newer coarse phosphor powders show very reasonable maintenance at frequencies as high as 10,000 cps, the first high-frequency "lifetime" can be long enough to be practically valuable. The purpose of this section is to illustrate this behavior by means of the maintenance contours to be described, and to show that the sequence HFLV followed by LFHV operation is the correct one to obtain the two "lifetimes" from an electroluminescent lamp.

One lamp made with standard green phosphor was deteriorated for 400 hr at high frequency (20 kcps) and low voltage (60 v rms) to 20% of initial brightness. This operating point is indicated by the cross in Fig. 9, which is a maintenance contour in frequency and voltage of the deteriorated lamp. The heavy lines and plotted points are apparent maintenance, in per cent of initial light output, as measured under frequency and voltage conditions other than those at which deterioration took place; that is, brightness was measured, before and after deterioration, at each combination of voltage and frequency. Note, for example, that this lamp shows no sign of deterioration at 160 v, 60 cps and that its light output under these conditions is equal to the initial light ouput before the original deterioration at HFLV.

The dashed lines of equal light emission illustrate the well-known observations (*a*) that the frequency dependence of electroluminescence becomes negligible at low voltage, where the voltage dependence of emission is strong, and (*b*) that the frequency dependence is strong at high voltage, where the voltage dependence is weak.[7] A change in operating conditions from HFLV to LFHV operation is more or less parallel to the equal-brightness lines; hence, light output under the latter conditions can be equal

[7] An explanation of these interdependences is given in ref. (14).

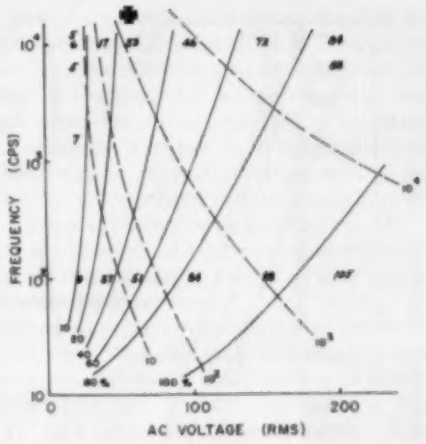

Fig. 9. Apparent maintenance (solid lines, per cent of initial brightness) at voltage and frequency other than that at which deterioration took place. Cross indicates conditions of deterioration (see text for time of deterioration). Dashed lines are initial brightness in arbitrary units. Standard green phosphor.

to or greater than the initial light output at the conditions under which deterioration took place.

Another lamp was deteriorated at a lower frequency (60 cps) and a higher voltage (150 v rms). For this case of initial LFHV operation, which resulted in deterioration of electroluminescence to 12% of initial, subsequent operation under the opposite HFLV conditions makes little difference in the observed state of deterioration, and no advantage is gained. Improvement results only by moving to lower frequency or higher voltage or both as in the previous case, but even then the recovery is not large (from 12% to about 30%).

Reasons based only on the mechanism of electroluminescence have led to the view (8) that an increase in frequency of excitation leads to more marked localization of the light-emitting and deterioration processes of electroluminescence. In a study of the field quenching of alpha particle scintillations, Alfrey and his associates (15) have obtained further and independent evidence that localization of the electric field is greater at high frequency. It is generally accepted that low voltages lead to greater localization of the high-field region or, put in another way, that with increase in voltage the high-field region extends farther and farther into the crystal (6). Such behavior will lead to maximum localization of deterioration effects if excitation is at high frequency-low voltage (HFLV), to the upper left in Fig. 9. Following deterioration under such conditions, marked recovery takes place if frequency is reduced or voltage increased or both. This is because in either case the light-emitting high-field region is extended into fresh regions of the phosphor crystal and the deterioration becomes proportionally less evident. In fact, in the voltage and frequency region below and to the right of the 100% line in Fig. 9, the active region extends so far into fresh parts of the crystal that the reduced emission from the original small region of excitation

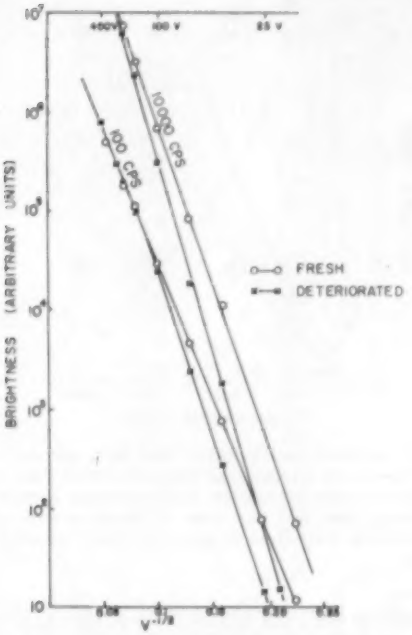

Fig. 10. Change in brightness-voltage dependence with deterioration (at 20,000 cps, 60 v, 15 hr). Standard green phosphor.

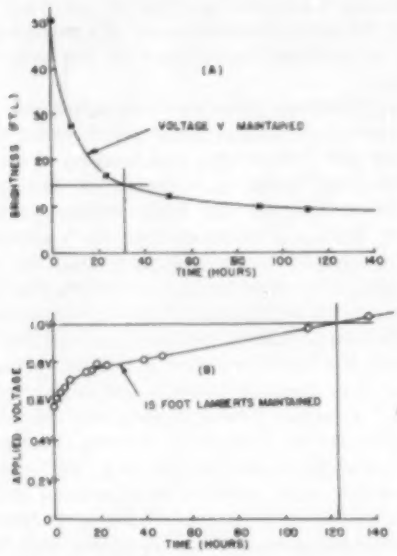

Fig. 11(A). Maintenance characteristic for constant voltage operation (4000 cps). Standard green phosphor.

Fig. 11(B). Maintenance characteristic for constant brightness operation (4000 cps). Standard green phosphor.

is masked, and deterioration effects are no longer seen. That the deterioration in the original active region is nonuniform is suggested by the observation that further localization of the active region by increasing the frequency or reducing the voltage from the conditions under which the deterioration took place, leads to even poorer apparent maintenance.

6. Localization of the electric field.—Further evidence that the excitation region in the phosphor is contracted by decrease in voltage or an increase in the frequency and expanded by an increase in voltage or a decrease in frequency appears in Fig. 10. The lamp from which the data for this figure were obtained was deteriorated at 20,000 cps and 60 v for 15 hr. Following this, the voltage-brightness characteristics were compared at 10,000 cps and at 100 cps with those for the fresh lamp. At 10,000 cps the effect of the deterioration is seen up to 400 v, but at 100 cps the effect is observed only up to 100 v. Apparently the "extent" of the high-field (excitation) region coincides with the volume of the phosphor crystal which was deteriorated at 100 v, 100 cps and at 400 v, 10,000 cps.

7. Constant brightness operation.—In lamp applications where there is a brightness control and where the desired brightness is less than the maximum brightness obtainable, operation is expected to be at constant brightness. Deterioration with operation is corrected for implicitly by resetting the brightness control (voltage) to a different setting as deterioration proceeds. The question was raised* whether a lamp operated at constant brightness would have a longer useful life than an identical lamp operated, as usual, at constant voltage. The question is made meaningful only if some restriction is made, such as that the rated voltage of the lamp should not be exceeded. Increasing the voltage during life should, by extending the excitation region into fresh parts of the phosphor crystal, result in longer life (see Section B-5 and B-6). This was confirmed by the results shown in Fig. 11. Operation was at 4000 cps. Two similar lamps were used, in each case V being the rated voltage at which the lamp brightness was initially 50 ft-L. The "desired" brightness was chosen at 15 ft-L. Figure 11 (A) represents a lamp operated at constant rated voltage V. This lamp deteriorated to 15 ft-L after about 30 hr of operation at 4000 cps, a typical maintenance figure for an early green-emitting ZnS:Cu,Cl phosphor. Figure 11 (B) represents the other lamp operated at the constant "desired" brightness of 15 ft-L. The applied voltage was about 0.6 v initially and rose to a value of V in about 120 hr. The useful life of the constant brightness lamp was therefore about four times that of the lamp operated at constant voltage. At the end of its "life" each lamp was operating at voltage V and a brightness of 15 ft-L. In one case the useful life is terminated by too low a brightness at rated voltage, and in the other case by too high a voltage to maintain rated brightness.

This increase in lifetime by constant brightness operation was confirmed* also at 400 cps. Different dielectric materials and lamp thicknesses were tested. The dielectric material had no effect. Lamp thickness does, however, have a strong effect; the thicker the lamp and the higher the breakdown voltage, the smaller the advantage in constant brightness operation. The reason is as follows: At a

* By S. Goldfarb, Wright Air Development Center, Dayton, Ohio.

* Data from R. W. Wollentin.

given required brightness the brightness-voltage dependence is stronger for the thicker lamp since the required field strength is lower. Therefore the initial voltage is a larger fraction of the final voltage, the voltage increase during life is smaller, and the utilization of fresh phosphor regions due to the voltage increase is less marked. The effect on lifetime is large indeed, since the thick lamps last only twice as long as with standard (constant-voltage) operation, while the lifetime of the thinner lamps is four times as long. This effect is beneficial, since lamps normally will be operated as near breakdown as possible to realize maximum brightness at minimum voltage (thin lamps), and such operation will lead to maximum improvement in lifetime due to constant brightness operation. In such a case, the maximum voltage obviously must not exceed the breakdown voltage of the lamp.

8. External series impedance.—The impedance of electroluminescent lamps is dependent on frequency and voltage of excitation (11, 16). The impedance of these lamps increases during life (see Section D below), and this effect is greatest with low frequency and high voltage operation. The impedance increase occurs in the phosphor powder itself; the dielectric material does not change its electrical properties with life if the lamp is properly finished and cured. Therefore, an added fixed impedance in series with the lamp will divide the voltage in such a way that the effective voltage on the lamp will automatically increase during life as the impedance of the lamp (phosphor) increases. This increase in effective voltage will tend to compensate for the normal decrease in brightness with life. Lamps were made with a poor maintenance blue phosphor in order to obtain the results in a short time, and were operated at 400 cps. Table IV identifies the series element, the total voltage applied to the lamp and series impedance combination, and the time in hours for the brightness to decay to half the initial brightness. Similar experiments have been conducted at 60 cps and increases in half-life of about five times have resulted from the addition of a series resistor equal to the initial impedance of the lamps.

It is interesting to note that operation of a lamp with a series impedance is inherently stable. The impedance of the lamp (phosphor) decreases with increasing field strength. Therefore, as the lamp impedance increases due to operation and the effective voltage across the lamp increases, this increase leads in turn to a reduction in lamp (phosphor) impedance at the new higher field strength. The effect is a type of negative feedback ensuring stability of operation. It should be borne in mind that the dielectric embedding material itself acts as an impedance in series with the phosphor crystals. At low phosphor concentrations where, on the average, each phosphor crystal is isolated in the dielectric, the maintenance is better than at high concentrations where each crystal is effectively in contact with one or more others and the series impedance effect is absent. Under certain conditions the maintenance is expected to improve upon addition of a clear coat, for the same reason. These effects are described in later sections.

9. Pre-aging effects.—Pre-aging at rated voltage and frequency leads to apparent improvements in maintenance since early deterioration is more rapid than later, and the "initial" brightness is then defined as that after some deterioration (the pre-aging) has taken place. Pre-aging is feasible so long as excess brightness is available. Pre-aging, at voltages and frequencies other than those under which the lamp is to be run, can lead to the same maintenance improvement in a much shorter time.

An improvement in 400 cps maintenance is associated with a certain cost in initial 400 cps brightness. This relation is given roughly in Table V, where L_o is the initial brightness and L_a is the brightness after aging, both measured under operating conditions rather than pre-aging conditions, and holds approximately regardless of the conditions of pre-aging. Various pre-aging conditions necessary to achieve the maintenance improvement in 1 and 2 of Table V are given in Table VI. Hence, for example, the 400 cps half-life of a lamp can be

Table IV. Effect of series impedance on maintenance

Lamp	Element	Total voltage	Half-life, hr
1	None	300	11
2	70×10^6 ohm	540	37
3	100×10^6 ohm	640	43
4	130×10^6 ohm	750	80 (extrapolated)
5	None	220	10
6	0.006 mf	400	32
7	0.003 mf	660	50

Table V. Relation of loss in initial brightness to half-life improvement by pre-aging

	Brightness ratio L_a/L_o, 400 cps	Half-life improvement factor
1	0.80	2
2	0.60	5
3	0.40	10
4	0.20	25

Table VI. Pre-aging conditions for specified half-life improvement

Frequency, cps	Voltage	Time, hr
Condition 1, 80% of initial output,* doubled half-life		
400	210	6
400	80	130
1200	240	3
1200	100	40
4000	280	1
4000	140	9
12000	280	0.3
12000	160	3
Condition 2, 60% of initial output* 5 × half-life		
400	160	130
400	360	6
1200	180	40
1200	400	3
4000	210	9
12000	250	3

* Measured under the aging conditions 280 v, 400 cps, rather than the pre-aging conditions.

improved by a factor of five at a reduction of 40% in initial brightness and this pre-aging can be accomplished in times varying from 3 to 130 hr depending on the frequency and voltage used for pre-aging.

C. Dependence of Maintenance on Lamp Construction

1. Phosphor concentration.—It has been customary to use a phosphor/plastic-dielectric weight ratio which yields maximum initial brightness within breakdown voltage requirements. It was found that this weight ratio also has an effect on maintenance and so this factor must be considered when arriving at an optimum ratio.

A set of lamps made with standard green phosphor and PVCA dielectric and utilizing a wide range of phosphor/plastic weight ratios (while maintaining constant lamp thickness) was subjected to accelerated life test at 4000 cps. At low phosphor concentrations or weight ratios, the maintenance is constant, independent of concentration. At a certain higher concentration the maintenance worsens rather abruptly and then remains constant at the poorer value for still higher phosphor concentrations. The corresponding half-life is reduced by a factor of two or three at high phosphor concentrations. Because of this peculiar result, these experiments were repeated by spraying an entirely new series of lamps. The results were essentially the same. The experiments were repeated for the third time to obtain more data in the transition region. These results are given in Fig. 12. The curve marked $t_{1/2}$ is the half-life in hours taken from the actual maintenance curve for operation at 120 v, 4000 cps. The transition is continuous as the phosphor/plastic weight ratio changes. The curve marked L_o is the initial brightness in ft-L at 120 v, 400 cps. Above a ratio of 5.0 some arcing occurs. The curve marked $L_o t_{1/2}$ is the product of L_o and $t_{1/2}$ and is indicative of the total light output during the life of the lamp.

2. Phosphor layer thickness.—It is intended only to re-emphasize here that the maintenance variation due to different applied voltages on lamps of constant thickness is also to be expected when lamps of various thicknesses are to be operated at a certain predetermined voltage. As shown in the preceding and following sections, phosphor concentration and clear coat thickness must be identical among lamps in which this phosphor layer thickness or field strength effect is to be utilized or studied.

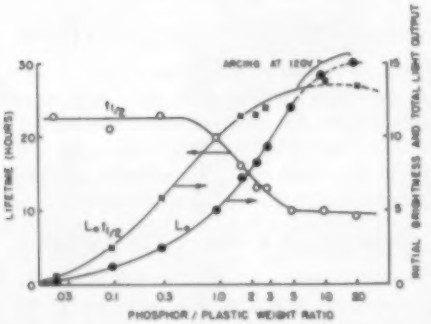

Fig. 12. Dependence of maintenance (hours to half of initial brightness at 120 v, 4000 cps), initial brightness (ft-L at 120 v, 4000 cps) and the product of these, in arbitrary units, on phosphor/plastic weight ratio. Standard green phosphor, constant thickness lamps.

Table VII. Dependence of maintenance on number of clear coats

No. clear coats	Half-life, cycles	Half-life, hr at 400 cps	Breakdown brightness, arb. units	Breakdown voltage, v
0	0.4×10^6	60	11	200
1	0.41	60	16	240
3	0.51	70	23	350
10	0.7	100	22	500
30	1.4	200	17	700
100	2.4	330	—	—

3. Clear coat thickness.—A clear coat is a layer of clear dielectric material containing no phosphor and is often applied to a lamp before or after the phosphor/plastic layer has been laid down. The half-life of conventional sprayed lamps has been observed to increase with the number of clear coats up to a factor of six times the half-life of an identical phosphor layer with no clear coat. Identical lamps consisting only of a thin phosphor/plastic layer were sprayed. Some were reserved as controls and the others were sprayed with from 1 to 100 very thin clear coats of PVCA lacquer-thinner solution. All lamps were operated at 150 v, 4000 cps. Table VII gives the half-life in number of cycles to half-brightness, the breakdown brightness, and the breakdown voltage as a function of the number of clear coats applied over the identical phosphor-plastic base layer. This indicates that in the particular case where a certain brightness is desired and excess voltage is available, maximum maintenance is obtained by utilizing as high a voltage as possible and increasing the clear coat to phosphor-layer ratio until the desired brightness is obtained. Previous indications that clear coats improve maintenance have sometimes been attributed to better moisture protection. The above experiments were carried out in an air-conditioned laboratory in about 30% relative humidity. The effect of clear coats on maintenance may also be that the clear coat behaves as a series impedance (primarily a capacitance) and the maintenance improvement may be the same as that observed when a series capacitor is connected to the lamp (see Section B-8).

D. Changes in Other Properties with Deterioration

1. Electrical properties.—In the fresh electroluminescent phosphor layer, both the capacitance and the conductance increase with increasing voltage (16). This behavior changes, however, with deterioration of the lamp (Fig. 13). The voltage dependence of both capacitance and conductance in the fresh lamp has largely disappeared in the deteriorated lamp, and this is observed over a wide range of frequencies of measurement and of deterioration. The reduction at high voltage of conductance leads to a reduction in power dissipation at high voltage; little change in either is observed at low voltage. The changes in power absorption and light emission during deterioration lead to drastically reduced efficiencies at low voltage. At high

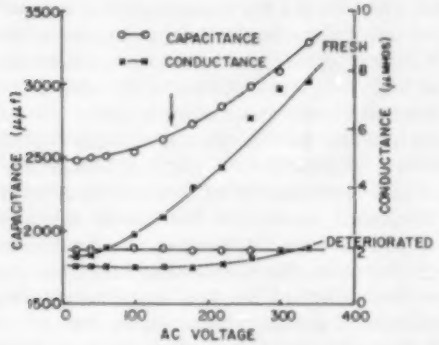

Fig. 13. Variation in capacitance and conductance for fresh and deteriorated lamps. Arrow indicates voltage at which deterioration took place. Standard green phosphor. 4000 cps, 150 v, 1000 hr.

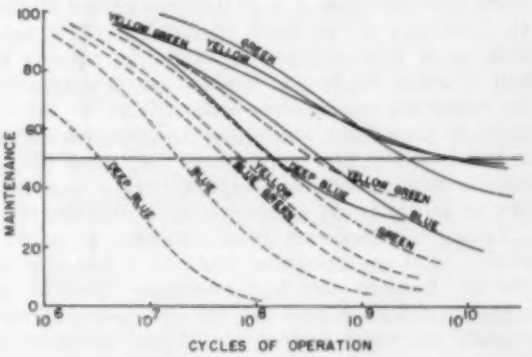

Fig. 14. Comparison of maintenance (per cent of initial brightness) characteristics of standard phosphors (dashed curves) and improved phosphors (solid curves), 150 v, 4000 cps.

voltage the efficiency can remain quite unchanged or can increase appreciably; this effect is a shift of peak efficiency toward higher voltage due to deterioration, and is another manifestation of the localization of deterioration effects in the phosphor crystal.

The gradual decrease with operation of the capacitance (5, 6) and conductance of a phosphor layer may be related directly to the electroluminescence process. Three cells were operated singly while in a bridge circuit for 120 hr at 150 v, 4000 cps. Cell A was a conventional sprayed phosphor-plastic layer of green-emitting ZnS:Cu, Cl phosphor. Cell B was similar except that no plastic dielectric was present. Cell C consisted of clear plastic dielectric with no phosphor, and the electrical characteristics of this cell did not change with operation. Components of the capacitance and of the conductance decrease roughly in proportion to the decrease in light output for both the conventional phosphor-plastic sprayed layer and the water-settled layer of phosphor powder alone.

2. Frequency response.—High-frequency deterioration depresses the light output more strongly in the frequency region where deterioration took place than at lower frequencies. Low-frequency deterioration depresses the brightness about equally at all frequencies. This observation also is related to the localization of electric field with increasing frequency discussed in Sections B-5 and B-6.

3. Emission spectrum.—No change in emission spectrum of ZnS:Cu, Cl phosphors with deterioration has ever been observed. In the case of conventional green-emitting phosphors, a quantitative search for such a spectral change was made and none found beyond slight discrepancies which could be attributed to darkening of the plastic dielectric material. The emission spectra of twelve phosphors (including ZnS:Cu, Cl emitting from the deep blue to yellow-green, ZnSSe:Cu,Cl emitting in the yellow, red ZnSe:Cu, Cl, blue-green ZnS:Cu, Pb_x Cl, and yellow ZnS:Cu, Mn, Cl) were compared when fresh and after long deterioration to a few per cent of initial brightness. Only the ZnSe:Cu, Cl phosphor appeared to shift slightly, toward longer wavelengths. The other phosphors showed no detectable change in emission spectrum.

D. Recent Maintenance Improvements

The phosphors described in this paper are predominantly conventional ZnS:Cu, Cl phosphors in which emission color shifts from the deep blue to the yellow-green as copper and chlorine additions are increased. The yellow-emitting manganese-activated ZnS:Cu, Mn, Cl phosphors behave much like those without manganese in their maintenance behavior, the manganese serving primarily to shift the blue or green "normal" emission to a relatively invariant yellow (17). The maintenance characteristics of earlier standard phosphors (dashed curves) are summarized in Fig. 14, where per cent of initial brightness is plotted against cycles of operation; the data were obtained at 150 v, 4000 cps, low humidity, and the resulting "universal curves" describe the maintenance behavior at frequencies of about 1000 cps or higher (Section B-1). Recent improvements in maintenance of the same basic phosphors have been made possible by alterations in activation and by modified firing procedures. These improved phosphors, covering the same range of emission color, are represented by the solid curves in Fig. 14; the same operating conditions as above were used in obtaining the data. These maintenance improvements do not usually sacrifice initial brightness. The old and new deep blue and greenish blue phosphors are about equivalent in brightness, the improved-maintenance green phosphors are often brighter than the original, and the improved maintenance yellow in Fig. 14, for example, has half the initial brightness of the original yellow shown, while its half-life is 100 times longer. This particular phosphor involves only an increase in Cu-Cl addition in accordance with Section A-1. The small losses in initial brightness as maintenance improves, as in the case of the yellow phosphor, are gradual and a compromise can be made at any point; however, integrated light output over the life of the lamp (lumen-hours) improves very rapidly indeed as maintenance improves. In fact, it is a property of some of the recent phosphors that a relatively high plateau of light emission is reached after long oper-

ation, as in the case of the improved yellow of Fig. 14. Obviously if the point of leveling off is near 50%, as in this example, the half-life, or time to half of initial brightness, is not a useful parameter for measuring maintenance since (*a*) minor differences in phosphors would lead to large variations in this quantity, and (*b*) defining the useful life to include deterioration to levels somewhat less than 50% of initial would increase it by a large factor.

Taking the improved green phosphor as an example, 1000 cps operation leads to a half-life of 750 hr. Because the high-frequency half-life in cycles is about doubled for 400 cps operation and roughly ten times greater for 60 cps operation of this type of phosphor (Section B-1), the corresponding extrapolated half-lives are 3750 hr at 400 cps, and 12,000 hr at 60 cps; such behavior requires good moisture protection and great patience to measure.

III. Discussion

The improvement in maintenance with increasing equal copper and chlorine additions can be explained as follows. The normal trapping or donor sites are associated with Cu-Cl centers in strongly electroluminescent ZnS:Cu, Cl phosphors. Excess chlorine (lower right hand region in Fig. 1-3) leads to phosphorescence and deeper traps which are detrimental to electroluminescence. The greater the copper-chlorine addition to the phosphor, the higher the expected concentration of normal traps or Cu-Cl centers, and the less rapid the quenching of electroluminescence either by a given rate of incoming deeper traps (8) or depletion of normal traps by outward diffusion (5). That the density of normal traps and good maintenance are strongly correlated is shown by Fig. 3, even though the deep traps, contributing to phosphorescence and not to electroluminescence, confuse interpretation in the low-copper high-chlorine region (lower right) of the figure. As the concentration of Cu-Cl centers increases, the electroluminescence brightness reaches a peak and then drops off (Fig. 2), perhaps due to self-quenching by the centers (concentration quenching), but maintenance apparently continues to improve. The degree of deterioration of electroluminescence after a period of operation is very likely related to the ratio of the concentration of deep traps which have appeared to the concentration of normal traps.

Maintenance improves with increasing particle diameter. If deterioration is due to the introduction of a foreign substance from the surface into the crystal volume, or to the escape from the volume to the surface of some entity necessary to electroluminescence, then an increase in the rate of deterioration with increase in surface to volume ratio is to be expected; experimentally the rate of deterioration is proportional to this ratio for all but the largest particle sizes.

Maintenance depends strongly on frequency and very little on voltage. An increase in frequency reduces the crystal volume experiencing the field and increases the maximum electric field in the crystal; therefore the rate of field-diffusion is increased and the volume affected by it is reduced and deterioration becomes more rapid. In the schematic inset of Fig. 6, E_1 and X_1 refer to the maximum field and extent at high frequency. As the active charge density decreases with deterioration, the slope dE/dX decreases and the field configuration approaches that of the low frequency case (E_2, X_2). Hence the light output also decreases toward that characteristic of low frequency excitation but never drops below since E_2 will always be less than E_1. An increase in voltage increases the maximum field but also increases the extent of the field so, although the rate of diffusion is greater, the volume into or out of which the diffusion takes place is also increased and the net effect on maintenance may be small. In the case of the blue phosphor (Section B-2) the copper-chlorine addition is relatively small so the volume concentration n of trapping or donor sites is expected to be small. It follows from Poisson's relation that the extent of the field will increase more rapidly with voltage if n is small. This blue phosphor (Table III) actually maintains output better at high voltages than at low voltages (at low frequency) as if in fact the excited crystal volume increased more rapidly with voltage than the rate of field-diffusion causing deterioration.

The temperature dependence of deterioration is very strong. If the diffusion of ions is involved, the electroluminescence half-life should be related to the ionic mobility (5) and should show an exponential temperature dependence. This dependence of half-life on temperature is shown experimentally in Fig. 7 and corresponds to an activation energy of about 0.1 ev.

In Section B-5 it was shown experimentally that electroluminescence deterioration is at least somewhat nonuniform, since contraction of the excitation region by reducing the voltage or increasing the frequency leads to a progressively smaller fraction of the light emission originally observed under the same conditions. This is to be expected. Any decrease of the positive charge density (the ionized donor or trapping sites active in the electroluminescence process) due either to incoming deeper traps or depletion of the normal traps by field-migration outward will reduce the field gradient gradually during deterioration and, at constant voltage, expand the high-field region into fresh parts of the phosphor crystal. Hence contraction of this region, as above, confines the excitation to phosphor parts which have been deteriorated the longest.

Evidence for the localization (8) of the electric field with increase in frequency was given in Sections B-5, B-6, and D-2. The pre-aging data of Section B-9 also indicate this effect. To pre-age a lamp to a given fraction of its initial brightness (measured at an arbitrary voltage and frequency) the voltage also must be increased if the frequency is increased; the contraction of the excitation region at the higher frequency must be counteracted by its expansion at higher voltage. Further evidence for this effect is implicit in the data of Sections B-1 and B-2. The blue phosphor, the only one showing better maintenance at high voltage (high fields),

also shows better maintenance as a longer half-life in terms of cycles of operation at high frequency (high fields). The other phosphors have longer half-lives in cycles at low frequency (low fields) and at low voltage (low fields). Incidentally, it was noticed recently that in his major 1947 paper (4) on electroluminescence, Destriau developed an analytical expression predicting higher active fields at higher frequencies of excitation.

The absence of even a slight shift in emission color, as deterioration proceeds to a point where brightness is only a few per cent of initial, suggests that the luminescence centers are not destroyed during electroluminescence deterioration for the following reason. All of the ZnS:Cu, Cl phosphors emit in both of the well-known blue and yellow-green emission bands of this type of phosphor; the blue-green and green emitters of this class, in particular, show substantial components of emission in both of these bands. If the blue and green centers differ significantly in their physical or electrical configuration, and if the motion of one constituent of the centers is involved in electroluminescence deterioration, then one of the centers is likely to be more vulnerable to destruction than the other by the deterioration process. No such effect seems to exist within the experimental error of a few per cent. On the other hand, the trapping and release of electrons is now considered to be an indispensable part of the electroluminescence process (14, 18-21). One theory (14) of electroluminescence in zinc sulfide explains the bulk of typical experimental data by considering only the trapping and release process without dealing explicitly with either recombination at the centers or the ionization process. If this trapping process is quenched by either or both the mechanisms described in Papers I or III, the electroluminescence brightness will deteriorate without destruction of the centers; as already pointed out, the maintenance of photoluminescence suggests that the luminescence centers remain intact.

In Section B-1 it was pointed out that some phosphors show a very definite slowly deteriorating component of light emission after long operation, and that probably all phosphors show this to some degree. In Fig. 15 the brightness-time data of a typical phosphor have been fitted by assuming

$$L = \frac{L_1}{1 + t/t_1} + \frac{L_2}{1 + t/t_2}$$

where $L_1 + L_2 = L_0$ and t_1 and t_2 are the widely different half-lives of the two components; here, $L_1 = L_2 = L/2$, $t_1 = 6$ hr and $t_2 = 97$ hr. In some cases according to such an analysis, the long-lived component deteriorates extremely slowly and is also a major fraction of the initial brightness; an example is the improved maintenance yellow phosphor of Fig. 14.

Acknowledgment

It is a pleasure to acknowledge the cooperation and valuable assistance of the author's associates. He wishes to thank particularly J. VanBroekhoven, W. Lehmann, and A. Wachtel for kindly supplying many of the phosphors, R. L. Fitzmaurice for making the countless lamps and for help in obtaining the data, J. M. Grasso and R. M. Potemski for their assistance, and H. F. Ivey for continued encouragement and helpful discussion.

Manuscript received March 24, 1960. This paper was prepared for delivery before the Chicago Meeting, May 1-5, 1960. Much of the work described in this paper was carried out under Contract AF33(616)5811 from the Wright Air Development Center.

Any discussion of this paper will appear in a Discussion Section to be published in the June 1961 JOURNAL.

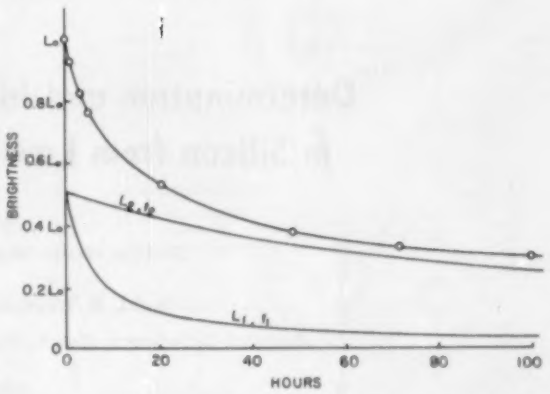

Fig. 15. Resolution of normal maintenance characteristic into short-lived and long-lived components. Standard green phosphor, 150 v, 4000 cps.

REFERENCES

1. H. F. Ivey, *IRE Trans. Electron Devices*, Vol. ED-6, p. 203, April, 1959 (complete bibliography).
2. G. Destriau and H. F. Ivey, *Proc. IRE*, **43**, 1911 (December 1955) (Review Paper).
3. G. Destriau, *J. Chim. Phys.*, **33**, 587 (1936).
4. G. Destriau, *Phil. Mag.*, **38**, 700, 774, 800, 885 (1947).
5. W. A. Thornton, *Bull. Amer. Phys. Soc., II*, **1**, 301 (1956); *J. Appl. Phys.*, **28**, 313 (1957) (Paper I).
6. S. Roberts, *J. Appl. Phys.*, **28**, 262 (1957) (Paper II).
7. S. Roberts, Unpublished work (1952).
8. W. A. Thornton, Papers presented at Electrochemical Society Meeting, New York City, April 27-May 1, 1958, and at International Symposium on Solid-State Physics, Brussels, June 2-7, 1958. (Paper III).
9. W. Hoogenstraaten, *This Journal*, **100**, 356 (1953).
10. F. A. Kröger and J. A. M. Dikhoff, *ibid.*, **99**, 144 (1952).
11. W. Lehmann, *ibid.*, **105**, 585 (1958).
12. P. Goldberg, *ibid.*, **106**, 34 (1959).
13. P. M. Jaffe, To be published.
14. W. A. Thornton, *Phys. Rev.*, **102**, 38 (1956).
15. G. F. Alfrey, I. Cooke, and K. N. R. Taylor, Paper presented at International Symposium on Solid-State Physics, Brussels, June 2-7, 1958. G. F. Alfrey and K. N. R. Taylor, *J. Electronics and Control*, **4**, 417 (1958).
16. W. Lehmann, *This Journal*, **103**, 24 (1956).
17. H. C. Froelich, *J. Opt. Soc. Amer.*, **43**, 320 (1953).
18. P. Zalm, Philips Research Repts., **11**, 353 415 (1956).
19. G. F. Alfrey and J. B. Taylor, *Proc. Phys. Soc. (London)*, **66B**, 775 (1955).
20. P. D. Johnson, W. W. Piper, and F. E. Williams, *This Journal*, **103**, 221 (1956).
21. C. H. Haake, *J. Appl. Phys.*, **28**, 117, 245 (1957); *This Journal*, **104**, 291 (1957); *J. Opt. Soc. Amer.*, **47**, 881 (1957).

Determination and Identification of Impurities in Silicon from Low-Temperature Hall Data

R. T. Bate

Battelle Memorial Institute, Columbus, Ohio

and L. R. Weingarten and D. J. Shombert

Research Laboratory, Merck, Sharp and Dohme, Rahway, New Jersey

ABSTRACT

Low-temperature measurements of the Hall effect have been used to determine donor and acceptor concentrations and in some cases to identify the major impurity in silicon. A simple apparatus for making these measurements with liquid helium is described. Typical results are presented and correlated with lifetime data at room temperature. Interpretation of the Hall coefficient measurements is discussed, and a simplified analysis of the case of the two types of donor impurity is suggested.

Experimental Apparatus

Low-temperature Hall measurements have been used by many workers to study impurity levels in silicon.[1, 2] This paper describes the use of such measurements to evaluate high-purity Merck silicon.

Figure 1 shows the Dewar used for these measurements, which is relatively simple in design. The liquid nitrogen Dewar which serves as a radiation shield has been omitted for clarity. The Dewar, made of Pyrex, is arranged so that four samples can be run at one time, and these are fastened to a relatively massive brass block which is surrounded by a tube containing helium gas at 1 atm. Outside this is a reflux column, in which the helium pressure can be varied to control the transfer of heat from the samples to the liquid helium bath above. The gasket seal at the top of this column is arranged so that the pressure cannot cause an explosion as the Dewar warms. Under proper conditions, the samples will warm from 20° to 80°K in 5-6 hr. Measurements are made by d-c potentiometry, and the magnetic field is monitored by NMR.

Theory of Hall Effect

In extrinsic silicon, the Hall coefficient in a homogeneous rectangular sample is given by Eq. [1], [2], and [3], shown below

$$R = 10^8 \frac{V_H T}{IH} \frac{\text{cm}^3}{\text{coulomb}} \qquad [1]$$

$$R_n = \frac{r_n}{ne}, \frac{1}{e} = 6.25 \times 10^{18} \text{ coulomb}^{-1} \qquad [2]$$

$$R_p = \frac{r_p}{pe} \qquad [3]$$

V_H is the Hall voltage, I is the current in amperes, T is the thickness in cm, and H is the magnetic flux density in gauss; p and n are the hole and electron concentrations, respectively, and r_n and r_p are the respective Hall coefficient factors. These factors depend in general on crystal orientation, impurity

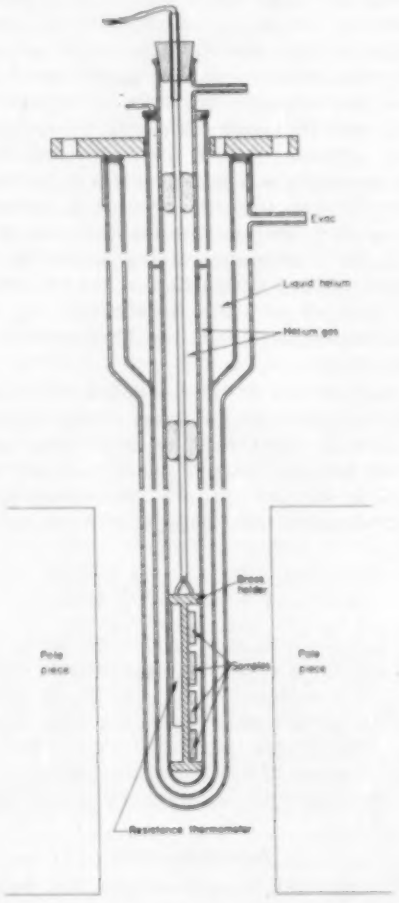

Fig. 1. Dewar for Hall measurements

[1] A method of determining the degree of compensation of p-type silicon from magnetoresistance measurements of liquid nitrogen temperature has been proposed also (1).

[2] References to much of this work are given in the review articles by Burton (2) and Kohn (3).

concentration, temperature, and magnetic field. If they can be determined, then the hole or electron concentration can be deduced directly from Hall measurements.

A discussion of the Hall coefficient factor for p-type silicon has been given by Beer and Willardson (4), and Gold and Roth (5) have studied n-type silicon. In p-type material, this factor is quite sensitive to ionized impurity scattering; however, the effect of impurity scattering in n-type material has not been calculated in terms of the exact conduction band structure. In high-purity silicon, the Hall coefficient factors are probably near unity below 40°K for reasonably strong magnetic fields. This assumption has been justified for p-type silicon by the careful work of Klein and Straub (6). Since our analysis of the Hall data required consideration only of the region below 40°K and the exhaustion region, correction for the Hall coefficient factor was necessary only in the determination of the exhaustion carrier concentration. The effect of impurity scattering in the exhaustion region in p-type material can be included by assuming initially that $r_c = 1$ at all temperatures and by calculating an approximate impurity concentration. This concentration is used then to calculate an impurity mobility from which the Hall coefficient factor can be evaluated by the method of Beer and Willardson. The Hall coefficient factor so determined then is used to correct the exhaustion carrier concentration.

The electron or hole concentration in extrinsic material is given by Eq. [4] or [5] below:

$$\frac{n(n+N_a)}{N_d-N_a-n} = A_c T^{3/2} \frac{\Sigma_i N_d^i f_d^i \exp(-\epsilon_d^i)/KT}{\Sigma_i N_d^i f_d^i},$$

$$A_c = 2.78 \times 10^{15} \frac{\text{deg}^{-3/2}}{\text{cm}^3} \quad [4]$$

$$\frac{p(p+N_d)}{N_a-N_d-p} = A_v T^{3/2} \frac{\Sigma_i N_a^i f_a^i \exp(-\epsilon_a^i)/KT}{\Sigma_i N_a^i f_a^i},$$

$$A_v = 5.62 \times 10^{15} \frac{\text{deg}^{-3/2}}{\text{cm}^3} \quad [5]$$

where N_a and N_d are the total acceptor and donor concentrations and N_a^i, f_a^i, and ϵ_a^i are the concentration, Fermi factor, and activation energy for a particular species of acceptor, N_d^i, f_d^i, and ϵ_d^i are the corresponding quantities for a particular donor. The Fermi factor for an impurity is just the probability that it is not ionized and for an acceptor is given by

$$f_a^i = \{1 + \tfrac{1}{4} \exp[(\epsilon_F - \epsilon_a^i)/KT]\}^{-1}$$

and for a donor by

$$f_d^i = \{1 + \tfrac{1}{2} \exp[(\epsilon_F - \epsilon_d^i)/KT]\}^{-1}$$

where ϵ_F is the Fermi energy. These equations are derived under the following assumptions: (*a*) only singly ionized (*i.e.*, groups III and V) impurities are present; (*b*) classical statistics hold; (*c*) no local interaction between impurities occurs; (*d*) excited bound states of carriers on impurities can be ignored (7); (*e*) the spin-orbit splitting of the degenerate ground state of the electron at the impurity site and perturbations of the band structure by the impurity can be assumed negligible (7); (*f*) the ground state of a donor is assumed doubly degenerate and that of an acceptor fourfold degenerate; and (*g*) impurity band conduction is not important. Under these assumptions, a unique activation energy can be defined which is just equal to the energy necessary to excite an electron from the valence band into the ground state of an acceptor or from the ground state of a donor into the conduction band.

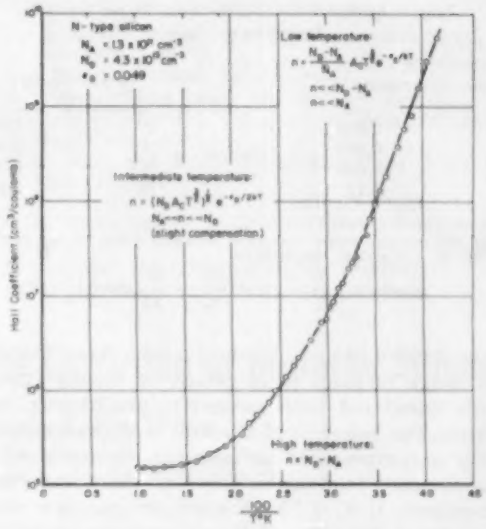

Fig. 2. Temperature dependence of Hall coefficient of n-type silicon.

Results and Discussion

Since the activation energies are known (8) for most singly ionized impurities in silicon, it is theoretically possible to identify those impurities and to determine the total donor and acceptor concentrations by fitting Hall data to these equations.

Figure 2 shows a temperature plot of the Hall coefficient for an n-type sample in which one donor (arsenic) seems to be predominant. This leads to the familiar situation in which three approximately linear regions appear on a semilog plot of the Hall coefficient *vs.* reciprocal temperature. The equations for the carrier concentration in each of these regions are given in the figure. The intermediate linear region occurs only in relatively uncompensated samples. The slope in this region is just half that in the low temperature region (neglecting the $T^{3/2}$ factor). The transition between these two regions occurs when the carrier concentration is approximately equal to the minority impurity concentration.

The fact that the intermediate linear region is observed in an n-type sample of this purity is rather surprising, since it suggests a very low boron concentration. Note from Fig. 2 that the analysis yields an acceptor concentration of the order of 10^{13} cm^{-3}. It is not clear whether this figure indicates the true boron content or whether some of the boron has become electrically inactive, possibly because of local interaction with some other impurity or defect.

The Hall plots for many undoped n-type samples show approximately linear regions between 20° and 40°K which correspond to activation energies in the

Table I. Activation Energies for Group III and Group V Impurities in Silicon

Group III acceptors	ev	Group V donors	ev
B	0.046	P	0.044
Al	0.057	As	0.049
Ga	0.065	Sb	0.039
In	0.16	Bi	0.067

For two donors whose activation energies differ by $\Delta\epsilon_1$ plot ln $(T^{3/2}/R)$ *vs.* $1/T$ at low temperature:

$$\text{Slope} = 1/k\left[\epsilon_1 + kT\ln\left(\frac{N_1}{N_d} + \frac{N_2}{N_d}e^{\Delta\epsilon/kT}\right)\right]$$

range 0.039–0.049 ev. As can be seen from Table I, this range includes three relatively closely spaced levels associated with antimony, phosphorus, and arsenic. The behavior of the Hall coefficient in relatively uncompensated samples can be explained if it is assumed that two or three of these impurities are present. If $N_a << N_d$, the low-temperature slope of a plot of $T^{3/2}$ x the Hall coefficient *vs.* reciprocal temperature for the case of two donors in an n-type sample is $1/k[\epsilon_1 + kT\ln(N_1/N_d + N_2/N_d \exp^{\Delta\epsilon/kT})]$ where N_1 is the concentration of the donors with the lower activation energy, N_2 is the concentration of those with the higher activation energy, and $\Delta\epsilon$ is the difference of their activation energies. This slope is somewhat temperature dependent, but it always lies between the slopes expected for donor one alone and donor two alone. Assuming that the average experimental slope is given approximately by its value at 25°K, we can define an effective activation energy for a pair, and the carrier concentration at 25°K then is given by an equation which is of the same form as the relation for a single donor. Thus the total donor and acceptor concentrations for the case of two donors can be determined from the Hall coefficient at 25°K, the slope of the $T^{3/2}R$ plot at 25°K, and the exhaustion Hall coefficient in the same way they are found in the case of a single donor. This procedure is valid only provided $n(25°K) << N_a << N_d$ because the relative populations of the two levels are influenced by compensation.

For the case of two donors, the effective activation energy is easy to compute, and Fig. 3 shows a plot for the pairs, Sb-P, P-As, and Sb-As as a function of relative concentration. If measurements are made carefully, these plots can be used to estimate the relative concentrations for different pairs which might be present.

Figure 4 shows a Hall plot for two p-type samples. The low-temperature slopes are both characteristic of boron, but number two, which is from a zone refined crystal, still exhibits the intermediate temperature characteristic at the lowest temperatures. This is indicative of extremely low compensation.

Table II gives a summary of the results of Hall and room temperature lifetime measurements on some single crystal silicon samples.

Conclusions

The activation energies of the p-type samples investigated were all characteristic of boron, and the

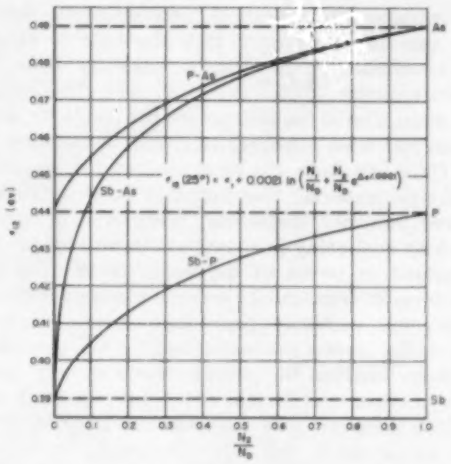

Fig. 3. "Effective" activation energy for pairs of donors in silicon at 25°K.

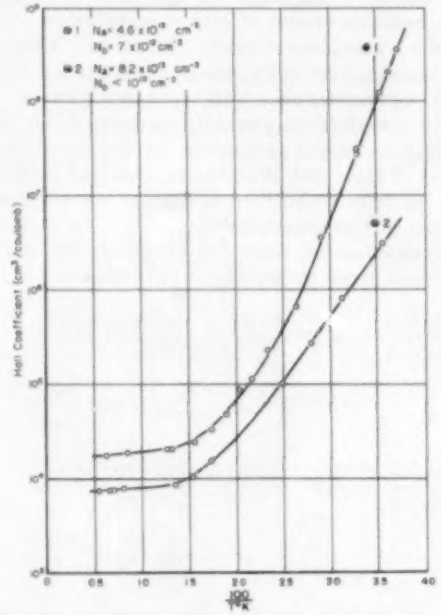

Fig. 4. Temperature dependence of Hall coefficient for two p-type silicon samples.

"effective" activation energies of the n-type samples were in the range 0.039–0.049 ev. It is concluded from this that the major acceptor impurity in all the samples investigated is boron and that it is present in concentrations of about 10^{15} cm^{-3}. The major

Table II. Lifetime Data on Some Single Crystal Silicon Samples

Sample	N_a, cm^{-3}	N_d, cm^{-3}	$N_a + N_d$, cm^{-3}	Lifetime, μ sec
B-95-5A	2.6×10^{15}	1.3×10^{15}	3.9×10^{15}	150
B-21-25B	8.3×10^{15}	$<10^{15}$	8.3×10^{15}	800
50-EX-126C	1.0×10^{15}	5×10^{13}	1.5×10^{15}	>1000
50-EX-122B	8.9×10^{15}	$<10^{15}$	9×10^{15}	600
B-15-17B	7×10^{15}	1.4×10^{15}	2.1×10^{15}	500
50-EX-126B	2.4×10^{15}	2.4×10^{15}	4.8×10^{15}	100
50-EX-122A	1.2×10^{15}	5.4×10^{15}	6.6×10^{15}	200
50-EX-111	1.6×10^{15}	3.2×10^{15}	4.8×10^{15}	600

donor impurities appear to be phosphorus, antimony, and arsenic, and their concentration is apparently reduced to less than 10^{15} cm^{-3} in some zone refined material.

Acknowledgment

The authors are indebted to J. J. Duga and F. J. Reid for making some of the Hall measurements, and to H. Leonard for sample preparation.

Manuscript received Feb. 11, 1960.

Any discussion of this paper will appear in a Discussion Section to be published in the June 1961 JOURNAL.

REFERENCES

1. Long, Motchenbacher, and Myers, *J. Appl. Phys.*, **30**, 353 (1959).
2. J. A. Burton, *Physica*, **20**, 845 (1954).
3. W. Kohn, "Solid State Physics," F. Seitz and D. Turnbull, Editors, Vol. 5, p. 257, Academic Press, New York (1957).
4. A. C. Beer and R. K. Willardson *Phys. Rev.*, **110**, 1286 (1958).
5. L. Gold and L. M. Roth, *ibid.*, **107**, 358 (1957).
6. C. A. Klein and W. D. Straub, Private communication.
7. E. H. Putley, *Proc. Phys. Soc.*, **72**, 917 (1958).
8. E. M. Conwell, *Proc. IRE*, **46**, 1281 (1958).

A Modified Closed Box System for the Diffusion of Boron in Silicon

R. S. Yatsko and J. S. Kesperis

U. S. Army Signal Research and Development Laboratory, Fort Monmouth, New Jersey

ABSTRACT

A modified closed box diffusion system has been investigated over a wide range of conditions. Boron layers have been diffused in silicon from B_2O_3-SiO_2 sources ranging from concentrations of 0.2% B by weight to pure B_2O_3. Non-melting source conditions have been varied to melting source conditions yielding surface concentrations ranging from 10^{19} to 10^{21} carriers/cc. Some effects of environmental atmospheres and materials are discussed. Applications to photovoltaic devices and double diffused transistors are described.

Boron diffusion is by far the most common approach today in the achievement of precision controlled p-type areas in silicon semiconductor devices. Yet methods currently in use for obtaining desirable surface concentrations of boron utilize widely varying diffusion techniques. Even techniques for the production of diffused areas of similar doping content and depth vary widely from one user to the other.

It is the objective of this paper to discuss the investigation of a general diffusion system for boron, capable of reproducibly attaining particular surface concentrations in the range 10^{19} to 10^{21} atoms/cc by using only simple variations of source concentration, temperature, and time. Experimental data, the capabilities, and limitations of this process are discussed, and although a complete investigation of the system is not presented, the results obtained have already been successfully applied to various semiconductor devices at these laboratories and should serve as useful information to those concerned with the design and fabrication of silicon devices.

Experimental

Figure 1 shows a typical diffusion boat consisting of quartz with provisions for holding a small platinum box in the center which carries the source material. Two center posts contain the box and separate it from two end compartments which carry the silicon wafers. The boat is constructed by sealing off tubular quartz and cutting a longitudinal section off, such that approximately ¾ of the cross-section area remains on the boat. The cut edges of the boat are carefully lapped flat with a 600 grit. A quartz flat plate acts as a cover plate. A 0.003 in. platinum sheet, equal in area to the quartz flat, acts as a gasket between the lapped edges and the cover plate. It is this gasket which forms a partial seal for the diffusion process. A single annealing process at 1100°C was sufficient to allow the platinum gasket to form on the contours of the quartz boat. The gasket could then be used many times with the same boat during subsequent diffusion runs with no further forming treatment. During the actual diffusion run, platinum wire was wrapped tightly about the entire assembly to prevent any movement of the parts during insertion and removal from the furnace.

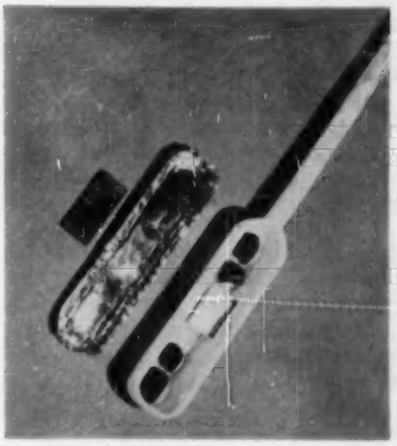

Fig. 1. Modified closed box showing quartz boat containing Pt source box and polished Si wafers. Formed Pt gasket is shown at left.

The boat thus constructed has only a partial seal and differs from a sealed capsule in this respect. However, the disadvantage of a finite leak rate was

not found to be significant as far as achievement of desired surface concentrations was concerned; the obvious advantages of ease in loading and re-use made it quite preferable to a sealed capsule technique.

Silicon wafers were polished carefully to a mirror finish using Linde A abrasive in an automatic bowl feed polisher. Diffusion was carried out in a Kanthal wound furnace using alundum tubes sealed off carefully at each end, with provisions for the insertion of the boat and dry argon gas.

Junction depths were measured by standard angle lapping and staining techniques (1). Evaluation of surface concentrations were made with four-point probe resistance measurements and the published data of Backenstoss (2).

Effects of system materials and environmental atmospheres.—The B_2O_3-SiO_2 source is reactive with quartz and must be isolated from the quartz in the system. Initial attempts to use a high purity graphite modified closed box resulted in very nonuniform silicon surface layers that could not be removed by HF, dilute NaOH, or boiling HNO_3 followed by HF rinses. Furthermore, a significant erosion of the actual silicon surface was observed. These difficulties are eliminated by the use of either an all-platinum system (with provisions for holding the silicon on quartz flats) or an all-quartz system with a platinum container for the source as was adopted for these experiments.

The nature of the surrounding atmosphere and particularly the presence of the water vapor is of major importance in a closed box system which is not sealed totally against leaks. Early attempts to use the modified closed box with a surrounding air ambient consistently produced diodes with very low forward inflection voltages. Solar converters produced in this manner gave corresponding open-circuit voltages in the 0.3-0.4 v range. It became necessary to make the diffusion tube air tight and to flush the system carefully with argon which was passed through two liquid nitrogen traps to insure an acceptable level of dryness. The incorporation of these methods improved the reproducibility of electrical characteristics and resulted in normal inflection voltages.

Preparation of the diffusion source.—Four selected sources were prepared for diffusion from boric and silicic acids. Compositions ranged from the equivalent of pure boron oxide to 0.2% boron in the following manner: pure B_2O_3, $4B_2O_3$-$1SiO_2$, $1B_2O_3$-$1SiO_2$, and 0.2% B. The composite sources were prepared by mixing boric and silicic acid powders together, adding distilled, deionized water, drying over low heat with constant stirring. The source was then placed in a platinum source box and sintered at the diffusion temperatures under a dry argon atmosphere.

Diffusion from composite oxide sources must be preceded by a suitable sintering at either the diffusion temperature or at temperatures slightly higher in order to obtain consistent diffusion results. The sintering or "bake out" process is used to dry and homogenize the source and at the same time probably acts to saturate the quartz box with boron. As can be expected, nonmelting oxide sources are much more difficult to homogenize than melting sources. Consistent diffusion results have been obtained with melting sources after 1.5-2 hr of bake out, depending on the diffusion temperature and SiO_2 concentration in the source, while bake out times of 6 to 7 hr were necessary with nonmelting oxide sources. Thurston (3) and co-workers have studied the bake out time required for 0.1% B sources by experimentally comparing the diffusivities of phosphorus and boron in silicon dioxide. Although boron showed five times the diffusivity of phosphorus in silicon dioxide, bake out of nonmelting boron-silicon dioxides required 7 hr while nonmelting phosphorus-silicon dioxide sources required only 3 hr. It was also found that when fresh sources of B_2O_3-SiO_2 were used in an already used quartz capsule, an additional 7 hr bake out was necessary. On the basis of these experiments, the saturation of the source and quartz capsule could not explain effectively the unusually long bake out time required for nonmelting B_2O_3-SiO_2 sources.

Results and Discussion

Runs 1 and 2 in Table I show the range of results obtained for diffusions at 1129°C with a 0.2% B nonmelting source. Runs 3 to 5 show the results at 1218°C. Surface concentrations varied only by one-half order of magnitude between these temperature extremes. Reproducibility of penetration and doping at a given temperature was very good. These diffusions were characterized by very uniform post diffusion oxides with a maximum oxide thickness of 2800Å at 1218°C for 30-min diffusion time. Excellent uniformity of surface concentration was found over the entire area of the diffused wafers.

In order to obtain high surface concentrations at temperatures practicable for device manufacture, it was found necessary to increase the B_2O_3 in the source. It was determined that the order of 0.2% B represented the maximum concentration for nonmelting conditions in the source at 1200°C. An order of magnitude increase in boron concentration produced partial melting at temperatures as low as 1125°C. Progressive increases in the B_2O_3 concentration changed the appearance of the baked out source from a white powder (0.2% B) to an agglomeration of small hemispherical globules (2% B), through a series of uniformly white translucent glasses to 50% B_2O_3, followed by an increase in the transparency of the melt as the pure B_2O_3 glass was approached. The change in source appearance from nonmelting to melting conditions was accompanied by a sharp departure in appearance of the post diffusion oxides. It was found impossible to maintain uniformity in the grown oxide with melting sources. These variations in oxide thickness were accompanied at certain temperatures with nonuniformity in sheet resistance over the area of the diffused wafer, but in most cases, very uniform results were obtained.

Diffusion from 50% B_2O_3 sources had to be carried out at 1125°C or higher in order to obtain uniform sheet resistances over the entire wafer area. Runs 6 and 7 (Table I) show the variation in sheet resistance obtained on two wafers at 1100°C. Variations

Table I. Tabulation of data summarizing obtainable surface concentrations under various conditions of diffusion source and temperature

Run	Source	Bulk carrier conc.	Time, min	Temp, °C	Sheet res., ohms/square	Junction depth, μ	Surface conc., carriers/cc
1	0.2% B	7×10^{15}	30	1129	1015	0.5	6×10^{19}
2	0.2% B	7×10^{15}	30	1129	1380	0.45	4×10^{19}
3	0.2% B	7×10^{15}	30	1218	134	2.3	9×10^{19}
4	0.2% B	7×10^{15}	30	1218	130	2.2	1×10^{19}
5	0.2% B	7×10^{15}	30	1218	145	2.3	8×10^{19}
6	50% B_2O_3	9×10^{15}	15	1100	17-29	1.1	2×10^{20}
7	50% B_2O_3	9×10^{15}	15	1100	82-104	1.1	3×10^{19}
8	50% B_2O_3	7×10^{15}	25	1125	7.0	1.9	3×10^{20}
9	50% B_2O_3	7×10^{15}	25	1125	3.4	2.3	4×10^{20}
10	50% B_2O_3	7×10^{15}	20	1125	3.9	1.9	4×10^{20}
11	50% B_2O_3	7×10^{15}	20	1125	9.0	1.8	2×10^{20}
12	50% B_2O_3	8×10^{15}	15	1200	0.82	4.0	8×10^{20}
13	50% B_2O_3	8×10^{15}	15	1200	1.0	3.6	8×10^{20}
14	50% B_2O_3	8×10^{15}	15	1200	0.94	3.9	8×10^{20}
15	50% B_2O_3	8×10^{15}	15	1200	1.8	3.8	5×10^{20}
16	50% B_2O_3	8×10^{15}	15	1200	0.85	3.2	1×10^{21}
17	80% B_2O_3	8×10^{15}	15	1125	5.5	1.5	3×10^{20}
18	80% B_2O_3	8×10^{15}	15	1125	4.6	1.9	3×10^{20}
19	80% B_2O_3	8×10^{15}	15	1125	8.3	1.8	2×10^{20}
20	80% B_2O_3	8×10^{15}	15	1125	7.3	1.5	4×10^{20}
21	80% B_2O_3	8×10^{15}	15	1125	5.2	1.6	4×10^{20}
22	B_2O_3	8×10^{15}	150	1000	15.5	1.3	2×10^{20}
23	B_2O_3	8×10^{15}	150	1000	14.2	1.3	2×10^{20}
24	B_2O_3	8×10^{15}	150	1000	17.6	1.2	1.5×10^{20}
25	B_2O_3	8×10^{15}	150	1000	16.8	1.2	1.5×10^{20}
26	B_2O_3	8×10^{15}	150	1000	15.2	1.3	2×10^{20}
27	B_2O_3	8×10^{15}	150	1000	19.2	1.2	1.5×10^{20}
28	B_2O_3	8×10^{15}	150	1000	14.3	1.3	2×10^{20}

of one order of magnitude in surface concentration were observed from wafer to wafer at 1100°C. Uniform sheet resistances were obtained at 1125°C and higher, with a much greater reproducibility in surface concentration. Runs 8 to 11 show the range of diffusion results for 25 min and 20 min diffusion time at 1125°C. Higher surface concentrations were obtained at 1200°C with the 50% B_2O_3 source. Runs 12 to 16 list the data obtained from the five wafers diffused at 1200°C.

In order to determine whether an increase in boron concentration would result in higher surface concentrations at 1125°C, five runs were made with an 80% B_2O_3 source (Runs 17-21). No significant difference was observed in surface concentration between the two sources at 1125°C. At 1200°C the difficulty encountered in removing postdiffusion oxide layers from the 80% source made a comparison with the 50% source impossible.

It was found that the postdiffusion oxides became more difficult to remove with longer diffusion times. Although no difficulties were encountered with the 50% and 80% source at 1125°C for diffusion times of 15 min to ½ hr, deep diffusions of 4 hr duration produced surface layers very difficult to remove. Diffusions for 4 hr at 1200°C produced surface layers which were impossible to remove. Diffusions from pure B_2O_3 sources had to be performed at temperatures below 1025°C to prevent pitting and erosion of the silicon surface. However at 1000°C, no difficulties were encountered for diffusion times as long as 2.5 hr.

Runs 22-28 list the data from 7 control runs made at 1000°C for 2.5 hr with pure B_2O_3 as the source. Excellent control of sheet resistance and penetration was obtained.

Fabrication of solar cells.—Five solar cells were fabricated utilizing the pure B_2O_3, 1000°C process. Since doping levels of 2×10^{20} were obtainable by this process, it was thought that the relatively low temperature required would be the least deleterious to the lifetime in the device, and this was the basis for choosing this as the beginning process in determining the optimum modified closed box process for solar cell fabrication. The diffused cells were given electroless nickel contacts to both p- and n-sides, followed with a solder dip. A polystyrene coating was placed over the active area to reduce reflection. Evaluation was conducted with a tungsten filament light source, filtered through a water bath to reduce the infrared. The illumination was calibrated to a radiation rate of 84.4 mw/cm². The total dark current series resistance amounted to 0.2 ohm. Surface concentrations and junction depths were as shown in Table I for the pure B_2O_3 runs. Results are indicated in Table II. Figure 2 shows the comparative light output current-voltage characteristics for cells 1 and 5 which represent the performance extremes from this group.

Application to Transistor Fabrication

The technique was applied to the fabrication of the emitter region of a p-n-p transistor. Table III

Table II. Tabulation of output efficiency data of 5 solar cells fabricated by diffusion from a pure B_2O_3 source at 1000°C

Cell	Area, cm²	E_{oc}, V	E_{mp}, V	I_{mp}, ma	P_{mp}, mw	Efficiency, %
1	1.80	0.560	0.442	38.5	17.0	11.2
2	1.44	0.555	0.420	32.3	13.8	11.2
3	1.67	0.550	0.409	37.2	15.2	10.8
4	1.71	0.550	0.420	38.1	16.0	11.1
5	1.50	0.550	0.420	32.3	13.6	10.7

Table III. Tabulation of data showing results of emitter diffusions using a modified closed box system

Run	Source	Time, min	Temp, °C	Sheet res., ohms/square	Junction depth, μ	Surface conc, carriers/cc	Junction depth base diffusion, μ	Base width, μ
1	80% B_2O_3	12	1120	6.0	1.4	3.5×10^{20}	2.4	1.0
2	80% B_2O_3	12	1120	4.0	1.4	4.0×10^{20}	2.4	1.0
3	80% B_2O_3	12	1120	6.0	1.3	4.0×10^{20}	2.4	1.1
4	80% B_2O_3	12	1120	4.5	1.3	3.5×10^{20}	2.4	1.1
5	50% B_2O_3	15	1125	11.3	1.4	2.0×10^{20}	2.5	1.1
6	50% B_2O_3	15	1125	11.2	1.4	2.0×10^{20}	2.5	1.1
7	50% B_2O_3	15	1106	15.5	1.0	2.0×10^{20}	2.5	1.5
8	50% B_2O_3	15	1106	14.4	1.1	2.0×10^{20}	2.5	1.4
9	50% B_2O_3	15	1106	15.7	1.1	2.0×10^{20}	2.5	1.4
10	Pure B_2O_3	150	1000	7.9	1.3	2.0×10^{20}	2.5	1.2
11	Pure B_2O_3	150	1000	8.0	1.3	2.0×10^{20}	2.5	1.2
12	Pure B_2O_3	150	1000	10.2	1.2	2.0×10^{20}	2.4	1.2
13	Pure B_2O_3	150	1000	10.3	1.2	2.0×10^{20}	2.4	1.2
14	Pure B_2O_3	150	1005	5.4	1.5	2.0×10^{20}	2.5	1.0
15	Pure B_2O_3	150	1005	6.2	1.6	2.0×10^{20}	2.5	1.0

shows results obtained for a number of emitter diffusion runs. The base region into which the boron emitters were diffused was diffused previously with antimony. The antimony depth of diffusion was approximately 2.5 μ and the surface concentration ranged from 1×10^{19} atoms/cc to 2×10^{19} atoms/cc. It was necessary to diffuse the boron emitters to shallow depths in order to maintain a thin base region. The aim was to diffuse the boron emitters to depths varying from 1.0 to 1.5 μ, attain a surface concentration greater than 10^{20} atoms/cc, and obtain masking in regions where the boron was not desired. Examination of Table III reveals that the sheet resistance of the group of wafers diffused with the 80% source ranged from 4 to 6 ohms/square. Diffusion depths varied from 1.3 to 1.4 μ for the temperature and time used, and the surface concentration achieved ranged from 3×10^{20} to 4×10^{20} atoms/cc for the temperature used. Diffusions with the 50% source were performed at two different temperatures, 1125° and 1106°C. At 1125°C the diffusion depths obtained were 1.4 μ and the sheet resistance was 11.2 ohms. At 1106°C the diffusion depths varied from 1.0 to 1.1 μ and the sheet resistances from 14.4 to 15.7 ohms. A surface concentration of 2×10^{20} atoms/cc was obtained at both temperatures at which the diffusions were made. Pure B_2O_3 was used for lower temperature diffusions. A surface concentration of 2×10^{20} atoms/cc was achieved at the temperature used. Sheet resistances varied from 8 to 10 ohms/square and junction depths ranged from 1.2 to 1.3 μ. No difficulty was encountered in removing the oxides from any of the diffused samples. Masking of boron where desired can be obtained by choosing a suitable combination of diffusion conditions and oxide thickness. For the diffusion conditions listed and an oxide thickness of approximately 1800Å complete masking of boron was achieved. The three melting sources have been used for forming emitters in fabricating a high-frequency p-n-p transistor. The nonmelting source is an excellent technique for forming a base region in a n-p-n or n-p-i-n structure.

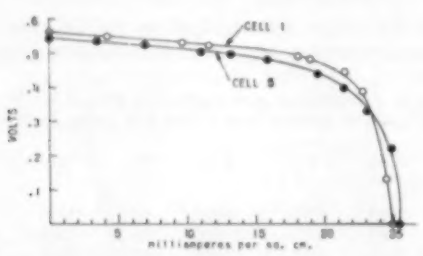

Fig. 2. Output current-voltage characteristics for cells 1 and 5 under 84 mw/cm² illumination.

Summary

The box technique described herein can be utilized with good advantage on many areas of silicon device technology. Specifically, the excellent control and uniformity of nonmelting sources (0.2% B max) is ideally suited for formation of base areas in n-p-n transistor structures where concentrations over 1×10^{19} carriers/cc are not required. Highly doped areas, 5×10^{20}-1×10^{21} can be obtained easily with the 50% B_2O_3 source. Moderate doping in the 1×10^{20}-5×10^{20} range is best obtained with the 50% and 80% B_2O_3 sources. Where low diffusion temperatures are required, pure B_2O_3 sources can consistently yield doping levels of 2×10^{20} at 1000°C. Consistently reproducible high efficiency solar converters in the 11% efficiency range are being made from pure B_2O_3 sources. Higher conversion efficiencies may be possible by increasing the surface concentration by diffusion from a composite source at higher temperatures, but this remains to be seen.

Emitter junctions have been made by three different diffusion sources, 80% B_2O_3, 50% B_2O_3, and pure B_2O_3. All three sources met specific device p n p requirements of doping (2×10^{20} min), successful oxide masking of the base, and ease of emitter oxide removal. The specific process for a particular device will depend of course on the best device yield as well as on meeting the design specifications.

General observations of the process can be summarized as follows: (*a*) long time diffusions (4 hr) with composite sources produced very tenacious surface layers and irregular junctions; (*b*) a minimum SiO_2 concentration of 50% was required for diffusion at 1200°C or above; (*c*) 50% sources required temperatures of 1125°C min for best repro-

ducibility of diffusion results; and (*d*) diffusion from pure B_2O_3 sources must be restricted to a maximum temperature of 1025°C to minimize surface erosion and pitting. At 1000°C, no difficulties are encountered.

Acknowledgment

The authors wish to thank Dr. Howard Loar of Bell Telephone Laboratories, Murray Hill, New Jersey, for the helpful discussions on the effects of environmental atmospheres on boron diffusions, and Messrs. J. Mandelkorn and A. LaRocque, USASRDL, for their helpful comments during the course of this work. Particular indebtedness is due Mr. W. Pharo, USASRDL, whose careful growth and preparation of silicon material made this work possible.

Manuscript received March 21, 1960. This paper was prepared for delivery before the Houston Meeting, Oct. 9-13, 1960.

Any discussion of this paper will appear in a Discussion Section to be published in the June 1961 JOURNAL.

REFERENCES

1. C. S. Fuller and J. A. Ditzenberger, *J. Appl. Phys.*, **27**, 544 (1956).
2. G. Backenstoss, *Bell System Tech J.*, **37**, 699 (1958).
3. M. O. Thurston ond J. Tsai, O.S.U. Research Foundation, Contract DA-36-039, sc-83874, Rpt 896-3 (1959).

Properties of PbSe Prepared by Powder-Metallurgy Techniques

J. F. Miller and R. C. Himes

Battelle Memorial Institute, Columbus, Ohio

ABSTRACT

The application of powder-metallurgy techniques to the preparation of bulk specimens of lead selenide was studied; both the hot-press and the press-and-sinter methods were employed. Compacting pressure, sintering temperature sintering time, and the particle size of the powder were treated as variables. Electrical and thermoelectric properties, densities, and microstructures of the specimens were studied.

Sound specimens of near-theoretical density and with electrical and thermoelectric properties similar to those of the best of cast lead selenide were prepared successfully by the hot-press method. Densities of hot-pressed specimens, which were highest for those prepared at 750°C, 8100 psi, were observed to decrease with sintering temperature in the range 750°-450°C, and with compacting pressure in the range 8100-2000 psi. The pressed-specimen density was not affected appreciably by variations of sintering time (in the range 5 min-5 hr at 750°C) or variations of the particle size of the powder (in the range —60 to —200 mesh). Electrical properties of specimens with densities in the range 90-98% of theoretical, which were prepared by both the hot-press and the press-and-sinter methods, did not change significantly as density varied in this range.

Lead selenide is a potentially useful semiconductor for several types of applications. Among these are applications which make use of (*a*) its thermoelectric properties, and (*b*) the (high) positive temperature coefficient of resistance of doped lead selenide in the extrinsic temperature range. However, when conventional casting techniques are used to prepare lead selenide circuit elements, several difficulties are encountered. Unless temperature and environment are controlled precisely, there is a pronounced tendency for pores or voids to form in the castings. If cooling rate is low enough to induce reasonable crystal growth, doping elements segregate. Both of these phenomena tend to produce electrically heterogeneous castings. In addition, when special shapes are required, they often cannot be cast at all or cannot be cast with the desired degree of precision. Use of powder-metallurgy techniques was seen as one possible means of satisfactorily circumventing these difficulties, providing specimens with acceptable physical and electrical properties could be prepared in this manner.

In this investigation of the application of powder-metallurgy techniques to the preparation of lead selenide, both the hot-press and the press-and-sinter methods were employed. Compacting pressure, sintering temperature, sintering time, and particle size of the powder were treated as variables. Electrical and thermoelectric properties, densities, and microstructures of the specimens were studied to evaluate the processes.

Experimental Procedures

The lead selenide used in this research was prepared initially by reacting high-purity (99.999%) lead and selenium in the molten state in evacuated, sealed, quartz containers. The master batch of n-type material, which was used in the majority of the experiments, was doped with 0.25 at. % excess lead and 0.025% by weight of bismuth. To ensure that this material would be as nearly uniform as possible, it was quenched in room-temperature oil from the molten state. The p-type lead selenide employed was from an ingot which was cast by the Bridgman method and doped with 0.02% by weight of arsenic.

Except as is otherwise noted, the powders were prepared, classified as to particle size, loaded into

the pressing equipment, and were pressed in an atmosphere of dry argon. The powder-metallurgical specimens prepared were cylinders ⅝ in. in diameter by approximately ½ in. long.

Hot pressing was done in inductively heated graphite dies. Design and operation of the hot-pressing apparatus has been described by Bourke, *et al.* (1). Hot pressing was done at three temperatures, 750°, 600°, and 450°C; at three compacting pressures, 8100, 4000, and 2000 psi; and for various sintering times in the range 5 min-5 hr. Powders of three particle-size ranges were used: −200 mesh; −100 + 200 mesh; and −60 + 100 mesh.

Specimens prepared by the press-and-sinter method were first compacted in latex tubes under 100,000-psi hydrostatic pressure. The compacts then were transferred to quartz tubes, which were evacuated and sealed with a minimum of free (vapor) space. The specimens were sintered at temperatures of 450°, 600°, and 750° for a period of 5 hr.

For anneal treatment, cast specimens also were sealed in close-fitting, evacuated quartz tubes. Similar cooling rates were established following the heat-treatment step in all three processes (*i.e.*, hot press, press and sinter, and anneal) so that specimens would be comparable in this respect.

Electrical measurements were made on bridge-type Hall specimens to which Chromel leads were attached by spot welding. Both d-c and a-c Hall measurements were made. In cases where both types of measurements were made on a given specimen, values for resistivity, Hall coefficient, and mobility obtained from the a-c data were generally lower (*e.g.*, mobilities lower by 5-10%) than those from the d-c measurements. A qualitatively similar change was noted in d-c values when procedure was altered from that of making measurements after a steady-state condition had been obtained to that of making measurements as soon as possible after current and magnetic field had been turned on. It is likely that the differences arise because of the relatively large Peltier effect in this high-Z material.[1]

Thermoelectric properties were determined by use of the "Z-meter" (2). This device makes possible reasonably accurate measurements of both the Seebeck coefficient and thermal conductivity of such small (1.5 cm long) specimens as were available for this research.

Densities were determined gravimetrically by the hydrostatic method and were measured with respect to both ethanol and methanol. It was found that water, which was initially tried as a reference fluid, does not "wet" lead selenide perfectly, and as a result yields scattered, low values. With the technique employed, multiple measurements were made yielding mean density values to which probable errors of less than ±0.01 g/cm³ could be ascribed in every case.

In preparing the specimens for metallographic examination, Murakami's electrolytic etch, containing 22 parts $K_3Fe(CN)_6$, 5 parts NaOH, and 945 parts water by weight, was used to bring out grain boundaries.

[1] The thermoelectric figure of merit $Z \equiv \alpha^2/K\rho$, where α is the Seebeck coefficient; K, thermal conductivity; and ρ, electrical resistivity.

Experimental Results and Discussion

Electrical properties.—The preparation, electrical properties, and densities of the powder-metallurgical specimens are summarized in Table I. (In this table, data on several of the specimens are repeated one or more times to facilitate comparisons.) Properties of specimens of the cast material (first group in table) are also given. Measured electron mobilities (Hall) for the cast lead selenide are low, presumably because of high concentrations of grain boundaries and defects in this quenched material. Heat treatment similar to that given the powder-metallurgical specimens in preparation (*i.e.*, anneal at 750°C for 5 hr, see specimen 74B-1) failed to change electrical properties significantly, however.

In general, electrical properties of the powder-metallurgical specimens compare favorably with those of the cast polycrystalline material and with those of polycrystalline and single-crystal lead selenide which are reported by others (3, 4). Resistivities and Hall mobilities for the powder-metallurgical specimens are similar to those for cast polycrystalline and single-crystal lead selenide of like purity that has solidified progressively and slowly from the molten state. Seebeck coefficients and temperature dependencies of Seebeck coefficient and resistivity in the range 300°-575°K, which were studied for a number of the powder-metallurgical specimens, were also similar to those for cast lead selenide.

For the n-type material, electrical properties vary somewhat from specimen to specimen. However, no correlation is apparent between the relatively minor variations in electrical properties observed and changes made in conditions under which the samples were prepared.

For the p-type lead selenide, resistivity and Hall coefficient of the hot-pressed specimen are significantly lower than those of the cast starting material, while on the other hand, mobility in the specimen remained quite good. Since just one experiment with p-type lead selenide was conducted in this exploratory study, it is not possible to say whether the changes noted are inevitably to be expected in hot pressing p-type material or are to be expected only under certain experimental conditions and/or with specific doping agents.

Density.—For a majority of the n-type hot-pressed specimens, determined densities are higher than both the theoretical value calculated from x-ray data and the measured density of sound specimens of similarly doped cast lead selenide. In addition, in a number of cases, measured densities are also higher than can be accounted for, even though consideration is given to concentrations of excess lead and bismuth which are present. The possibility of an effect of pressure on the lattice is suggested.

Density of both the hot-pressed and the pressed-and-sintered specimens varied in a normal manner with respect to sintering temperature and compacting pressure. Density of the 5-hr hot-pressed specimens decreased as sintering temperature was reduced in the range 750°-450°C (with pressure held constant, consider specimens 79-81), and as compacting pressure was reduced in the range 8100-

Table I. Preparation and properties of powder-metallurgical lead selenide specimens

Specimen	Method	Remarks	Specimen preparation: Size of powder particles, mesh	Compacting pressure, psi	Sintering: Temperature, °C	Sintering: Time, hr	Room-temperature properties: Electrical properties: Resistivity, 10^{-3} ohm-cm	Hall coefficient, cm^3/coulomb	Hall mobility, cm^2/v-sec	Carrier concentration, $10^{18}/cm^3$	Density: Measured value, g/cm^3	Density: Per cent of theoretical[a]
			Cast N-type (starting material) lead selenide									
74A	Cast-quench	From lower end of ingot	—	—	—	—	0.92	−0.74	840	8.5	—	—
74B	Cast-quench	From middle of ingot	—	—	—	—	0.52	−0.32	620	20	—	—
74C	Cast-quench	From upper end of ingot	—	—	—	—	1.1	−0.60	550	10	—	—
74B-1	Cast-quench-anneal	74B, annealed at 750°C, 5 hr	—	—	—	—	0.64[b]	−0.46	770	14	—	—
36	Cast-Bridgman drop		—	—	—	—	—	—	—	—	8.25	99.8
			Variable—temperature									
79	Hot press		−200	8,100	750	5	1.46	−1.7	1200	3.7	8.30	100.4
80	Hot press		−200	8,100	600	5	2.09	−2.1	1000	3.0	8.28	100.2
81	Hot press		−200	8,100	450	5	2.18	−2.2	1000	2.9	8.23	99.6
76	Hot press		−200	8,100	750	2.5	1.38	−1.6	1200	3.9	8.27	100.1
84	Hot press		−200	8,100	600	2.5	1.67	−2.1	1300	3.0	8.29	100.3
							1.57[b]	−1.8	1100	3.5	—	—
			Variable—time									
79	Hot press		−200	8,100	750	5	1.46	−1.7	1200	3.7	8.30	100.4
76	Hot press		−200	8,100	750	2.5	1.49[b]	−1.7	1100	3.7	8.27	100.1
82	Hot press		−200	8,100	750	(5 min)	1.29	−1.5	1200	4.2	8.27	100.1
78	Hot press		−100 + 200	8,100	750	5	1.40	−2.0	1400	3.1	8.31	100.6
							1.36[b]	−1.7	1200	3.7	—	—
75	Hot press		−100 + 200	8,100	750	1.5	1.27	−1.5	1200	4.2	8.30	100.4
80	Hot press		−200	8,100	600	5	2.09	−2.1	1000	3.0	8.28	100.2
84	Hot press		−200	8,100	600	2.5	1.67	−2.1	1300	3.0	8.29	100.3
			Variable—atmosphere									
77	Hot press	Powder ground and loaded in argon	−60 + 100	8,100	750	5	1.28	−1.5	1200	4.2	8.29	100.3
86	Hot press	Powder ground and loaded in air	−60 + 100	8,100	750	5	1.33	−1.5	1100	4.2	8.30	100.4
			Variable—pressure									
79	Hot press		−200	8,100	750	5	1.46	−1.7	1200	3.7	8.30	100.4
90	Hot press	Powder ground and loaded in air	−200	4,000	750	5	1.24[b]	−1.6	1300	3.9	8.21	99.3
91	Hot press	Powder ground and loaded in air	−200	2,000	750	5	1.62[b]	−1.7	1000	3.7	7.67	92.8
			Variable—size of powder particle									
79	Hot press		−200	8,100	750	5	1.46	−1.7	1200	3.7	8.30	100.4
78	Hot press		−100 + 200	8,100	750	5	1.40	−2.0	1400	3.1	8.31	100.6
77	Hot press		−60 + 100	8,100	750	5	1.28	−1.5	1200	4.2	8.29	100.3
			Press-and-sinter method									
89A	Press and sinter		−200	100,000	750	5	1.11	−1.2	1100	5.2	7.48	90.5
89B	Press and sinter		−200	100,000	600	5	1.38	−1.6	1200	3.9	8.04	97.3
89B							1.31[b]	−1.3	1000	4.8	—	—
89C	Press and sinter		−200	100,000	450	5	1.74	−1.8	1000	3.5	8.12	98.2
			P-type lead selenide									
24	Cast-Bridgman drop		—	—	—	—	4.73[b]	+4.9	1100	1.3	—	—
92	Hot press	Powder ground and loaded in air	−200	8,100	750	5	1.17[b]	+1.4	1200	4.3	8.25	99.8

[a] Theoretical value 8.265 g/cm^3; calculated from precision x-ray lattice constant (a_0 = 6.1265 ± 0.0003Å.
[b] A-c measurements.

2000 psi (with temperature held constant, consider specimens 79, 90, 91). For the press-and-sinter method, in which samples were initially compressed to near-theoretical density, density of the sintered specimens decreased as firing temperature was increased through the range 450°-750°C. In the ranges studied, density did not vary appreciably with hot-press time (5 min-5 hr at 750°C, 2.5-5 hr at 600°C) or particle size (−60 to −200 mesh).

The study was not sufficiently comprehensive to permit a full evaluation of combined effects of the variables. However, if the hot-press process variables are considered singly, it may be noted that near-theoretical densities were attained at minimums of 8100 psi compacting pressure, 600°C sintering temperature, and 5 min hot-press time; densities roughly equal to that of cast material were attained at minimums of 4000 psi compacting pressure, and 450°C sintering temperature.

Density of the p-type specimen, which was hot pressed for 5 hr at 750°C, is significantly lower than that of similarly treated n-type material. The excess lead, which was present in the n-type material, apparently has a salutary effect on the sintering process. The sintering of p-type lead selenide, which may proceed by different mechanisms, should be the subject of a separate study.

It is considered significant that, although densities of the sintered specimens ranged down to about 90% of theoretical, electrical properties did not change appreciably, Such low-density powder-metallurgical materials, because of the possible effect of the high concentrations of grain boundaries and voids (*i.e.*, lattice discontinuities) on thermal conductivity, may possess superior over-all thermoelectric properties.

Microstructures.—Microstructures of the hot-pressed lead selenide specimens, Fig. 1, show clearly the effects of variation of sintering temperature and time on average grain size, and of variation of compacting pressure on density.

At 750°C, 8100 psi, (Fig. 1a) considerable growth of crystals was obtained in the course of a 5-hr treatment, but at 450°C under otherwise similar conditions (Fig. 1b) little or no crystal growth occurred. However, some crystal growth is seen to have occurred in only 5 min at the higher temperature (Fig. 1c). In photomicrographs 1a, d, and e, the decrease in average grain size and density (*i.e.*, increase in concentration and size of voids) as compacting pressure is decreased from 8100 to 2000 psi may be seen. Differences between 8100 and 4000 psi are slight, but at 2000 psi both density and average grain size are considerably reduced.

Even though an extremely high compacting pressure (100,000 psi) was used in the press-and-sinter method, crystals present in the specimens were small and densities were relatively low (Fig. 1f).

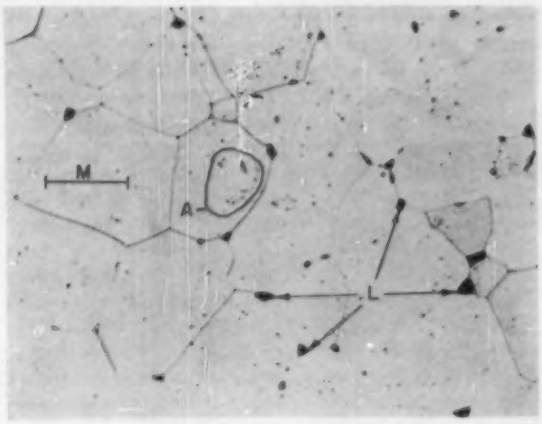

Fig. 1. Microstructures of powder-metallurgy specimens of lead selenide: M, maximum initial particle diameter; L, lead-rich phase; A, fine structure includes (a) deposits of the lead-rich phase, (b) some etch pits, and (c) some deposits of an oxide phase; V, voids. Fig. 1a. Specimen 79, —200 mesh powder, hot pressed at 8100 psi, 750°C, 5 hr. Magnification of microstructures 250X before reduction for publication.

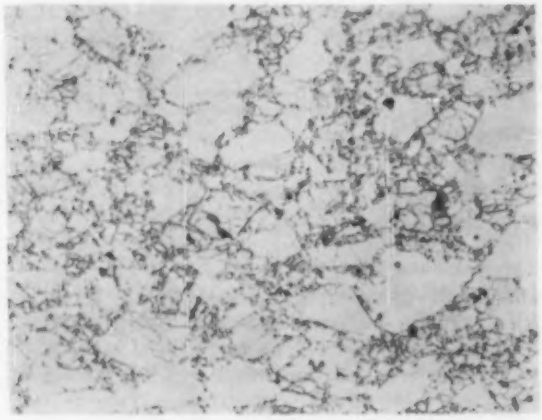

Fig. 1b. Specimen 81, —200 mesh powder, hot pressed at 8100 psi, 450°C, 5 hr.

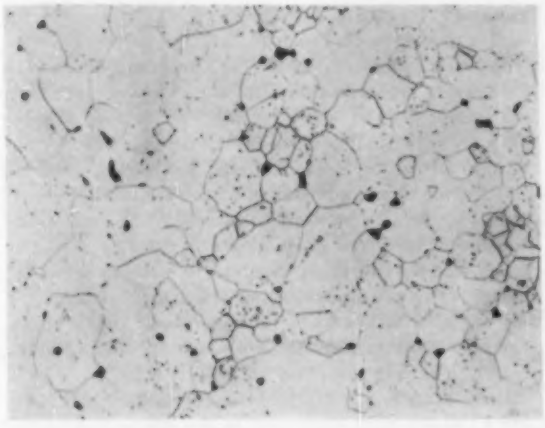

Fig. 1c. Specimen 82, —200 mesh powder, hot pressed at 8100 psi, 750°C, 5 min.

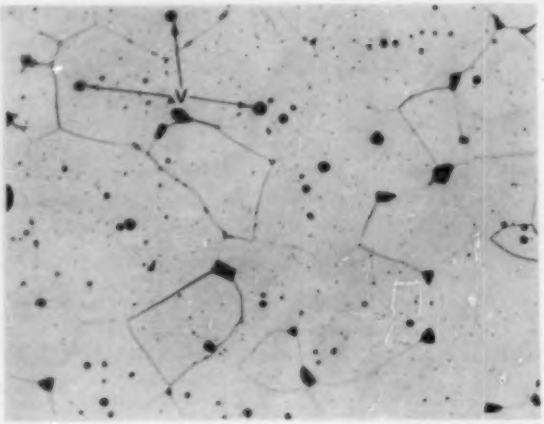

Fig. 1d. Specimen 90, —200 mesh powder, hot pressed at 4000 psi, 750°C, 5 hr.

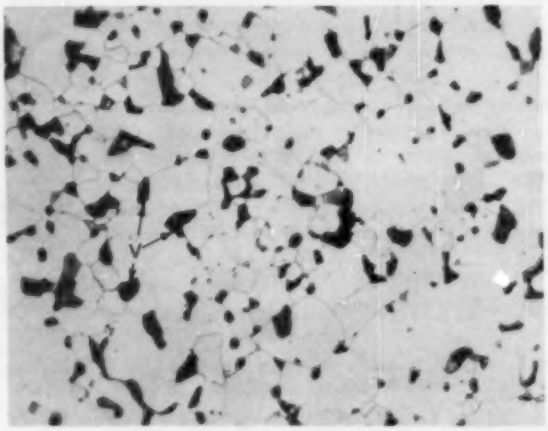

Fig. 1e. Specimen 91, —200 mesh powder ground and loaded in air, hot pressed at 2000 psi, 750°C, 5 hr.

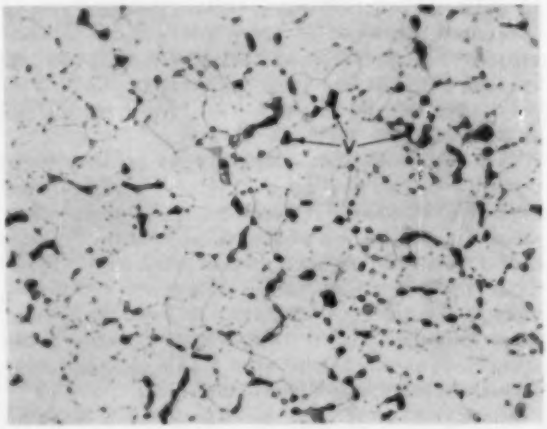

Fig. 1f. Specimen 89A, —200 mesh powder, pressed at 100,000 psi, sintered 750°C, 5 hr.

With a similar heat treatment, larger crystals and higher densities were obtained by the hot-press method (Fig. 1a, d).

The majority of the specimens were prepared from powder which was ground and handled in argon. Nevertheless, small inclusions of an oxidic

Table II. Thermoelectric properties of hot-pressed and of cast n-type lead selenide

	Hot-pressed: Specimen 77, −60 + 100-mesh powder hot pressed at 750°C, 8100 psi, 5 hr	Cast: Specimen 35, Bridgman drop at ½ in./hr
Z-meter measurements		
Mean temperature, $\overline{T}$, °K	297.4	298.4
Resistivity, ρ, ohm-cm	1.18×10^{-3}	7.7×10^{-4}
Seebeck coefficient, α, μv/°K	−168	−135
Thermal conductivity, K, watt/cm °K	0.020	0.021
Thermoelectric figure of merit, Z, $°K^{-1}$	$1.2_8 \times 10^{-3}$	$1.1_5 \times 10^{-3}$
Hall measurements		
Resistivity, ρ, ohm-cm	1.28×10^{-3}	8.4×10^{-4}
Hall coefficient, R_H, cm^3/coul	−1.5	−0.89
Hall mobility, μ, cm^2/v-sec	1200	1100
Carrier concentration, n, cm^{-3}	4.2×10^{18}	7.2×10^{18}

phase were found in all specimens. However, metallographs showed that concentrations of this phase were considerably higher in specimens which were prepared from powder that was exposed to air in the course of grinding and loading operations.

Thermoelectric properties.—Thermoelectric properties of a typical high-density hot-pressed lead selenide specimen, which are given in Table II, indicate that material with a good thermoelectric figure of merit can be prepared by this method. It should be noted that these favorable indications have been obtained without any effort to optimize the powder-metal product with respect to thermoelectric properties. As has been suggested previously, thermoelectric properties of low-density powder-metallurgical lead selenide may be of special interest and should be the subject of future studies.

Conclusions

Sound specimens of n-type lead selenide with electrical and thermoelectric properties similar to those of cast lead selenide can be prepared by hot pressing.

Near-theoretical densities can be obtained by hot pressing for only 5 min at 750°C, 8100 psi, and for 2.5 hr at 600°C, 8100 psi. Density of the specimens decreases with sintering temperature in the range 750°-450°C, and with compacting pressure in the range 8100-2000 psi. No appreciable effect on density is produced by variation of sintering time (in the range 5 min-5 hr at 750°C, 2.5-5 hr at 600°C). Variation of size of powder particle in the range −200 to −60 mesh likewise produces no noticeable effect.

Electrical properties of hot-pressed p-type lead selenide deviate from those of the cast starting material to a greater degree than do those of the n-type material. Density of the p-type material is significantly lower than that of n-type material which is hot-pressed under similar conditions.

Specimens produced by the hot-press method contain larger crystallites and are of higher density than those prepared by the press-and-sinter method (100,000 psi). Specimens with densities in the range 90-98% of theoretical can be prepared by both methods. Anomalously high densities (above 100% of theoretical) can be attained by hot pressing. Of possible significance is the fact that electrical properties of the lead selenide that is doped suitably for thermoelectric use do not change appreciably as density varies in the range covered in this investigation.

Acknowledgments

The authors wish to express their thanks to J. E. Mock, who prepared the specimens, F. J. Reid and B. Paris, who made the electrical measurements, and J. L. McCall, who prepared the metallographs.

Manuscript received April 29, 1960. This investigation was supported by The Selenium and Tellurium Development Committee.

Any discussion of this paper will appear in a Discussion Section to be published in the June 1961 JOURNAL.

REFERENCES

1. R. C. Bourke, R. Simon, and E. H. Lougher, Abstract of paper presented at Spring Semiconductor Symposium, The Electrochemical Society, Chicago, May 2, 1960.
2. T. C. Harman, J. H. Cahn, and M. J. Logan, *J. Appl. Phys.*, **30**, 1351 (1959).
3. E. H. Putley, *Proc. Phys. Soc. (London)*, **68B**, 22 (1955).
4. R. S. Allgaier and W. W. Scanlon, *Phys. Rev.*, **111**, 1029 (1958).

Brief Communications

The JOURNAL accepts short technical reports having unusual importance or timely interest, where speed of publication is a consideration. The communication may summarize results of important research justifying announcement before such time as a more detailed manuscript can be published. Consideration also will be given to reports of significant unfinished research which the author cannot pursue further, but the results of which are of potential use to others. Comments on papers already published in the JOURNAL should be reserved for the Discussion Section published biannually.

Submit communications in triplicate, typewritten double-spaced, to the Editor, Journal of The Electrochemical Society, 1860 Broadway, New York 23, N. Y.

Kinetics of the Formation of the Iron-Tin Alloy $FeSn_2$

Robert P. Frankenthal[1] and Alexei W. Loginow

Applied Research Laboratory, United States Steel Corporation, Monroeville, Pennsylvania

ABSTRACT

The kinetics of the formation of the iron-tin alloy $FeSn_2$ have been studied at temperatures below and above the melting point of tin (232°C). At all temperatures studied, the growth obeyed the parabolic-rate law. This is indicative of a diffusion mechanism. An Arrhenius plot of the data gives a straight line below the melting point of tin and a straight line above the melting point of tin, with a sharp break at the melting point. The activation energy is the same below and above the melting point of tin and is 29.3 ± 1 kcal/mole. The kinetics of the growth were also studied as a function of various properties associated with the tin plate: tin-coating weight, steel base, and the type of pickle to which the steel base was subjected prior to electroplating of the tin. No effect due to any of these variables was found.

At temperatures up to 496°C, iron and tin react to form the intermetallic compound $FeSn_2$ (1). This compound will form not only above the melting point of tin (232°C) but also below it (2), contrary to the findings of Davies and Hoare (3). Little data have been published on the rate and mechanism of formation of this alloy: Seybolt (4) measured the rate of alloying when steel is immersed in a bath of molten tin at constant temperature and found the parabolic-rate law to be obeyed. This is indicative of a diffusion mechanism. Thwaites (2) has studied the formation of the alloy and its metallography as a function of the rate of change of temperature, at temperatures above the melting point of tin. He also reported a few results on the formation of the alloy at constant temperatures below the melting point of tin. Lambert (5) studied the alloy-growth rate on commercial tin plate at temperatures below the melting point of tin. However, because of the short times investigated and the thin tin coatings on his samples, he was not able to determine whether the alloy grew by a diffusion mechanism; also, his experiments were done with an initial alloy coating present and this unnecessarily complicated the calculations. He also stated that according to the phase diagram, at temperatures below the melting point of tin the alloy FeSn must be formed; however, this was not verified by analysis. Moreover, Stoll and Birch (6) have not been able to observe by electron diffraction any patterns other than that of $FeSn_2$ on alloys formed at temperatures up to 260°C.

The present work represents an analysis of the rate of formation curves at constant temperatures below and above the melting point of tin and the effect of temperature on the rate of formation of the alloy. Since the alloying was performed on steel covered with an electroplated tin coating, the effect of (*a*) variations in the thickness of the tin coating, (*b*) the steel base, and (*c*) surface preparation of the steel prior to electroplating on the rate of formation of the alloy were also examined.

[1] Present address: E. C. Bain Laboratory for Fundamental Research, United States Steel Corporation, Monroeville, Pa.

Experimental

The samples were prepared by electroplating the tin onto Type L (low metalloid; % Fe > 99) steel sheets from a phenolsulfonic acid electrolyte to thickness of 0.29 mg/cm², 0.50 mg/cm², 0.72 mg/cm², and 1.05 mg/cm². The tin plate with a coating of 0.72 mg/cm² was prepared with four different pickling treatments of the steel base prior to electroplating, to determine whether steel preparation had any effect on the rate of alloy formation. All pickling treatments were performed at room temperature (approximately 27°C): (*a*) electrolytic pickle in 5% H_2SO_4, 1.5 sec cathodic, 1.5 sec anodic; (*b*) electrolytic pickle in 5% HNO_3, 1.5 sec cathodic, 1.5 sec anodic; (*c*) 5-sec dip in 5% H_2SO_4; (d) 5-sec dip in 5% HNO_3. The steel came from four different coils produced in different steel mills at different times to determine coil to coil variations on the rate of alloy formation.

The alloys were prepared by heating the samples in a constant-temperature oil bath for various times ranging from 2 sec to 6 hr, these times being dependent on the temperature under study, which ranged from 175° to 316°C. The melting point of tin is 232°C. The temperature of the oil bath was controlled to ±0.5°C for temperatures up to 260°C. At the higher temperatures, the control was ±2°C. Upon removal from the oil bath, the samples were quenched immediately to room temperature in water or in an organic liquid. The quantity of alloy formed was determined coulometrically by the method of Kunze and Willey (7), as was the tin coating weight of the material used. In this method, the tin and the alloy are anodically stripped at constant current in 1M HCl. When all the tin has been stripped and again when all the alloy has been stripped, the potential of the sample, as measured with a silver-silver chloride reference electrode, becomes more positive. The potential-time behavior of the sample was followed on a recorder (chart speed of 30 in./min). From the measured time required to strip the tin and the alloy and from the

known current, the quantity of tin and alloy present could be calculated making use of Faraday's Laws of electrolysis. It was possible to determine the alloy to ±0.002 mg/cm² by this means.

Results and Discussion

The rate of alloy growth at all temperatures studied decreased with time, as would be expected if the parabolic-rate law were obeyed; this is typical for alloying reactions and is indicative of a diffusion mechanism. Seybolt (4) found this in his study of the tin-iron system above the melting point of tin. Therefore, the data were plotted (Fig. 1 and 2) according to the parabolic-rate law, w^2 vs. t, where w is the quantity of alloy formed at time t. Linear plots are observed, but they do not go through the origin as would be expected if the parabolic-rate law were obeyed from the beginning of the reaction ($t = 0$). This type of phenomenon is frequently observed in gas-metal reactions, such as oxidation (8) or sulfidization reactions (9), and is attributed to an interface reaction between the metal and the gas that establishes the initial reaction layer, after which diffusion through the reaction layer becomes rate-controlling. It would be natural to expect the same situation to exist in this study since the conditions are analogous, except that either a solid-solid or a solid-liquid reaction exists at the interface instead of a solid-gas reaction. The mathematics of the metal-gas reaction were treated initially by Fischbeck (10) and by Wagner (11) and more recently by Dravnieks and Samans (9), who assumed first-order kinetics for the interface reaction. This approach was applied to the data obtained in these studies in the hope of determining the rate of the interface reaction. However, the data did not follow this relationship and thereby indicated that the interface reaction did not obey simple first-order kinetics. No further attempt was made to study the interface reaction.

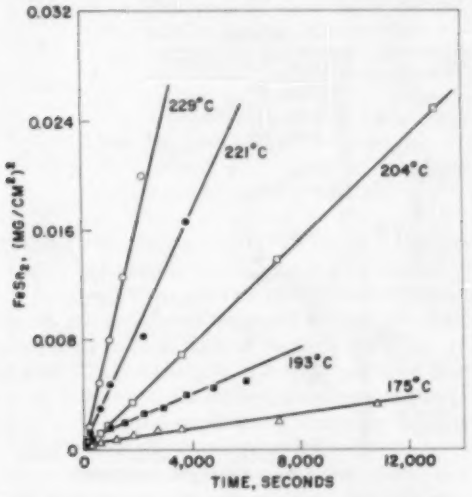

Fig. 1. Rate of growth of $FeSn_2$ at temperatures below the melting point of tin: parabolic plot.

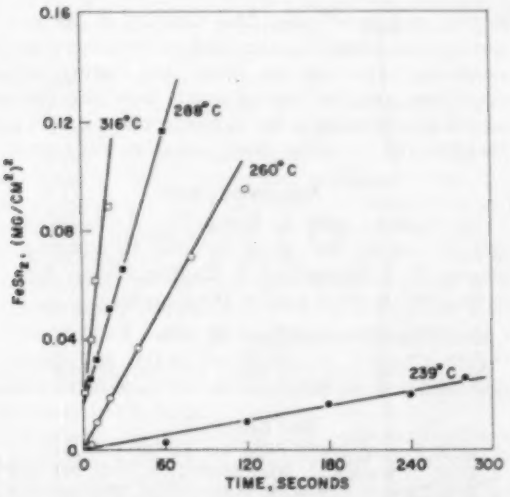

Fig. 2. Rate of growth of $FeSn_2$ at temperatures above the melting point of tin: parabolic plot.

Table I. Parabolic-rate constant as a function of temperature

Temperature	$k \times 10^6$, mg²/cm⁴/sec
175	0.26
192	0.62
193	0.89
193	0.61
202	1.46
203	2.12
204	1.92
221	4.7
222	5.8
229	8.3
239	10.3
245	17.2
260	39.
260	88.
288	167.
316	495.

Parabolic-rate constants for the diffusion reaction at the various temperatures, the slopes of the plots in Fig. 1 and 2, are given in Table I. An Arrhenius plot of the log of the parabolic-rate constant vs. the reciprocal of the absolute temperature is shown in Fig. 3. Table I and Fig. 3 include data not shown in previous figures. Two straight lines with a sharp break at the melting point of tin are observed. The

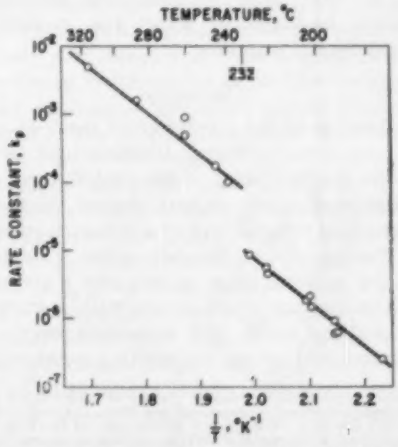

Fig. 3. Rate of formation of $FeSn_2$ with temperature.

calculated activation energy below and above the melting point is the same within experimental error and is 29.3 ± 1 kcal/mole. This value is in good agreement with the value of 28.6 kcal/mole[5] found by Seybolt (4). No similar results for analogous systems have been found in the literature. The sharp increase in the reaction rate above the melting point of tin is believed due to increased contact area at the Sn-Fe interface, compared with solid tin electrodeposited on iron.

The intercepts of the parabolic plots on the ordinate, Fig. 1 and 2, average at approximately 0.006 mg/cm². From the density of $FeSn_2$ (12), 7.74 g/cm³ and the lattice parameters (13) of the alloy, a = 6.53Å and c = 5.33Å, this is calculated to be equivalent to a thickness of 11 unit cells of the alloy, which does not seem to be an unreasonable thickness, at which the interface reaction ceases to be rate-determining and the diffusion reaction commences to be rate-determining.

Tin-coating weight.—In early experiments, it was observed that some of the tin was dissolved from the samples in the oil bath, but it was not known how this affected the results. Hence, the effect of the thickness or weight of the tin coating on the rate of growth of the alloy was studied. Results are shown in Fig. 4 for 204° and 239°C. It is apparent that there is no effect except possibly at the high alloy weight levels for the 0.29 mg/cm² plate, in which case the results are low. These are low because there was insufficient tin on the plate (some having dissolved in the oil bath) to form more alloy, as evidenced by the fact that these samples had no free tin left on them when they were removed from the oil bath.

Steel base.—Data in Fig. 3 were obtained using the steel from the four different coils described previously. Alloy-growth studies with each steel were made at temperatures below and above the melting point of tin. Since the data from each of the coils lie on the observed lines, it is concluded that coil to coil variations do not affect the kinetics or mechanism of the growth of the alloy.

Pickle.—Figure 5 shows the effect of the various pickling treatments prior to electroplating on the rate of formation of the alloy layer at 202° and 240°C. No effect is evident, although these different treatments undoubtedly affect the surface of the steel in different manners.

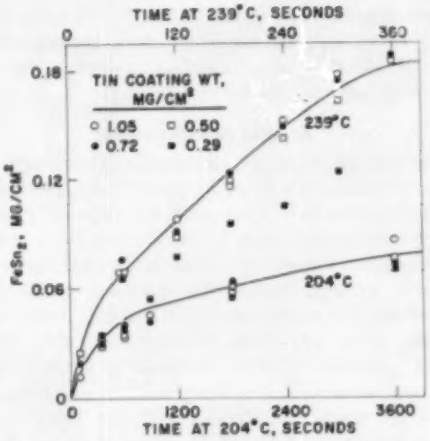

Fig. 4. Formation of $FeSn_2$ as affected by tin-coating weight.

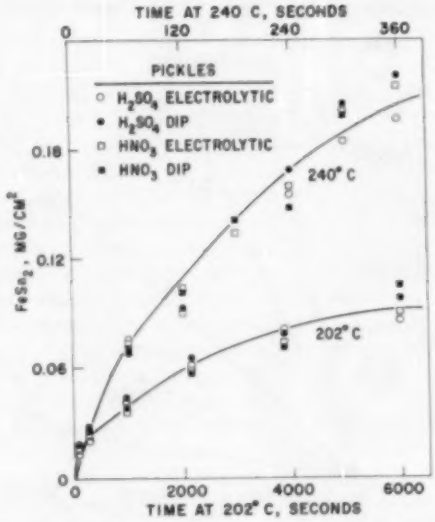

Fig. 5. Formation of $FeSn_2$ as affected by pickling conditions.

Summary

The kinetics of the formation of the iron-tin alloy $FeSn_2$ have been studied at temperatures below and above the melting point of tin (232°C). At all temperatures studied, the growth obeyed the parabolic-rate law. This is indicative of a diffusion mechanism. An Arrhenius plot of the data gives a straight line below the melting point of tin and a straight line above the melting point of tin, with a sharp break at the melting point. The activation energy is the same below and above the melting point of tin and is 29.3 ± 1 kcal/mole. The kinetics of the growth were also studied as a function of various properties associated with the tin plate: tin-coating weight, steel base, and the type of pickle to which the steel base was subjected prior to electroplating of the tin. No effect due to any of these variables was found.

[5] Seybolt reported an activation energy of 14.3 kcal/mole. However, his rate constants were calculated from the slope of a w vs. $t^{1/2}$ plot and are thus equal to the square root of the rate constants calculated from a w^2 vs. t plot; the activation energy calculated from the former rate constants will be equal to one-half that calculated from the latter rate constants.

Acknowledgment

The authors wish to thank Drs. R. T. Davis, Jr., and C. Luner for their helpful discussions and Messrs. R. F. Higgs and E. C. Brendlinger for preparing the tin plate used in these studies.

Manuscript received April 22, 1960.

Any discussion of this paper will appear in a Discussion Section to be published in the June 1961 JOURNAL.

REFERENCES

1. O. E. Romig, *Metal Progress*, **42**, 899 (1942).
2. C. J. Thwaites, *J. Iron Steel Inst.*, **183**, 244 (1956).
3. J. E. Davies and W. E. Hoare, *ibid.*, **168**, 134 (1951).
4. A. U. Seybolt, *Trans. ASM*, **29**, 937 (1941).
5. W. N. Lambert, *Corrosion*, **11**, 454 (1955).

6. P. J. Stoll and H. J. Birch, Private communication.
7. C. T. Kunze and A. R. Willey, *This Journal*, **99**, 354 (1952).
8. O. Kubaschewski and B. E. Hopkins, "Oxidation of Metals and Alloys," p. 42, Fig. 18a, Butterworth Scientific Publications, London (1953).
9. A. Dravnieks and C. H. Samans, *This Journal*, **105**, 183 (1958).
10. K. Fischbeck, L. Neundenbel, and F. Salzer, *Z. Elektrochem.*, **40**, 517 (1934).
11. C. Wagner and K. Grunewald, *Z. physik. Chem.*, **B40**, 455 (1938).
12. R. A. Covert and H. H. Uhlig, *This Journal*, **104**, 537 (1957).
13. H. Nowotny and K. Schubert, *Metallforsch.*, **1**, 17 (1946).

Properties of Vanadium-Columbium Alloys

S. T. Wlodek

Metals Research Laboratory, Union Carbide Metals Company,

Division of Union Carbide Corporation, Niagara Falls, New York

ABSTRACT

The development of a series of vanadium-columbium alloys is described. The exploitation of this alloy system allows the design of high-strength, low-density compositions possessing good aqueous corrosion resistance in boiling, oxidizing, or reducing acids and sufficient oxidation resistance to allow their fabrication by conventional hot-working techniques in air. In the warm-worked condition, the spectrum of properties measured under inert atmosphere conditions (strain rate 0.005^{-1} sec) includes ultimate tensile strengths of 120,000 to 35,000 psi over the temperature range of 700°-1000°C and stress-rupture properties at 700°C corresponding to 100-hr life at stresses in excess of 100,000 psi. Tensile strengths as high as 70,000 psi at 1000° and 40,000 psi at 1200°C were observed at higher rates of loading in the warm-worked and stress-relieved conditions.

The high melting point (1900°C) and low density (6.1 g/cc) of vanadium suggest a material of promising mechanical properties at elevated temperature with an advantageous strength-to-weight ratio for applications where such a factor would be of importance. Unfortunately, the high melting point of pure vanadium is not accompanied by the expected degree of high-temperature strength (1). This drawback, common to the other VB periodic group refractory metals, columbium and tantalum, is offset by the excellent room-temperature fabricability and ductility down to liquid nitrogen temperature. Vanadium possesses good liquid metal corrosion resistance, and because all of its short-lived isotopes decay without emitting excessively strong decay products it is often regarded as a promising structural material for nuclear applications. Of all the refractory metals, however, pure vanadium is probably the least resistant to oxidation and aqueous corrosion. The low melting point of V_2O_5 (660°C), the main oxidation product on a vanadium-base material, produces such catastrophic rates of reaction above 660°C, that the hot-working of vanadium is a most uneconomical procedure. The protection of a vanadium-base material against oxidation by means of coatings is also made a most difficult, if not impossible, problem. The poor corrosion resistance of vanadium, in either oxidizing or strongly reducing acids or high chlorine concentrations, limits its application in chemical environments.

Attempts at improving the properties of vanadium by alloying have involved the use of titanium with further additions of a third element, such as: chromium, aluminum, or silicon for strength, and oxidation resistance, as well as carbon for improved fabricability. These studies, performed primarily by Rostoker, Yamamoto, and Riley (2), and recently fully summarized by Rostoker (3), have resulted in an appreciable improvement over the properties of pure vanadium. Ultimate tensile strengths of 130,000-90,000 psi and 100-hr rupture strengths of 100,000-10,000 psi were obtained in the temperature range 500°-700°C. A different system of alloys based on the vanadium-titanium binary and containing additions of tantalum, columbium, molybdenum, or carbon in amounts not exceeding 1 weight per cent (w/o) has been proposed by Smith and Van Thyne (4) for applications requiring medium strength combined with high fabricability and good aqueous or liquid metal corrosion resistance.

It is the purpose of this paper to present some preliminary results on the oxidation resistance, mechanical properties, and aqueous corrosion behavior of a family of alloys based on a vanadium-columbium system in the region of 20-50 w/o columbium.

The vanadium-columbium phase diagram portrays a system of complete solid solution with a minimum in the liquidus at 1810°C, corresponding to a composition of 35 w/o columbium (5). Of all the elements that are completely miscible with vanadium, columbium possesses the largest degree of atomic mismatch combined with complete solid solubility. The high-melting points of this alloy system and the large atomic size difference between vanadium and columbium suggest a system with good high-temperature properties. The complete miscibility of vanadium and columbium suggests a minimum loss in fabricability on alloying with a maximum increase in strength. Although the columbium-vanadium system is of the liquidus minimum type, a

Table I. Analyses of materials

	Vanadium, %	Columbium, %
Carbon	0.043	0.030
Oxygen	0.090	0.070
Hydrogen	0.001	—
Nitrogen	0.038	0.030

characteristic often associated with systems that undergo clustering or disproportionation at some lower temperature, no evidence of the formation of a second phase was ever observed in this study. Even in columbium-vanadium alloys containing 20-50 w/o columbium and annealed for up to 100 hr at a temperature range of 700-900°C only single-phase structures were observed. This is in agreement with the work of Wilhelm, *et al.* (6), who similarly failed to find the sigma phase reported by Rostoker and Yamamoto (7).

Turning now to the oxides, the Cb_2O_5-V_2O_5 system may be roughly described as a simple peritectic type with appreciable amounts (about 20 vol %) of Cb_2O_5 being soluble in V_2O_5 at 600°C. The addition of Cb_2O_5 to V_2O_5 raises the melting point of vanadium pentoxide to the point that an equimolar mixture of V_2O_5 and Cb_2O_5 is completely solid at temperatures up to 950°C. The greater affinity of columbium for oxygen and the complete miscibility of columbium and vanadium metal all indicated the possibility that columbium might increase the oxidation resistance of vanadium by promoting the formation of a higher melting point oxide.

These were the reasons for considering this study as being a likely approach to a series of vanadium-base alloys possessing better mechanical properties and superior oxidation resistance.

Preparation of Alloys

Commercial-grade vanadium and columbium as produced by Union Carbide Metals Company with the analyses given in Table I were used throughout this study. The other alloying elements employed were also of commercial purity.

All aqueous corrosion and some oxidation samples were prepared by the nonconsumable arc melting of 70-g, 2-in. diameter buttons. The charge was prepared by compacting the vanadium and columbium as 10-mesh powders with the titanium being added in the same form. Additions of aluminum, silicon, and chromium were made by means of the intermetallic compounds Al_3Cb, $CbCr_2$, or $CbSi_2$, these master alloys having been prepared previously by melting the elemental powders. After compaction, the charge was melted four times, twice on each side, on a water-cooled copper hearth using a tungsten electrode, the melting operation being carried out in an atmosphere of pure argon with currents in the order of 200-500 amp at 24-26 v.

Wrought material for mechanical property and certain oxidation studies was obtained from consumable 1½-in. diameter 800-g ingots. The consumable electrodes were formed by welding together five 4-in. long bars of the alloy composition, the bars having been previously prepared by nonconsumable, tungsten electrode melting using the same technique described above for buttons. Satisfactory ingots with an equiaxed as-cast grain size were prepared by d-c arc melting with currents of 600-1000 amp and in an atmosphere of 120 mm Hg of argon. After dressing, these ingots were extruded in air at temperatures of 1100°-1200°C. To keep the extrusion times as short as possible, induction heating was used to preheat the billets, and the actual extrusion, at a 4-to-1 ratio, was performed in a fast-acting, flywheel activated, impact-extrusion press at speeds of 40-100 ips. Subsequent hot-working to ⅜-in. diameter was performed by swaging in the temperature range of 1000°-1100°C or by cold-working at room temperature. An argon atmosphere was used for preheating the billets prior to the extrusion and swaging operations. All fabricating procedures were performed in air; no canning or in-plant coating techniques were used.

As given in Table II, this technique of wrought sample preparation produced compositions close to the nominal analysis with a slight amount of oxygen pickup from the swaging operation.

The fabrication of most of these alloys, below about 1100°C, is tantamount to warm-working. For 0.5-hr annealing times, the recrystallization temperature of binary vanadium alloys containing 30-40 w/o columbium is about 1150°C. Very little grain growth occurs as the annealing temperature is increased to 1300°C. The recrystallization temperature for the vanadium-columbium-titanium ternary alloys, especially if modified with quaternary aluminum or silicon additions, is somewhat lower, ranging as low as 1100°C for the 50% V-40% Cb-10% Ti alloy to 1050°C for the 45% V-40% Cb-10% Ti-5% Al composition. The microstructures

Table II. Sample analyses of consumable arc melted alloys

	V	Cb	Ti	Al	Si	C*	O*	N*
Nominal	60.0	40.0	—	—	—	—	—	—
Analyzed	59.78	39.60	—	—	—	0.050	0.26	0.023
Nominal	50.0	40.0	10.0	—	—	—	—	—
Analyzed	49.89	40.00	9.40			0.039	0.23	0.020
Nominal	49.0	40.0	10.0	—	1.0	—	—	—
Analyzed	50.23	38.70	9.00		0.90	0.080	0.23	0.022
Nominal	45.0	40.0	10.0	5.0	—	—	—	—
Analyzed	45.15	39.80	9.20	4.73	—	0.030	0.20	0.020

* Carbon, oxygen, and nitrogen analyses obtained on wrought material after tensile testing. Additional pickup of oxygen probably occurred during creep-rupture testing. The above oxygen levels were the maximum observed. Values as low as 0.15 w/o oxygen were sometimes encountered.

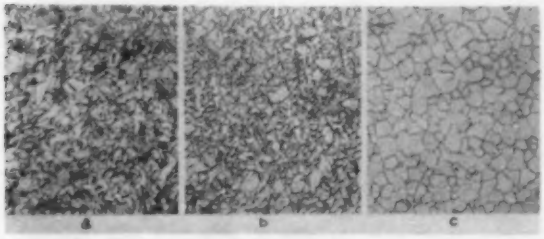

Fig. 1. 60% Vanadium-40% columbium alloy, all etched in 1 HF:1 HNO_3:3 glycerol. Magnification 100X before reduction for publication. (a) Swaged at 1000°C, annealed 0.5 hr at 1000°C, hardness 243 VPH; (b) swaged at 1000°C, annealed 0.5 hr at 1100°C, hardness 242 VPH; (c) swaged at 1000°C, annealed 0.5 hr at 1200°C, hardness 210 VPH.

illustrated in Fig. 1 for the 60% V-40% Cb composition as-swaged at 1000°C and annealed for 0.5 hr at 1000°, 1100°, and 1200°C exemplify the structure of these alloys. All the compositions given in Table II were single phase. The amount and extent of slip bands shown in Fig. 1 were characteristic of the warm-worked state, with deformation twins being readily observed in the compositions cold-worked at room temperature. Both types of deformation markings were less prevalent in titanium-containing alloys.

Corrosion Testing

Corrosion tests were performed on as-cast specimens of columbium-vanadium binary alloys over the range 20-50 w/o columbium with and without ternary titanium additions at the 10-20 w/o level. As shown in Fig. 2, the addition of columbium to vanadium greatly increased the corrosion resistance to boiling 65% HNO_3, boiling 5, 10, and 15% HCl, and boiling 10, 20 and 30% H_2SO_4 solutions. Further improvements, especially in regard to the corrosion resistance in boiling 65% HNO_3, were obtained on the addition of columbium in the presence of 10 and 20% titanium. The addition of titanium to the vanadium-columbium base, however, was found to increase the rate of corrosion in HCl and H_2SO_4 solutions. The addition of 20-50 w/o columbium, with and without further titanium additions, improved the room-temperature resistance to wet chlorine attack at room temperature to the point that corrosion rates of less than 1 mil/year were obtained. All these data were derived from 48-hr duplicate tests with the exception of the chlorine corrosion data which were obtained from 90-hr periods.

With the exception of boiling 65% HNO_3 solutions, where vanadium-columbium-titanium alloys behaved best, the most corrosion-resistant composition studied was the 50% Cb-50% V alloy. Exhibiting a corrosion rate in 65% HNO_3 of 17 mils/year, this composition corroded in boiling 5, 10 and 15% HCl at rates of 8, 50, and 83 mils/year, respectively. In addition, the 50% V-50% Cb alloy was found to corrode in boiling H_2SO_4 solutions of 5, 10, 20, and 30% concentration by weight at rates of 11, 17, 31, and 63 mils/year. By means of a bar diagram of the type first introduced by Stern and Bishop (8) the over-all corrosion resistance of the 50% V-50% Cb alloy is compared with other corrosion-resistant alloys and pure vanadium in Fig. 3. In this type of diagram, the total area below each horizontal bar denotes the range of environments in which that composition resists attack. Although the nature of this diagram is highly qualitative, the over-all degree of corrosion resistance possessed by the 50% V-50% Cb alloy is evident. This ability to withstand oxidizing or reducing acids in the presence or absence of chlorides is an appreciable improvement over pure vanadium, which, as shown in Fig. 3, is only able to withstand relatively dilute reducing solutions and relatively low chloride environments.

Oxidation Testing

The rate of oxidation of vanadium-columbium alloys containing from 20 to 40 w/o columbium with or without further additions of titanium, silicon, chromium, and aluminum in ternary or quaternary combinations was evaluated by means of continuous weight-gain measurements and intermediate exposure tests involving the subsequent measurement of the amount of metal consumed.

Continuous weight-gain measurements were obtained in an atmosphere of pure and dry oxygen at 700°, 800°, and 900°C. Test samples consisted of as-cast parallelepipeds (1.5 x 0.8 x 0.8 cm) abraded

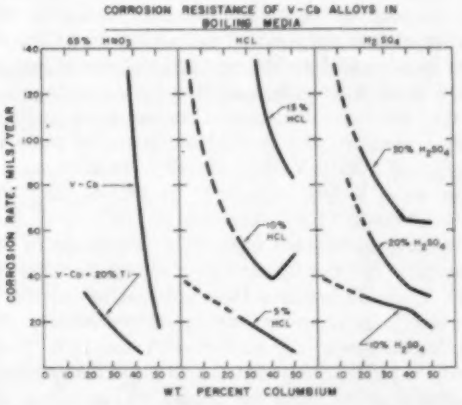

Fig. 2. Effect of columbium additions on the corrosion of vanadium in boiling 65% HNO_3, HCl, and H_2SO_4. Effect of a 20% titanium addition on the behavior of a V-Cb alloy in 65% HNO_3 is also shown.

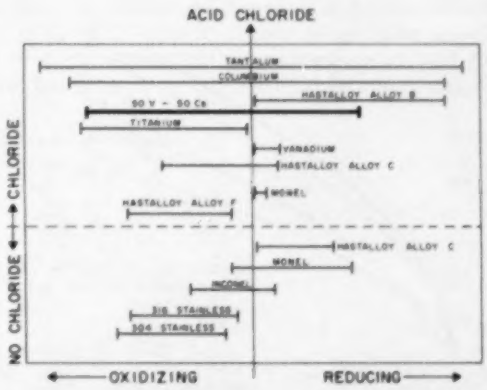

Fig. 3. Comparison of corrosion resistance of 50V-50Cb to other materials (8). Each alloy exhibits adequate corrosion resistance in all environments below its solid line.

Table III. Oxidation rates of vanadium-columbium alloys

Alloy composition, w/o				Rate of steady-state oxidation* in pure oxygen, mg/cm²/hr		
V	Cb	Ti	Other	700°C	800°C	900°C
70	30	—	—	14.4	32.6†	Liquid
60	40	—	—	9.8	57.4	64.0†
50	50	—	—	8.7	312.0	510.0†
50	30	20	—	6.4	18.2	41.3
50	40	10	—	7.2	9.0	18.8
40	40	20	—	13.1	54.2	115.0
55	40	—	5 Al	10.5	18.8	38.6†
55	40	—	5 Cr	20.5	15.0	24.9†
55	40	—	5 Si	20.9	58.8†	Liquid
50	35	10	5 Al	8.6	9.6	20.0
55	30	10	5 Si	18.0	13.1	14.9
48	40	10	2 Si	7.1	14.1	48.7
45	40	10	5 Si	7.7	12.2	18.7

* Rate of steady-state reaction, often attained after about 5.0 hr of oxidation.
† Some liquid phase present at some period during oxidation process.

under kerosene through 0000 emery paper and then rinsed in benzene before testing. The sample was suspended from one arm of a Mauer (9) automatically recording, gravimetric balance by means of a quartz rod and a platinum sling. Pure dried oxygen at a flow rate of 22.4 l/hr was passed over the specimen, the resulting increase in weight being recorded to the nearest 1.0 mg. The average length of the oxidation test was of the order of 6-8 hr.

The most significant results obtained in the rate measurements are tabulated in Table III in terms of the instantaneous oxidation rate exhibited by the alloy after 5.0 hr exposure, an interval which allowed some semblance of steady-state kinetics to be achieved. This method of comparing oxidation rates had to be adopted in view of the varying kinetic forms of oxidation exhibited by vanadium-base alloys. As shown in the weight gain *vs.* time plots in Fig. 4, various combinations of reaction rates were observed during oxidation even at 700°C.

On the basis of these results, it was possible to conclude that, while the addition of columbium to vanadium does suppress the formation of a liquid oxide, a maximum reduction in oxidation rate can be obtained only by the addition of titanium,

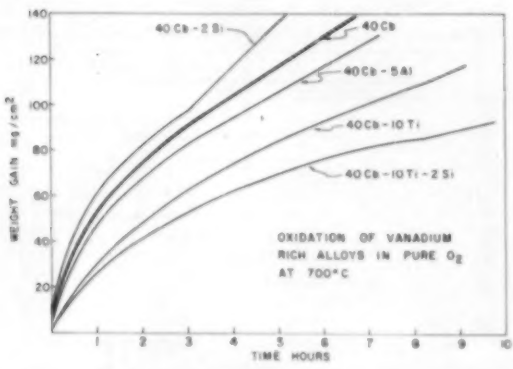
40 Cb - 2 Si
40 Cb
40 Cb - 5 Al
40 Cb - 10 Ti
40 Cb - 10 Ti - 2 Si
OXIDATION OF VANADIUM RICH ALLOYS IN PURE O2 AT 700°C
WEIGHT GAIN mg/cm²
TIME HOURS

Fig. 4. Oxidation of columbium containing vanadium alloys as characterized by weight-gain values at 700°C.

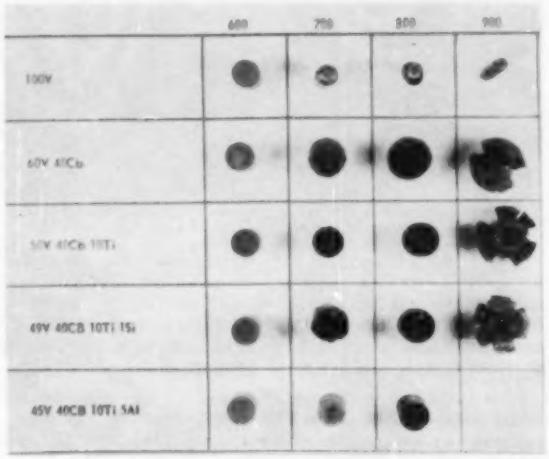

Fig. 5. Appearance of ⅜-in. diameter samples after 5.0 hr exposure in air.

especially in the presence of small amounts of silicon or aluminum.

Oxidation measurements by means of metal loss techniques, wherein the decrease in sample diameter after oxidation is measured, were made on pure vanadium and four alloys. The alloys were:

60% V-40% Cb
50% V-40% Cb-10% Ti
49% V-40% Cb-10% Ti-1% Si
45% V-40% Cb-10% Ti-5% Al

These compositions were selected on the basis of the weight-gain measurements described above to combine the minimum oxidation rate with a single phase structure. Tests were performed on wrought ⅜-in. diameter specimens over a temperature range of 600°-900°C for time periods of up to 10 hr at 900°C and up to 100 hr at lower temperatures. The 45% V-40% Cb-10% Ti-5% Al alloy was also evaluated at 1000°C. The visual appearance of some of the samples after oxidation is portrayed in Fig. 5. Following exposure in undried static air at the proper temperature and time combination, oxidation products were removed by abrasion and etching in a 20% KOH-5% $KMnO_4$ solution, and the amount of metal consumed, the metal loss, was measured with a micrometer to the nearest mil (0.001 in.). The decrease in sample diameter in terms of metal loss expressed in mils per side is plotted for a constant 5-hr period of air exposure against temperature in Fig. 6. Figure 7 presents the rate of oxidation of pure vanadium and a 50% V-40% Cb-10% Ti alloy as well as the 49% V-40% Cb-10% Ti-1% Si and 45% V-40% Cb-10% Ti-5% Al alloys at 700°C.

These measurements indicate a reduction in oxidation rate for the quaternary alloys and for the simple V-Cb-Ti ternary that approaches a five- to sevenfold improvement over pure vanadium. The rate of oxidation of the 45% V-40% Cb-10% Ti-5% Al alloy is particularly outstanding for a vanadium-base composition with no liquid oxide being observed at temperatures up to 1000°C. Liquid vanadium pentoxide was definitely noted on the other compositions tested at 900°C, and in the case of the

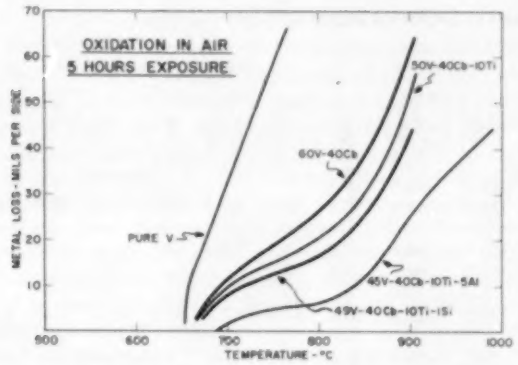

Fig. 6. Effect of temperature on oxidation of vanadium-columbium alloys.

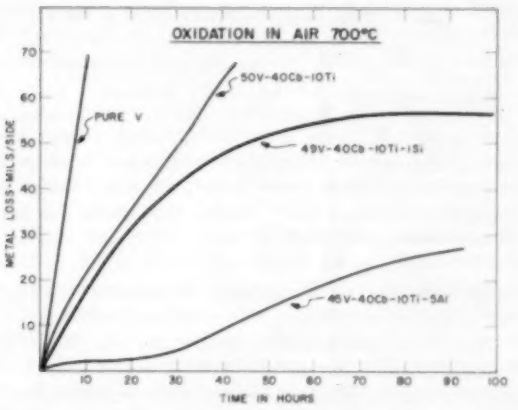

Fig. 7. Oxidation of vanadium-columbium alloys as characterized by a size decrement value at 700°C.

60% V-40% Cb alloy, small amounts of liquid oxide were observed on samples exposed at 800°C. The appearance of liquid vanadium pentoxide during the oxidation of these alloys is to some extent time-dependent, becoming more pronounced as the oxidation process proceeds. In all samples examined, no subscale surface hardening of the type encountered in columbium-base alloys or pure vanadium was noticed.

Mechanical Properties

The determination of the mechanical properties of vanadium-columbium alloys was focused primarily on the compositions of promising oxidation and corrosion resistance.

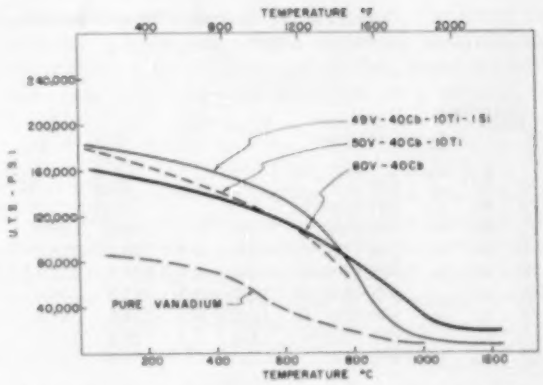

Fig. 8. Effect of temperature on tensile strength of alloys tested at 0.005^{-1} sec.

Tensile tests were performed on wrought materials using a button-head type miniature tensile specimen, with all tests being performed in vacuum. The tensile properties of as-swaged vanadium-columbium alloys with and without further additions of titanium, silicon, and aluminum are presented in Table IV for room temperature, 700° and 1000°C. These data augmented by results obtained at 1200°C are plotted in Fig. 8 for the stronger alloys in the as-swaged condition. The as-swaged condition is equivalent to warm-worked material for all alloys with the possible exception of the 45% V-40% Cb-10% Ti-5% Al composition. The effect of cold-work on the mechanical properties of the 70% V-30% Cb and 50% V-40% Cb-10% Ti alloys is presented in Table V, which also includes data on the effect of heat-treatment on the properties of warm-swaged vanadium-columbium alloys. All alloys studied could be cold-swaged at room temperature after a primary breakdown by extrusion. The high compressive strength of these materials, however, produced very frequent die failures during swaging, and since cold working did not affect the mechanical properties appreciably, the production of cold-swaged material was limited. Cold work decreased the room-temperature ductility of these materials without producing appreciable elevated temperature strengthening, even at temperatures well below the recrystallization temperature. Annealing warm-worked material in the temperature range of 1100°-1300°C tended to produce some reduction in mechanical properties which was more than made up by increased room-temperature duc-

Table IV. Tensile properties of vanadium-columbium alloys*

				R.T.			700°C			1000°C			
V	Cb	Ti	Other	U.T.S. psi × 10^{-3}	0.2% Y.S. psi × 10^{-3}	E %	U.T.S. psi × 10^{-3}	0.2% Y.S. psi × 10^{-3}	E %	U.T.S. psi × 10^{-3}	0.2% Y.S. psi × 10^{-3}	E %	Density lb/in.^{3}
70	30	—	—	Brittle failure			127.0	91.1	24.0	—	—	—	—
60	40	—	—	Brittle failure			102.3	91.0	7.4	34.8	30.8	8.0	0.25
50	40	10	—	Brittle failure			91.8	84.2	15.8	—	—	—	0.24
49	40	10	1% Si	182.0	140.0	3.0	121.0	86.4	22.3	12.8	8.85	74.0	0.23
45	40	10	5% Al	Brittle failure			91.2	69.0	5.3	7.9	5.9	142.0	—

* All impact extruded 4:1 reduction at 1100°-1200°C followed by 50% reduction by swaging at 1000°C. All tests performed at 0.005^{-1} sec strain rate.

Table V. Effect of processing variables on mechanical properties*

Alloy composition, w/o V	Co	Ti	Swaged condition†	Annealed Temp, °C	Time, hr	R.T. U.T.S. psi × 10^{-3}	R.T. 0.2% Y.S. psi × 10^{-3}	R.T. E %	700°C U.T.S. psi × 10^{-3}	700°C 0.2% Y.S. psi × 10^{-3}	700°C E %	1000°C U.T.S. psi × 10^{-3}	1000°C 0.2% Y.S. psi × 10^{-3}	1000°C E %	1200°C U.T.S. psi × 10^{-3}	1200°C 0.2% Y.S. psi × 10^{-3}	1200°C E %
70	30	—	30% C.W.	—	—	Brittle failure			128.6	109.6	5.2	—	—	—	—	—	—
70	30	—	50% 1100°C	—	—	Brittle failure			130.2	112.0	6.0	70.1	63.7	89	23.2	22.4	43.6
70	30	—	50% 1100°C	1100	0.5	124.1	125.6	2.2	—	—	—	—	—	—	—	—	—
70	30	—	50% 1100°C	1200	0.5	123.8	118.2	2.0	121.7	90.7	69.0	68.2	65.0	72	—	—	—
70	30	—	50% 1100°C	1300	0.5	123.6	114.7	5.0	126.0	90.7	25.0	—	—	—	—	—	—
60	40	—	50% 1000°C	1000	0.5	143.3	136.9	2.0	—	—	—	—	—	—	—	—	—
60	40	—	50% 1000°C	1100	0.5	154.6	141.6	62.5	140.2	131.8	40.5	68.3	63.0	35.3	22.8	22.3	14.0
60	40	—	50% 1000°C	1300	0.5	125.8	115.3	7.7	—	—	—	—	—	—	19.8	19.0	21.1
50	40	10	40% C.W.	—	—	181.0	177.2	4.0	86.7	75.5	2.8	—	—	—	—	—	—

* All tests performed at 0.02^{-1} sec strain rate.
† Preceded by extrusion 4:1 reduction at 1100°-1200°C.

tility. The sparsity of data makes even these comments questionable, but the generalization that the room-temperature ductility of these materials can be increased by the proper heat-treatment is definite. This, of course, is valid only for conditions of tensile loading applied at the strain rate used (0.005-0.02^{-1} sec). Although the tensile properties of the vanadium-columbium type of alloys are not affected appreciably by variations in strain rate within this spectrum of rate of load application, much higher rates of loading will decrease the ductility parameters and markedly increase the ultimate tensile strength. This has been observed even at 1200°C. The ultimate tensile strength of a warm-worked 60% vanadium-40% columbium alloy will vary from some 20,000 psi to 40,000 psi at 1200°C as the strain rate is increased from 0.02^{-1} sec to 0.20^{-1} sec.

The concluding step in these mechanical studies involved creep-rupture tests on as-swaged 60% V-40% Cb, 50% V-40% Cb-10% Ti, and 49% V-40% Cb-10% Ti-1% Si compositions. All tests were performed at 700°C in an atmosphere of pure helium gettered by a titanium collar placed around the creep-rupture specimen. The stress-rupture properties of these alloys at 700°C are shown in Fig. 9. Stress levels for a 100-hr life to rupture of 110,000 psi for the 60% V-40% Cb alloy, 85,000 psi for the 50% V-40% Cb-10% Ti alloy, and 90,000 psi for the 49% V-40% Cb-10% Ti-1% Si, were reflected in a correspondingly high creep resistance. As given in Table VI, the 100,000 psi minimum

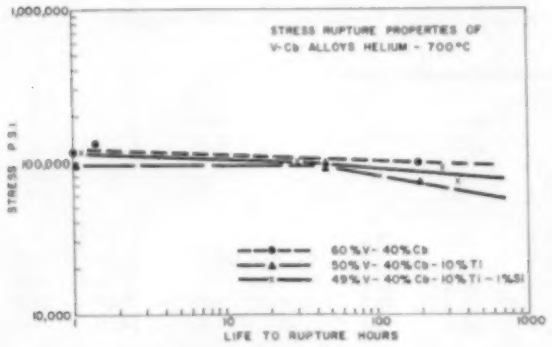

Fig. 9. Stress-rupture properties of some V-Cb alloys tested in helium.

Table VI. Creep properties of V-Cb alloys* at 700°C

Alloy composition w/o	Minimum creep rate (in./in./hr) for 75,000 psi	90,000 psi	100,000 psi
60 V-40 Cb	—	—	1.05×10^{-4}
50 V-40 Cb-10 Ti	3.58×10^{-5}	1.15×10^{-4}	1.0×10^{-4}
49 V-40 Cb-10 Ti-1 Si	8.0×10^{-5}	1.7×10^{-4}	1.85×10^{-4}

* As-swaged at 1000°-1100°C.

creep rate of the vanadium-columbium alloys at 700°C varied from 1.0 to 1.85×10^{-4} in./in./hr.

The high mechanical properties of the 60% V-40% Cb and the 49% V-40% Cb-10% Ti-1% Si alloys are even more attractive when compared with the properties of other materials on the strength-to-density basis. Such a comparison is presented in Fig. 10 where the strength-to-weight ratio of these two compositions is compared to the same ratio for the strongest iron-, titanium-, and molybdenum-base alloys. In this plot, the ultimate tensile strength of the vanadium-columbium alloys refers to the warm-worked condition as evaluated at a strain rate of 0.005^{-1} sec. If data obtained at strain rates of 0.20^{-1} sec had been used, the 60% V-40% Cb composition would approach the strength-to-weight ratio of the molybdenum-0.5 titanium alloy at 1200°C (2192°F).

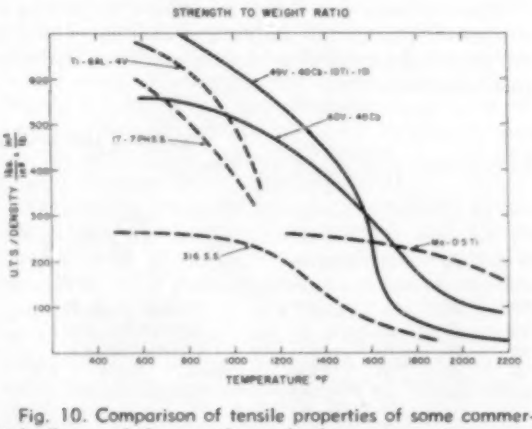

Fig. 10. Comparison of tensile properties of some commercial alloys and the vanadium-columbium compositions on a strength-to-weight basis.

Summary and Discussion

The aqueous corrosion and oxidation resistance as well as the high-temperature strength that can be imparted to vanadium by columbium additions present an appreciable improvement over other vanadium base systems (3, 4). Relatively simple alloys such as the 50% V-50% Cb or 60% V-40% Cb compositions exhibit degrees of corrosion resistance and elevated temperature strength that compare favorably with the best materials in present day commercial use. More complex alloys as exemplified by the 45% V-40% Cb-10% Ti-5% Al begin to show a level of oxidation resistance that would at least assure reliability in a coated structure, while even the simple binary combinations exhibit sufficient resistance to liquid V_2O_5 formation to allow their fabrication at elevated temperatures without cumbersome canning or coating procedures. None of these alloys, of course, is oxidation resistant enough above 660°C to permit prolonged service in air.

The degree to which columbium additions will increase the high-temperature strength of vanadium is an excellent example of the solid solution strengthening that can be imparted by adding a solute of high solubility that produces the maximum amount of lattice strain for a minimum decrease of the solvent's melting point. The small loss in fabricability and the retention of ductility after recrystallization that is made possible by such a strengthening mechanism are also beneficial. Nevertheless, the alloys are highly strain-rate sensitive, a condition that can be improved at the expense of strength by titanium additions.

The solubility of Cb_2O_5 in V_2O_5 and the resultant increase of the melting point of the vanadium pentoxide are partially responsible for the observed improvement in oxidation. Equally significant is the complete intersolubility that exists in the metallic phase and higher affinity of columbium for oxygen. Both of these latter two factors are believed to promote the inclusion of columbium in the oxide phase. A further reduction in reaction rate can be obtained by titanium and aluminum additions.

The observed increase in corrosion resistance is probably a reflection of the passivity inherent to columbium, a property which for this metal is usually associated with the presence of a protective film.

In closing, it may be noted that, although each of these possible mechanisms requires a high level of columbium in terms of weight per cent, the atomic concentration of columbium is roughly one-half of that expressed on a weight basis. The properties exhibited by these vanadium-columbium alloys can, therefore, be correctly ascribed to a vanadium-rich system and regarded as a further development in the alloy systems of this refractory metal.

Acknowledgment

The author is indebted to Mr. C. R. Bishop for the corrosion results presented here and to Mr. J. L. Wilson for his help and advice in the fabrication of these alloys.

Manuscript received May 9, 1960. This paper was prepared for delivery before the Chicago Meeting, May 1-5, 1960.

Any discussion of this paper will appear in a Discussion Section to be published in the June 1961 JOURNAL.

REFERENCES

1. J. W. Farrell, Paper presented at The Electrochemical Society Symposium on Vanadium, May 1-5, 1959, in Chicago.
2. W. Rostoker, A. S. Yamamoto, and R. E. Riley, *Trans. A.S.M.*, **48**, 560 (1956).
3. W. Rostoker, "The Metallurgy of Vanadium," John Wiley & Sons, Inc., New York (1958).
4. K. F. Smith and R. J. Van Thyne, Metallurgical Society Conferences, Reactive Metals, **2**, 403 (1959); Interscience.
5. M. Hansen and K. Anderko, "Constitution of Binary Alloys," 2nd ed., McGraw-Hill Book Co., New York (1958).
6. H. A. Wilhelm, O. N. Carlson, and J. M. Dickinson, *Trans. A.I.M.E.*, **200**, 915 (1954).
7. W. Rostoker and A. Yamamoto, *Trans. A.S.M.*, **46**, 1136 (1954).
8. M. Stern and C. R. Bishop, *ibid.*, **52**, 239 (1960).
9. F. A. Mauer, *Rev. Sci. Instr.*, **25**, 598 (1954).

Correction

Subject to the publication of the paper "Oxidation of Niobium in the Temperature Range 350°-750°C" by D. W. Aylmore, S. J. Gregg, and W. B. Jepson in the June 1960 issue of the Journal, the authors have been informed by Messrs. Murex Ltd. that the figure for the carbon content of the niobium (Batch A) was incorrectly quoted. The correct value is 0.01%.

Technical Notes

NMR Measurements of the Knight Shift in Conducting PbO_2

D. A. Frey and H. E. Weaver[1]

Instrument Division, Varian Associates, Palo Alto, California

According to the quantum mechanical model, nuclei possessing units of angular momenta and a nonzero magnetic moment are allowed only discrete orientations in an applied magnetic field. In the case of the Pb^{207} isotope where the nucleus has a spin of ½ units, there are two separate field-dependent energy levels. The energy of these levels is given by

$$E = \vec{\mu} \cdot \vec{H}$$

or

$$\nu = \gamma H, \text{ for the transition frequency,}$$

ν being the frequency, μ the magnetic moment, H the value of the magnetic field, and γ the gyromagnetic ratio for a given nucleus.

By varying the applied magnetic field, H, and simultaneously irradiating the sample containing the isotope under investigation with an oscillating magnetic field of frequency, ν, an NMR (nuclear magnetic resonance) absorption of energy from the rf-field may be detected when the value of the field-frequency satisfies the relation, $\nu = \gamma H$. NMR techniques have a wide range of application in the study of the molecular environment and its influence on the resonance character of the nuclei in an external magnetic field.

The effective magnetic field at the nucleus may differ from that of the applied field because of the influence of the external field on the environmental electrons of the nuclei, be they valence or conduction electrons. The magnitude and sign of the "chemical shifts" associated with a particular compound containing the resonating nucleus can easily be measured via the techniques of NMR. In the case of nuclei of high atomic number these relative shifts can amount to several per cent of the applied field (1). For conductors this "chemical shift" has the name Knight shift (1) after its discoverer.

Lead dioxide has long been known to be a conductor of electricity but until recently (2, 3) little quantitative data were available on its physical properties. In an earlier note Piette and Weaver (4) measured the resonance of Pb^{207} in PbO_2 and other lead compounds relative to that in the metal and found that the data were indeed consistent with the concept that PbO_2 does behave as a metal. Thomas (2) measured the conductivity and Hall coefficient for rather dense samples of PbO_2 and found that the carriers were electrons and that the temperature coefficient of conductivity is negative. Rüetschi, *et al.* (3) have measured the electrochemical properties of both α- (orthorhombic) and β- (tetragonal) forms of PbO_2. They have made extensive measurements on the effect of oxygen removal from PbO_2 on the electrical properties of both allotropic forms. It has been established that PbO_2 never has the stoichiometric composition, but rather shows an oxygen deficiency yielding a mixture with a formula more like $PbO_{1.98}$ to $_{1.96}$. The lack of stoichiometric composition is generally felt to be the origin of the conductivity.

Lead dioxide is generally available in powder form with particle sizes of less than 1 μ. In this form it is ideally suited for NMR at 8 mc/sec and even EPR (electron paramagnetic resonance) at 9000 mc/sec, since the particles are smaller than the skin depth. Nuclear and electron resonance techniques are the "noncontacting" type, thereby requiring essentially no sample preparation and specifically no electroding.

Piette and Weaver (4) have measured the chemical shift of Pb^{207} in several representative lead compounds, in particular commercial PbO_2 (presumably β-form) relative to the resonance in lead metal. Rocard, *et al.* (5) reported later on a similar set of measurements, but with some variation in the Knight shift in PbO_2 compounds depending on the assay. They ascribed these differences to impurity content. Accordingly a series of experiments were designed to investigate the variation of the chemical shift (or Knight shift) of the Pb^{207} resonance in as many different forms of PbO_2 as were available. This note then deals exclusively with NMR and EPR measurements in PbO_2 and Pb metals.

Instrumentation

In those room-temperature measurements involving NMR a standard Varian V4200 wide line spectrometer was employed. A standard probe with the Dewar insert with associated transfer Dewar and heat exchanger were employed for measurements made at other than room temperature. By adjusting the flow rate of dry nitrogen gas, the temperature of the sample could be continuously varied from room temperature down to −185°C. For the EPR measurements a standard V4500 spectrometer plus cryogenic accessories were used. The magnet employed was V4012-3B with 2⅝ in. air gap with associated current stabilization.

[1] Present address: Physik-Institut Der Universität Zurich, Zurich, Switzerland. Dr. Weaver is on leave of absence from Varian Associates.

Table I. Summary of PbO_2 NMR measurements at room temperature

Compound	Knight shift	Relative intensity
β-PbO_2 B & A 95%	$0.58 \pm 0.02\%$	1.00
β-PbO_2 B & A 90%	$0.56 \pm 0.02\%$	0.52
β-PbO_2 E S B —	0.63 ± 0.02	0.67
β-PbO_2 N L Co.	$0.62 \pm 0.02\%$	0.55
α-PbO_2 E S B	0.48	—

Measurements

The NMR experiments performed fell into two major classifications: (i) room-temperature measurements as a function of sample preparation and crystal symmetry, (ii) measurement of the Knight shift as a function of temperature, and thermal decomposition of PbO_2 with increased temperature above 200°C. EPR experiments were designed merely to detect a resonance.

Nuclear magnetic resonance.—NMR measurements of the Knight shift relative to Pb metal were made on all available samples. Table I indicates that at least two separate shifts appear to have been observed for the β group and a third for the α sample. Since the Knight shift in the PbO_2 resonance is dependent on the density of conduction electrons near the top of the Fermi distribution, Knight shift values for these samples can be said to correspond qualitatively with their conduction properties. However, the mechanism by which conduction electrons are made available is not completely understood.

Oxygen deficiency rather than impurity content probably is responsible for the conduction electron density, hence the fluctuations among the β group. It is noteworthy that both the 90% and 95% B & A samples have approximately the same Knight shift (relative to the metal), while the ESB and NL Co. samples have considerably higher values.

To obtain further quantitative information, first moments indicative of the relative intensities were calculated from the resonance curves obtained from each of the β samples, normalizing the B & A 95% moment (or intensity) to one. In Fig. 1 (a-e) are shown typical traces of the lead resonance in various available forms of PbO_2. The signal-to-noise of ESB-α-PbO_2 (Fig. 1e) was particularly poor because of a small amount of sample. Microscopic examination of the samples at an optical magnification of 800 gave no conclusive information regarding the relative particle size which would affect the density of the sample and hence the signal-to-noise obtained from a given volume.

Variations in NMR Knight shift measurements were also used as an indication of the change in PbO_2 conductivity with thermal decomposition. Table II clearly shows a decrease in the Knight shift (or an increase in the shift relative to the metal) as the thermal decomposition progresses. This suggests that the compound goes through the transition from conductor to semiconductor before becoming an insulator in the form of PbO. It is interesting to note that further loss of oxygen (prior to an actual crystal phase change) does not improve the conduction properties, which at best is anomalous in light of the model proposed: *viz.*, it is just this initial oxygen deficiency that is responsible for the conductivity.

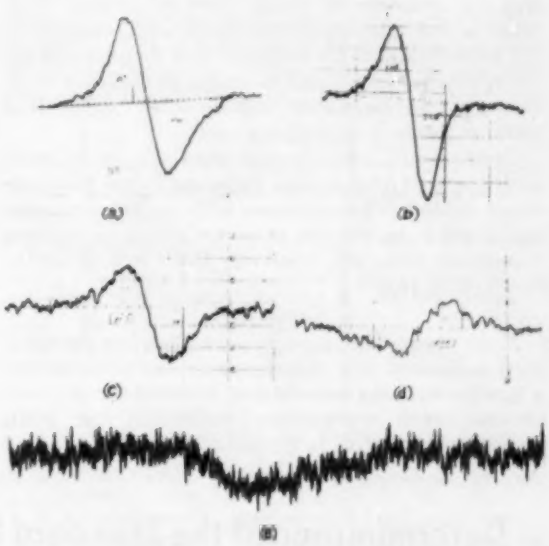

Fig. 1. Representative NMR traces of PbO_2 at 7.5 Mc/s. (a) B & A β—PbO_2 95%; gain x-10-2; (b) ESB β—PbO_2; gain x-10-3; (c) B & A β—PbO_2, 90%; gain x-10-3; (d) NL Co. β— PbO_2; gain x-10-4; (e) ESB α-PbO_2; gain x-10-4.

Electron paramagnetic resonance.—Since the particle size of the PbO_2 samples was less than the skin depth even at microwave frequencies it seemed worthwhile to investigate them for possible electron resonance. The resonance, if detected, could stem then either from paramagnetic impurity, presumably transition elements in a favorable environment, or from the conduction electrons themselves. Accordingly samples were prepared and a series of experiments were made from room temperature down to less than 2.0°K.

To date the results have been inconclusive. Lines which might be ascribed to the β-PbO_2 seem not to follow an expected pattern. Further, because of the excessive width of the observed resonance the amplitude is small and hence the attendant signal-to-noise is poor. The lack of a well-defined conduction electron resonance is not at all surprising in light of the proposed mechanism of oxygen deficiency to account for the conductivity. This model implies that there is a rather large concentration of "free" lead ions interstitially located in the regular PbO_2 lattice,

Table II. Summary of relative NMR shifts for heat-treated samples of β— B & A (95%) PbO_2

Temperature, °C	Shift* relative to untreated samples (gauss)
Room	0.0
200	−2.2
285	−6.5
330	−12.7
360	−15.3

* A negative shift implies a shift in the resonance toward higher fields.

and the presence of these "foreign" atoms could cause severe inhomogeneous temperature-independent broadening of the resonant line thereby making the resonance impossible to detect. Such seems to be the case. No resonance was detected in the lead metal powders.

Conductivity.—An experiment was performed with the low-temperature facilities at the Westinghouse Research Laboratories with β-PbO_2 commercial grade in an attempt to detect a superconducting transition. None was observed down to a temperature of 1°K (6).

Conclusion

From these data it is evident that the chemical shift associated with the resonance of Pb^{207} is indeed a Knight shift characteristic of a conductor. A series of controlled experiments measuring the NMR Knight shift relative to Pb metal as the oxygen-lead ratio is varied might well yield much more conclusive data.

Manuscript received May 11, 1960.

Any discussion of this paper will appear in a Discussion Section to be published in the June 1961 JOURNAL.

REFERENCES

1. For an excellent review of the technique of MNR see G. E. Pake, "Solid State Physics," Vol. II, p. 2, Academic Press Inc., New York (1956); W. D. Knight, *ibid.*, p. 93.
2. U. B. Thomas, J. (*and Trans*) *Electrochem. Soc.*, **94**, 42 (1948).
3. P. Rüetschi and B. D. Cahan, *This Journal*, **105**, 369 (1958).
4. L. Piette and H. Weaver, *J. Chem. Phys.*, **28**, 735 (1958).
5. J. Rocard, M. Bloom, and L. Robinson, *Can. J. Phys.*, **37**, 522 (1959).
6. P. C. Chester, Private communication.

Determination of the Standard Free Energy of Formation of Lead Selenide

Cabell B. Finch[1] and J. Bruce Wagner, Jr.

Department of Metallurgy, Yale University, New Haven, Connecticut

In conjunction with diffusion studies in this laboratory on the semiconducting compounds, PbS, PbSe, and PbTe, measurements have been carried out to determine the standard free energy of formation of lead selenide. Following the suggestions of Wagner (1-5), a galvanic cell involving a solid electrolyte

$$Pb(s) \mid PbCl_2 + 1\%\ KCl(s) \mid PbSe(s), Se(l) \qquad (I)$$

was used. The virtual cell reaction of cell (I) on passing two faradays is

$$Pb(s) + Se(l) = PbSe(s) \qquad [1]$$

The lead selenide was prepared by synthesis from its elements. Lead, 99.999% pure, was reacted with 99.99+% selenium by a method used for the synthesis of cuprous sulfide (4). The synthesized PbSe was mixed with an excess of the pure selenium and pressed into pellets at a pressure of about 350 kg/cm^2. The solid ionic electrolyte, $PbCl_2$ + 1% KCl, was prepared as described elsewhere (6) and pressed into pellets. Crucibles to contain the molten selenium coexisting with PbSe were made by drilling a hole in one side of the electrolyte pellet. The galvanic cell was assembled by placing a 99.999% lead pellet in a graphite crucible. The crucible of electrolyte which contained the PbSe pellet with excess selenium was placed on top of the lead pellet. Glass wool or asbestos was packed between the walls of the graphite and electrolyte crucibles in order to prevent vapor transport of selenium to the pure lead. A graphite electrode was placed in contact with the PbSe pellet and the entire cell was placed in a glass tube under argon as described in ref. (3).

A controller maintained the temperature better than ±1°C and the temperature was measured with a chromel-alumel thermocouple which was calibrated previously against the melting points of lead, zinc, and aluminum. The electromotive force measurements were consistent on increasing and decreasing the temperature between 200° and 300°C, and

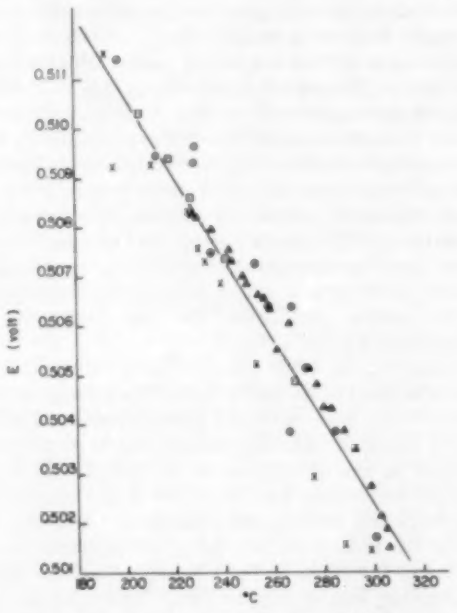

Fig. 1. EMF vs. temperature for the cell, Pb(s) | $PbCl_2$ + 1% KCl | PbSe(s), Se(l)

[1] Present address: Oak Ridge National Laboratory, Oak Ridge, Tenn.

the results of four separate experiments are shown in Fig. 1. Using a least squares analysis of all these data the standard free energy of formation of lead selenide in the range of 200° to 300°C may be expressed by the equation

$$\Delta G^\circ = -nFE = [-23{,}352 + 3.8(t - 250)] \text{ cal} \quad \text{(II)}$$

where **F** is the Faraday constant, *E* the electromotive force, and *t* the temperature in °C.

All but two of the emf data, one at the high temperature and one at the low temperature, lie between ±1.5 mv of the least square curve. This corresponds to ±69 cal in ΔG°. Thus with a temperature variation of ±1°C the total estimated accuracy is better than ±80 cal in ΔG°.

Below about 200°C, the attainment of steady values was very sluggish. Above about 300°C, the vapor pressure of selenium was sufficiently high that vapor transport sometimes caused contamination of the lead pellet. At the end of each experiment, the lead was examined for selenium contamination and any results obtained under these conditions were discarded. In addition, the higher temperatures favored plastic deformation of some of the cell components causing short circuits. Therefore the present measurements were restricted to the range of 200° to 300°C. The present value of the standard free energy of formation agrees well with unpublished data of Lorenz and Wagner (5).

Acknowledgment

The authors wish to thank Professor Carl Wagner for advice and the Office of Naval Research for financial support.

Manuscript received May 18, 1960.

Any discussion of this paper will appear in a Discussion Section to be published in the June 1961 JOURNAL.

REFERENCES

1. C. Wagner, Proc. of the Seventh Meeting of the International Committee of Electrochemical Thermodynamics and Kinetics, Lindau (1955), p. 361 [Published as a separate paper without changes in pagination by Butterworths Scientific Publications (1957)].
2. K. Kiukkola and C. Wagner, *This Journal*, **104**, 308 (1957).
3. K. Kiukkola and C. Wagner, *ibid.*, **104**, 379 (1957).
4. J. B. Wagner and C. Wagner, *J. Chem. Phys.*, **26**, 1602 (1957).
5. G. Lorenz and C. Wagner, Unpublished research at the Massachusetts Institute of Technology (1956).
6. J. B. Wagner and C. Wagner, *This Journal*, **104**, 509 (1957).

Microalloy Junction for Silicon

L. Maissel

Research Division, Philco Corporation, Philadelphia, Pennsylvania

The development of the germanium microalloy junction (1) brought about considerable improvement in the frequency response of transistors made by electrochemical techniques (2); its main features are high injection efficiency and very shallow depth of penetration (approximately 0.001 mil). It consists, basically, of an indium-gallium dot alloyed at as low a temperature as possible.

In searching for a similar contact for silicon it was first necessary to analyze the general requirements for a satisfactory microalloy junction. By definition, the metal used in forming the junction must be such as to dissolve only a small percentage of its own volume of semiconductor when alloying takes place. The metal semiconductor phase diagram should, therefore, be of the general form of Fig. 1.

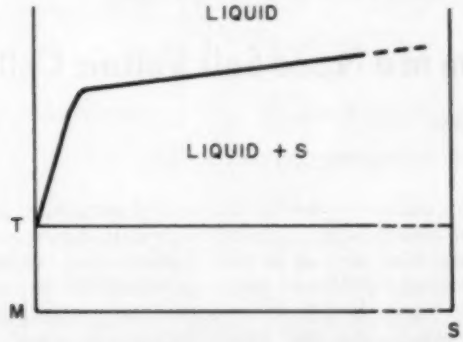

Fig. 1. Metal semiconductor phase diagram

In the case of germanium the metals that have this type of liquidus curve are indium, bismuth, lead, and gallium. Gallium cannot be used in practice because of its low melting point. Any of the other three would be suitable if it were not for the requirement that the microalloy junction must possess high injection efficiency as well as shallow penetration. This means that a small percentage of some suitable dopant must be included with the alloying metal. The only two dopants that are sufficiently soluble in germanium, to give a high injection efficiency junction, are aluminum and gallium. The former is, however, almost completely immiscible at all temperatures with all three of the possible alloying metals. Gallium is immiscible with bismuth and lead but, fortunately, not with indium. The indium-gallium combination is thus the only one suitable for a germanium microalloy[1] if alloying is allowed to proceed to equilibrium.

Similar reasoning applied to silicon indicates that either tin or antimony might be suitable metals for microalloying. The former, however, has shallow penetration only at relatively low temperatures (below 600°C) where dopant solid solubilities are also low. Antimony has shallow penetration below 800°C and has the additional advantage of also being a donor element with reasonable solid solubility in silicon at these temperatures.

Accordingly, an attempt was made to make an

[1] Microalloy junctions also can be formed by using a very rapid heating cycle, so that equilibrium and hence full penetration is not reached. However, it will be shown that nonequilibrium alloying is unsuitable for silicon.

alloyed junction of pure antimony in silicon. Initial attempts failed because of "balling up" of the antimony during alloying. That this was not surprising can be seen from the following considerations

If a given liquid is to wet a solid, it is a necessary (although not sufficient) condition that the surface tension of the solid must exceed that of the liquid. The surface tension of liquid antimony is approximately 350 dynes/cm; the values for solid silicon and solid silicon dioxide are approximately 600 dynes/cm and 300 dynes/cm, respectively (3). Thus the condition for antimony wetting is satisfied by silicon but not by its oxide. In view of the invariable presence of a thin oxide layer on the surface of silicon the net effect is that antimony will not wet silicon.

Since the surface tension of almost all liquid metals is greater than 300 dynes/cm it would seem that very few metals should ever wet silicon. However, the oxide film is generally of a porous nature so that metal and silicon are in fact in direct contact in a limited number of places. If the metal and the silicon have a eutectic reaction then, as long as the temperature is kept below the melting point of the pure metal (but above the eutectic point) fusion can begin in the regions of direct metal-to-silicon contact. The liquid so formed spreads out as it dissolves silicon so that the oxide film is undercut and, eventually, dislodged. In the absence of a eutectic reaction it should still be possible to promote wetting of the silicon by the metal provided the latter can be constrained from "balling up" long enough for the process of oxide film undercutting to become effective.

Direct mechanical constraint of the liquid antimony by suitable jigging was not considered feasible because of the extremely delicate nature of the electrochemically formed base region. Several other ways of achieving the required constraint were explored. Alloying was attempted in an oxidizing atmosphere in the hope that the skin of antimony oxide that formed prior to the melting of the antimony would be tough enough to hold it in position. Some success was obtained but results were not reproducible. A layer of refractory metal was tried in place of the oxide but this invariably broke contact with the silicon and simply floated on the surface of the antimony.

Alloying of antimony to silicon then was attempted by use of the technique of "dip alloying." The principle behind this method is as follows: suppose silicon, with a dot of plated antimony on its surface, is plunged into a fused salt bath. Provided the melting point of the bath is greater than that of antimony, the crust of salt that freezes on the surface of the cold silicon when it first enters the bath will still be solid when the antimony reaches its melting point. During the brief period before the crust remelts the antimony is thus constrained by a tough close-fitting jacket, so that wetting can occur by the mechanism discussed above. A number of salt baths were investigated for use in this connection and successful alloying of antimony to silicon was obtained in both KCl and KBr. Most compounds that were tried had to be rejected because they reacted with either antimony or silicon or both.

In order to establish that a true microalloy junction was being formed during dip-alloying, a number of test transistors were fabricated as follows: blanks of 5 ohm-cm p-type silicon were jet-etched to a thickness of approximately 0.4 mil. Dots of antimony 20 and 40 mils in diameter were then jet-plated onto opposite sides of the etch pit from an ethylene glycol solution containing 10 g SbF_3 and 60 g HF per liter. After dip-alloying in KCl for 30 sec at 800°C, units were rinsed in deionized water (to remove KCl) and were then clean-up etched. Whereas the antimony dots had shown only weak rectification before alloying, the alloyed units exhibited alpha-values of approximately 0.9. To measure the junction thickness, punch-through voltages before and after alloying were compared. These measurements showed the depth of penetration to be approximately 2×10^{-4} in., about twice that of a typical germanium microalloy junction. The feasibility of microalloying silicon was thus demonstrated.

Acknowledgments

The author wishes to thank Mr. V. C. Sirvydas for his assistance in the fabrication of the punch-through units.

Manuscript received April 11, 1960.

Any discussion of this paper will appear in a Discussion Section to be published in the June 1961 JOURNAL.

REFERENCES

1. A. D. Rittman, G. E. Messenger, R. A. Williams, and E. Zimmerman, *I.R.E. Trans.* on Electron Devices 49, April 1958.
2. J. W. Tiley and R. A. Williams, *Proc. I.R.E.*, **41**, 1706 (1953).
3. A. Bondi, *Chem. Rev.*, **52**, No. 2 (1953).

Electrolytic Production of Zirconium in a Fused Salt Voltaic Cell

Meyer L. Freedman

Refractory Metals Laboratory, General Electric Company, Cleveland, Ohio

The production of refractory metal powders by electrolysis of their compounds in molten salt solutions has been investigated intensively because of the valuable properties of high purity and coarsely crystalline form which may be obtained (1). The low oxygen, carbon, and nitrogen contents which can be achieved are particularly valuable for titanium, zirconium, boron, silicon, and beryllium, since these metals cannot be purified readily during processing. Also, because of their particle sizes, the electrolytically produced metal powders are consolidated more readily by conventional metallurgical processing than the metal sponges produced by chemical reduction. These advantages apply in part

also to vanadium, columbium, tantalum, chromium, molybdenum, and tungsten.

Electrolytic extraction has not been utilized more widely for the refractory metals because of problems inherent in the anode reactions. The anodic generation of corrosive gas at high temperature may require the use of graphite containers sometimes resulting in high maintenance costs (2). Anodic polarization effects may be troublesome especially with fluoride salts (3). The problems resulting from anode reactions can be largely eliminated by the use of soluble anodes (4). Cell corrosion and anode effects are avoided, but the process then becomes one of electrorefining rather than electrowinning.

Sodium metal can be used for obtaining all of the refractory metals as sponges or fine powder by high-temperature reduction of their appropriate compounds (5). The use of sodium metal as the soluble anode in a fused salt cell should eliminate corrosion problems while generating *in situ* the current required for effecting the cathodic reduction. Refractory metals could thus be produced with the desirable properties of electrolytic powders while avoiding the difficulties of fused salt electrolysis.

Production of metal powder by this voltaic cell action was observed while experimenting with the sodium reduction of K_2TaF_7. A nickel crucible was filled with a bottom layer of K_2TaF_7, a middle layer of NaCl-KCl eutectic, and a top layer of sodium metal. The layers were separated by porous diaphragms made from Monel screen. After melting under argon, large flakes and crystals of tantalum metal were found adhering to the lower diaphragm and to the crucible wall beneath the unreacted tantalum salts. Spectrographic analysis of the washed tantalum showed it to contain less than 0.01% of copper, iron, or nickel as major impurities. The metal flakes were soft, ductile, and easily compacted into mechanically strong pellets.

The voltaic cell metals extraction phenomena was investigated on a larger scale with the apparatus shown in Fig. 1. The 10 cm diameter stainless steel container was placed in a pot furnace. Vacuum drying of the loaded cell before melting was accomplished by the use of a steel cover and rubber gasket which rested on the flange. A charge of 650 g of equimolar C.P. NaCl-KCl provided a 6 cm layer of molten salt at 750°C. Access of air was prevented by a stream of argon. After melting the salt, the cathode was lowered to the cell bottom and 25 to 50 g of sodium metal was added to the cell by melting through a porous stainless steel filter to remove oxides. Five grams of vacuum dried technical grade K_2ZrF_6 was then added to the cathode chamber to give a concentration in the molten salt of about 3% by weight. Additional 5-g portions were added at 30-min intervals during the course of the reaction. At the conclusion of a run the cathode was raised slowly to permit drainage of molten salt and then cooled under argon in the upper chamber. The cathode was then dismantled and the zirconium crystals separated from adhering salts by boiling first with water and then with dilute HCl.

A number of cathode arrangements were tried. With a basket made of 40 mesh Monel screen, the zirconium deposited only on the cell bottom and baffle wall. Thick pads of zirconium crystals formed on both the inside and exterior of a hollow cathode made from perforated nickel foil. The cathode shown in Fig. 1 was constructed from a 5 cm diameter nickel tube which was perforated with two rows of closely spaced 0.6 cm holes. A porous nickel diaphragm covered these holes and was folded over the end of the tube to support a sheet nickel bottom plate. The diaphragm was made by filling the openings of 40 mesh Monel screen with a paste of nickel powder, drying, and sintering in hydrogen at 1100°C.

In one run, 40 g of K_2ZrF_6 was added over a 4-hr period and 11.5 g of washed zirconium crystals were obtained for a yield of 89%. The addition of 50 g of K_2ZrF_6 in 3 hr reduced the cathode yield to 80% of theoretical. The metal was deposited as a thick pad of dendritic crystals over the interior walls and bottom of the cathode. This permitted drainage of

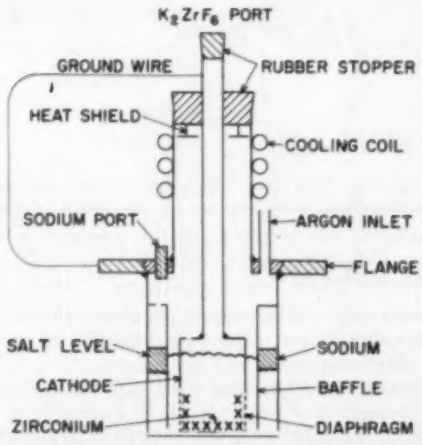

Fig. 1. Zirconium extraction cell

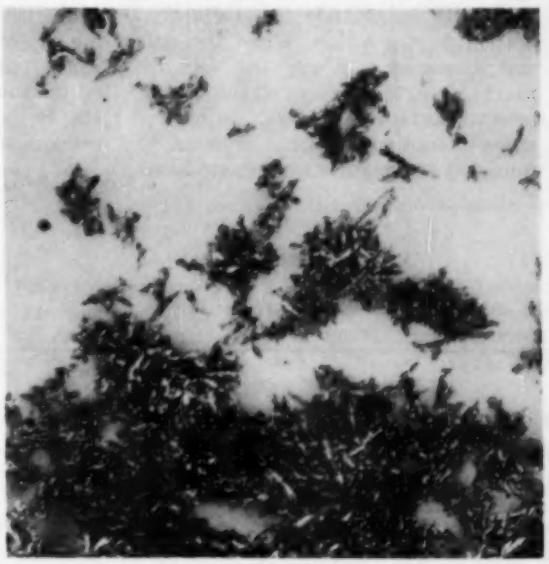
Fig. 2. Zirconium crystals. Magnification 20X before reduction for publication.

molten salts so that a weight of salt equal to only about twice that of the zirconium was retained by the cathode. The recovered metal powder was a silvery gray color with a bulk density of 0.9 g/cc. Figure 2 shows the dendritic form of these zirconium crystals. A 100 mesh screen retained approximately 50% so the average particle size was estimated as 150 μ. A qualitative spectrochemical analysis indicated only traces of iron and nickel impurities. While the particle size is similar to that reported for electrolytic zirconium (6) the dendritic form is more pronounced. Compaction to 80% of theoretical density was obtained on pressing at 50 tons/in.^{2}. The sample thus compares favorably in this respect to hydride zirconium powders (7). A Rockwell B hardness of 90 was determined on a pellet which had been further consolidated by electron beam melting. This value is well within the range for commercially pure zirconium.

The design of this experimental cell did not permit successful reuse of the salt charge. The zirconium obtained in the second run with the same salt bath was a mixture of dendritic crystals and fine black powder similar to the powder obtained by direct reduction of K_2ZrF_6 with sodium. During the time required for the removal of one cathode and the insertion of a second, atomic sodium had apparently diffused into the bulk of the molten salt. This then reacted directly with the K_2ZrF_6 as it was added to the new cathode. For continuous use of the salt bath, provision must thus be made for sealing off the sodium compartment between runs. Otherwise, a second porous diaphragm might be used to restrict the atomic diffusion of sodium while permitting ionic transport.

The anode slit height, fixed by the distance between the bottom of the baffle and the cell bottom, was also found to greatly influence the character of the extracted zirconium. A slit height of approximately 2 mm was generally used. A voltmeter connected in place of the ground wire then registered 0.6 v with the cathode raised slightly above the cell bottom during a run. When the anode slit height was increased to 5 mm the volt meter registered nearly zero. Zirconium was still deposited on the interior surface of the cathode in good yield. However, instead of dendritic crystals, the metal now consisted of irregular gray flakes having rough pebbled surfaces. The zirconium in this form prevented the drainage of molten salt from the cathode at the end of the run and was also difficult to wash free of salt. With the enlarged anode slit the concentration of atomic sodium in the molten salt adjacent to the cathode must have been nearly as high as the concentration within the sodium compartment. Under these conditions, the outer surface of the cathode itself would serve as the anode.

While fluoride salts were used in these experiments, the voltaic cell process should be more advantageous with a chloride feed. In the absence of fluorides, a porous ceramic diaphragm could be used to enclose the cathode volume while a porous metallic diaphragm would confine the sodium. Continuous operation could then be obtained with solid cathodes and molten NaCl.

Other methods have been reported for using molten inert salts in the production of refractory metal powders by sodium reduction. Thus, Vaughan partially submerges a metal grid in a fused salt bath containing a refractory metal halide and sprays sodium metal upon the grid (8). The sodium is claimed to wet the grid and to be carried along the grid surface beneath the melt where it reacts to form crystals of the refractory metal. Dean produces large crystals of refractory metals by reacting very dilute solutions of sodium and refractory metal halides in a molten salt medium (9).

Manuscript received May 25, 1960.

Any discussion of this paper will appear in a Discussion Section to be published in the June 1961 JOURNAL.

REFERENCES

1. G. L. Miller, Powder Metallurgy (1958) No. 1/2 p. 53.
2. G. T. Miller, *J. Electrochem. Soc.*, **106**, 815 (1959).
3. C. L. Mantell, "Industrial Electrochemistry," p. 477, McGraw-Hill Book Co., Inc., New York (1950).
4. R. S. Dean, "Electrolytic Titanium," Chicago Development Corp., Riverdale, Md. (1957).
5. M. Sittig, "Sodium," p. 230, Reinhold Publishing Corp., New York (1956).
6. M. A. Steinberg, M. E. Sibert, E. Wainer, *J. Electrochem. Soc.*, **101**, 63 (1954).
7. H. Hausner, Ed., "Powder Metallurgy in Nuclear Engineering," H. Hirsch, Chapter IV, p. 51, American Society for Metals, Cleveland, Ohio (1958).
8. J. L. Vaughan (To National Research Corp.) U. S. Pat. 2,847,298, Aug. 12, 1958.
9. R. S. Dean (To Chicago Development Corp.) U.S. Pat. 2,875,038, Feb. 24, 1959.

June 1961 Discussion Section

A Discussion Section, covering papers published in the July–December 1960 JOURNALS, is scheduled for publication in the June 1961 issue. Any discussion which did not reach the Editor in time for inclusion in the December 1960 Discussion Section will be included in the June 1961 issue.

Those who plan to contribute remarks for this Discussion Section should submit their comments or questions in triplicate to the Managing Editor of the JOURNAL, 1860 Broadway, New York 23, N. Y., *not later than March 1, 1960*. All discussion will be forwarded to the author(s) for reply before being printed in the JOURNAL.

Fuel Cell Thermodynamics

Andre J. deBethune

Chemistry Department, Boston College, Chestnut Hill, Massachusetts

ABSTRACT

A simple fuel cell, operated reversibly, puts out, either electrochemically or in osmotic-mechanical form, an amount of useful work equal to the chemical potential (free enthalpy, Gibbs free energy) $-\Delta G$ released isothermally by the fuel plus oxygen upon their combination. This may be larger than the corresponding Carnot output $(-\Delta H)\,(T_h - T_l)/T_h$ of the same amount of fuel used to fire a reversible heat engine.

A coupled (regenerative) fuel cell regenerates the cell reagents by decomposing the reaction products at a high temperature (obtainable from a nuclear reactor). It thus acts as a heat engine in converting heat from the nuclear reactor into useful work. Its reversible work output, given by the summation of $-\Delta G$ for all isothermal steps, is exactly equal to that predicted from the heat inputs by Carnot's theorem in integral or differential form, for any fuel cell reaction, and for zero and finite values of ΔC_p for the cell reaction. The useful work output of an idealized practical irreversible fuel cell cycle is also given.

Simple Fuel Cell

A simple fuel cell (1) puts out directly and isothermally as useful work (2) the chemical potential released by a fuel (reductant) plus oxygen (oxidant) upon their conversion to combustion (reaction) products. If the cell operates electrochemically, the useful work output appears as electrical work, which is, under reversible conditions, equivalent to the charging up of a condenser. If the cell operates through semi-permeable membranes as an osmotic reaction engine, the useful work may appear in mechanical form, equivalent to the lifting up of weights (2, 3). Living systems function through the mechanism of osmotic membranes (4). The biological cell might therefore be described thermodynamically as an osmotic-mechanical fuel cell.

The maximum (reversible) useful work output $W_{e,max}$ of the reaction

Fuel (reductant) + oxidant
= combustion (reaction) products [1]

conducted isothermally in a fuel cell, operating at a temperature T_f, is equal to the chemical potential (free enthalpy) released $-\Delta G_f$. In contrast, the same amount of fuel, firing a conventional power plant, yields a maximum useful work output equal to the heat (enthalpy) released $-\Delta H_h$ (at a high temperature T_h) multiplied by the Carnot efficiency $(T_h - T_l)/T_h$, where the low temperature T_l cannot ordinarily be less than ambient. The ratio of the first to the second of these work outputs, *i.e.*, the "fuel cell gain ratio," may be expressed in the form

$$\text{"Fuel Cell Gain Ratio"} = \frac{(-\Delta H_l) + T_f \Delta S_l - \int_l^f \Delta C_p\, dT + T_f \int_l^f \Delta C_p\, d\ln T}{(-\Delta H_l) - \int_l^h \Delta C_p\, dT} \cdot \frac{T_h}{T_h - T_l} \quad [2]$$

where h, f, and l refer to the temperatures T_h, T_f, and T_l, respectively, and the integrals contain summations of all enthalpies or entropies of transition that may be involved. In the special case where the reaction entropy ΔS_l and heat capacity ΔC_p are both zero, expression [2] shows that fuel cell operation permits a complete recovery of the reaction enthalpy drop $-\Delta H_l$ as useful work, without Carnot limitation.

Liebhafsky (1) discusses the thermodynamics of the reaction

$$H_2(g) + \tfrac{1}{2}O_2(g) = H_2O(g) \quad [3]$$

From his data and from Latimer (5), one can obtain the figures: $W_{e,max}(\text{fuel cell}) = -\Delta G^\circ_{298} = 54{,}635$ cal per molal reaction unit at 298°K. By comparison, $W_{e,max}(\text{power plant}) = -\Delta H^\circ_h(T_h - T_l)/T_h$. This has the values (taking $T_l = 298$°K)

T_h (°K)	400	500	1,000	2,000
$W_{e,max}$ (power plant) (cal)	14,080	23,500	41,600	51,200

Thus the comparative advantage of the fuel cell is marked, especially at low temperatures, but tends to diminish, or even turn to a disadvantage, at

higher temperatures (1). The latter difficulty tends to arise especially for negative values of ΔS and ΔC_p, as shown by Eq. [2]. The simple fuel cell is free from the Carnot-efficiency limitation of the fuel-fired power plant, since it yields its work isothermally. The thermodynamic price paid, in either case, is the permanent conversion of a quantity of fuel to combustion products. The desirable thermodynamic properties for a simple fuel cell reaction are ΔG negative, ΔS zero or positive, ΔC_p zero or positive.

These thermodynamic properties are related to the reversible cell emf E as follows

$$-\Delta G = -\Delta H + T\Delta S = n\mathbf{F}E \qquad [4]$$

$$\Delta S = n\mathbf{F}(dE/dT) \qquad [5]$$

$$\Delta C_p = n\mathbf{F}T(d^2E/dT^2) \qquad [6]$$

These quantities can be evaluated from electrode potentials (5, 6), and from their temperature coefficients (6), and second temperature coefficients (7). An illustrative calculation is given below for reaction [3].

The following numbers give standard Gibbs-Stockholm (8) electrode potentials V°, and their first and second isothermal temperature coefficients (6, 7), for hydrogen and oxygen electrodes.

	V°, v	$(dV^\circ/dT)_{\text{isoth}}$, mv/deg	$(d^2V^\circ/dT^2)_{\text{isoth}}$, μv/deg^2
$H_2 = 2H^+ + 2E^-$	0.0000	0.000	0.000
$2H_2O(l) = O_2 + 4H^+ + 4E^-$	+1.229	−0.846	+0.552
$2H_2O(g) = O_2 + 4H^+ + 4E^-$	+1.185	−0.230	−0.173

For cell reaction [3], the above numbers yield $E^\circ = 1.185$ v, $dE^\circ/dT = -0.230$ mv/deg, and $d^2E^\circ/dT^2 = -0.173$ μv/deg^2 at 25°C. The reaction entropy ΔS° is therefore $2\mathbf{F}(-0.230$ mv/deg$) = -10.6$ cal/deg, while $-\Delta G^\circ = 2\mathbf{F}(1.185$ v$) = 2.370$ v$\mathbf{F} = 54.6$ kcal, and $-\Delta H^\circ = -\Delta G^\circ - T\Delta S^\circ = 57.8$ kcal. The reaction heat capacity ΔC_p° is $2\mathbf{F}(298°\text{K})(-0.173$ μv/deg$^2) = -2.38$ cal/deg.

For a similar cell reaction with liquid water as the final product, $E^\circ = 1.229$ v, $dE^\circ/dT = -0.846$ mv/deg, and $d^2E^\circ/dT^2 = +0.552$ μv/deg^2. The reaction entropy ΔS° is now $2\mathbf{F}(-0.846$ mv/deg$) = -39.0$ cal/deg, while $-\Delta G^\circ = 2\mathbf{F}(1.229$ v$) = 56.7$ kcal, and $-\Delta H^\circ = 68.3$ kcal. The reaction heat capacity ΔC_p° is now $2\mathbf{F}(298°\text{K})(+0.552$ μv/deg$^2) = +7.59$ cal/deg at 25°C.

Coupled (Regenerative) Fuel Cell

An electrochemical (or an osmotic-reaction) cell can be coupled with a high temperature source of heat (*e.g.*, a nuclear reactor) to decompose the combustion (reaction) products and regenerate the reactants of reaction [1]. Such a device is also termed a fuel cell (1), although in this case, cell reaction [1] no longer is the primary source of energy but is merely a step in a cycle that converts heat from the high temperature source into work. Such a coupled fuel cell is not ordinarily a simple Carnot cycle (*i.e.*, a cycle of two isothermals and two adiabatics), but if it is operated reversibly, it has a useful work output determined exactly by Carnot's theorem in either integral or differential form. This was proved to be true for the integral form by Liebhafsky (1) for the case where ΔC_p is zero. He also proved this to be approximately true, by a numerical example, for an idealized practical case in which only the heat exchanges during the warming-cooling portions of the cycle were allowed to be irreversible.[1]

For complete reversibility, the output of a regenerative fuel cell obeys Carnot's theorem in differential form exactly, even when ΔC_p is not zero. This can be proved by considering the following cycle of operations

$$\mathrm{M} + \mathrm{X} = \mathrm{MX} \text{ (at } T_1) \qquad [A]$$

$$\mathrm{MX}(T_1) = \mathrm{MX}(T_2) \qquad [B]$$

$$\mathrm{MX} = \mathrm{M} + \mathrm{X} \text{ (at } T_2) \qquad [C]$$

$$\mathrm{M} + \mathrm{X}(T_2) = \mathrm{M} + \mathrm{X}(T_1) \qquad [D]$$

All reactants and products are in their arbitrarily chosen standard states. All steps are completely reversible. Reaction A has a useful work output $W_{uA} = -\Delta G_A$. For a reversible reaction, the heat input $Q_A = T_1\Delta S_A$. The enthalpy change (2) is $\Delta H_A = Q_A - W_{uA}$. The thermodynamic properties of step A are summarized in Table I.

[1] Liebhafsky's efficiency of 73.3%, compared with a Carnot efficiency of 75%, should have been reported as 71.8%.

Table I. Thermodynamic properties of the four-step regenerative fuel cell cycle A-B-C-D

Step	ΔG	ΔH	ΔS	W_u	Q
A	ΔG_A	$T_1\Delta S_A + \Delta G_A$	ΔS_A	$-\Delta G_A$	$T_1\Delta S_A$
B and D combined	$\int_1^2 \Delta C_p dT$ $-\Delta S_A(T_2 - T_1)$ $-T_2\int_1^2 \Delta C_p d\ln T$	$\int_1^2 \Delta C_p dT$	$\int_1^2 \Delta C_p d\ln T$	0	ΔH_{BD}
C	$-\Delta G_A$ $+\Delta S_A(T_2 - T_1)$ $-\int_1^2 \Delta C_p dT$ $+T_2\int_1^2 \Delta C_p d\ln T$	$-\Delta H_A$ $-\int_1^2 \Delta C_p dT$	$-\Delta S_A$ $-\int_1^2 \Delta C_p d\ln T$	$-\Delta G_C$	$T_2\Delta S_C$
Cycle	0	0	0	$-\Delta G_A - \Delta G_C = -\Delta S_A(T_2 - T_1)$ $+\int_1^2 \Delta C_p dT - T_2\int_1^2 \Delta C_p d\ln T$	

The heating and cooling steps B and D are in general not adiabatics, but they can be conducted as reversible heatings or coolings in the usual fashion, i.e., by the conceptual use of an infinite number of heat reservoirs whose temperatures differ by intervals of dT. The heat absorbed in step B is then $\int_i^h C_p(\mathrm{MX})\,dT$, while the heat released in step D is $\int_h^i C_p(\mathrm{M}+\mathrm{X})\,dT$. Both integrals are understood to contain any heats of transition that may be involved. The net heat absorbed in heating and cooling combined is $\int_i^h \Delta C_p\,dT$ where $\Delta C_p = C_p(\mathrm{MX}) - C_p(\mathrm{M}) - C_p(\mathrm{X})$. At constant pressure, the useful work output is zero (2). The other thermodynamic properties of steps B and D combined are given in Table I, and all integrals are understood to contain summations of all enthalpies or entropies of transition.

At the high temperature T_h, the decomposition of MX, reaction C, has a further useful work output (which may in actual cases be negative, *e.g.*, as for an electrolytic decomposition and separation of M and X) equal to $-\Delta G_c$. The thermodynamic properties of step C are given in Table I.

For the whole cycle, the total useful work output, equal to the net heat input from all sources, is

$$W_u(\text{cycle}) = \oint dQ = -\Delta G_h - \Delta G_c$$
$$= -\Delta S_h(T_h - T_i) + \int_i^h \Delta C_p\,dT - T_h \int_i^h \Delta C_p\,d\ln T \quad [7]$$

According to Carnot's theorem in differential form, the useful work of the cycle should be given by

$$W_u(\text{cycle}) = \int_i^h dQ(T - T_i)/T \quad [8]$$

where dQ is an infinitesimal amount of heat received reversibly by the system from a heat reservoir at temperature T. Equation [8] can be expanded to give

$$W_u(\text{cycle}) = Q_c(T_h - T_i)/T_h + \int_i dQ_{s.p}\,(T - T_i)/T \quad [9]$$

where $dQ_{s.p} = \Delta C_p\,dT$. Evaluation of the two terms in Eq. [9] leads to the expression already given in Eq. [7]. Thus the work output of the cycle satisfies Carnot's theorem exactly, for a reversible operation throughout.

In practice, one of the chief sources of irreversibility in a regenerative fuel cell lies in the heat exchanges during heating and cooling (1). These can be minimized by having ΔC_p as close to zero as possible. The desirable thermodynamic properties for a regenerative fuel cell reaction are therefore

ΔG_h negative

ΔS_h negative

ΔC_p as close to zero as possible.

Finally, it is of interest to write expressions for the useful work output of a regenerative fuel cell cycle in which the two isothermal steps are reversible, while the heating and cooling steps are allowed to be irreversible. This is a much closer approximation to the actual situation for ΔC_p different from zero than the completely reversible cycle discussed above. From a consideration of the entropy-temperature diagram (9), it can be shown that this work is $S^*(T_h - T_i)$ where S^* is the quantity of entropy which falls reversibly through the temperature drop from T_h to T_i in driving forward the operation of one cycle. The useful work will therefore be $(-\Delta S_h)(T_h - T_i)$ or $\Delta S_c(T_h - T_i)$, whichever is smaller. For ΔC_p negative, the useful work output is

$$(-\Delta S_h)(T_h - T_i) = -\Delta G_h - \Delta G_c$$
$$-\{\int_i^h \Delta C_p\,dT - T_h \int_i^h \Delta C_p\,d\ln T\} \quad [10]$$

For ΔC_p positive, the useful work output is

$$\Delta S_c(T_h - T_i) = (-\Delta S_h - \int_i^h \Delta C_p\,d\ln T)(T_h - T_i) =$$
$$-\Delta G_h - \Delta G_c - \{\int_i^h \Delta C_p\,dT - T_i \int_i^h \Delta C_p\,d\ln T\} \quad [11]$$

In both Eq. [10] and [11], the expressions in braces represent the dissipated energy of the irreversible cycle, a quantity which is always positive.

Manuscript received Jan. 30, 1960.

Any discussion of this paper will appear in a Discussion Section to be published in the June 1961 JOURNAL.

REFERENCES

1. H. A. Liebhafsky, *This Journal*, **106**, 1068 (1959).
2. A. J. deBethune, *Ind. Eng. Chem.*, **50**, 129 (1958).
3. J. H. van'tHoff, *Z. physik. Chem.*, **1**, 481 (1887).
4. H. T. Clarke and D. Nachmansohn, "Ionic Transport across Membranes," Academic Press, New York (1954).
5. W. M. Latimer, "Oxidation Potentials—The Oxidation States of the Elements and their Potentials in Aqueous Solutions," 2nd ed., Prentice Hall, New York (1952).
6. A. J. deBethune, T. S. Licht, and N. Swendeman, *This Journal*, **106**, 616 (1959).
7. A. J. deBethune and G. R. Salvi, Unpublished results.
8. J. Willard Gibbs, "Equilibrium of Heterogeneous Substances (1875-1878)" in "Collected Works, Vol. I—Thermodynamics," pp. 332-349, Longmans Green, New York (1928); "Electrochemical Thermodynamics (1887)," *ibid.*, pp. 406-412; "On the Equations of Electric Motion (1899)," *ibid.*, p. 429. J. A. Christiansen and M. Pourbaix, Compt. Rend. 17th Conf. I.U.P.A.C. (Stockholm), pp. 82-84, Maison de la Chimie, Paris (1954). T. S. Licht and A. J. deBethune, *J. Chem. Educ.*, **34**, 433 (1957).
9. J. Willard Gibbs, "Graphical Methods in the Thermodynamics of Fluids (1873)" in "Collected Works, Vol. I—Thermodynamics," pp. 9-12, Longmans Green, New York (1928).

FUTURE MEETINGS OF
The Electrochemical Society

Indianapolis, Ind., April 30, May 1, 2, 3, and 4, 1961
Headquarters at the Claypool Hotel
Sessions probably will be scheduled on
Electric Insulation, Electronics (including Luminescence and Semiconductors), Electrothermics and Metallurgy, Industrial Electrolytics (including a Symposium on Fuel Cells) and Theoretical Electrochemistry

★ ★ ★

Detroit, Mich., October 1, 2, 3, 4, and 5, 1961
Headquarters at the Statler Hotel

★ ★ ★

Los Angeles, Calif., May 6, 7, 8, 9, and 10, 1962
Headquarters at the Statler Hilton Hotel

★ ★ ★

Boston, Mass., September 16, 17, 18, 19, and 20, 1962
Headquarters at the Statler Hilton Hotel

Papers are now being solicited for the meeting to be held in Indianapolis, Ind., April 30-May 4, 1961. Triplicate copies of each abstract *(not exceeding 75 words in length)* are due at Society Headquarters, 1860 Broadway, New York 23, N. Y., *not later than January 2, 1961* in order to be included in the program. *Please indicate on abstract for which Division's symposium the paper is to be scheduled, and underline the name of the author who will present the paper.* Complete manuscripts should be sent in triplicate to the Managing Editor of the JOURNAL at 1860 Broadway, New York 23, N. Y.

Presentation of a paper at a technical meeting of the Society does not guarantee publication in the JOURNAL. However, all papers so presented become the property of The Electrochemical Society, and may not be published elsewhere, either in whole or in part, unless permission for release is requested of and granted by the Editor. Papers already published elsewhere, or submitted for publication elsewhere, are not acceptable for oral presentation except on invitation by a Divisional program Chairman.

Current Affairs

ECS Membership Dues and Journal Subscription Price Increases Voted by Board of Directors, Effective 1961

The cost of operating the Society constantly increases. The principal cause for increased costs is the publication of the JOURNAL which is expanding rapidly with respect to the number of papers published. Since the last increase of dues, which took place in 1953, our operating expenses also have increased from year to year. Thus, in order to compensate for these expanded activities and increased costs, the Board of Directors has voted the following rates to be effective in 1961:

Active Member Dues	$20.00
Nonmember Journal Subscriptions	$24.00

News Notes in the Electrochemical Field

Outdoor Exposure Confirms Laboratory Tests on Thicker Chromium Plate

Results of outdoor exposure tests over the past year on thousands of chromium-plated sample panels in Detroit and in the seashore atmosphere at Kure Beach, N. C., have confirmed the earlier results with accelerated laboratory tests on excellent corrosion resistance of thicker chromium plate over bright nickel.

The outdoor corrosion tests show that thicker chromium, such as crack-free and duplex chromium, applied over bright nickel gives better protection than the standard chromiums.

The two accelerated tests which were used to screen the new finishes were the CASS test (copper-accelerated acetic acid salt spray) and the Corrodkote test, both developed as a result of a research project sponsored by the American Electroplaters' Society and used by General Motors, Ford, and Chrysler. A new process must pass these accelerated tests to be accepted initially by the electroplating industry, but confirmation in outdoor exposure gives added confidence.

ACS to Confer Awards on H. A. Laitinen and J. C. Bailar, Jr.

The American Chemical Society recently announced the winners of 17 awards to be presented at its 139th National Meeting in St. Louis in the spring of 1961.

Among those to be honored are two Electrochemical Society members, Dr. Herbert A. Laitinen, professor of analytical chemistry, and Dr. John C. Bailar, Jr., professor of chemistry, both at the University of Illinois in Urbana.

Dr. Laitinen will receive the Fisher Award in Analytical Chemistry, and Dr. Bailar the Scientific Apparatus Makers Award in Chemical Education.

Dr. Laitinen currently is a member of the ECS Publication Committee as Editor of Monographs and Special Publications.

Thermoelectric Alloy Shows High Energy-Conversion Efficiency

Studies under way at Bell Telephone Laboratories on one of the most efficient thermoelectric materials yet developed were discussed on August 29 at the International Conference on Semiconductors at Prague, Czechoslovakia. The compound, first discovered by J. H. Wernick of Bell Labs., is silver antimony telluride ($AgSbTe_2$).

Thermoelectric devices currently being considered by industry are based on principles discovered over a century ago. The effects in metals are quite small, but, with the accelerated study of semiconductors, much more efficient materials were found.

Extensive development work is now being carried out on practical devices such as heat-to-power converters and localized coolers, especially for miniature electronic devices. Although inadequate for many proposed applications, the materials most widely used in present-day thermoelectric devices are lead telluride and bismuth telluride. The search for improved materials at Bell Labs. centered on ternary intermetallic semiconductor compounds, many of which have a cubic crystal structure similar to sodium chloride. The desired crystal formation is somewhat disordered and contains heavy atoms such as tellurium. Many compounds, and alloys of compounds, some with as many as seven elements, have been produced and studied. The best of these discovered to date has been silver antimony telluride. This material is now being widely studied in laboratories in this country and around the world.

Synthesis of these alloys by Dr. Wernick involves the direct fusion of stoichiometric quantities of the desired elements. Zone refining is then used to produce pure samples.

The material possesses a very low thermal conductivity, necessary in order to maintain a temperature differential between two ends of a device. Its thermoelectric figure of merit, "Z," recently has been measured by scientists at Radio Corp. of America, and is reported to be about $1.75 \times 10^{-3}/°C$ over a range of 200° to 500°C, which is the best yet observed for p-type thermoelements in this range. While the material is always thermoelectrically p-type, its Hall effect is p-type in some specimens, and n-type in others, even when taken from a single ingot.

Dr. R. Wolfe, Dr. J. H. Wernick, and S. E. Haszko, all of Bell Labs., ascribe this anomalous behavior to the presence of a small amount of a

second phase consisting of silver telluride, which is swept to one end by zone refining. This n-type compound appears to dominate the room temperature Hall coefficient at concentrations as low as 10 to 20%, while the p-type silver antimony telluride dominates the thermoelectric properties. Further studies of these anomalies are in progress and are expected to advance considerably the knowledge of semiconductors in general.

H-VW-M Increases Grand Rapids Chemical Capacity 300%

J. C. Miller Division, Hanson-Van Winkle-Munning Co., has announced the completed expansion of the manufacturing facility in Grand Rapids, Mich. By the addition of reactors, filtration equipment, and mixing equipment, the company has increased the monthly production capacity of the plant by a factor of three. The company recently has enlarged its line of proprietary and other chemicals for electroplating and other metalfinishing.

Solvay Process Division to Expand Chlorine-Caustic Soda Production

Plans for expansion of its mercury cell chlorine-caustic soda plant at Brunswick, Ga., have been announced by Solvay Process Division, Allied Chemical Corp. The new facilities will increase chlorine-caustic soda production capacity by approximately 100 tons per day.

This will be the second expansion of the Brunswick plant since it was constructed in 1956.

In addition to its Brunswick plant, Solvay has chlorine-caustic soda facilities at Syracuse, N. Y.; Baton Rouge, La.; and Moundsville, W. Va.

1961 Bound Volume

Members and subscribers who wish to receive bound copies of Vol. 108 (for 1961) of the JOURNAL can receive the volume for the low, prepublication price of $6.00 if their orders are received at Society Headquarters, 1860 Broadway, New York 23, N. Y., *by December 1, 1960*. After that date, members will be charged $12.00, and nonmembers, including subscribers, $18.00, subject to prior acceptance.

Bound volumes are *not* offered independently of JOURNAL subscription.

Electric Storage Battery Co. Enters Nickel-Iron Battery Market

The Edison storage battery business recently was purchased by the Electric Storage Battery Co. from the McGraw-Edison Co.

Now known as the Nickel Alkaline Battery Division, the former Thomas A. Edison Industries storage battery unit of McGraw-Edison continues to be headed by Robert A. Weeks, Jr., division manager, and by James A. Mustard, Jr., general sales manager. The new division reports to Monroe G. Smith, vice-president of ESB.

With manufacturing facilities at West Orange and the Silver Lake section of Bloomfield and Belleville, N. J., the division continues to manufacture the nickel-iron battery invented by Thomas A. Edison. It also will produce other alkaline types of industrial storage batteries.

ESB has made numerous moves in recent years to diversify its basic business of manufacturing packaged power devices. The addition of the nickel-iron battery to ESB's alkaline battery line is another step in the broadening of its line of batteries required by industry.

Nickel-iron batteries, having operating characteristics different from lead-acid batteries, have important applications in the industrial storage battery field.

PSI Administrative Headquarters Moves to Lawndale Complex

Administrative offices of Pacific Semiconductors, Inc., Culver City, Calif., a Thompson Ramo Wooldridge subsidiary, were moved in mid-August to a newly completed module of a $10,000,000 Diode and Rectifier facility at 14520 Aviation Blvd., Lawndale.

PSI will retain its Culver City buildings and continue to operate there with approximately 350 employees. Departments remaining here will include Research and Development, Microelectronics Engineering, and the Manufacture of Diode Equipment which PSI designs and produces for its own production lines.

The new corporate headquarters at Lawndale now consists of 193,000 square feet. The new module adds 106,000 square feet to the facility, in which 1700 persons are employed.

Technical Conference Held on "Metallurgy of Elemental and Compound Semiconductors"

Five sessions with a total of 33 papers were held at the Technical Conference on "Metallurgy of Elemental and Compound Semiconductors, August 29-31, in the Statler Hotel, Boston, Mass. The program was sponsored by the Semiconductors Committee of the Institute of Metals Division of the Metallurgical Society of the American Institute of Mining, Metallurgical, and Petroleum Engineers and the Boston Section of AIME.

Morning and afternoon sessions on August 29 were on "Esaki-Tunnel Diodes"; the morning of August 30 was devoted to papers on "Dendritic Growth" and the afternoon to "Vapor Growth"; with the August 31 closing program on "Growth of Other Materials."

The papers and discussions at the Conference will be published as one of the continuing series of "Metallurgical Society Conferences," printed by Interscience Publishers, Inc.

ISA Continues Russian Technical Publication Translation Program

Publication of four Russian technical journals, translated into English, will be continued with the 1960 issues during the coming year by the Instrument Society of America, under a grant from the National Science Foundation. Undertaken as a service to American science and industry, the ISA "Soviet Instrumen-

Notice to Subscribers

Your subscription to the JOURNAL of The Electrochemical Society will expire on *December 31, 1960*. Avoid missing any issue. Send us your remittance now in the amount of $24.00 for your 1961 subscription. (Subscribers located outside the United States must add $1.00 to the subscription price for postage, and payment must be made by Money Order or New York draft, not local check.) An expiration notice has been mailed to all subscribers.

A bound volume of the 1961 JOURNALS can be obtained at the prepublication price of $6.00 by adding this amount to your remittance. However, no orders will be accepted at this rate after *December 1, 1960*, when the price will be increased to $18.00 subject to prior acceptance. Bound volumes are *not* offered independently of your JOURNAL subscription.

tation and Control Translation Series" is now in its fourth year. It affords U. S. Scientists and engineers an excellent means to be better informed on the latest developments in the field of Soviet instrumentation. Included in the series are:

Automation and Remote Control (Avtomatika i Telemekhanika)—considered to be the leading Soviet journal in the automatic control field. Published monthly by the Institute of Automation and Remote Control of the Academy of Science, U.S.S.R., it carries approximately 150 pages per issue of articles on all phases of automatic control theories and techniques.

Measurement Techniques (Izmeritel'naia Tekhnika)—Approximately 100 pages per issue, published monthly by the Committee of Standards, Measures, and Measuring Instruments of the Council of Ministers, U.S.S.R. Of particular interest to those engaged in the study and application of fundamental measurement.

Instruments and Experimental Techniques (Pribory i Tekhnika Eksperimenta)—Published bimonthly, more than 175 pages per issue, by the Academy of Sciences, U.S.S.R., each issue contains articles relating to the function, construction, application, and operation of instruments in various fields of instrumentation.

Industrial Laboratory (Zavodskaya Laboratoriya)—Published monthly by the Ministry of Light Metals, U.S.S.R., it contains approximately 125 pages per issue. Articles appearing are on instrumentation for analytical chemistry, and physical and mechanical methods of material research and testing.

The 1960 translations as well as translations of previous years published under ISA's program, are available at low subscription rates ranging from $20 to $35 per annual subscription. On a combined order for all four journals, special rates apply. Libraries of nonprofit academic institutions are also offered subscriptions at special rates.

For subscriptions or information, write to Foreign Translations Dept., Instrument Society of America, 313 Sixth Ave., Pittsburgh 22, Pa.

1961 Palladium Medal Award, ECS

The sixth Palladium Medal of The Electrochemical Society will be awarded at the Fall Meeting of the Society to be held in Detroit, Mich., October 1-5, 1961.

The medal was established in 1951 by the Corrosion Division for distinguished contributions to fundamental knowledge of theoretical electrochemistry and of corrosion processes. It is awarded biennially to a candidate selected by a committee appointed by the Society's Board of Directors.

Sections, Divisions, and members of the Society are invited to send suggestions for candidates, accompanied by supporting information, to the National Office of the Society, 1860 Broadway, New York 23, N. Y., attention of Robert K. Shannon, Executive Secretary, for forwarding to the committee Chairman. *Deadline for submission of suggestions is March 15, 1961.*

Candidates may be citizens of any country and need not be members of the Society. Previous medalists have been: Carl Wagner, Max Planck Institut für Physikalische Chemie; N. H. Furman, Princeton University; U. R. Evans, Cambridge University; K. F. Bonhoeffer, Max Planck Institut für Physikalische Chemie (posthumous award); and A. N. Frumkin, Electrochemical Institute of the U.S.S.R.

Electronics Division Enlarged Abstracts

Copies of past issues of the Electronics Division Enlarged Abstracts booklets are available as follows::

1956—Vol. 5, No. 1, at $2.50
1959—Vol. 8, No. 1, at $3.00
1960—Vol. 9, No. 1, at $3.50

Please send order and check directly to:

Austin E. Hardy
Secretary-Treasurer
Electronics Division
Electrochemical Society
c/o RCA
Lancaster, Pa.

New Members

In October 1960, the following were elected to membership in The Electrochemical Society by the Admissions Committee:

Active Sustaining Members

C. G. Kepple, Motorola Inc., 2553 N. Edgington Ave., Franklin Park, Ill.

E. A. Oster, Jr., A.A.T. Dept., General Electric Co., 950 Western Ave., Lynn, Mass. (Battery)

Active Members

L. G. Austin, Pennsylvania State University; Mail add: 1165 S. Atherton St., State College, Pa. (Battery)

B. K. Balasubramanyam, Amco Batteries (Private) Ltd., Mysore Rd., Bangalore, South India (Battery)

A. B. Barakat, Jr., Raytheon Manufacturing Co.; Mail add: 23 Rich Rd., Woburn, Mass. (Electronics)

Harry Boyko, Jr., R.C.A.; Mail add: 531 Tiffin Ave., Findlay, Ohio (Electronics)

H. R. F. Braun, Climax Molybdenum Co., Talstrasse 70, Zurich, Switzerland (Electrothermics & Metallurgy)

E. W. Brewster, Sylvania Lighting Div., 60 Boston St., Salem, Mass. (Electronics)

R. C. Chirnside, Research Labs., General Electric Co., Ltd., Wembley, Middlesex, England (Corrosion, Electric Insulation, Electrodeposition, Electronics, Electrothermics & Metallurgy)

Harold Cohen, Ciba Pharmaceutical Products, Inc., 556 Morris Ave., Summit, N. J. (Electro-Organic, Theoretical Electrochemistry)

L. E. Fay, III, Bryant Computer Div., Excello Corp.; Mail add: 1800 S. Coats Rd., Oxford, Mich. (Electronics)

R. W. Guard, Metallurgical Products Dept., General Electric Co.; Mail add: 4175 Kenmore Rd., Berkley, Mich. (Electrothermics & Metallurgy)

W. E. L. Haas, Philco Corp.; Mail add: 1351 Unruh Ave., Philadelphia 11, Pa. (Electric Insulation)

R. V. Harrington, Corning Glass Works; Mail add: 1 Oakwood Dr., Corning, N. Y. (Electronics)

W. R. Hewitt, National Carbon Co.; Mail add: 3030-81st Place S.E. 7, Mercer Island, Wash. (Industrial Electrolytic)

Fumio Hine, Western Reserve University; Mail add: 2040 Stearns Rd., Cleveland 6, Ohio (Corrosion,

Notice to Members

Re Voting Ballot

By now you have received your official voting ballot from Society Headquarters. If you have not already done so, please return the ballot *by December 15* so that your vote can be included in the final election count.

By action of the Board of Directors of the Society, all prospective members must include first year's dues with their applications for membership.

Also, please note that, if sponsors sign the application form itself, processing can be expedited considerably.

Electrodeposition, Industrial Electrolytic)

Donald Hogle, Westinghouse Research Labs., Beulah Rd., Churchill Boro., Pittsburgh 35, Pa. (Electric Insulation)

R. W. Hyde, Arthur D. Little, Inc.; Mail add: 93 Cedar St., Lexington, Mass. (Electrothermics & Metallurgy)

R. H. Jones, Baker Contact Div., Engelhard Industries; Mail add: 19 Willow Rd., Lawrenceville, N. J. (Electronics)

S. P. Jones, Baker Contact Div., Engelhard Industries; Mail add: P. O. Box 56, Mt. Arlington, N. J. (Electronics)

E. J. Kalil, Self-Employed, Patent Attorney; Mail add: 42 Broadway, Rm. 1901, New York 4, N. Y. (Electrodeposition, Electrothermics & Metallurgy)

D. A. Kallander, Motorola Inc.; Mail add: 606 Solana Dr., Tempe, Ariz. (Electronics, Electrothermics & Metallurgy)

Steven Karlik, Jr., Aerovox Corp.; Mail add: 742 Belville Ave., New Bedford, Mass. (Electric Insulation)

S. R. Kresses, Titanium Alloy Manufacturing Div., National Lead Co.; Mail add: 359 Spruce Ave., Niagara Falls, N. Y. (Electrothermics & Metallurgy)

F. W. Keuther, Honeywell Research Center, 500 Washington Ave. S., Hopkins Minn. (Electrothermics & Metallurgy)

Y. L. Ko, P. R. Mallory & Co., Inc., 3029 E. Washington St., Indianapolis, Ind. (Battery, Industrial Electrolytic)

D. K. Lyon, Kollstan Semiconductor Elements, Inc.; Mail add: P. O. Box 742, Golden, Colo. (Electronics)

J. J. Meehan, Stanford University; Mail add: 356-26th Ave., San Francisco 21, Calif. (Electrodeposition)

R. E. Moore, Semiconductor Products Dept., General Electric Co.; Mail add: 105 Oakley Dr., North Syracuse 12, N. Y. (Electronics)

R. M. Pierson, Delco Radio Div., General Motors Corp., Kokomo, Ind. (Electronics)

ECS Membership Statistics

The following three tables give breakdown of membership as of Nov. 1, 1960. The Secretary's Office feels that a regular accounting of membership will be very stimulating to membership committee activities. In Table I it should be noted that the totals appearing in the right-hand column are *not* the sums of the figures in that line since members belong to more than one Division and, also, because Sustaining Members are not assigned to Divisions. But the totals listed are the total membership in each Section. In Table I, Sustaining Members have been credited to the various Sections.

Table I. *ECS Membership by Sections and Divisions*

Section	Division: Battery	Corrosion	Electric Insulation	Electrodeposition	Electronics	Electro-Organic	Electrothermics & Met.	Industrial Electrolytic	Theoretical Electrochem.	No Division	Total as of 1/1/60	Total as of 11/1/60	Net Change
Boston	18	35	13	37	84	5	24	10	28	5	168	172	+ 4
Chicago	24	33	10	37	29	16	19	14	34	7	134	147	+13
Cleveland	54	28	1	47	42	8	30	30	38	6	198	192	— 6
Columbus, Ohio	5	14	2	13	13	2	30	5	11	2	62	60	— 2
Detroit	21	21	4	51	17	8	9	7	37	6	97	103	+ 6
India	11	10	2	24	9	6	8	10	17	3	35	42	+ 7
Indianapolis	30	10	10	13	24	6	14	6	14	2	53	68	+15
Midland	10	16	1	5	2	3	10	15	9	0	43	42	— 1
Mohawk-Hudson	7	23	17	7	17	1	12	1	20	5	70	74	+ 4
New York	107	113	31	172	185	41	103	73	128	34	575	614	+39
Niagara Falls	13	19	2	25	26	6	71	59	13	11	180	166	—14
Ontario-Quebec	8	19	2	13	8	2	42	29	13	4	93	91	— 2
Pacific Northwest	6	9	1	8	1	0	9	11	12	3	43	39	— 4
Philadelphia	38	22	7	38	76	9	28	24	44	16	205	208	+ 3
Pittsburgh	4	43	5	30	35	5	37	23	36	1	136	128	— 8
San Francisco	14	14	1	28	34	3	15	21	24	3	78	97	+19
S. Calif.-Nevada	23	25	5	38	67	4	31	21	38	4	135	146	+11
Texas	4	21	2	14	38	3	9	24	31	1	0	98	+98
Washington-Baltimore	37	39	9	37	27	5	13	7	25	2	140	142	+ 2
U. S. Non-Section	61	71	11	78	68	33	65	51	86	26	452	352	—100
Foreign Non-Section	60	66	15	71	37	29	48	62	82	82	285	300	+15
Total as of Jan. 1, 1960	479	658	117	755	748	198	569	502	718	331	3182		
Total as of Nov. 1, 1960	555	651	151	786	839	195	627	503	740	223		3281	+99
Net Change	+76	—7	+34	+31	+91	—3	+58	+1	+22	—8			

Table II. *ECS Membership by Grade*

	Total as of 1/1/60	Total as of 11/1/60	Net Change
Active	2761	2859	+98
Faraday (Active)	32	34	+ 2
Deutsche Bunsen Gesellschaft (Active)	18	17	— 1
Delinquent	88	85	— 3
Active Representative Patron Members	10	10	0
Active Representative Sustaining Members	111	107	— 4
Total Active Members	3020	3112	+92
Life	17	16	— 1
Emeritus	48	65	+17
Associate	33	38	+ 5
Student	57	43	—14
Honorary	7	7	0
Total	3182	3281	+99

The figures pertaining to Patron and Sustaining Member Representatives, and Faraday and Deutsche Bunsen Gesellschaft members subscribing to the JOURNAL, have been added to reflect reclassifications and changes in membership status.

Table III. *ECS Patron and Sustaining Membership*

	Total as of 1/1/60	Total as of 11/1/60	Net Change
Patron Member Companies	5	5	0
Sustaining Member Companies	160	157	— 3

R. K. Riel, Semiconductor Dept., Westinghouse Electric Corp.; Mail add: Frick Apts., R.D. No. 3, Irwin, Pa. (Electronics)

A. J. Rosenberg, Tyro, Inc.; Mail add: 30 Burlington Rd., Bedford, Mass. (Electronics)

William Rostoker, Armour Research Foundation; Mail add: 2052 W. 108th Place, Chicago 43, Ill. (Electrothermics & Metallurgy)

J. S. Russo, Sperry Gyroscope Co.; Mail add: 63 Ontario Ave., Massapequa, N. Y. (Electrodeposition)

A. N. Salomon, Capacitor Dept., General Electric Co.; Mail add: 27 First St., Hudson Falls, N. Y. (Electric Insulation, Electronics)

Judith A. Siragusa, Ciba Pharmaceutical Products, Inc., 556 Morris Ave., Summit, N. J. (Electro-Organic)

W. F. Sringgate, Bell Telephone Labs., Inc., 1600 Osgood St., North Andover, Mass. (Electric Insulation)

L. C. Suhostavsky, Convair Scientific Research Lab.; Mail add: 1911 Glen Ridge Rd., Escondido, Calif. (Electrodeposition)

R. C. Thomas, Semiconductor Products Dept., General Electric Co.; Mail add: 23 Curtis Ave., Baldwinsville, N. Y. (Electronics)

P. V. Vedanarayan, Western Battery Corp., 108, Bazaar Ward, Kurla, Bombay 37, India (Battery)

Joe Vikin, Ciba Pharmaceutical Products, Inc.; Mail add: 412 Morris Ave., Summit, N. J. (Electro-Organic, Theoretical Electrochemistry)

Tsu-Hsing Yeh, Product & Development Lab., I.B.M., Inc., Poughkeepsie, N. Y. (Electronics)

Associate Members

P. I. Enz, P. R. Mallory & Co., Inc.; Mail add: 222 Ohmer Ave., Indianapolis 19, Ind. (Battery)

R. A. Litman, Raytheon Corp.; Mail add: 1295 Commonwealth Ave., Boston 34, Mass. (Electronics)

W. G. Pierson, Ciba Pharmaceutical Products, Inc.; Mail add: 119 Coolidge St., Irvington, N. J. (Electro-Organic, Theoretical Electrochemistry)

S. J. Salva, Western Electric Co.; Mail add: 200 N. Sterling, Kansas City 21, Mo. (Electronics)

E. F. Uhler, Jr., R.C.A.; Mail add: 111 Bertram Ave., South Amboy, N. J. (Battery, Electronics)

Student Associate Members

S. J. Acello, Rensselaer Polytechnic Institute; Mail add: 139 West High St., Ballston Spa, N. Y. (Corrosion)

I. Y. Chang, University of Texas; Mail add: Box 7705, University Station, Austin 12, Texas (Theoretical Electrochemistry)

A. J. Greif, Metallurgy Dept., Rensselaer Polytechnic Institute, Troy, N. Y. (Corrosion)

Rajindra Manocha, School of Mines, 403, Columbia University, New York 27, N. Y. (Corrosion, Electrothermics & Metallurgy, Industrial Electrolytic)

Deceased Members

Michael Borushko, Detroit, Mich.
Karl Dengg, Mentor, Ohio
S. L. Siegel, New York, N. Y.
Lawrence Whitby, Palo Alto, Calif.

Harry K. Ihrig

Harry K. Ihrig, vice-president in charge of research, Allis-Chalmers Manufacturing Co., Milwaukee, Wis., died of a heart attack on August 22, 1960. He was 62 years old.

Dr. Ihrig was born in Appleton, Wis. He studied at Carleton College, Northfield Minn., receiving his B.S. degree in 1919 and his M.S. degree in 1920 from the University of North Dakota, and his Ph.D. degree in 1923 from the University of California.

He held 22 United States patents. One of his best-known inventions, a process to make steel resistant to corrosion and acid, was developed in 1936 while he was with the Globe Steel Tubes Co. He had been vice-president and director of laboratories for Globe Steel for 17 years before joining Allis-Chalmers in 1950.

In addition to The Electrochemical Society, which he joined in February 1943, Dr. Ihrig was a member of the American Chemical Society, American Institute of Chemical Engineers, American Society for Metals, American Institute of Mining and Metallurgical Engineers, National Society of Professional Engineers, and Industrial Research Institute.

He is survived by his wife, Luella, of Shorewood, and two sons, Judson L. and Harry Karl, Jr.

Division News

Industrial Electrolytic Symposium on Fuel Cells, Spring 1961

A Symposium on Fuel Cells sponsored by the Industrial Electrolytic Division will be held on May 1, 2, and 3, 1961 during the Spring Meeting of the Society in Indianapolis, Ind.

Since fuel cells are an electrochemical process with great industrial potential, the members of the

Manuscripts and Abstracts for Spring 1961 Meeting

Papers are now being solicited for the Spring Meeting of the Society, to be held at the Claypool Hotel in Indianapolis, Ind., April 30, May 1, 2, 3, and 4, 1961. Technical sessions probably will be scheduled on Electric Insulation, Electronics (including Luminescence and Semiconductors), Electrothermics and Metallurgy, Industrial Electrolytics (including a Symposium on Fuel Cells), and Theoretical Electrochemistry.

To be considered for this meeting, triplicate copies of abstracts (*not exceeding 75 words in length*) must be received at Society Headquarters, 1860 Broadway, New York 23, N. Y., *not later than January 2, 1961. Please indicate on abstract for which Division's symposium the paper is to be scheduled and underline the name of the author who will present the paper.* Complete manuscripts should be sent in triplicate to the Managing Editor of the JOURNAL at the same address.

Presentation of a paper at a technical meeting of the Society does not guarantee publication in the JOURNAL. However, all papers so presented become the property of The Electrochemical Society, and may not be published elsewhere, either in whole or in part, unless permission for release is requested of and granted by the Editor. Papers already published elsewhere, or submitted for publication elsewhere, are not acceptable for oral presentation except on invitation by a Divisional program Chairman.

Industrial Electrolytic Division are interested in both the theoretical and practical aspects. Fuel cells also are of interest from the point of view that they may be used as a source of d-c current for other electrochemical processes and that they may make use of by-product hydrogen from an electrochemical plant.

Those interested in participating by the presentation of a paper must submit abstracts of National Society Headquarters, 1860 Broadway, New York 23, N. Y., *by January 2, 1961.*

J. E. Curry, *Sec.-Treas.*

Announcements from Publishers

"Mechanism of Electroreduction of Chromic Ion at the Mercury Cathode," May 1960. AEC Report IDO-14505,* 55 pages; $1.50.

"Corrosion" (Ten-Year Bibliography), SB-401,* 10 cents.

"Study of Energy Conversion Devices (Report No. 1)," R. E. Shearer, MSA Research Corp., for U. S. Army, Oct. 1959. Report PB 161690,* 29 pages; $1.00.

"Research in Radiation Damage in Semiconductors," J. W. Harrity and others, General Dynamics Corp., for U. S. Air Force, Feb. 1960. Report PB 161673,* 157 pages; $3.00.

"High-Temperature Semiconductor Devices," edited by F. D. Rosi and P. Rappaport, Radio Corp. of America, for U. S. Air Force, Oct. 1959. Report PB 161541,* 124 pages; $2.75.

"A Practical Interpretation of Dielectric Measurements up to 100-MC," J. J. Chapman and L. J. Frisco, Johns Hopkins University, for the U. S. Army, Dec. 1958. Report PB 161545,* 207 pages; $3.50.

"The Hill Reaction as a Model for Chemical Conversion of Solar Energy," R. J. Marcus, Stanford Research Institute, for Air Force Office of Scientific Research, Dec. 1959. Report PB 161462,* 6 pages; 50 cents.

"Study of Electrical and Physical Characteristics of Secondary Emitting Surfaces," W. G. Shepherd, University of Minnesota, for Wright Air Development Center, U. S. Air Force, Dec. 1959. Report PB 161491,* 65 pages; $1.75.

"Magnetic Properties of Some Ferrite Micropowders," A. E. Berkowitz and W. J. Schuele, Franklin Institute Labs. for Research and Development, for Wright Air Development Center, U. S. Air Force, Nov. 1959. Report PB 161533,* 15 pages; 50 cents.

"Preparation and Properties of Some Polyphenyls," G. F. Woods, University of Maryland, for Wright Air Development Center, U. S. Air Force, Sept. 1959. Report PB 161508,* 178 pages; $3.00.

"Pressure Induced Crystallization in Polyethylene," S. Matsouka and B. Maxwell, Army Signal Corps and Office of Naval Research, for the U. S. Army, April 1959. Report PB 161455,* 92 pages; $2.25.

"Methods of Purification of Metals and Intermetallic Compounds," S. Susman, Armour Research Foundation, for Wright Air Development Center, U. S. Air Force, Nov. 1959. Report PB 161415,* 86 pages; $2.25.

* Order from Office of Technical Services, U.S. Dept. of Commerce, Washington 25, D.C.

Personals

C. A. Butler has joined the chemical consulting firm of R. B. MacMullin Associates, Niagara Falls, N. Y., as a partner and manager of their Cleveland office. Mr. Butler formerly was director of engineering and director of commercial development of the Diamond Alkali Co., Cleveland.

Alden Stevenson has been named director of research for Pacific Semiconductors, Inc., Culver City, Calif. In addition to his new responsibilities, he will continue as materials research program director. Dr. Stevenson joined the Thompson Ramo Wooldridge subsidiary four years ago after three years as development physicist with Minneapolis-Honeywell Regulator Co.

Gunther A. Wolff has joined the Harshaw Chemical Co. as a senior research group leader on semiconductor materials and crystal kinetics. He will make his headquarters at the Main Office of the company in Cleveland, Ohio. Dr. Wolff formerly was associated with the Signal Corps at Fort Monmouth, N. J.

Research Post For

PHYSICAL CHEMIST

and/or

INORGANIC CHEMIST

M.S. or Ph.D.

Experience: Research experience preferred, but not essential. Applicant should have interests in one or more of research fields below, and good educational background.

Areas of Work: Materials studies; chemistry of preparation and purification of new materials; energy conversion; solid-state devices; fuel cells.

Battelle offers: Especially attractive combination of individual freedom and collateral aid from fellow scientists and technologists. Facilities, including outstanding library, among the best. Creativity in both basic and applied research most highly valued . . . Salary commensurate with education and experience; attractive extra benefits; opportunity to combine work and additional graduate study at adjacent Ohio State University . . . Write L. G. Hill.

BATTELLE MEMORIAL INSTITUTE

55 King Avenue

Columbus 1, Ohio

ADVANCED NAVAL REACTOR DEVELOPMENT
at the
Knolls Atomic Power Laboratory

CHALLENGE AND OPPORTUNITY IN
POSITIONS OF MAJOR RESPONSIBILITY

CORROSION ENGINEER

5 to 10 years experience. Evaluate materials for use in high temperature water, including measurement uniform corrosion, galvanic corrosion, stress corrosion, corrosion fatigue, and wear. Design and conduct or direct experiments. Prepare proposals, experimental design and reports. Work closely with metallurgists and design engineers.

CORROSION SCIENTIST

Originate, carry out and report results of programs on: Corrosion rates and mechanisms in high temperature water; Nature and transport of corrosion products.

Superior laboratory facilities. Publications encouraged.

Write to Mr. A. J. Scipione, Dept. ES-K.

The Knolls Atomic Power Laboratory is operated for the A.E.C. by

GENERAL ELECTRIC

Schenectady, New York

U.S. Citizenship Required

ELECTROCHEMIST

Doctor's Degree—5 to 10 Years' Experience

To head a newly organized group of electrochemists and physical chemists devoted to research on fuel cells.

This is a challenging position in a new field. It requires considerable theoretical background, experimental skill and inventive talent.

Work is strongly supported by the Corporation and directed at commercial exploitation. The position has excellent potential for growth.

A new laboratory building has been erected in our plant at East Hartford, Connecticut.

Send resume and minimum salary requirements to Mr. P. R. Smith, Office 61,

PRATT & WHITNEY AIRCRAFT
Division of United Aircraft Corporation
East Hartford 8, Connecticut

PHYSICAL CHEMISTS

ELECTRO-CHEMISTS

CHEMICAL ENGINEERS

Important research positions are available in the Electrochemistry Laboratory at Lockheed Missiles and Space Division, located 40 miles south of San Francisco.

The laboratory is engaged in the field of electrochemical energy conversion such as fuel cell systems, and requires outstanding personnel qualified by extensive experience or academic background in the following areas:

CHEMICAL ENGINEERS
PROCESS & EQUIPMENT DESIGN
MASS TRANSFER
PILOT OPERATIONS

CHEMISTS
SOLID STATE CHEMISTRY
SURFACE CHEMISTRY
HETEROGENEOUS KINETICS
CATALYSIS
ELECTROCHEMISTRY
PHOTOCHEMISTRY

These positions provide an excellent opportunity in a young and growing new technology with an assured future. If you are experienced in work related to the above areas, you are invited to write: Research and Development Staff, Dept. K-26, 962 W. El Camino Real, Sunnyvale, Calif. U.S. citizenship or existing Department of Defense industrial security clearance required.

Lockheed
MISSILES AND SPACE DIVISION

Sunnyvale, Palo Alto,
Van Nuys, Santa Cruz,
Santa Maria, California
Cape Canaveral, Florida
Hawaii

Literature from Industry

"Some Plain Talk About Fuel Cells," GED-4111. Illustrated, 12-page booklet discusses basic facts about fuel cells, including how they work, problem areas, various types of cells under development, special features of the new G. E. ion-membrane fuel cell, technical performance data, and application information. General Electric Co., Schenectady, N. Y.

Sel-Rex Electrion pH Meter. Illustrated data sheet shows how precise, reproducible readings within ±0.02 pH accuracy are obtained with the Electrion, a palm-sized pH meter using a single "combination" electrode and requiring standardization only once a week or less. Sel-Rex Instruments Inc., Nutley, N. J.

Sargent Catalog. A 60-page catalog (Booklet 60) of laboratory instruments, including the Sargent recorders, Models MR and SR, along with the Sargent polarographs, Models XV and XXI, is available on request. E. H. Sargent & Co., Dept. 60, 4647 W. Foster Ave., Chicago 30, Ill.

Direct-Traverse Trimmer Capacitors. Seven models of direct-traverse trimmer capacitors with pan terminals and five models with wire terminals are described in a new engineering reference sheet. The special direct traverse mechanism provides smooth, linear tuning without backlash. The trimmers' hardware and special glass dielectric give them excellent performance under shock and vibration. Designed for communications and instrumentation circuits, they have capacitances between 0.5 and 12 $\mu\mu$f.

Advertiser's Index

American Brass Company 252C
Battelle Memorial Institute 258C
Bell Telephone Laboratories, Inc. 249C
General Electric Company 259C
General Motors Research Laboratories 248C
Great Lakes Carbon Corp., Electrode Division ..... Cover 2
Lockheed Missiles & Space Division 259C
Pratt & Whitney Aircraft 259C
Sylvania Electric Products Inc. 251C

Sheet CE-4.01 is available on request on company letterhead from Corning Electronic Components, a department of Corning Glass Works, Bradford, Pa.

New Products

Cathodic Protection Rectifiers. Complete, one-unit cathodic protection rectifiers in four standardized case sizes are being offered by EICOR, Div. of the Scranton Corp. Each transformer is custom-designed and manufactured with a sufficient safety factor for intermittent overloads and long life.

Detailed specifications with output rating charts and other information available on request from EICOR, 4059 West North Ave., Chicago 39, and 2225 Burbank, Dallas, Texas.

Fiberglas Flake Protective Coating, a spray coating providing a corrosion-resistant surface to metals, wood, and concrete, has been developed by Owens-Corning Fiberglas Corp. Accelerated weathering tests have shown virtually no deterioration of the coating, and laboratory tests of the coating show the following: vapor transmission, less than 0.01 perms; shear strength, 800 psi; dielectric strength, 500 v per mil.

Inquiries should be directed to J. S. McBride, Owens-Corning Fiberglas Corp., 717 Fifth Ave., New York 22, N. Y., or Henry M. Kidd, De Vilbiss Co., 300 Phillips Ave., Toledo 1, Ohio.

Formfitting Silvercel Primary Battery. A high-rate, two-section Silvercel battery, curved for optimum space utilization in missiles, was shown for the first time by Yardney Electric Corp., New York City, at the 1960 Western Electronic Show and Convention. The new Yardney powerpack, Model P-3000, is a primary (one-shot) unit designed for wide variations in discharge rates (as high as 100 amp continuously). Its sections, "A" and "B," each consist of 20 cells of 3-amp-hr nominal capacity. In typical application, the battery can meet voltage regulation requirements for Section "A" that allow a variation of only ± 0.7 v. In such use, Section "A" would supply continuous drains ranging from 24 amp to 26.8 amp with 33.2-amp pulses every 60 sec, at 28.7 v, for 3.5 min. Section "B," in the same application, would provide continuous drains ranging from 65 to 38.5 amp, at 26.7 to 28.2 v, for 3.5 min, with a peak pulse of 145 amp, at 24 v.

Employment Situations

Positions Available

Research Chemists—Research and development group seeks chemist or chemical physicist for solid-state work on cathodoluminescent and electroluminescent materials, photoconductors, and chemicals for electronic applications. Candidates should have Ph.D. or equivalent and be capable of independent work. Modern and well-equipped laboratories in Northeastern Pennsylvania. Publication of work encouraged.

Send résumé to: Dr. J. S. Smith, Manager of Chemical Research and Development, Chemical and Metallurgical Division, Sylvania Electric Products Inc., Towanda, Pa.

Four challenging research positions for experienced surface chemists, in fully-equipped laboratory devoted to research and development on aluminum and copper alloys, involving: A. Electrochemical kinetics, adsorption, and oxide film structure investigations related to finishing processes. B. Studies of interfacial surface reactions between polymeric resins and metal oxide surfaces relating to strength and permanence of joints in the adhesive bonding of metals. C. Mechanisms relating to surface phenomena, associated with liquid metal-solid metal inter-action as applied to soldering and brazing. D. Surface and electrochemical reactions effecting the kinetics of general, localized, and stress corrosion processes. Pleasant living, with access to major university. Send reply to R. H. Endriss, Personnel Manager, Olin Mathieson Chemical Corp., 125 Munson St., New Haven, Conn.

Position Wanted

Chemical Engineer, B.S.—Thirteen years of electrolytic background in development and production work. Supervisory experience. Desires responsible position in either process engineering or production. *Reply to Box No. 370, c/o The Electrochemical Society, 1860 Broadway, New York 23, N. Y.*

The Electrochemical Society

Patron Members

Aluminum Co. of Canada, Ltd., Montreal, Que., Canada

International Nickel Co., Inc., New York, N. Y.

Olin Mathieson Chemical Corp., Niagara Falls, N. Y.
- Industrial Chemicals Div., Research and Development Dept.

Union Carbide Corp.
- Divisions:
  - Union Carbide Metals Co., New York, N. Y.
  - National Carbon Co., New York, N. Y.

Westinghouse Electric Corp., Pittsburgh, Pa.

Sustaining Members

Air Reduction Co., Inc., New York, N. Y.

Ajax Electro Metallurgical Corp., Philadelphia, Pa.

Allen-Bradley Co., Milwaukee, Wis.

Allied Chemical & Dye Corp.
- General Chemical Div., Morristown, N. J.
- Solvay Process Div., Syracuse, N. Y. (3 memberships)

Allied Research Products, Inc., Detroit, Mich.

Alloy Steel Products Co., Inc., Linden, N. J.

Aluminum Co. of America, New Kensington, Pa.

American Metal Climax, Inc., New York, N. Y.

American Potash & Chemical Corp., Los Angeles, Calif. (2 memberships)

American Smelting and Refining Co., South Plainfield, N. J.

American Zinc Co. of Illinois, East St. Louis, Ill.

American Zinc, Lead & Smelting Co., St. Louis, Mo.

American Zinc Oxide Co., Columbus, Ohio

M. Ames Chemical Works, Inc., Glens Falls, N. Y.

Basic Inc., Maple Grove, Ohio

Bell Telephone Laboratories, Inc., New York, N. Y. (2 memberships)

Bethlehem Steel Co., Bethlehem, Pa. (2 memberships)

Boeing Airplane Co., Seattle, Wash.

Burgess Battery Co., Freeport, Ill. (4 memberships)

Canadian Industries Ltd., Montreal, Que., Canada

Carborundum Co., Niagara Falls, N. Y.

Catalyst Research Corp., Baltimore, Md.

Ciba Pharmaceutical Products, Inc., Summit, N. J.

Columbian Carbon Co., New York, N. Y.

Columbia-Southern Chemical Corp., Pittsburgh, Pa.

Consolidated Mining & Smelting Co. of Canada, Ltd., Trail, B. C., Canada (2 memberships)

Continental Can Co., Inc., Chicago, Ill.

Cooper Metallurgical Associates, Cleveland, Ohio

Corning Glass Works, Corning, N. Y.

Diamond Alkali Co., Painesville, Ohio (2 memberships)

Dow Chemical Co., Midland, Mich.

Wilbur B. Driver Co., Newark, N. J. (2 memberships)

E. I. du Pont de Nemours & Co., Inc., Wilmington, Del.

Eagle-Picher Co., Chemical Div., Joplin, Mo.

Eastman Kodak Co., Rochester, N. Y.

Thomas A. Edison Research Laboratory, Div. of McGraw-Edison Co., West Orange, N. J.

Electric Auto-Lite Co., Toledo, Ohio
- C & D Division, Conshohocken, Pa.

Electric Storage Battery Co., Yardley, Pa.

Englehard Industries, Inc., Newark, N. J. (2 memberships)

The Eppley Laboratory, Inc., Newport, R. I. (2 memberships)

Erie Resistor Corp., Erie, Pa.

Exmet Corp., Tuckahoe, N. Y.

Fairchild Semiconductor Corp., Palo Alto, Calif.

Food Machinery & Chemical Corp.
- Becco Chemical Div., Buffalo, N. Y.
- Westvaco Chlor-Alkali Div., South Charleston, W. Va.

Foote Mineral Co., Paoli, Pa.

Ford Motor Co., Dearborn, Mich.

General Electric Co., Schenectady, N. Y.
- Chemistry & Chemical Engineering Component, General Engineering Laboratory
- Chemistry Research Dept.
- General Physics Research Dept.
- Metallurgy & Ceramics Research Dept.
- Aircraft Accessory Turbine Dept., West Lynn, Mass.

General Instrument Corp., Newark, N. J.

(Sustaining Members cont'd)

General Motors Corp.
Delco-Remy Div., Anderson, Ind.
Guide Lamp Div., Anderson, Ind.
Research Laboratories Div., Detroit, Mich.
General Transistor Corp., Jamaica, N. Y.
Gillette Safety Razor Co., Boston, Mass.
Globe-Union, Inc., Milwaukee, Wis.
Gould-National Batteries, Inc., Minneapolis, Minn.
Grace Electronic Chemicals, Inc., Baltimore, Md.
Great Lakes Carbon Corp., New York, N. Y.
Hanson-Van Winkle-Munning Co., Matawan, N. J. (2 memberships)
Harshaw Chemical Co., Cleveland, Ohio (2 memberships)
Hercules Powder Co., Wilmington, Del.
Hill Cross Co., Inc., New York, N. Y.
Hoffman Electronics Corp., El Monte, Calif.
Hooker Chemical Corp., Niagara Falls, N. Y. (3 memberships)
Hughes Aircraft Co., Culver City, Calif.
Industro Transistor Corp., Long Island City, N. Y.
International Business Machines Corp., Poughkeepsie, N. Y.
International Minerals & Chemical Corp., Skokie, Ill.
ITT Laboratories, Nutley, N. J.
Jones & Laughlin Steel Corp., Pittsburgh, Pa.
K. W. Battery Co., Skokie, Ill.
Kaiser Aluminum & Chemical Corp.
Div. of Chemical Research, Permanente, Calif.
Div. of Metallurgical Research, Spokane, Wash.
Kennecott Copper Corp., New York, N. Y.
Keokuk Electro-Metals Co., Keokuk, Iowa
Libbey-Owens-Ford Glass Co., Toledo, Ohio
M. & C. Nuclear, Inc., Attleboro, Mass.
Mallinckrodt Chemical Works, St. Louis, Mo.
P. R. Mallory & Co., Indianapolis, Ind.
McGean Chemical Co., Cleveland, Ohio
Merck & Co., Inc., Rahway, N. J.
Metal & Thermit Corp., Detroit, Mich.
Minnesota Mining & Manufacturing Co., St. Paul, Minn.
Monsanto Chemical Co., St. Louis, Mo.
Motorola, Inc., Chicago, Ill.
National Cash Register Co., Dayton, Ohio
National Lead Co., New York, N. Y.
National Research Corp., Cambridge, Mass.
National Steel Corp., Weirton, W. Va.
New York Air Brake Co., Kinney Vacuum Div., Boston, Mass.
Northern Electric Co., Montreal, Que., Canada
Norton Co., Worcester, Mass.
Olin Mathieson Chemical Corp., Research & Engineering Operations, Energy Div., New Haven, Conn.
Ovitron Corp., Long Island City, N. Y.
Peerless Roll Leaf Co., Inc., Union City, N. J.
Pennsalt Chemicals Corp., Philadelphia, Pa.
Phelps Dodge Refining Corp., Maspeth, N. Y.
Philco Corp., Philadelphia, Pa.
Philips Laboratories, Inc., Irvington-on-Hudson, N. Y.
Pittsburgh Metallurgical Co., Inc., Niagara Falls, N. Y.
Poor & Co., Promat Div., Waukegan, Ill.
Potash Co. of America, Carlsbad, N. Mex.
Radio Corp. of America
Tube Div., Harrison, N. J.
RCA Victor Record Div., Indianapolis, Ind.
Ray-O-Vac Co., Madison, Wis.
Raytheon Manufacturing Co., Waltham, Mass.
Reynolds Metals Co., Richmond, Va. (2 memberships)
Rheem Semiconductor Corp., Mountain View, Calif.
Schering Corporation, Bloomfield, N. J.
Shawinigan Chemicals Ltd., Montreal, Que., Canada
Speer Carbon Co.
International Graphite & Electrode Div., St. Marys, Pa. (2 memberships)
Sprague Electric Co., North Adams, Mass.
Stackpole Carbon Co., St. Marys, Pa.
Stauffer Chemical Co., New York, N. Y.
Sumner Chemical Co., Div. of Miles Laboratories, Inc., Elkhart, Ind.
Sylvania Electric Products Inc., Bayside, N. Y. (2 memberships)
Tennessee Products & Chemical Corp., Nashville, Tenn.
Texas Instruments, Inc., Dallas, Texas
Three Point Four Corp., Yonkers, N. Y.
Titanium Metals Corp. of America, Henderson, Nev.
Tung-Sol Electric Inc., Newark, N. J.
Udylite Corp., Detroit, Mich. (4 memberships)
Universal-Cyclops Steel Corp., Bridgeville, Pa.
Upjohn Co., Kalamazoo, Mich.
Victor Chemical Works, Chicago, Ill.
Western Electric Co., Inc., Chicago, Ill.
Wyandotte Chemicals Corp., Wyandotte, Mich.
Yardney Electric Corp., New York, N. Y.